Behavior of lightweight framing systems for buildings

by

Abdelfattah Elnur Abbaker

A thesis submitted in partial fulfilment of the requirements for the degree of Doctor of Philosophy in Civil Engineering

School of Engineering, University of Warwick

June 2006

Contents

Acknowledgements

Declaration

Publications

Abstract

Notations

1 Introduction **1**

1.1 Modern methods of construction 1

1.2 Shear flexible frame analysis 5

2 Review of Modular Construction **11**

2.1 Introduction 11

2.1.1 Modular elements 13

2.2 Thin-walled cold-formed sections 13

2.3 Manufacturing of cold-rolled sections 14

2.4 Novel ε-section 15

3 Strength of Cold-form Thin-walled Columns **22**

3.1 Introduction 22

3.2 Flexural buckling 25

3.2.1 Boundary condition 27

3.2.2 Initial imperfection 28

3.3 Local buckling 29

3.3.1 Post buckling 30

3.3.2 Effective area approach 30

3.4 Inelastic buckling 32

3.5 Flexural torsional buckling 34

4 Inelastic Stability of Curved Plates **42**

4.1 Introduction 42

4.2 Inelastic stability of curved plate element 43

4.2.1 Displacement field 47

4.2.2 Internal forces 47

4.2.3 Strain energy 54

4.2.4 Rayleigh-Ritz method 57

4.2.5 Application to curved plate subjected to edge forces 57

4.3 Development of the plasticity reduction factor for curved plate element 68

5 Experimental Method for Characterisation of Stub and Stud ε-columns **72**

5.1 Introduction 72

5.2 Tensile coupon tests 73

5.3 Stub column tests 74

5.3.1 Introduction 74

5.3.2 Preparation of specimens 74

5.3.3 Test procedure 75

5.3.4 Instrumentation 76

5.3.5 Loading and measurements 77

5.4 Stud column testing 77

5.4.1 Introduction 77

5.4.2 Preparation of specimens 78

5.4.3 Test procedure 80

5.4.4 Instrumentation 82

5.4.5 Loading sequence 83

5.4.6 Measurements 84

6 Stub Column Study with 1.5 mm Thick ε-section 94

6.1 Introduction 94

6.2 Results of the tensile coupon tests 94

6.3 Analysis of stub column testing 99

6.3.1 Plasticity reduction factor, η, for curved element 102

6.3.2 Prediction of inelastic critical load for ε-section 103

6.3.3 Effective area, A_{eff} 106

7 Stud Column Test Results and their Evaluation 115

7.1 Introduction 115

7.2 Test results for stud columns 116

7.2.1 Effective length of ε-columns 120

7.2.2 Effect on buckling resistance of intermediate stiffening 121

7.2.3 Influence on buckling resistance of the wall thickness 123

7.2.4 Influence on buckling resistance of the cross-section configuration 123

7.2.5 The overall effective load eccentricity in the series of ε-column tests 124

7.2.6 ε-column design strengths 127

8 Conclusions and Recommendations for Further Work on the ε-column Study 145

8.1 Conclusions on the ε-column study 145

8.2 Recommendations for further work 149

9 Analysis of Frames of Fibre Reinforced Polymer Sections 151

9.1 Introduction 151

9.2 Pultruded structural shapes and systems 152

9.3 The pultrusion process 153

9.4 Uses of FRPs in civil engineering 154

9.5 Merits and drawback 155

9.6 Frame analysis 156

9.7 In-house frame analysis software called sframe 157

10 Elastic Critical Load of Framed Structures 161

10.1 Introduction 161

10.2 The stability concept of structures 164

10.2.1 Element shear deformation 166

10.2.2 Shear-stiff stability functions for isotropic elements 169

10.2.3 Shear-flexible stability functions for FRP elements 170

10.2.4 Verification of developed $\overline{\phi_i}$ functions 174

10.3 Semi-rigid joint action in frame analysis 175

10.4 Analysis for the elastic critical buckling load of frames 178

10.5 Summary for the sframe analysis tool 182

11 Parametric Study Using sfame to Determine the Elastic Critical Buckling Loads of Shear-flexible Frames 189

11.1 Introduction 189

11.2 Portal frames with shear-rigid members and rigid joints 190

11.3 Shear-flexible members and rigid joints 192

11.4 Shear-rigid members and semi-rigid joint action 195

11.5 Shear-flexible members and semi-rigid joint action 196

12 Conclusions and Recommendations for Further Work on the sframe Analysis 201

12.1 Conclusions on the sframe analysis 201

12.2 Recommendations for further work 203

Appendix A Load-displacement plots

Appendix B Modified stability functions

Appendix C Guide for using sframe program to analysis plane frames of shear flexible members

References

List of figures

1.1	Modular construction for a large family house in Japan (from SCI publication P272)	9
1.2	Modular construction for a fast food restaurant (from SCI publication P272).	9
1.3	Example of a framed structure using steelwork (from RM Construction, website)	10
2.1	Main types of modular construction, (a) Mobile offices (from Portakabin website), (b) Building system (Charter School, from NRB website)	18
2.2	Examples of cold formed steel sections (from SCI publication P276)	19
2.3	Cold rolling process for thin walled steel sections	20
2.4	Cross-section of ε-section with 1.5 mm wall thickness	20
2.5	Prototype modular unit fabricated by Modula 2000 Ltd	21
3.1	Euler's assumed column deformation	39
3.2	Effective length for different end restraints	39
3.3	Initial lack of straightness	40
3.4	Distribution of σ_z stress across width of plate in post-buckling regime	40
3.5	Effective width concept for a flat plate	41
3.6	Deformations of a general asymmetric cross-section under axial	41

compression

4.1 Curved plate geometry and displacements components 70

4.2 Curved plate moment and force intensities 70

4.3 Curved plate under axial compression force 71

5.1 Cross-section of ε-column with the Major axis (x-x) the horizontal plane through the centre of the cross-section 85

5.2 Stub column specimens 85

5.3 Strain gauges locations on specimens S7 and S8 86

5.4 Local buckling test arrangement with specimen S7 86

5.5 Photos for strain gauges locations on specimen S7 (a) front view, (b) back view 87

5.6 ε-columns stiffeners locations, (a) WU104&105, (b) WU106&107, (c) WU108&109, (d) WU110&111, (e) WU112 (from Peter Dann Ltd). 90

5.7 WU series ε-column with end load end fixtures (from Peter Dann Ltd). 91

5.8 Test rig, (a) Schematic of test rig, (b) Photo of test rig with 2.7 m height stud column ready for testing 91

5.9 Displacement transducers at mid-length to measure lateral deflection in the major x- and minor z-direction 92

5.10 Base fixture and 120 kN load cell 92

5.11 Top fixture, load jack and axial displacement transducer 93

5.12 Hydraulic Jacks and data logger 93

6.1 Tensile stress v strain curve for ε-section steel, from coupon 109

———, from Equation (6.2) — — —

6.2	Mean axial shortening versus compression stress from 8 stub columns of the 1.5 thick ε-section at a height of 200 mm	109
6.3	Axial strain from gauge No. 8 versus compression stress from stub column S7 of the 1.5 thick ε-section at a height of 200 mm	110
6.4	Post-test deformations of stub specimens S1 to S8	111
6.5	Strain profiles at mid height for different axial compressive stress levels, using stub column specimen	112
6.6	Locations of strain gauges Nos. 1 to 8 at the mid-height for stub column specimens S7 and S8	112
6.7	Assumed buckling elements of the ε-stub column	113
6.8	Calculated plasticity reduction factor $\overline{\eta}$ with compressive stress for the 1.5 mm ε-section	113
6.9	Assumed flange length for ε-section having wall thickness of 1.5 mm	114
7.1	Typical specimen deformation at maximum test load	136
7.2	Load-displacement curve for column of type WU104	136
7.3	Load-displacement curve for column of type WU105	137
7.4	Load-displacement curve for column of type WU106	137
7.5	Load-displacement curve for column of type WU107	138
7.6	Load-displacement curve for column of type WU108	138
7.7	Load-displacement curve for column of type WU109	139
7.8	Load-displacement curve for column of type WU110	139
7.9	Load-displacement curve for column of type WU111	140
7.10	Load-displacement curve for column of type WU112	140

7.11 Determination of the point of zero curvature, (a) Locations of the strain gauges, (b) Location of the point of zero curvature from the ends of a ε-column 141

7.12 Effect on buckling load of number and location of stiffeners, from testing columns of types WU104, WU106 and WU108 142

7.13 Effect on buckling load of number and location of stiffeners, from testing columns of types WU105, WU107 and WU109 142

7.14 Influence on buckling resistance of ε-section wall thickness, with column type WU104 at 1.5 mm and WU105 at 2 mm 143

7.15 Influence on load-displacement response and buckling resistance of having ε-section fully-opened in column types WU104 and WU105 and fully-enclosed in column types WU110 to WU112 143

7.16 Central deflection, (a) Δ_e of a beam-column member due to load eccentricity, (b) $\Delta_{MA\theta A}$ of a beam-column member, without axial compression, due to equal end-moments 144

9.1 Application of FRPs in civil engineering. (a) West Mill Bridge in Oxfordshire, UK (b) Wall façade fabricated from FRP at Dubai International airport 159

9.2 Standard and non-standard PFRP sections (from Strongwell, web site) 159

9.3 Schematic diagram showing the salient stages in the pultrusion process 160

10.1	Second-order P-Δ and P-δ moments, (a) Sway permitted, (b) Sway restrained (Galambos 1998)	184
10.2	Frame deformation shapes, (a) side-sway frame, (b) no-side-sway frame	185
10.3	Force and nodal displacements for shear-flexible beam-column element	186
10.4	Beam-column element generalised deformation	186
10.5	Beam-column element subjected to end rotations and no sway	186
10.6	Influence of the shear-flexible parameter μ on the shear-flexible ϕ_1 function	187
10.7	Typical connections details for joints in pultruded FRP frames (Mottram 1994)	187
10.8	Joints classification, (a) rigid joint, (b) pinned joint, (c) semi-rigid joint	188
10.9	Moment-rotation curve for semi-rigid connection in pultruded FRP frames	188
10.10	The hybrid element comprising beam-column element with end rotational springs to simulate semi-rigid joint action	188
11.1	Portal frames, (a) Sway loading case, (b) No-sway loading case	197
11.2	Two-storey, sinlge bay sway frame problem	198
11.3	ρ_{crsh} with μ for the Al-Sarraf (1979) single bay two storey frame problem	198
11.4	Portal sway frame with semi-rigid beam-column joints	199
11.5	Elastic critical buckling load parameter ρ_{cr} with changing $(S_j l)/(EI)$ for a simple frame problem with shear-rigid members	199

11.6 Elastic critical buckling load parameter ρ_{crsh} with changing $(S_j l)/(EI)$ and moduli ratio E/G for a simple portal frame problem 200

List of tables

5.1	Geometric properties of stud column ε-sections	80
5.2	Nominal steel mechanical properties	80
6.1	Mechanical properties to the steel in the ε-section of 1.5 mm thick	97
6.2	Moduli of steel determined at different stress levels	98
6.3	Summary of inelastic critical buckling stresses from experiments and theory	106
7.1	Fifty-four concentric full length ε-column test results	118
7.2	Column failure loads and overall effective load eccentricities	127
7.3	ε-column strength test and theoretical results	131
7.4	Column resistances based on the series of ε-column tests	134
7.5	Perry coefficient based on the series of ε-column tests	135
11.1	Comparison of elastic critical buckling loads for simple portal frame examples with shear-rigid members	192

Acknowledgements

Praises and thanks belong only to Allah S.W.T for giving me the opportunity to work with wonderful academic members, colleagues and friends who made this thesis possible. I greatly appreciate their assistance and support.

I would like to thank the members of my PhD panel who monitored my work and took effort in providing me with valuable comments; I would like also to thank Colin Banks and my colleague at postgraduate hall.

Specially, I would like to thank my advisor Toby Mottram for his great efforts and advice.

For financial support, I thank Modular 2000 Ltd for the studentship and Gordon memorial trust for contribution toward my academic fees.

Finally I am indebted to my wife, parents and the entire extended family for their understanding, endless patience and encouragement.

Alhamulillah

Declaration

Hereby I declare that, the research within this thesis has been conducted by the author such material as has been obtained from other sources has been acknowledged. The material contained within this thesis has not previously been submitted for any degree or academic qualification to any other university or institution.

Publications

Abbaker, A. and Mottram, J. T., (2004), 'The influence of shear-flexibility on the elastic critical elastic load for frames of pultruded fibre reinforced plastic section,' in *Proceedings 2nd International Conference on Advanced Polymer Composites for Structural Applications in Construction* (ACIC04), Woodhead Publishing Ltd., Cambridge, 437-444.

A. Abbaker, and J. T. MOTTRAM (2004), *'Stud column tests for the Modula 2000 advanced building system,'* Progress Report No.1 to Modula 2000 for period 1st October 2003 to 1st February 2004, University of Warwick, p. 38.

A. Abbaker, and J. T. MOTTRAM (2004), *'Stud column tests for the Modula 2000 advanced building system,'* Progress Report No.2 to Modula 2000 for period 1st February 2004 to 13th April 2004, University of Warwick, p. 6.

A. Abbaker, and J. T. MOTTRAM (2005), *'Fifty-four 2.7 m high stud column tests for the Modula 2000 advanced building system,'* Progress Report No.3 to Modula 2000 for period 1st October 2004 to 1th May 2005, University of Warwick, p. 52.

Abstract

Presented in this thesis are the results from two distinct investigations on the behaviour of lightweight framing systems for buildings. One investigation concerns the characterisation of cold-formed steel sections of novel shape for the design of columns in modular construction, and this is reported in the first part of thesis. The second new investigation is for a theoretical analysis to determine the elastic critical buckling load for shear-flexible frames of fibre reinforced polymer sections. This work is detailed in the second part to the thesis.

Modular 2000 Ltd. fabricated the column specimens that were characterized for the research on lightweight steel modular construction. To determine the resistance of nine different column types a series of nominal concentric strength tests were conducted on specimens of 2.7 m length having a new ε-section shape. The novelty to the shape is that it has no flat elements and is continuously curved in plan. Open ε-sections are of S350 structural grade steel, are nominally 100x43 mm in plan, and have wall thicknesses of either 1.5 or 2 mm. Various bracket and enclosure combinations were the variables in the nine column types tested. These were connected to the ε-sections by MIG plug-welding. Except for the 100x40x1.5 mm C-enclosure of S350, the other attachment components were of steel grade CR4, at 1.5 mm thickness. There were five column types with ε-sections of 2.0 mm thickness and four with 1.5 mm thickness. Reported are the salient results from 54 strength tests, where the mode of failure was global buckling about the minor-axis of the ε-column. To also determine the local buckling strength, and the effective area, a small series of stud column tests were performed on 200 mm long specimens of the 1.5 mm open ε-section only.

To support the understanding gained from the series of full-sized physical tests on ε-columns, a programme of theoretical work is presented which is used to determine the design strengths of the column types and to predict the elastic and inelastic critical loads of a curved panel. Theory is also used to find a plasticity reduction factor for the ε-section, which is required to establish the effective area for local buckling.

BS 5950-5: 1998 gives a code of practice for the design of cold-formed thin-gauge sections. This current guidance is specific to steel sections comprising simple shaped members that are of flat elements bounded either by free edges or by bends. The new results from the combined theoretical and experimental studies to characterise ε-columns are evaluated and used to make recommendations on how BS 5950-5: 1998, and, in particular, Section 6 for members in compression, can be used with ε-sections to design modular units.

In the second part of the thesis the author shows how a static analysis for plane frames of shear-flexible members, written by a previous Warwick University PhD student, can be modified to calculate the elastic critical buckling load for overall instability. The modified sframe programme provides

a practical analysis tool that, importantly, includes non-linearity by way of second-order P-Δ effects with shear-flexible functions and semi-rigid joint action. In conventional frame analysis shear-flexibility is ignored when members are of isotropic material (steel), and by way of a preliminary parametric study the author shows why the influence of shear deformation on reducing the buckling load of shear-flexible frames should not be neglected when the material is of fibre reinforced polymer. By studying the change in critical load in simple frame problems it is found that there is an interaction between shear-flexibility and the torsional stiffness given to the beam-to-column joints. Moreover, the study on the instability of shear-flexible frames provides evidence to suggest that the relative stiffness values for joint classification boundaries are likely to be lower than those for steel frames by Eurocode 3 (BS EN 1993-1: 2005). This is an important finding for when a structural Eurocode or other code of practice is drafted for lightweight framed structures of fibre-reinforced polymer materials.

Although the work presented in this thesis is from two distinct investigations the deliverables are important to the sustainable development of lightweight framing systems for buildings.

Notations

A cross-section area

b plate width

b_{eff} plate effective width

b_i plasticity coefficients for middle surface strain terms

C section centroid

$\bar{c}$ shear-flexible carry-over function

c_i plasticity coefficients for curvature terms

C_w warping constant of a section

e_i strain intensity

e_u percentage elongation

E elastic modulus

$\bar{E}$ reduced modulus

E_s secant modulus

E_t tangent modulus

E_{nom} nominal elastic modulus

$\mathbf{F}$ internal forces

G shear modulus

H applied horizontal load

I second moment of area about minor axis of the cross section

I_o polar moment of area about the shear centre

I_x second moment of area about x-axis

I_z second moment of area about z-axis

J St Venant torsion constant of a section

k effective length factor

K buckling coefficient

$\mathbf{K}$ overall stiffness matrix

$K_{\min}$ minimum buckling coefficient

$[\bar{k}]^{(e)}$ element stiffness matrix

l element length

L column length

L_E column effective length

m number of half-waves in z-direction

M bending moment

M_x edge bending moment x-direction

M_y edge bending moment y-direction

M_{xy} edge twisting moment

$\overline{M}^e$ member end moment

N_x edge force in x-direction

N_y edge force in y-direction

N_{xy} edge shear force

p_E mean axial stress at Euler load

p_y mean axial stress at first yield

P compressive centrally applied load

P_E Euler critical load

P_T torsional buckling load

P_y load at first yield

P_{cs} short column capacity

P_{Ex} Euler critical load about x-axis

P_{Ey} Euler critical load about y-axis

P_{TF} torsional flexural buckling load

r radius of gyration

$\bar{s}$ shear-flexible stiffness function

S shear centre

S_j rotational stiffness

S_x equivalent stress in x-direction

S_z equivalent stress in z-direction

t plate thickness

u displacement along x-axis

$\bar{u}^e$ member end axial displacement

U_b bending strain energy

U_m membrane strain energy

U_s ultimate tensile strength

$\bar{U}^e$ member end axial force

v displacement along y-axis

$\bar{v}^e$ member end sways

V work done by applied force

$\bar{V}$ shear force

$\bar{V}^e$ member end shear force

w displacement along z-axis

$y_{o,}$ y-coordinates of the shear centre

$\bar{y}_0$ neutral surface coordinate

z_o z-coordinates of the shear centre

Y_s material yield stress

α effective length multiplier for torsional flexural buckling

β shear correction factor

$\{\bar{\delta}\}^{(e)}$ vector for the element's nodal displacements

Δ lateral drift of the frame

γ_{xy} shear strain

ϕ rotation of the cross-section

φ plate aspect ratio

ϕ_i shear stiff phi functions

$\bar{\phi}_i$ shear-flexible phi functions

ε_x strain in x-direction

ε_z strain in z-direction

ε_1 middle surface strain in z-direction

ε_2 middle surface circumferential direction

ε_3 middle surface shear strain

η Perry coefficient factor

$\bar{\eta}$ plasticity reduction factor

λ critical load factor

ν $\dfrac{l^2}{12EI}$

$\bar{\theta}$ member end rotation

ρ non-dimensional Euler critical load

μ shear-flexible parameter

Π total potential energy

σ_e stress at the edge

σ_i stress intensity

σ_x normal stress in x-direction

σ_z normal stress in z-direction

σ_{cr} critical stress

σ_{max} compressive stress on the effective element

$\sigma_{0.2}$ 0.2% proof stress

τ_{xy} shear stress

χ_1 change of curvature in z-direction

χ_2 change of curvature in x-direction

χ_3 twist

ψ $\dfrac{\beta}{GA}$

ζ $1-\mu\rho$

Chapter 1 Introduction

This thesis presents the results from two distinct investigations on the behaviour of lightweight framing systems for buildings. The first of the investigations concerns the characterisation of a cold-formed steel section of novel shape for the design of columns in modern methods of construction, and this is reported in Chapter 2 to 8 of thesis. The second investigation is for a theoretical analysis to determine the elastic critical buckling load for shear-flexible frames of fibre-reinforced polymer sections. This work is detailed in Chapter 9 to 12 in the thesis. The author will now present an introduction to the two distinct investigations in order of their reporting

1.1 Modern methods of construction

For a number of political, social and economic reasons there is much interest within the construction sector to find efficient ways to deliver quickly, and at low cost, well-designed buildings. For housing, schools, hotels and student accommodation there is a potential to find energy-efficient solutions using Modern Methods of Construction (MMC). MMC is a term used to embrace a range of technologies and processes involving various forms of supply-chain specifications. Often the production process is carried out off-site, in a specially designed factory. And as the Energy saving trust's publication CE139 (2005) shows, the MMC product library will include: panel building systems, modular building systems, hybrid construction and other sub-assembles or components. The panel system comprises walls, floors and roofs in the form of flat pre-engineered panels that are transported to the site and assembled to the desirable structural form. The modular system is in the

form of ready-made rooms that can be fitted together to make, for example, a whole house. Between 80 to 95% of such modular buildings can be executed in the factory and then delivered to the site for final assembly. Hybrid systems combine panellised and modular methods of construction. Finally, the sub-assembled method, although predominantly traditional, utilises factory fabricated sub-assemblies or components.

In Chapter 2 to 8 the author will present research on the behaviour of columns, with a novel sectional shape, to the development of lightweight steel framing for panel and modular building systems. Such solutions provide a number of advantages over the more familiar traditional construction methods, in terms of environmental, economic, constructional and health and safety impacts. In the preface to a 1964 book, published for the Architect and Building News, it states that: "system building is bringing the construction industry into the machine age and will enable all of us to live in clean and healthy surroundings, pleasing to our aesthetic feeling, at a cost which will be within everybody's pocket". Eatherley and Perera (2003) list the following seven factors for these advantages:

- Prefabrication can result in significant environmental benefits by reducing waste and minimising pollution by carrying out the work under controlled conditions.
- The use of light gauge steel panels tends to minimise transportation costs (both financial and environmental) and difficulties of site access.

- Fully fitted three-dimensional construction reduces the on-site construction time, and secures the quality of relatively high-value components.
- High levels of insulation result in low energy consumption.
- Low weight of construction results in economics in foundation and load-transfer structures.
- The structure can be dismantled and a high proportion reused at the end of its life; making this approach more sustainable.

Statistics from the United Kingdom government in 2003 indicate that there will be a need over the next 20 years for 3.8 million additional households in England (Eatherley and Perera 2003). The construction industry has a vital role to play in meeting this expected demand, and doing so in a sustainable manner. The Parliamentary Office of Science and Technology declared, in Postnote (2003), that a majority of new UK homes are still being constructed of traditional 'brick block' masonry. Within the last few years we have witnessed an increased exploitation of MMC in housing. Many UK companies, in this business sector, are now choosing to go the modular construction route, because of the greater control they can exert over quality, speed and reliability, which are all seen as financially related benefits. A range of factors, including the demand for faster construction and a lack of skills shortages, is driving this change.

USA and Japan are amongst the leading countries that now widely used MMC. The Steel Construction Institute has reported (SCI P272 1999) that the

Japanese house building market is dominated by modular construction, with over 150k new units per annum. A typical spacious Japanese house of modular construction is shown Figure 1.1. Good examples of the move from conventional to modular construction are also found with hotels and fast-food restaurants. Shown in Figure 1.2 is one such example for which the on-site construction time may well have been reduced by 60% from that required by a traditional approach.

Chapters 2 to 8 report the research that shall be used to prepare guidance for the design of ε-section stud columns in modular construction. Chapter 2 provides a brief introduction to modular construction systems and their application. Chapter 3 presents a review of the relevant literature on previous research to understand the behaviour of cold-formed thin-walled columns. Chapter 4 describes the theoretical approach, based on an energy method, that the author used to obtain predictions to the inelastic critical load, and the development of a new plasticity reduction factor for a curved section that represents the ε-section. A description of the research methodology used to conduct the full-sized series of physical column tests is given in Chapter 5. By an investigation presented in Chapter 6 on stub columns (i.e. of 200 mm length), the effective area for the 1.5 mm thick ε-section is obtained. Results from a comprehensive series of 2.7 m long column tests under nominal concentric load are presented and evaluated in Chapter 7. Findings and conclusions from this work, and future recommendations and some final remarks on the ε-section are given in Chapter 8.

1.2 Shear flexible frame analysis

Figure 1.3 shows a typical steel frame arrangement that consists of a series of steel components for columns, beams, and other members that are connected together by standard joint details, which are essential to the stability of the building as a whole. Its structure serves to carry and transmit dead and live loads safely to the foundation, and to perform satisfactorily over the design working life, that is > 25 years. Traditionally, components are manufactured from steel, reinforced concrete or timber. Engineers have been in search of alternative structural materials that can be shown to be cost effective and corrosive resistant. Advanced FRPs are a class of composite material with proven efficiency and economy for new build applications. It is noted that the mechanical properties of FRPs make them ideal for widespread exploitation in the construction sector. Glass and carbon fibres are up to six times stronger than structural grades of steel, one-fifth the weight, and are non-corrosive and non-magnetic (Anon 1989, Anon 1995, Anon 1999). Their high strength and light-weight, and the fact that FRPs are now readily available in the form similar to traditional standard steel sections, make them an attractive alternative and economical solution where these properties are required.

The combinations of components, and their arrangement, determine the mechanisms by which the loading is transmitted and cause the frame to deform. In framed structures, it is significant that, irrespective of the behaviour of the individual members, the overall structure acts as an integral unit, where the stiffer and stronger members and joints assist the more

flexible and weaker ones. The overall response of the structure to the loading is therefore determined by an interaction between all its components. Ultimate failure of the frame will occur when the applied load condition generates an internal stress field that exceeds the structure's resistance. If the component material is steel then design practice can rely on the ultimate failure mode to be the result of loss of stability by plastic hinge formation. If, however, the components have linear elastic properties to material rupture then ultimate frame failure can be by general elastic instability. This will be the situation if the member sections are of Fibre Reinforced Polymer (FRP) material. Such sections, mimicking the traditional steel I- and H-shapes, are produced by the pultrusion process and are available off-the-shelf, from pultruders such as Strongwell, Fiberline Composites A/S and Creative Pultrusion Inc. A second effect, which this change in material has on frame behaviour, is to make it necessary to include the effect of shear deformation, which for the same member geometry is dependent on the moduli ratio E/G. Such shear deformation is neglected in the analysis of metal frames because its presence has little influence on how the frame deforms and its eventual mode of failure. This is not the situation when the material is of FRP as E/G is much higher than 2.6, and with carbon fibre reinforcement can be as high as 80. The higher this ratio is, the more does shear flexibility influence both member and frame response to the loading.

In Chapter 9 to 12 the author present a plane frame analysis that can be used to predict static response (Zheng 1998) and elastic critical loads of frames of FRP sections. It is the latter analysis capability that is the author's

new contribution. To cope with members of FRP material the generalised column-beam element is shear-flexible. The analysis accounts for second-order P-Δ effects by the inclusion of shear-flexible stability functions, and semi-rigid action by the inclusion of the non-linear moment-rotation characteristics of the joints. These options will allow plane frames to be analysed for their joint actions, deformations and their elastic critical buckling loads.

For the purposes of analysis and design of steel frames they have traditionally been regarded as belonging to one of the two categories of pin-jointed (simple construction) or rigid-jointed (continuous construction). In order to provide guidance on the most appropriate type of analysis to use Eurocode 3 (ECS, 1993) has introduced the frame classification, as described by Galambos (1998).

Frames may be classified as braced (simple or moment resisting) if their side sway resistance is stiffened by a bracing system, while the unbraced frame (moment resisting) system resists the lateral forces by means of rigid or semi-rigid beam-to-column connections. A frame may be classified as non-sway, whether or not it is braced, if its side sway is such that the secondary moments due to non-verticality of columns can be neglected. According to Eurocode 3 (ECS, 1993) any other frame shall be treated as a sway frame and the effects of the horizontal displacements of its nodes taken into account in its design.

The author's work, has been to further the sframe code (Zheng 1998) so that, when the analysis is run, it will determine the elastic critical load for shear-flexible frames of fibre reinforced polymer sections. In Chapter 9, a brief introduction to fibre reinforced polymer materials and their application is given. Chapter 10 describes the theoretical approach used to obtaining elastic critical load of frame with semi-rigid joints, using nonlinearities due to P-Delta effect, and shear flexible stability functions. Verification of the sframe analysis is made in Chapter 11 by a preliminary parametric study. Conclusions on this new contribution to shear flexible fame analysis, and some remarks and recommendations for further work are given in Chapter 12.

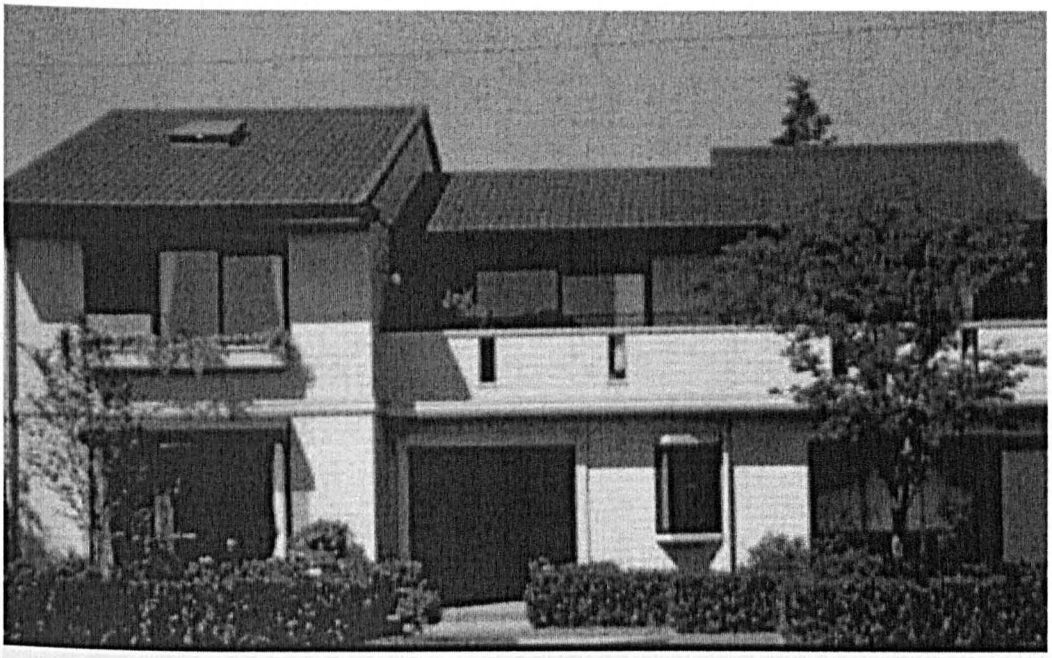

Figure 1.1. Modular construction for a large family house in Japan (from SCI publication P272).

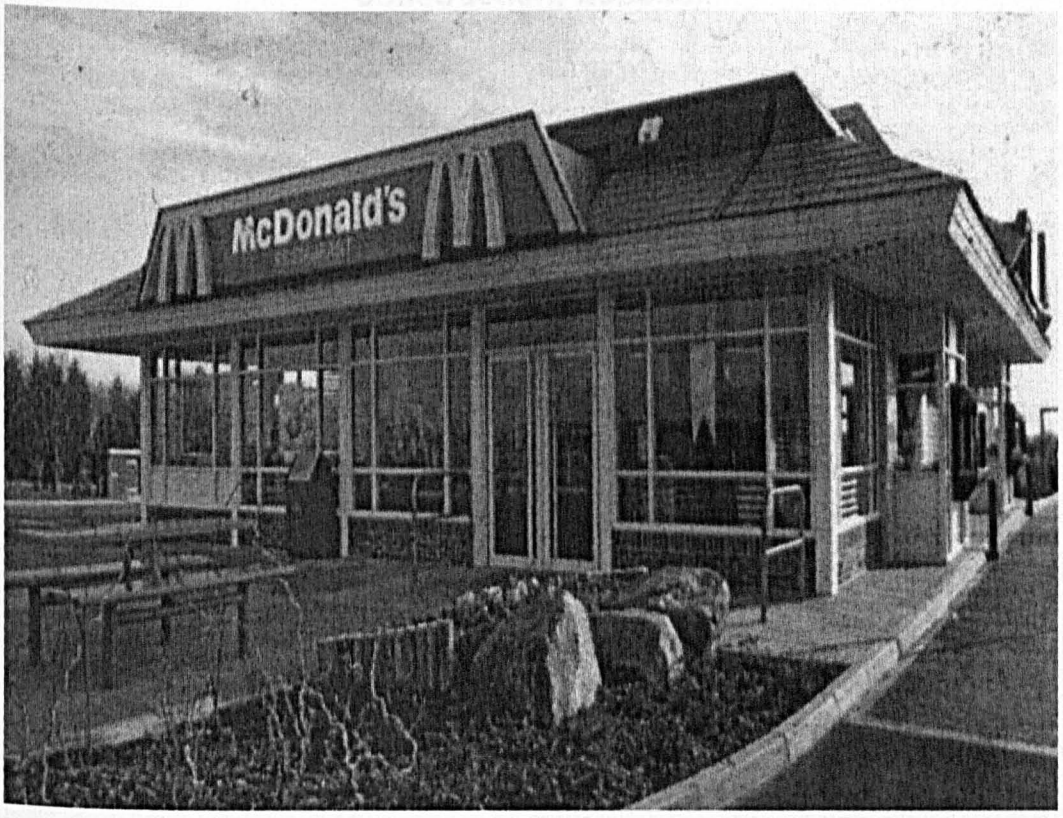

Figure 1.2. Modular construction for a fast food restaurant (from SCI publication P272).

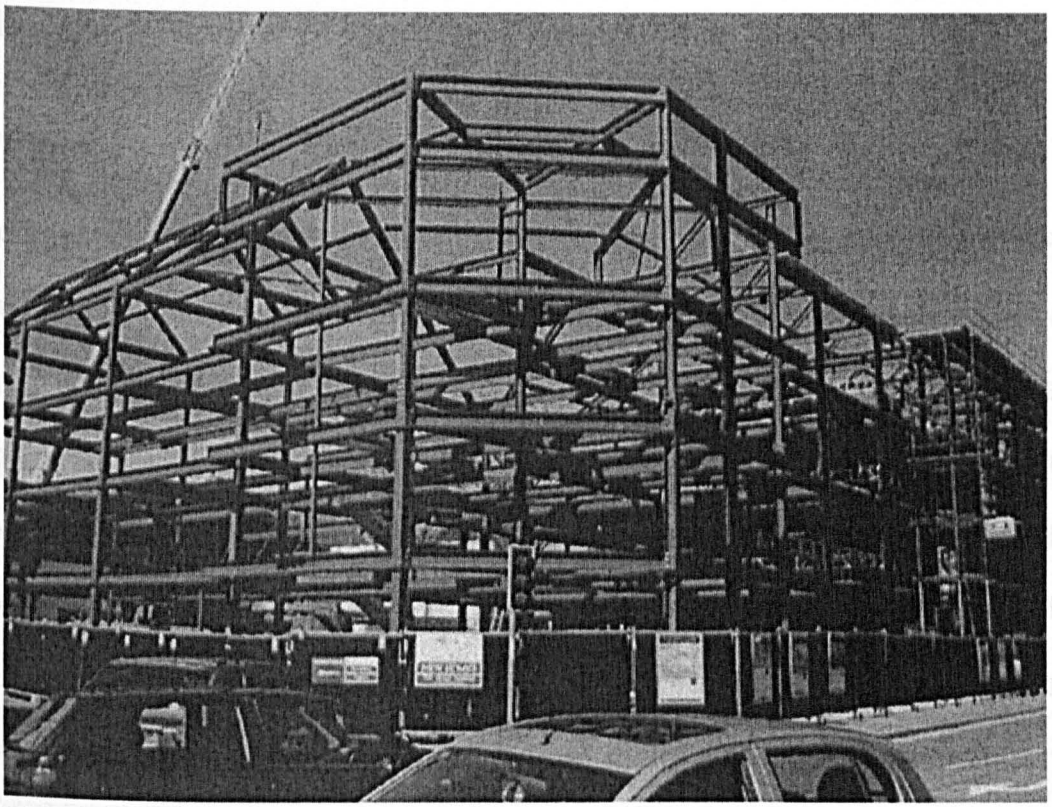

Figure 1.3. Example of a framed structure using steelwork (from RM Construction, website).

Chapter 2 Review of Modular Construction

2.1 Introduction

Modular construction is a term used for the factory production of pre-engineered building units, which are then delivered to site and assembled as large volumetric components or substantial elements to building structures. The modular units may form complete rooms, parts of rooms, or separate serviced units, such as toilets or lifts. There are two main types of modular construction, as shown in Figure 2.1, for mobile offices and modular buildings. With both types of buildings, construction takes place in a factory-controlled environment using the same materials utilized for traditional construction. Unlike traditional building approaches the modular alternative can provide us with design constraints. Since the building will be transported by road, there are, for example, some dimensions constraints (SCI News 2005). Each module typically ranges in size from 2 m to 3.6 m wide and from 5.4 m to 9 m long. Modules for residential buildings have a recommended internal wall height of 2.4 m and for educational buildings and offices the preferred internal wall height increases to 2.7 m.

Similar to traditionally made buildings, modular buildings can be occupied for many different purposes. They can range from portable classrooms to research lab facilities to a medical clinic. There are a variety of finishes you can choose for your modular building exterior. They include wood, steel, brick, aggregate and aluminium. You can also customize your exterior with windows, multiple doors, and various roof treatments. Numerous options exist for finishing the interior as well.

The motivation for using modular construction lies in the business-related benefits that make this form of construction more attractive to the client than alternative forms of conventional site-built construction. Frustrations with contractors, bad weather, scheduling delays, supplier problems, work stoppages. These are just some of the reasons why clients will turn to the modular construction solution. Modular construction offers numerous advantages over what has typically been defined as "conventional" or site-built construction methods. According to SCI P272 (1999) the client's preference for choosing a MMC is most strongly influenced by:

- Speed of construction on-site, since rapid construction leads to business-related benefits to the client, due to early completion and early return on capital investment.
- Avoidance of disruption and loss of operation of adjacent buildings, such as hotels, hospitals and nursing homes.
- Buildings or components with a high degree of services; these require careful site installation, and pre-compliance trials, which are better carried out off site and off the critical construction path.
- A large number of regular or repetitive units; factory production can facilitate transportation and can achieve economy of scale in production.
- A short 'weather window', or other site constraints to the construction operation.
- Lack of suitable skills at site; this might be the case at a remote site.

- Client requirements for an exceptionally high degree of quality control; this can best be achieved by off-site manufacture and pre-installation checks.
- A requirement for a single-point procurement route; this can be achieved through a design, manufacture and build service, which the modular industry provides.
- Construction operations can be controlled more precisely when modular units are used, and this is good for security or other related issues on site.

2.1.1 Modular elements

Each module consists of lightweight steel elements for columns, floor joists, wall studs and edge beams. The collection of discrete modular units usually forms a self-supporting structure in its own right or for tall buildings, may rely on an independent structural framework (SCI P272 1999). In order to maximise structural efficiency, load paths are made as direct as possible by avoiding transfer structures and by ensuring that wall studs and floor joists are aligned at every junction. The principal vertical loads are carried to the ground by cross walls.

2.2 Thin-walled cold-formed sections

Wang *et al.* (2001) observe that, because of a number of favourable factors, cold-formed thin-walled steel sections (width-to-thickness ratios greater than 20) are used extensively in the execution of buildings, automobiles, aircrafts, and ships. Included in these factors is: a high strength-to-weight ratio, an

ease of mass production, a simple maintenance regime, a good aesthetic appearance, and a high corrosion resistance (Hancock *et al.* 2001). To meet the various end-user requirements, cold-rolled sheet products are designed to provide specific attributes such as high formability and strength. Cold-formed thin-walled open-sections may be considered as one of the most appropriate technological solutions adopted for economical use of the high-strength raw materials. This is because they promote a minimum use of natural resources to form structural systems that can sustain the design loads. Sections are currently used in the construction sector for primary structural members in the modular construction systems for residential and commercial building structures.

Cold-formed steel products have been classified by AISI (2005) into the three categories of members, panels and prefabricated assemblies. Typical structural members, for studs, joists and "bracing" angles are shown in Figure 2.2. Panel and deck units, not only constitute the useful "surfaces" for floors, roofs and walls, but are used to resist the in-plane and out-plane loads. The third category of prefabricated assemblies is for roof trusses, panelised walls and floors.

2.3 Manufacturing of cold-rolled sections

Cold-rolled thin-walled elements are generally made from steel sheet, strip, or bars in roll-forming machines or by press brake operations. A rolling machine for lightweight steel sections is shown in Figure 2.3. The first step in the manufacture of cold-rolled sheet products involves cold reducing the coils

of hot-rolled product to the required gauge thickness in the range from 0.14 mm to 3.2 mm. This cold-reduction operation induces very high strains (work hardening) into the sheet that not only makes the sheet thinner, but also makes the steel much harder, less ductile, and more difficult to form. However, the work-hardened sheet can be made very soft and formable by annealing, which occurs by heating the material to high temperatures up to 850 °C (Meyzaud and Parniere 1977). In fact, the combination of cold reduction and annealing leads to a refinement in the steel itself that provides very desirable and unique forming properties for subsequent use by the fabricator of the cold-rolled sections.

2.4 Novel ε-section

Straight-sided thin-walled sections, such as the range shown in Figure 2.2, are currently dominant in the market place for lightweight steel framing. Among the manufacturers of thin-walled sections are Corus International Ltd, Ispat International Ltd and Phoenix Metal Product Ltd. BS 5950-5:1998 provides a code of practice for the design of building structures from cold-formed sections having straight sides. A possible disadvantage of using these conventional profiles is that not all of their cross-sectional area is effective after local buckling occurs (Rhodes and Harvey (1976), Seah *et. al.* (1993), and Khong (1994)). That is their effective area, as defined in Clause 4.7 in BS 5950-5:1998, can be less than the area of the cross-section. Another disadvantage is that tolerances can make sections, such as lipped C-sections, lose their geometric symmetry. These factors, for example, will reduce the design capacity of columns to concentric loading. Despite their

disadvantages straight-sided sections are successfully used as they can be readily joined together in a variety of ways to form frames and many of the existing modular systems use them. Prominent in the marketplace are system from Framing Solutions Plc., Yorkon Limited, and Portakabin Limited.

The trend to optimize member geometry by embracing modern manufacturing technology can be a way of introducing high performance cross-sectional shapes into the construction industry. This approach has led to a new section shape with continuous curvature in the plane of the cross-section. In this thesis this cross-sectional form is referred to as the ε-section. Figure 2.4 shows the novel ε-section for stud columns, as invented by Mr John Window of Modula 2000 Ltd. (Patent No. WO2004051024). The purpose of this new section, of nominal size 100x43 mm^2 in plane, is to increase member strength compared to the straight-sided equivalents, without adding to overall weight. In fact the ε-section can, if so desired, be used to replace straight-sided thin-walled sections in any modular construction system. Modula 2000 Ltd fabricated a prototype modular unit using the ε-section is shown in Figure 2.5. The method of connection between the components is by plug welds using MIG brazing method.

Walls are manufactured in single storey heights. Each are fabricated of 100 mm deep ε-section studs that are at the standard 600 mm spacing. The ends of the studs are set into unlipped tracks and the components are MIG welded together in the factory. Steel thickness of the ε-section is either 1.5 mm or 2 mm, depending on the number of storeys to the building. The light gauge

steel sections are inevitably classed as slender and so stability is an important consideration in their structural design, and so this aspect is the theme of the first of the distinct investigations reported in this thesis.

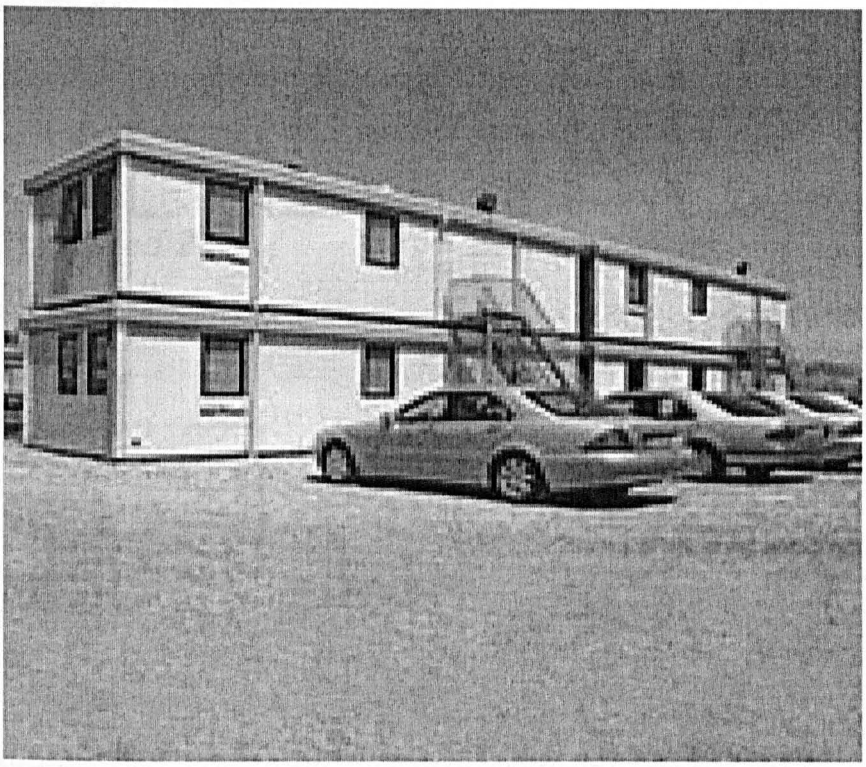

(a)

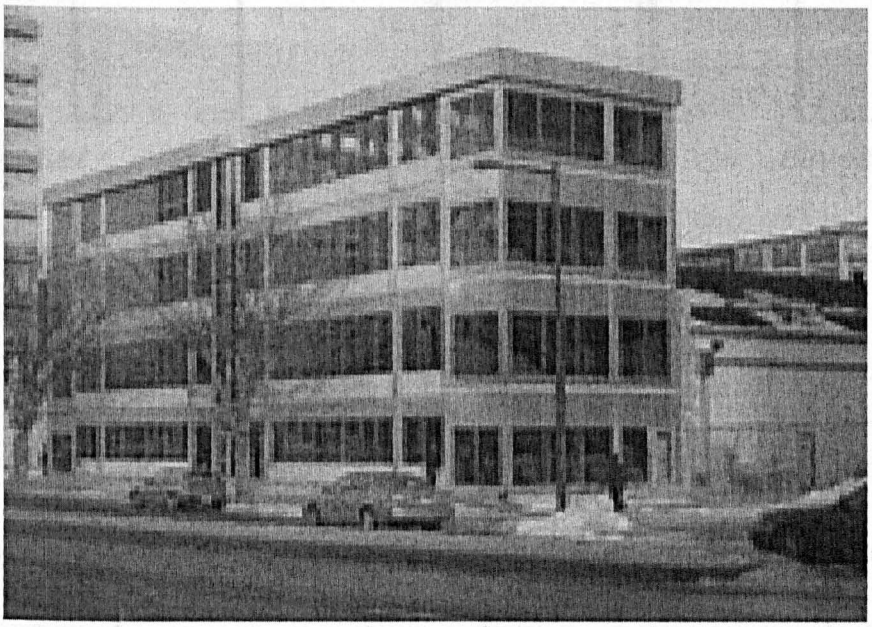

(b)

Figure 2.1. Main types of modular construction, (a) Mobile offices (from Portakabin website), (b) Building system (Charter School, from NRB website).

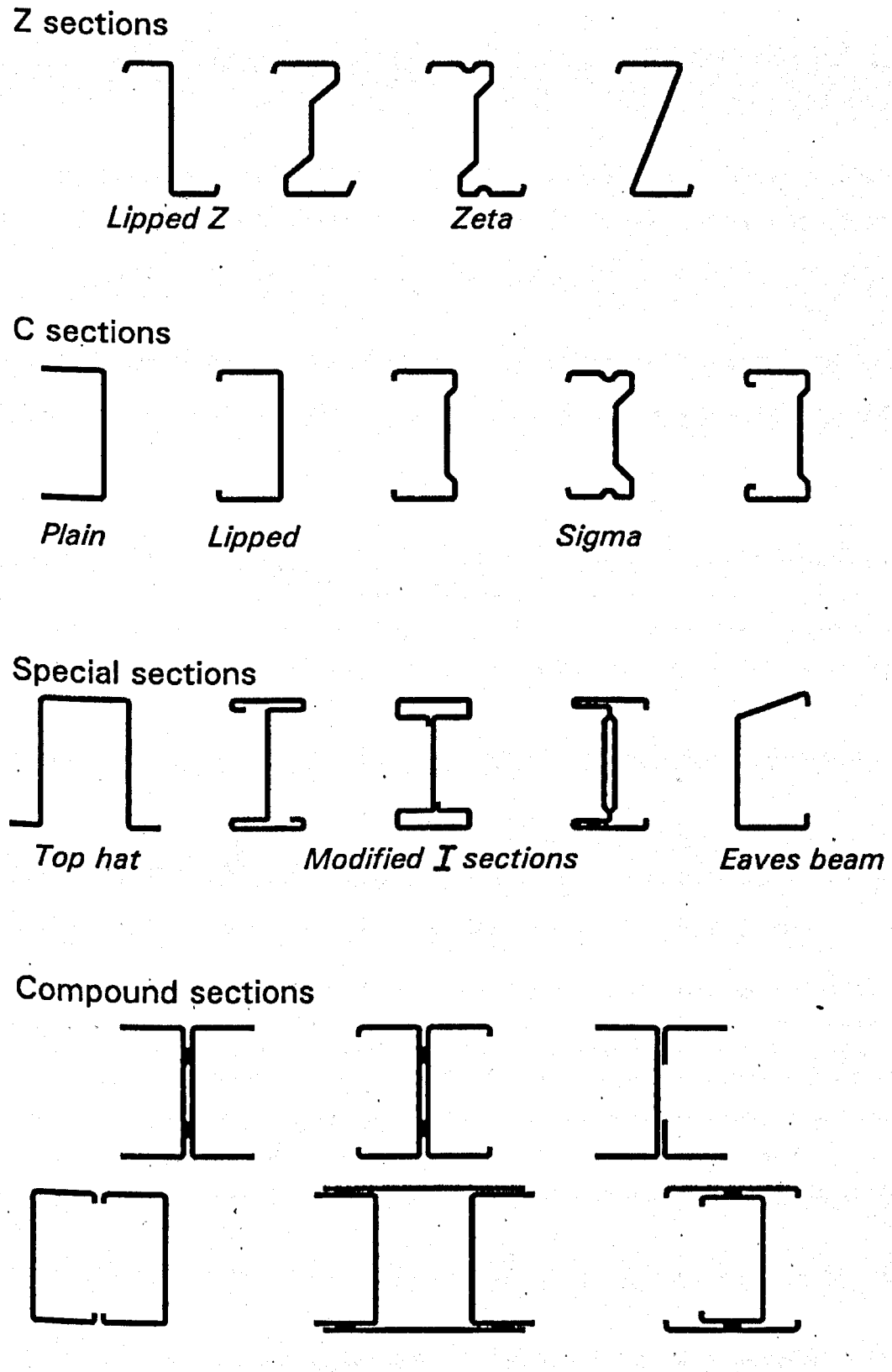

Figure 2.2. Examples of cold formed steel sections (from SCI publication P276).

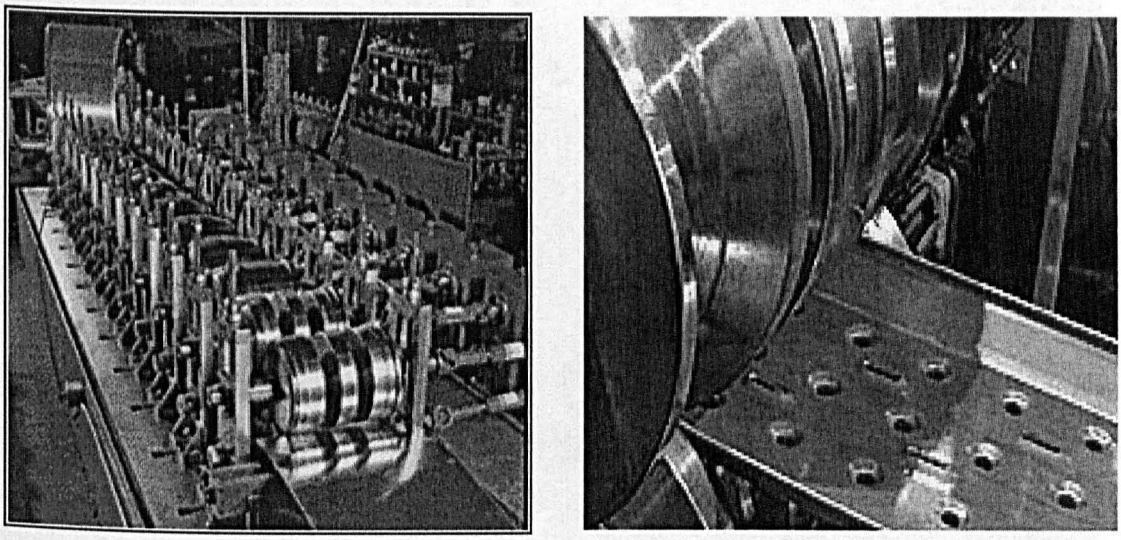

Figure 2.3. Cold rolling process for thin walled steel sections.

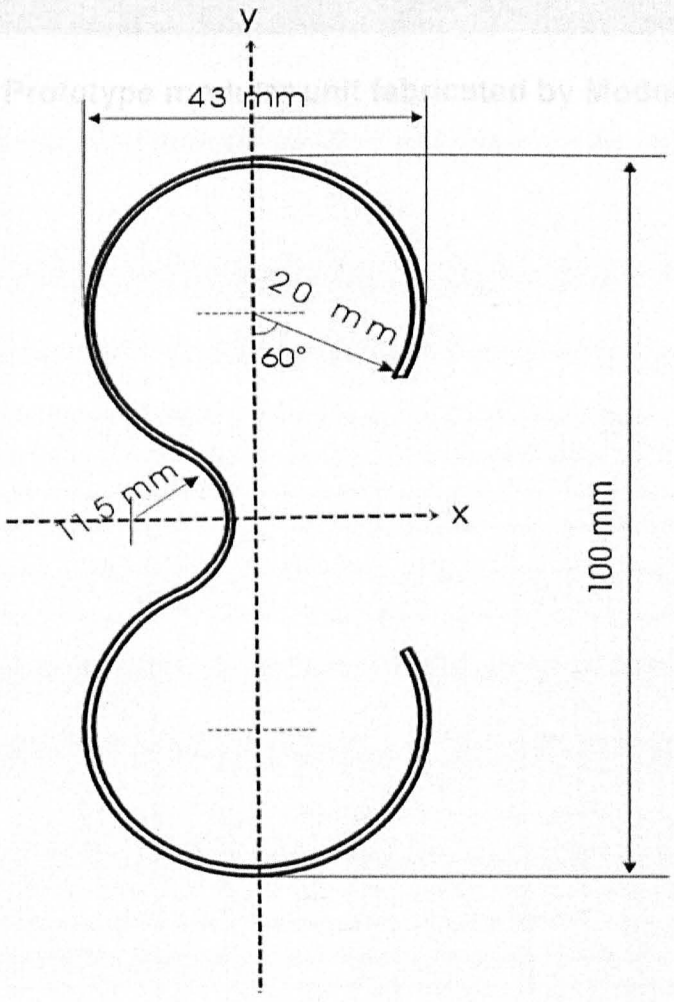

Figure 2.4. Cross-section of ε-section with 1.5 mm wall thickness.

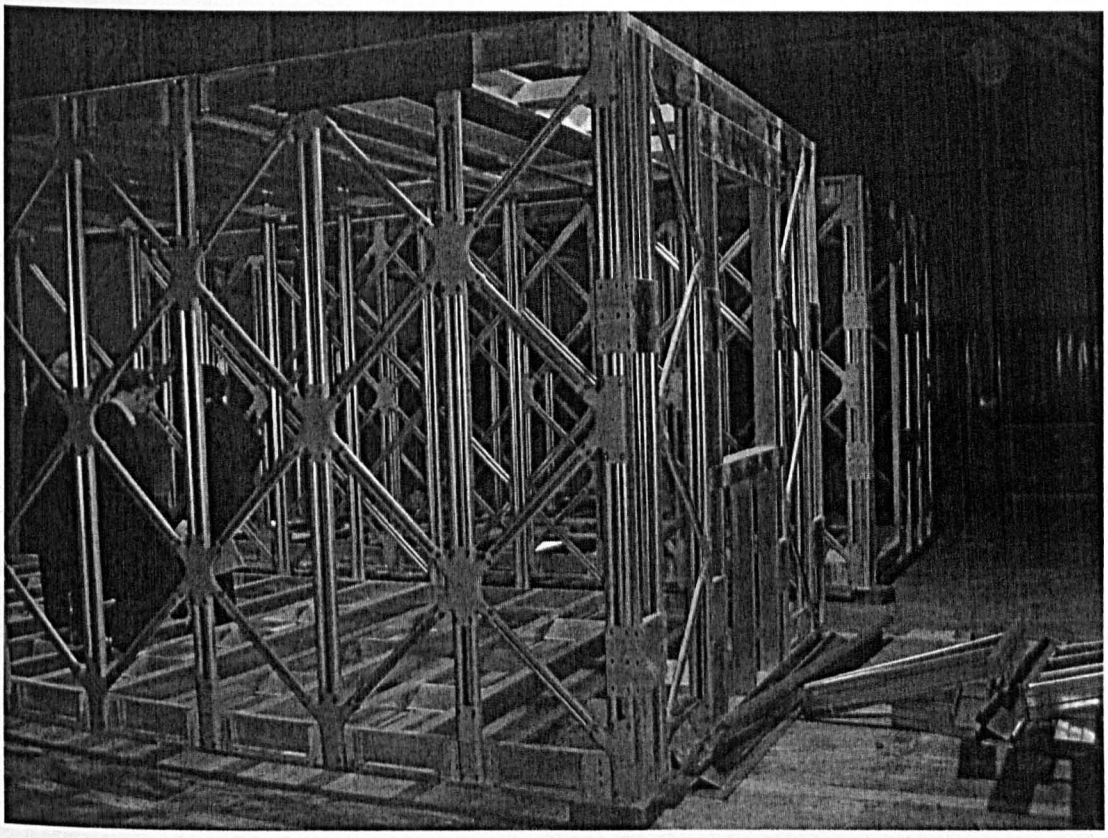

Figure 2.5. Prototype modular unit fabricated by Modula 2000 Ltd.

Chapter 3 Strength of Cold-form Thin-walled Columns

3.1 Introduction

Cold-formed steel members are produced by press-braking or bending flat sheet of hot- or cold-rolled steel strips at ambient temperature, to form any desirable shape of structural element, which fulfils their intended application requirements. By way of considerable developments in manufacturing technology, we now have more complex shapes of cold-formed thin-walled members that can be utilized in the construction industry. The most commonly available thin-walled members for building applications as shown in Figure 2.2, are of open non-symmetrical section, such as C-section, Z-section and slightly different forms like top-hat or modified I-sections. These steel sections acquired the thin-walled classification because their thickness is much less than the other dimensions. Cold-formed steel sections have gained popularity due to the advantages they give over their hot-rolled section counterparts. As Lawson *et al.* (2002) states the advantages of cold forming are sections that are light, easy to shape and resist corrosion.

Lightness and ease to shape are two of the reasons that initiated the new building approach known as Modern Methods of Construction (MMC). Structural units are now prefabricated in a factory as modules, delivered and assembled on site, to form part or even complete structure, for residential and commercial buildings. In such buildings thin-walled members have been utilized as primary elements in a form of stud columns, roof trusses and floor joists, to carry compression, tension and bending actions. The achievement

of optimum shape, reduced weight and aesthetic appearance has led to increasingly more complicated and slender shapes being produced and when used as compression members they are more likely to fail by stability rather than by steel yielding. It is well known that thin-walled members under compression will tend to fail due to one of three competing buckling modes local, global (flexural or flexural–torsional) and distortional or their interaction (Hancock *et al.* 1994, Cheng and Schafer 2003, Teter and Kolakowski 2004). To be able to design against these stability modes of failure or their potential interaction contributes to the complications in the design procedures for such members.

Many researchers have extensively studied stability problems of thin-walled members. Bleich (1952) presents a summary of the literature on buckling resistances of metal structures. Another of the seminal books on this topic is "The Theory of Elastic Stability" by Timoshenko (1961). In this book Timoshenko provides the fundamental theory to the buckling of bars, rings, curved bars, thin plates and shells. For a summary on the stability of flat plate problems one can refer to the key source by Bulson (1970). Chen and Atsuta (1976) presents the principles and methods for analysis of beam-column, which forms the basis for structural design of frames and shows how these theories, may be used in the solution of practical design problems. Trahair (1993) provides detailed summaries for the understanding of flexural-torsional buckling and for an up-to-date treatment of modern methods of analysing flexural-torsional buckling, which can be used by both designers and researchers. Recently, Wang *et al.* (2005) published an excellent

summary on the closed-form solution to the buckling of columns, beams, arches, rings, plates and shells. In spite of all these investigations, there is still a lack on literature in the area of the instability of curved plate elements that needs further research.

The most commonly used thin-walled members are of the cross-sectional shapes shown in Figure 2.2 that consist of relatively slender flat-plate elements (flanges, webs, lips). Under concentric compression action, instead of failure through material yielding their resistance is often governed by instability. These flat-sided sections have been extensively investigated and design rules are available for such structural members in the main codes of practice. These include BS 5950-5:1998 and Eurocode 3: 1993 Part 1.3. Hancock (2003) reviewed the major research developments for cold-formed steel structures. He mentions that research on the behaviour of compression members has concentrated on sections of three shapes, which are channels, angles and perforated sections. These members all comprise of elements of straight sides. The new ε-section shown in Figure 2.4 has a shape with a distinct continuous curve profile. It is the compression behaviour of this section shape that has been studied for the new research presented herein.

In practice a column carrying capacity may be influenced by many factors, such as boundary conditions, geometrical imperfections, local buckling and flexural torsional buckling (Chen 1980, Bjorhovde and Birkemoe 1979, and Young and Rasmussen 2000). When a thin-walled member buckles locally, the stiffness properties of the cross-section may changed, but the member

might still posses some post-buckling capacity, since the translation and/or rotation of the entire cross section is not involved. If the same member fails in the global buckling mode, the entire cross section of the member is displaced and this may lead to overall loss of stability. The form of the global buckling mode mainly depends on the shape of the cross-section itself. For the case of doubly symmetrical sections, the flexural buckling in the direction of minimum cross-section stiffness is dominant. While, single symmetric cross section a mixed flexural-torsional buckling is relevant. The rest of this chapter presents a review on the factors that are known to affect the column's load-carrying capacity.

3.2 Flexural buckling

Columns under concentric compression may fail by loss of stability before reaching material yielding. Commonly there are two different analysis approaches for tackling the stability problem Chen and Atsuta (1976). These are the load-deflection approach, in which the problem is approached from the standpoint of deflection and an eigen-value approach, in which an attempt is made to determine the stability load in a direct manner without calculating the member's deflection. For the eigen-value approach it is assumed that the member is an ideal one, without geometric or material imperfections, and is loaded in such an ideal manner that only the deformation taking place at loading below the critical buckling value is that of axial shortening. The initial theoretical research into elastic buckling is dedicated to Euler, who by using eigen-value approach obtained the first analytical method of prediction for the strength of slender columns. In 1744

he found the smallest critical load, for concentrically loaded column with pinned ends condition and linear elastic material behaviour, to be given by

$$P_E = \pi^2 \frac{EI}{L^2} \tag{3.1}$$

In Equation (3.1) E is the elastic modulus, I is the second moment of area of the cross-section and L is the column length. Euler mode of failure is associated with slender members. Whereas, short and compact members under compression may fail due to yielding of the material. The short column capacity is then given by $P_{cs} = A_{eff}\, p_y$, in which A_{eff} is the effective cross-sectional area and p_y is the mean axial stress. The physical model for the ideal column before failing at the Euler critical buckling load is illustrated in Figure 3.1a. In such a situation deformation due to compression is that of axial shortening. The load lateral displacement curve is coincident with load axis until it reaches the critical point, when bifurcation kicks in and the curve diverts from the load axis. This response is illustrated in Figure 3.1c. At this point, the load is known as the Euler critical buckling load and the member loses its stability. However, columns used in practice will inherently have some imperfections that include initial out-of-straightness, load eccentricity and residual stresses. Reality therefore requires the researcher to study the influence of each of these aspects on the resistance of real columns, in order to include in design procedures the reduction to strength that imperfections cause.

3.2.1 Boundary condition

Figures 3.2(a) to (c) represent the deformed configurations of a member under compression with respectively pinned, semi-rigid and rigid boundary conditions.

The elastic critical load obtained by Euler is for simply supported ends. In general column design carrying capacity is determine as a function of this critical load and the expression accounting for different boundary conditions can more generally expressed by $P_E = \pi^2 \frac{EI}{L_E^2}$. Now the effective length L_E shown in Figure 3.2b and 3.2c, is been used in Equation (3.1), rather than the actual length of the member, that is given in Figure 3.2a. The effective length defined as the distance between points of contra-flexure (i.e. the point of zero curvature), is $L_E = kL$ in which k is the effective length factors. It has value of 0.5 for the perfectly fixed ends and 1.0 for the perfectly pinned ends. For practical joints the end restraints are neither fully fixed nor fully pinned. This semi-rigid situation is shown in Figure 3.2b. Chen (1980) presents a review of column design approaches and a description of the effect of end restraint that might be included in column design. He highlights the need for research with end-restrained columns as one of parameters that has not received sufficient attention in the past. Chapuis & Galambos. (1982) determined numerically the effective length factor for crooked columns. Ding *et al.* (2003) presents a method for estimating the effective length factors for solid round steel leg members of lattice towers with cross bracing.

3.2.2 Initial imperfection

The assumption of a perfect member is unrealistic. Real columns suffer from imperfections in terms of geometry and material properties. Horne and Merchant (1965) have considered a pin-ended strut with initial lack of straightness defined by mid-height deflection x_o, as a sinusoidal deflection shape as shown in Figure 3.3a.

Figure 3.3b shows that due to the presence of x_o the load deflection curve of the column follows a new path with gradual increase in lateral deflection, x, with increasing P. Horne and Merchant (1965) shows theoretically that the influence of the applied axial load on x is to magnify, by a factor of $1/(1- P/P_E)$, deflection x_o. It is evident from the form of the magnification factor that when P approaches P_E the mid-height deflection x approach infinity. It is clear that the geometric imperfection makes the member's Euler load unobtainable. Horne and Merchant (1965) also show that for the column with initial geometric imperfection deflection x_o, the applied load is resisted by a combination of axial and flexural rigidities and given by

$$p_y = \frac{1}{2}\left\{Y_s + (1+\eta)p_E - \sqrt{\left[(Y_s + (1+\eta)p_E)^2 - 4Y_s p_E\right]}\right\} \qquad (3.2)$$

In Equation (3.2) Y_s is the yield stress, p_y is the mean axial stress at the load for first yield P_y, p_E is the mean axial stress at P_E and η is the Perry coefficient factor used to take into account the effect of initial geometric imperfection on column resistance. Equation (3.2) is the Perry-Robertson formula and is used as the basis for the design of steel columns in current BS codes. Bjorhovde and Birkemoe (1979), Little (1982) and Chernenko and Kennedy (1991) are

researchers "among others" whom have investigated column resistance when the member has out-of-straightness.

3.3 Local buckling

Flat plates under compression may be susceptible to cross-sectional instability at critical stresses, but they behave in a different manner than columns at the moment of bifurcation. Plates at bifurcation exhibit a stable equilibrium with a substantial amount of post-bucking strength (Bulson 1970). Local buckling is commonly encountered in the component plate of thin-walled members and characterised by the relatively short wavelength mode of failure BS 5950-5:1998. In 1891 Bryan presented an analysis for the elastic critical stress of a rectangular plate, simply supported along all edges, and subjected to a uniform longitudinal compressive stress. Equation (3.3), taken from Bulson (1970), is the solution for the critical buckling stress.

$$\sigma_{cr} = \frac{K_{\min}\pi^2 E}{12(1-\nu^2)}\left(\frac{t}{b}\right)^2 \tag{3.3}$$

in Equation (3.3) t is the plate thickness, b is the plate width, ν is the Poisson's ratio and $K_{\min}$ is a buckling coefficient determined by solving the characteristic equation defining the stability of a flat plate and represents the influence of the boundary conditions and the plate geometry.

The Bryan equation is for the case of a perfectly linear elastic plate, which buckles at an elastic critical stress. The onset of local buckling of a flat plate does not guarantee ultimate failure since post-buckling stability with an increase in strength is usually expected. Since the out-of-plane deformation

at buckling does not coincide with ultimate failure, a thin plate can be economically designed on the basis of its post-buckling strength. In the determination of design rules for local buckling failure, both the critical stress and the post-buckling strength are important parameters.

3.3.1 Post buckling

As supported plates do not collapse when the elastic buckling strength is reached they experience a considerable amount of post-buckling resistance due to stretching of the middle plane. The axial stress distribution is uniform over the area of the plate prior to elastic buckling occur. After buckling, the stresses at the middle part approach the critical stress σ_{cr}, the stiffness of the plate reduces away from the edges and a non-uniform stress distribution is developed. The redistribution of stress continues until the stress σ_e at the edge reaches the yield stress Y_s at onset of ultimate plate failure. The post-buckling stress distribution across the width, b, is shown in Figure 3.4.

The well-known effective-width approach is based on the stress distribution associated with that in Figure 3.4. Graves-Smith (1967) showed that ultimate failure occurs once the stress at the edge areas of the compressed width of the plate becomes equal to the material yield strength.

3.3.2 Effective area approach

Van Karman introduced the concept of the effective width given by notation b_{eff} (Bulson 1970). He proposed that the two strips in Figure 3.5b could be

considered as rectangular plates each of width $\frac{b_{eff}}{2}$ and when their stress equal Y_s, ultimate failure occurs. Many others have developed further this concept, among which is the important work of Winter and Uribe (1967) and his contribution will be discussed later. The effective-width approach assumes that, instead of the actual non-uniform stress distribution, the total load is carried by a fictitious effective width, subjected to a uniformly distributed stress equal to the maximum stress σ_e that occurs at the unloaded plate edges. This is shown in Figure 3.5.

The effective width is selected so that the area under the curve of the actual non-uniform stress distribution is equal to the sum of the two parts of the equivalent rectangular area with a total width b_{eff}. Mathematically this is given by (Figure 3.4 and 3.5)

$$\int_1^2 \sigma_z(x)dx = b_{eff}\sigma_e \tag{3.4}$$

It may also be considered that the effective width represents a particular plate that buckles when the compressive stress reaches the yield point of steel. This resulted in the van Karman formula for b_{eff}, which is developed from test data

$$\frac{b_{eff}}{b} = \sqrt{\frac{\sigma_{cr}}{Y_s}} \tag{3.5}$$

Based on his extensive investigation on cold-formed steel sections Winter (1967) indicates that Equation (3.5) is equally applicable to the plate element in which the maximum stress is below the yield point Y_s. In addition, it has been verified that Equation (3.5) is suitable for plates with different boundary

conditions. By introducing an empirical correction factor, to account for an accumulation of imperfections, this led to the modified Winter's formula of

$$\frac{b_{\text{eff}}}{b} = \sqrt{\frac{\sigma_{\text{cr}}}{\sigma_e}}\left(1 - 0.22\sqrt{\frac{\sigma_{\text{cr}}}{\sigma_e}}\right) \qquad (3.6)$$

It is this equation, or comparable ones, that present a practical description of the actual post-buckling strength of individual flat plates. Furthermore, it presents the basis for the local buckling behaviour of cross section as used in the design clause in section 4 of BS 5950-5:1998.

3.4 Inelastic buckling

The interaction between plastic behaviour and instability is important for stocky plates, or plates where the residual stresses represent a significant factor in their design. The Bryan Equation (3.3) for elastic buckling stress includes the value of the elastic modulus, E, but does not involve the limits of elastic behaviour. Consequently, the plate material may yield before the theoretical elastic critical stress predicted, by Equation (3.3), is reached in practice. In this case the plate might buckle and collapse at a lower value of stress than the theoretical prediction. This is known as inelastic or plastic buckling and shall be referred to be the former in this thesis. Considere, Engesser and van Karman, were the first three researchers to realise the possibility of replacing the elastic Young's modulus in Euler's formula with a reduced modulus for the inelastic zone of strut buckling (Bleich 1952). To predict inelastic buckling of a plate element Bleich assumed anisotropic behaviour of the plate. When the edge stress σ_e exceeded the proportional limit Y_s, the reduced modulus is assumed to be effective for strips of plate in

the z-direction (coincident with applied load direction), whereas, the elastic modulus remained valid for perpendicular strips in the x-direction. To simplify the concept it was assumed that twisting moments acting on these strips were governed by $\sqrt{\frac{\overline{E}}{E}}$. This term was then introduced into the conventional isotropic differential equation for flat plate element

$$D\left[\frac{\overline{E}}{E}\left(\frac{\partial^4 v}{\partial z^4}\right)+\sqrt{\frac{\overline{E}}{E}}\left(\frac{2\partial^4 v}{\partial^2 z\partial^2 x}\right)+\frac{\partial^4 v}{\partial x^4}\right]=-\sigma_z t\frac{\partial^2 v}{\partial z^2} \tag{3.7}$$

With $\overline{E}$ is the reduced modulus and σ_z is normal compressive stress applied to ends of the plate.

Alternatively, Ros and Eichinger (1932) assumed that the plate remains isotropic even when the stress exceeded the proportional limit, with the reduced modulus applying in all directions (Bulson 1970). This gave

$$D\frac{\overline{E}}{E}\left[\frac{\partial^4 v}{\partial z^4}+\frac{2\partial^4 v}{\partial z^2\partial x^2}+\frac{\partial^4 v}{\partial x^4}\right]=-\sigma_z t\frac{\partial^2 v}{\partial z^2} \tag{3.8}$$

Neither of these approaches was particularly satisfactory, although the former gave closer agreement with physical test results, so attempts were made to introduce the laws of plastic theory into the plate-buckling analysis (Bulson 1970). Ilyushin (1947), among others used the total strain theory to define the actual stress-strain relationships. Stowell (1948) modified the plate buckling theory by Ilyushin, using the total strain theory, which states that the relationship between direct stress and direct strain takes the form $\sigma = E_s\varepsilon$ in which E_s is the secant modulus for material which is being loaded (Bulson

1970). Stowell's governing differential equation for inelastic plate buckling has the form

$$\left(\frac{1}{4}+\frac{3E_t}{4E_s}\right)\frac{\partial^4 v}{\partial z^4}+\frac{2\partial^4 v}{\partial z^2\partial x^2}+\frac{\partial^4 v}{\partial x^4}=\frac{\sigma_x t}{D'}\frac{\partial^2 v}{\partial z^2} \tag{3.9}$$

where $D'=\frac{E_s t^3}{12(1-\nu)}$, and E_t is the tangent modulus. The solution of Equation (3.9) for a rectangular plate simply supported along all edges and subjected to a uniform longitudinal compressive stress, σ_z, gave the inelastic critical stress, $\bar{\sigma}_{cr}$ to be

$$\bar{\sigma}_{cr}=\frac{\pi^2 E_s}{9}\left(\frac{t}{b}\right)^2\left[\left(\frac{1}{4}+\frac{3E_t}{4E_s}\right)\frac{1}{\varphi^2}+\varphi^2+2\right] \tag{3.10}$$

Where $\varphi\left(=\frac{a}{b}\right)$ is the plate aspect ratio.

To simplify the prediction of the theoretical inelastic critical stress, $\bar{\sigma}_{cr}$, a plasticity reduction factor is introduced. This plasticity reduction factor ($\bar{\eta}$) is define as the ratio of minimum inelastic buckling stress to the minimum elastic buckling stress, and for the simply supported flat plate case it is given by (Bulson 1970)

$$\bar{\eta}=\frac{E_s}{E}\left(\frac{1}{2}+\frac{1}{2}\sqrt{\frac{1}{4}+\frac{3E_t}{4E_s}}\right)\frac{(1-\nu^2)}{0.75} \tag{3.11}$$

In Chapter 4 the author will establish an equivalent formula for the case when the plate is curved so that a plasticity reduction factor can be applied to ε-section to predict its inelastic critical stress and the effective area.

3.5 Flexural torsional buckling

Flexural-torsional buckling is a primary consideration in design as it might be a mode of failure that governs the compressive load-carrying capacity. In this mode of buckling a member suddenly deforms by deflecting laterally and twisting out-of-the plane of the load direction (Bradford and Pi 2005). This form of buckling may occur in a thin-walled member of open cross section, which has low lateral bending and torsional stiffness compared with its stiffness in the plane of loading, such as those sections shown in Figure 2.2.

Shown in Figure 3.6 is a general asymmetric cross-section (in which the centroid of the cross-section does not coincide with the shear centre). The element is of length L, thickness t and has compressive load P. The principal centroidal axes of the cross-section are given by y and x respectively, the coordinates of the shear centre (S) by (y_0, x_0), and its displacements by w (in z-direction), v (in y-direction), and u (in x-direction). Under the applied compressive load the column may buckle through a combination of bending and torsion. In the deformed configuration, the shear centre moves from (S) to (S`) and the centroid from ($C$) to ($C$`). The cross-section translates and rotates about the new position of the shear centre (S`). By denoting the rotation of the cross-section by ϕ then the final position of the centroid (C``) is as shown in Figure 3.6.

At the critical load the stable equilibrium of the straight column is at its limit and there exists a slightly deflected configuration of the column, which can also satisfy equilibrium condition (see Figure 3.1b). For this configuration,

under the assumption of small deflection, the differential equations of the elastic curve of the deflected and rotated column are.

$$EI_y \frac{d^2u}{dz^2} = P(u + y_0 \cdot \phi) \tag{3.12}$$

$$EI_x \frac{d^2v}{dz^2} = P(v - x_0 \cdot \phi) \tag{3.13}$$

$$GJ\frac{d\phi}{dz} - EC_w \frac{d^3\phi}{dz^3} = P \cdot y_0 \cdot \frac{du}{dz} - P \cdot x_0 \cdot \frac{dv}{dz} + \frac{p}{A} \cdot I_0 \cdot \frac{d\phi}{dz} \tag{3.14}$$

In these three equations EI_x and EI_y are the flexural rigidities about the minor and major axes respectively, GJ is the tosional rigidity, EC_w is warping rigidity, and I_0 is the polar moment of area about the shear centre (S).

The three simultaneous differential Equations (3.12) to (3.14) for buckling by flexural and torsion can be used to determine the critical loads. By using the sine wave function for the first mode shape one can obtained, for a non-trivial solution the following instability determinant equation (Timoshenko 1961).

$$\begin{vmatrix} P - P_{Ey} & 0 & Py_0 \\ 0 & P - P_{Ex} & -Px_0 \\ Py_0 & -Px_0 & \frac{I_0}{A}(P - P_T) \end{vmatrix} = 0 \tag{3.15}$$

P_{Ex} and P_{Ey} in Equation (3.15) are the Euler critical loads about the x and y axes, respectively, and P_T is the critical load for torsional buckling given by

$$P_T = \frac{A}{I_0}\left(GJ + \frac{\pi^2}{L}EC_w\right) \tag{3.16}$$

Solving Equation (3.15) for the case of asymmetric sections, with the y-axis is an axis of symmetry, we have a quadratic equation whose roots give the critical load P_{cr} to be either

$= P_{Ex}$

or

$$= P_{TF} = \frac{1}{2\left(1 - \frac{A \cdot y_0^2}{I_0}\right)}\left[P_T + P_{Ey} - \sqrt{\left(P_T + P_{Ey}\right)^2 - 4\left(1 - \frac{A \cdot y_0^2}{I_0}\right)P_T \cdot P_{Ey}}\right] \tag{3.17}$$

The smaller of the two values of the critical load is of the practical interest. When the second of expressions, for torsional flexural mode governs by giving the lowest critical load, this means we shall observe twisting of the column's cross-section during buckling.

In part 5 of BS 5950 the effect on column design of torsional flexural buckling is dealt with in Section 6. Clause 6.3.2 state that the design of members which have at least one axis of symmetry and which are subjected to torsional flexural buckling, may be in accordance with Clause 6.2 provided that a factored slenderness ratio, $\alpha\frac{L_E}{r}$, is used in place of the actual slenderness ratio. Values of the effective length multiplier for torsional flexural buckling, α, are determined as follows

For $P_E \leq P_{TF}$, the factor $\alpha = 1$

For $P_E > P_{TF}$, the factor $\alpha = \sqrt{\frac{P_E}{P_{TF}}}$,

$P_E = \pi^2 \frac{EI}{L_E^2}$, and P_{TF} is the torsional flexural buckling load given by its expression in Equation (3.17).

For the work presented in this thesis factors influencing a study on instability failure have been reviewed in this Chapter. These effects may be taken into account by means of effective geometrical properties concept such as effective area and effective length.

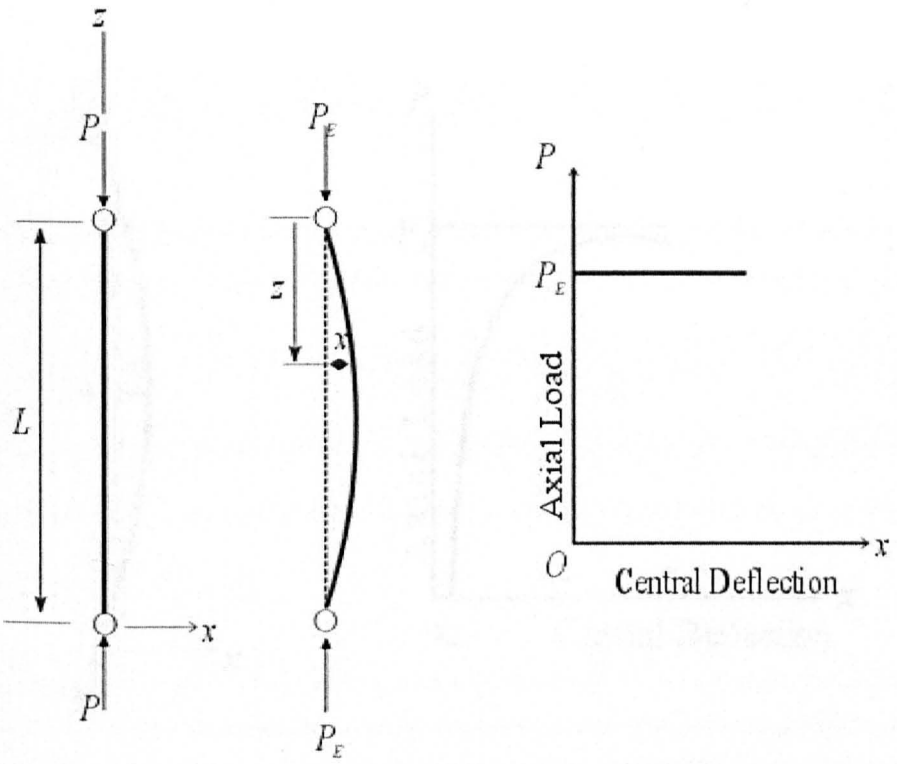

(a) (b) (c)

Figure 3.1. Euler's assumed column deformation.

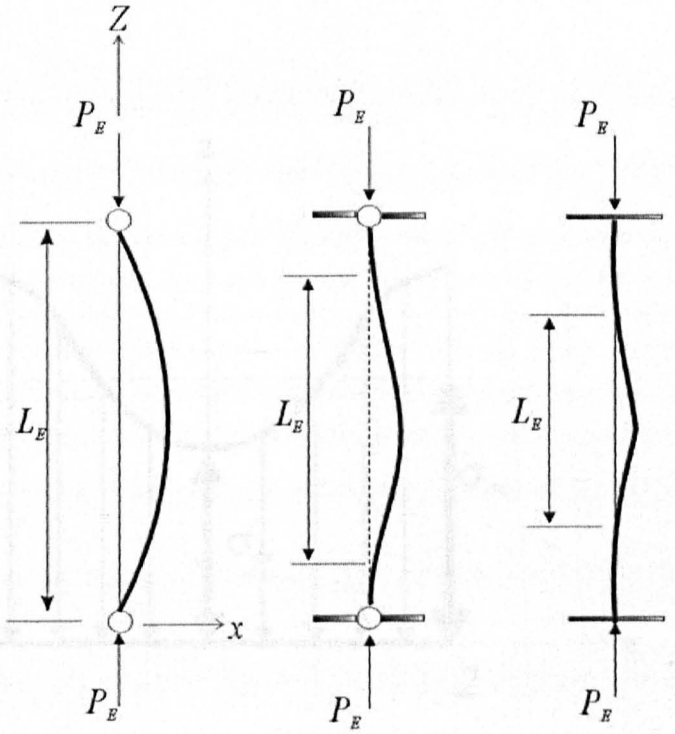

(a) (b) (c)

Figure 3.2. Effective length for different end restraints.

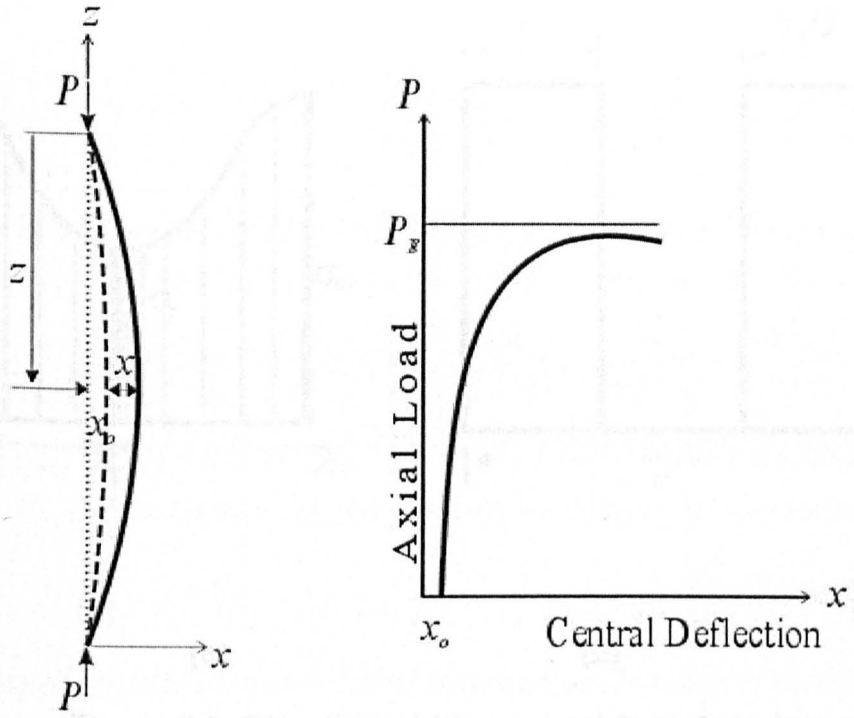

(a) (b)

Figure 3.3. Initial lack of straightness.

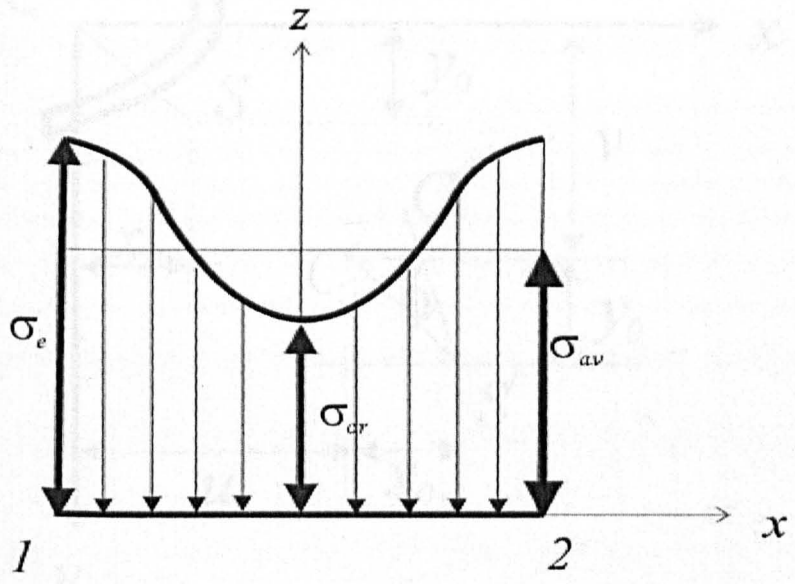

Figure 3.4. Distribution of σ_z stress across width of plate in post-buckling regime.

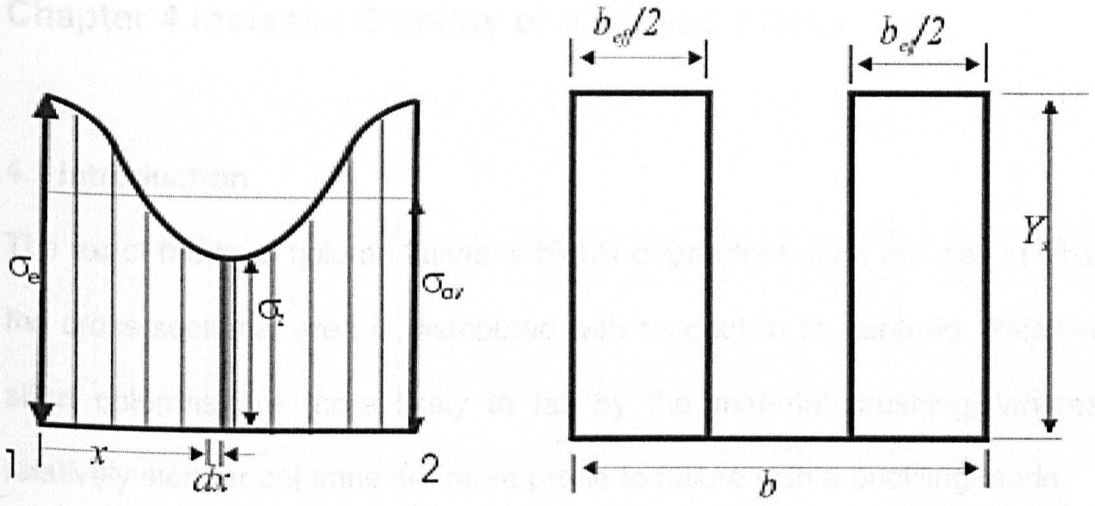

(a) (b)

Figure 3.5. Effective width concept for a flat plate.

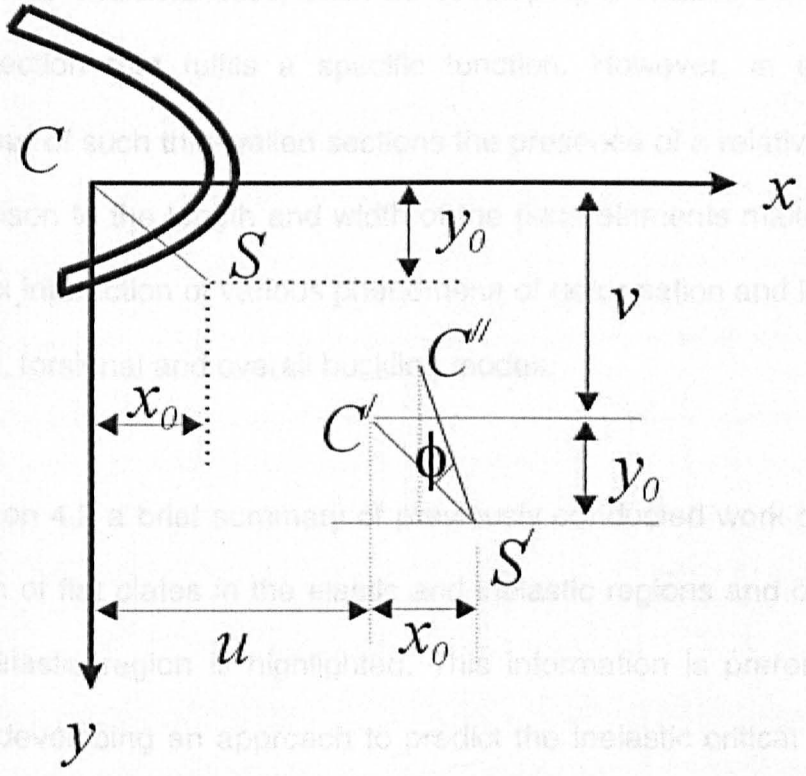

Figure 3.6. Deformations of a general asymmetric cross-section under axial compression.

Chapter 4 Inelastic Stability of a Curved Plates

4.1 Introduction

The exact mode of column failure is highly dependent upon the way in which the cross-sectional area is distributed with respect to its centroid. Relatively short columns are more likely to fail by the material crushing, whereas relatively slender columns are more prone to failure with a buckling mode.

Construction engineers and designers have always been concerned with the implementation of optimum structures to reduce the cost and provide efficient, safe and reliable facilities for improving the life style. The optimization objective of the structural elements is based upon enhancing some of its characteristics, such as developing a reliable configuration, like the ε-section that fulfils a specific function. However, in examining the behaviour of such thin-walled sections the presence of a relatively thin wall in comparison to the length and width of the plate elements makes evident the complex interaction of various phenomena of deformation and instability such as local, torsional and overall buckling modes.

In Section 4.2 a brief summary of previously conducted work on the stability problem of flat plates in the elastic and inelastic regions and of curved plate in the elastic region is highlighted. This information is prerequisite for the author developing an approach to predict the inelastic critical local buckling load for a curve plate element, and applying it to establish the stub column failure load of the ε-section.

4.2 Inelastic stability of curved plate element

Stability in elastic and inelastic ranges of deformation of columns and flat plates has been the subject of extensive studies by several researchers. Key primary texts are those by Timosheko (1961), Bleich (1952) and Bulson (1970). Further theoretical modelling of inelastic local buckling was proposed by Kato (1965), Graves-Smith (1967), Azhari and Bradford (1993), Bradford and Azhari (1994), and Moller *et al.* (1997). The stability problem of a curved plate under axial compression has received little attention, especially beyond the elastic regime. For buckling in the elastic region, relevant information may be found in Redshaw (1938), Batdorf *et al.* (1947), Gerard and Becker (1957) and Parks and Yu (1989), and in the inelastic range there are the papers by Levy (1943) and Wang and Rakotonrainibe (1978). Redshaw developed an expression on the basis of the classical energy method, to predict the elastic local critical buckling stress of curved plate under axial compression. Its general form is

$$\sigma_{cr} = K_{\min} \frac{\pi^2 E}{12(1-\upsilon^2)}\left(\frac{t}{b}\right)^2 \tag{4.1}$$

this has the same form as Equation (3.3) except b is now the circumferential length of plate.

He developed the following expressions for $K_{\min}$ depending on the boundary condition of the plate's longitudinal sides, and on which no compressive stress is applied. The other two edges with uniform compression are assumed to be simply supported.

For simply supported longitudinal sides with $y = 0$ and $y = b$ he gives

$$K_{min} = 4 + \left(\frac{192}{\pi^4}\right)(1-\upsilon^2)\left(\frac{d}{t}\right)^2, \text{ for } \frac{d}{t} \leq 1.47, \text{ and } (\nu = 0.25, \text{ light metal alloy}) \quad (4.2a)$$

If the two longitudinal sides are clamped the minimum critical stress coefficient is given by

$$K_{min} = 2\left(\sqrt{\frac{16}{3} + \frac{768}{\pi^4}\left(\frac{d}{t}\right)^2} + 1\right) \quad (4.2b)$$

For the longitudinal side $y = 0$ simply supported and side at $y = b$ free Redshaw obtained

$$K_{min} = \frac{2}{\pi^2}\left(16 \cdot \sqrt{3}\left(\frac{d}{t}\right) + 3(1-\upsilon)\right) \quad (4.2c)$$

And finally for the longitudinal side $y = 0$ clamped and side at $y = b$ he gives

$$K_{min} = \frac{1}{\pi^2}\left[2\left(\frac{162}{13} + 768\left(\frac{d}{t}\right)^2\right)^{\frac{1}{2}} + \frac{135}{91}(6-7\upsilon)\right] \quad (4.2d)$$

where distance d in Equations (4.2a) to (4.2d) is defined refer to Figure 4.1 at start of analysis. Redshaw highlighted the dependency of the coefficient K_{min} of the curved plate on the curvature of the plates and the ratio L/mb, which is the length of plate divided by the product of the circumferential length and the number of half waves in the axial direction. Redshaw (1938) also mentions that the experimental data presented by Cox and Clenshaw for the two cases given by Equations (4.2a) and (4.2b) give K_{min} values that are lower than the corresponding theoretical values by 40 to 50%. He attributed this discrepancy to imperfections and the actual nature of the edge boundary conditions being different to these assumed in the analytical treatment.

Strut buckling was the first structural problem to be studied in the inelastic range. Engesser (Bleich 1952) proposed the replacement of the tangent modulus (reduced modulus) for the Young's modulus of elastic in Euler's formula. Alternatively, Considere (Bleich 1952) introduced the use of the effective modulus, which has a value that lies between the tangent modulus and the Young's modulus. The effective modulus concept was further refined by von Karman based on his unloading concept at the onset of buckling, and this led to what is generally known as the double modulus. Shanley (1947) conducted tests on columns and managed to show that the unloading on one side of the column, as postulated by von Karman, does not occur at buckling and that the correct reduced modulus for determining the critical buckling stress is actually the tangent modulus.

For inelastic buckling of a plate element as briefly presented in Section 3.4. Bleich handled the problem by assuming the reduced modulus was effective for strips of plate in the applied load-direction, whereas the elastic modulus remained valid for strips in the direction perpendicular to the applied load. Alternatively, Ros and Eichinger (1932) assumed that the plate remains isotropic even when the stress exceeded the proportional limit, with the reduced modulus applying in all direction. But according to Bulson (1970), neither of these two approaches is particularly satisfactory, although the Bleich work gave closer agreement with physical test results. Attempts have therefore been made by researchers to improve the theoretical treatment introducing the laws of plastic theory into the inelastic plate-buckling analysis. Ilyushin (1947) based his solution for the plastic stability problem on von

Karman's concept be that, on onset of the plastic deformation, "unloading takes place on the convex side of the bent plate as this side behaves elastically whereas concave side behaves plastically". Similarly as in the column case, Stowell (1948) modified the inelastic plate buckling theory by Ilyushin, using Shanley's contribution that "no strain reversal occurs in any part of the plate beyond the elastic limit". Stowell took Poisson's ratio equal to 0.5, thereby following the method by Ilyushin. The effect of any error due to this value of ν is partially eliminated by this technique of using the concept of plasticity reduction factor to obtain the inelastic critical buckling stress. The plasticity reduction factor is calculated by dividing the inelastic critical stress by the critical stress computed on the assumption of perfect elasticity, but with $\nu = 0.5$ instead of $\nu = 0.3$. Then the inelastic critical stress is computed from multiplying the plasticity reduction factor by the elastic critical buckling stress.

In Sections 4.2.1 to 4.2.5 the inelastic stability problem of a curved plate compressed in axial direction by a uniformly distributed load in the plane of the plate is investigated. The contribution is based on the original work by Redshaw for curved plates in the elastic region. Furthermore, stability theories for plastic buckling by Ilyushin and Stowell are followed to develop an energy expression. The Principle of Minimum Potential Energy is then implemented to obtain a set of algebraic equations, which are solved using numerical techniques for inelastic critical buckling stress then implemented to develop the new plasticity reduction factor expression that can be used with curved plates.

4.2.1 Displacement field

In developing the relationship between the applied load and the member's deformation the description of deformed configuration first needs to be established by displacement expressions. In considering the deformed configuration of the curved plate Kirchhoff assumptions are implemented to describe the nature of the displacement field through the thickness of the plate. The straight elements, which are normal to the middle surface of generic cross-section, remain straight and normal to the deformed surface. The wall thickness is small in comparison with the radii of curvature. For the new theoretical treatment the in-extensional assumption is relaxed Redshaw (1938).

The geometry of a profile with constant thickness and generic curved cross-section is shown in Figure 4.1. An orthogonal curvilinear coordinates system (x,y,z) is adopted with x-axis along the line of curvature, y-axis normal to the middle surface and z-axis in axial direction. The corresponding displacement components are $u(x,y,z)$, $v(x,y,z)$, and $w(x,y,z)$, respectively and given by

$$w(x,y,z) = w_o(x,z) - y \cdot \frac{\partial v}{\partial x} \tag{4.3a}$$

$$u(x,y,z) = u_o(x,z) + y \cdot \frac{\partial v}{\partial y} \tag{4.3b}$$

$$v(x,y,z) = w_o(x,z) \tag{4.3c}$$

4.2.2 Internal forces

Before we can use the energy method to obtain an expression giving the critical load, the basic concept behind the energy expressions is established.

The inelastic buckling of a curved plate element requires the knowledge of stress-strain relation beyond the elastic range. In this study Ilyushin and Stowell stability theories of plastic buckling are adopted. In the case of two-dimensional state of stress, the intensities of stress and strain according to the Von Mises fundamental hypothesis of the theory of plasticity are given by.

$$\sigma_i = \sqrt{\sigma_x^2 + \sigma_z^2 - \sigma_x \sigma_z + 3\tau_{xz}^2} \tag{4.4}$$

$$e_i = \frac{2}{\sqrt{3}} \sqrt{\varepsilon_x^2 + \varepsilon_z^2 + \varepsilon_x \varepsilon_z - \frac{\gamma_{xz}^2}{4}} \tag{4.5}$$

In Equation (4.4) σ_i is stress intensity that produces the strain intensity e_i, in Equation (4.5). σ_x and σ_z are normal stresses and τ_{xz} is the shear stress. ε_x and ε_z are the normal strains and γ_{xz} is the shear strain.

According to plasticity theory the intensity of stress σ_i is, for any given material, a uniquely defined function of the intensity of strain e_i, and the corresponding stress-strain relations are

$$\varepsilon_z = \frac{\sigma_z - \upsilon \sigma_x}{E_s} = \frac{S_z}{E_s} \tag{4.6}$$

$$\varepsilon_x = \frac{\sigma_x - \upsilon \sigma_z}{E_s} = \frac{S_x}{E_s} \tag{4.7}$$

$$\gamma_{xz} = \frac{2(1+\upsilon)\tau_{xz}}{E_s} \tag{4.8}$$

In Equations (4.6) to (4.8) E_s is the secant modulus that is defined by $\frac{\sigma_i}{e_i}$, S_x and S_z are equivalent stresses in the x-axis and z-axis directions respectively. According to Stowell (1948) the Poisson's ratio in the plastic

region can be assumed to be 0.5. On substituting ν = 0.5 in the Equations (4.6) to (4.8), and solving for the stresses the following expressions are obtained

$$\sigma_z = \frac{4}{3}(S_z + 0.5S_x) \tag{4.9}$$

$$\sigma_x = \frac{4}{3}(S_x + 0.5S_z) \tag{4.10}$$

$$\tau_{xz} = \frac{E_s}{3}\gamma_{xz} \tag{4.11}$$

At onset of buckling, the slight distortion of the plate gives rise to variation in the strain components. This variation arises partly from the variation of the middle surface strains (membrane stresses) and partly from strains due to bending of the plate. These variations are given by

$$\delta\varepsilon_z = \varepsilon_1 - y\delta\chi_1 \tag{4.12}$$

$$\delta\varepsilon_x = \varepsilon_2 - y\delta\chi_2 \tag{4.13}$$

$$\delta\gamma_{xz} = 2\varepsilon_3 - 2y\delta\chi_3 \ , \tag{4.14}$$

where ε_1 is the middle surface strain in the z-direction, ε_2 is the middle surface strain in the circumferential direction, and ε_3 is the middle surface shear strain. Although an x, y and z coordinate system is used to introduce the theoretical treatment it is more convenient to adopt the polar coordinate system for curved sections. This enables circumferential continuity to be ensured easily. The transformation is made by introducing the expression $x = R\theta$, where R is radius and θ is angle of rotation (see Figure 4.1). principal strain components are now related to the displacements by way of

$$\varepsilon_1 = \frac{\partial w}{\partial z} \tag{4.15}$$

$$\varepsilon_2 = \frac{v}{R} + \frac{\partial u}{\partial \theta} \tag{4.16}$$

$$\varepsilon_3 = R\frac{\partial u}{\partial z} + \frac{1}{R}\frac{\partial w}{\partial \theta} \tag{4.17}$$

In Equations (4.12) to (4.14) $\delta\chi_1$, $\delta\chi_2$ and $\delta\chi_3$ are the changes of curvature and in term of displacements w, u and v they are given by:

$$\delta\chi_1 = \frac{\partial^2 v}{\partial z^2} \tag{4.18}$$

$$\delta\chi_2 = \frac{1}{R^2}\left(v + \frac{\partial^2 v}{\partial \theta^2}\right) \tag{4.19}$$

$$\delta\chi_3 = \frac{1}{R}\left(\frac{\partial^2 v}{\partial z \partial \theta}\right) - \frac{\partial u}{\partial z} \tag{4.20}$$

The corresponding variations of the equivalent stresses can now be obtained by using Equation (4.6) (with $S_z = E_s\varepsilon_z$) to derive

$$\delta S_z = E_s\delta\varepsilon_z - \frac{\varepsilon_x}{e_i}\left(\frac{\sigma_i}{e_i} - \frac{d\sigma_i}{de_i}\right)\delta e_i \tag{4.21}$$

The work done by the internal forces when the plate passes from the initial undeformed to the loaded deformed configuration is given by

$$\sigma_i\delta e_i = \sigma_x\delta\varepsilon_x + \sigma_y\delta\varepsilon_y + 2\tau_{xy}\delta\gamma_{xy} \tag{4.22}$$

Then after substitution for the strain variations given by Equations (4.12) to (4.14) in Equation (4.22) the variation of strain intensity is given by

$$\delta e_i = \frac{\sigma_z\varepsilon_1 + \sigma_x\varepsilon_2 + 2\tau_{xz}\varepsilon_3 - y(\sigma_z\delta\chi_1 + \sigma_x\delta\chi_2 + 2\tau_{xz}\delta\chi_3)}{\sigma_i} \tag{4.23}$$

At neutral surface of the curved plate element the variation of strain intensity is zero (i.e. $\delta e_i = 0$), and hence the y-distance to the neutral surface ($\bar{y}_0$) is given by

$$\bar{y}_0 = \frac{\sigma_z \varepsilon_1 + \sigma_x \varepsilon_2 + 2\tau_{xz}\varepsilon_3}{\sigma_z \delta\chi_1 + \sigma_x \delta\chi_2 + 2\tau_{xz}\delta\chi_3} \tag{4.24}$$

By substituting the strain intensity variation δe_i into the variation of equivalent stress S_z, and introducing the neutral surface coordinate $\bar{y}_0$ we have that

$$\delta S_z = E_s(\varepsilon_1 - y\delta\chi_1) + \frac{\varepsilon_z}{\sigma_i e_i}(E_s - E_t)(\sigma_z \delta\chi_1 + \sigma_x \delta\chi_2 + 2\tau_{xy}\delta\chi_3)(y - \bar{y}_0) \tag{4.25}$$

Similarly, the following expressions can be obtained for the other two stresses variations δS_x and $\delta\tau_{xz}$

$$\delta S_x = E_s(\varepsilon_2 - y\delta\chi_2) + \frac{\varepsilon_x}{\sigma_i e_i}(E_s - E_t)(\sigma_z \delta\chi_1 + \sigma_x \delta\chi_2 + 2\tau_{xz}\delta\chi_3)(y - \bar{y}_0) \tag{4.26}$$

$$\delta\tau_{xz} = \frac{2}{3}E_s(\varepsilon_3 - z\delta\chi_3) + \frac{\gamma_{xz}}{3\sigma_i e_i}(E_s - E_t)(\sigma_z \delta\chi_1 + \sigma_x \delta\chi_2 + 2\tau_{xz}\delta\chi_3)(y - \bar{y}_0) \tag{4.27}$$

Where $E_t = \frac{d\sigma_i}{de_i}$ is the tangent modulus.

On each of the four sides (at $z = 0$, $z = L$, $y = 0$ and $y = b$) of the element the surface traction can be replaced by resultant normal forces applied at the mid-plane of the sides and resultant bending moments acting about the relevant axis. Since the curved plate is thin, the sides of the element of width δx can be considered as a rectangle. Figure 4.2 defines the resultant force and moment intensities on the sides of the element. Hence, the variations of the resultant forces and resultant moments are.

$$\delta N_z = \int_{-\frac{t}{2}}^{\frac{t}{2}} \delta\sigma_z dy \tag{4.28}$$

$$\delta N_x = \int_{-\frac{t}{2}}^{\frac{t}{2}} \delta\sigma_x dy \tag{4.29}$$

$$\delta N_{xz} = \int_{-\frac{t}{2}}^{\frac{t}{2}} \delta\tau_{xz} dy \tag{4.30}$$

$$\delta M_z = \int_{-\frac{t}{2}}^{\frac{t}{2}} \delta\sigma_z y dy \tag{4.31}$$

$$\delta M_x = \int_{-\frac{t}{2}}^{\frac{t}{2}} \delta\sigma_x y dy \tag{4.32}$$

$$\delta M_{xz} = \int_{-\frac{t}{2}}^{\frac{t}{2}} \delta\tau_{xz} y dy \tag{4.33}$$

By substituting for σ_z from Equation (4.9), and for $\delta\varepsilon_z$ and $\delta\varepsilon_x$ from Equations (4.25) and (4.26) in Equation (4.28) we can obtain

$$\delta N_z = \frac{4}{3}\int_{-\frac{t}{2}}^{\frac{t}{2}} (\delta\varepsilon_z + 0.5\delta\varepsilon_x) dy \tag{4.34}$$

$$\delta N_z = \frac{4}{3}\left[E_s(\varepsilon_1 + 0.5\varepsilon_2)\int_{-\frac{t}{2}}^{\frac{t}{2}} dy - E_s(\delta\chi_1 + 0.5\delta\chi_2)\int_{-\frac{t}{2}}^{\frac{t}{2}} y dy + \frac{\varepsilon_x + 0.5\varepsilon_x}{\sigma_i e_i}(E_s + E_t)(\sigma_z\delta\chi_1 + \sigma_x\delta\chi_2 + 2\tau_{xy}\delta\chi_3)\int_{-\frac{t}{2}}^{\frac{t}{2}} (y - \bar{y}_0) dy \right]$$

The integrals to the equivalent stress variations $\delta\varepsilon_z$, $\delta\varepsilon_x$ and $\delta\varepsilon_{xz}$ in the plastic region have been taken over the entire thickness of the plate, with the

assumption that no part of the plate is being unloaded (i.e. the cross-section is fully yielded). On carrying out the integration the force term is developed to be

$$\delta N_z = \frac{4}{3} E_s t \left[(\varepsilon_1 + 0.5\varepsilon_2) + \frac{\varepsilon_z + 0.5\varepsilon_x}{\sigma_i e_i} \left(1 - \frac{E_t}{E_s} \right) (\sigma_z \delta\chi_1 + \sigma_x \delta\chi_2 + 2\tau_{xz} \delta\chi_3) \bar{y}_0 \right]$$

$$\delta N_z = \frac{4}{3} E_s t \left[(\varepsilon_1 + 0.5\varepsilon_2) + \frac{0.75\sigma_z}{E_s \sigma_i e_i} \left(1 - \frac{E_t}{E_s} \right) (\sigma_z \varepsilon_1 + \sigma_x \varepsilon_2 + 2\tau_{xz} \varepsilon_3) \bar{y}_0 \right] \qquad (4.35)$$

Similarly, for the remaining two stresses variations we can establish the expressions

$$\delta N_x = \frac{4}{3} E_s t \left\{ \begin{aligned} &\left[1 - \frac{3}{4} \left(\frac{\sigma_x}{\sigma_i} \right)^2 \left(1 - \frac{E_t}{E_s} \right) \right] \varepsilon_2 \\ &+ \frac{1}{2} \left[1 - \frac{3}{2} \frac{\sigma_x \sigma_z}{\sigma_i^2} \left(1 - \frac{E_t}{E_s} \right) \right] \varepsilon_1 - \frac{3}{2} \frac{\sigma_x \tau_{xz}}{\sigma_i^2} \left(1 - \frac{E_t}{E_s} \right) \varepsilon_3 \end{aligned} \right\} \qquad (4.36)$$

$$\delta N_{xz} = \frac{2}{3} E_s t \left\{ \left[1 - \frac{3\tau_{xz}^2}{\sigma_i^2} \left(1 - \frac{E_t}{E_s} \right) \right] \varepsilon_3 - \frac{3}{2} \left(\frac{\sigma_z \tau_{xz}}{\sigma_i^2} \varepsilon_1 + \frac{\sigma_x \tau_{xz}}{\sigma_i^2} \varepsilon_2 \right) \left(1 - \frac{E_t}{E_s} \right) \right\} \qquad (4.37)$$

Similarly by substituting for σ_z from Equation (4.9), and for δS_z and δS_x from Equations (4.25) and (4.26) into Equation (4.31) we find

$$\delta M_z = \frac{4}{3} \int_{-\frac{t}{2}}^{\frac{t}{2}} (\delta S_z + 0.5\delta S_x) y dy \qquad (4.38)$$

$$\delta M_z = \frac{4}{3} \left[E_s (\varepsilon_1 + 0.5\varepsilon_2) \int_{-\frac{t}{2}}^{\frac{t}{2}} y dy - E_s (\delta\chi_1 + 0.5\delta\chi_2) \int_{-\frac{t}{2}}^{\frac{t}{2}} y^2 dy + \frac{\varepsilon_z + 0.5\varepsilon_x}{\sigma_i e_i} (E_s + E_t)(\sigma_z \delta\chi_1 + \sigma_x \delta\chi_2 + 2\tau_{xz} \delta\chi_3) \int_{-\frac{t}{2}}^{\frac{t}{2}} (y^2 - y\bar{y}_0) dz \right]$$

Following the procedure for developing Equations (4.35) to (4.37) we established that

$$\delta M_z = \frac{4}{3}\frac{E_s t^3}{12}\left[-(\delta\chi_1 + 0.5\delta\chi_2) + \frac{\varepsilon_z + 0.5\varepsilon_x}{\sigma_i e_i}\left(1 - \frac{E_t}{E_s}\right)(\sigma_z \delta\chi_1 + \sigma_x \delta\chi_2 + 2\tau_{xz}\delta\chi_3)\right]$$

$$\delta M_z = -D'\left\{\begin{aligned}&\left[1 - \frac{3}{4}\left(\frac{\sigma_z}{\sigma_i}\right)^2\left(1 - \frac{E_t}{E_s}\right)\right]\delta\chi_1 \\ &+\frac{1}{2}\left[1 - \frac{3}{2}\frac{\sigma_x\sigma_z}{\sigma_i^2}\left(1 - \frac{E_t}{E_s}\right)\right]\delta\chi_2 - \frac{3}{2}\frac{\sigma_z\tau_{xz}}{\sigma_i^2}\left(1 - \frac{E_t}{E_s}\right)\delta\chi_3\end{aligned}\right\} \quad (4.39)$$

Similarly, it can be shown that

$$\delta M_x = -D'\left\{\begin{aligned}&\left[1 - \frac{3}{4}\left(\frac{\sigma_x}{\sigma_i}\right)^2\left(1 - \frac{E_t}{E_s}\right)\right]\delta\chi_2 \\ &+\frac{1}{2}\left[1 - \frac{3}{2}\frac{\sigma_x\sigma_z}{\sigma_i^2}\left(1 - \frac{E_t}{E_s}\right)\right]\delta\chi_1 - \frac{3}{2}\frac{\sigma_x\tau_{xz}}{\sigma_i^2}\left(1 - \frac{E_t}{E_s}\right)\delta\chi_3\end{aligned}\right\} \quad (4.40)$$

$$\delta M_{xz} = -\frac{D'}{2}\left\{\left[1 - \frac{3\tau_{xz}^2}{\sigma_i^2}\left(1 - \frac{E_t}{E_s}\right)\right]\delta\chi_3 - \frac{3}{2}\left(\frac{\sigma_z\tau_{xz}}{\sigma_i^2}\delta\chi_1 + \frac{\sigma_x\tau_{xz}}{\sigma_i^2}\delta\chi_2\right)\left(1 - \frac{E_t}{E_s}\right)\right\} \quad (4.41)$$

in which $D' = \frac{E_s t^3}{9}$.

4.2.3 Strain energy

In the extensional method the strain energy of a deformed element is composed of the strain energy due to bending and the extension of the middle surface. The total work done due to variation in moments is

$$\delta U_b = -\frac{1}{2}\iint(\delta M_z \delta\chi_1 + \delta M_x \delta\chi_2 + 2\delta M_{xz}\delta\chi_3)dxdz \quad (4.42)$$

Substituting for the moments their expressions from Equations (4.39) to (4.41) the energy integral of the entire element due to bending during the

transition from the primary configuration to deformed one may be represented by (Stowell 1948).

$$\delta U_b = \frac{1}{2} D' \iint [c_1 \delta\chi_1^2 - c_2 \delta\chi_1 \delta\chi_3 + c_3 (\delta\chi_3^2 + \delta\chi_1 \delta\chi_2) - c_4 \delta\chi_2 \delta\chi_3 + c_5 \delta\chi_2^2] dA$$

Where

$$c_1 = 1 - \frac{3}{4}\left(\frac{\sigma_z}{\sigma_i^2}\right)^2 \left(1 - \frac{E_t}{E_s}\right), \quad c_2 = 3\left(\frac{\sigma_z \tau_{xz}}{\sigma_i^2}\right)\left(1 - \frac{E_t}{E_s}\right), \quad c_3 = 1 - \frac{3}{4}\frac{\sigma_x \sigma_z + 2\tau^2}{\sigma_i^2}\left(1 - \frac{E_t}{E_s}\right),$$

$$c_4 = 3\left(\frac{\sigma_x \tau_{xz}}{\sigma_i^2}\right)\left(1 - \frac{E_t}{E_s}\right), \quad c_5 = 1 - \frac{3}{4}\left(\frac{\sigma_x}{\sigma_i^2}\right)^2 \left(1 - \frac{E_t}{E_s}\right).$$

The membrane strain energy due to the additional stretching of the middle surface is

$$\delta U_m = \frac{1}{2} \iint (\delta N_z \varepsilon_1 + \delta N_x \varepsilon_2 + \delta N_{xz} \varepsilon_3) dA \qquad (4.43)$$

When substituting for the forces their expressions given by Equations (4.35) to (4.37) the energy integral of the entire element due to membrane forces during the transition from the unstressed configuration to the deformed one is

$$\delta U_m = \frac{2}{3} E_s t \iint [b_1 \varepsilon_1^2 + b_2 \varepsilon_1 \varepsilon_2 - b_3 \varepsilon_1 \varepsilon_3 + b_4 \varepsilon_2^2 - b_5 \varepsilon_2 \varepsilon_3 + b_6 \varepsilon_3^2] dA$$

Where

$$b_1 = c_1, \quad b_2 = 1 - \frac{3}{2}\frac{\sigma_x \sigma_z}{\sigma_i^2}\left(1 - \frac{E_t}{E_s}\right), \quad b_3 = 0.75 c_2, \quad b_4 = c_5, \quad b_5 = 0.75 c_4,$$

$$b_6 = \frac{1}{2} - \frac{3}{2}\left(\frac{\tau_{xz}}{\sigma_i^2}\right)^2 \left(1 - \frac{E_t}{E_s}\right).$$

Therefore the total change in the strain energy of a curved plate element is

$$\delta U = \begin{bmatrix} \frac{2}{3}E_s t \iint \left[b_1\varepsilon_1^2 + b_2\varepsilon_1\varepsilon_2 - b_3\varepsilon_1\varepsilon_3 + b_4\varepsilon_2^2 - b_5\varepsilon_2\varepsilon_3 + b_6\varepsilon_3^2 \right] dA + \\ \frac{1}{2}D' \iint \begin{bmatrix} c_1\delta\chi_1^2 - c_2\delta\chi_1\delta\chi_3 + c_3\left(\delta\chi_3^2 + \delta\chi_1\delta\chi_2\right) \\ -c_4\delta\chi_2\delta\chi_3 + c_5\delta\chi_2^2 \end{bmatrix} dA \end{bmatrix} \tag{4.44}$$

In order to apply the Principle of Minimum Potential Energy we need to have an expression for the loss in potential energy V of external loads due to the deformation of the plate's middle plane. V is equal to the negative product of the external forces and the displacement in the direction of the applied force, and may be expressed by (Redshaw 1938)

$$\delta = \left[\frac{\partial w}{\partial z} + \frac{1}{2}R^2\left(\frac{\partial u}{\partial z}\right)^2 + \frac{1}{2}\left(\frac{\partial y}{\partial z}\right)^2 \right] \delta z \tag{4.45}$$

The work done by applied force on the panel is

$$V = \sigma_z t \iint \left[\frac{\partial w}{\partial z} + \frac{1}{2}R^2\left(\frac{\partial u}{\partial z}\right)^2 + \frac{1}{2}\left(\frac{\partial v}{\partial z}\right)^2 \right] dz R d\theta \tag{4.46}$$

The total potential energy of the internal and the external forces acting on the curved plate element is then obtained by adding the strain energy due to deformation to the work done by the forces applied at the boundary of the plate, as follows

$$\Pi = U + V \tag{4.47}$$

Using the strains and change in curvatures from Equations (4.15) to (4.20), Equation (4.47) will yield the governing potential energy integral, that is

$$\Pi=\left[\begin{array}{l}\dfrac{2}{3}E_s t\iint\left[\begin{array}{l}b_1\left(\dfrac{\partial u}{\partial x}\right)^2+b_2\left(\dfrac{\partial u}{\partial x}\right)\cdot\left(\dfrac{w}{R}+\dfrac{\partial v}{\partial\theta}\right)-b_3\left(\dfrac{\partial u}{\partial x}\right)\cdot\left(R\dfrac{\partial v}{\partial x}+\dfrac{1}{R}\dfrac{\partial u}{\partial\theta}\right)+b_4\left(\dfrac{w}{R}+\dfrac{\partial v}{\partial\theta}\right)^2\\ -b_5\left(\dfrac{w}{R}+\dfrac{\partial v}{\partial\theta}\right)\cdot\left(R\dfrac{\partial v}{\partial x}+\dfrac{1}{R}\dfrac{\partial u}{\partial\theta}\right)+b_6\left(R\dfrac{\partial v}{\partial x}+\dfrac{1}{R}\dfrac{\partial u}{\partial\theta}\right)^2\end{array}\right]dA+\\ \dfrac{1}{2}D\iint\left[\begin{array}{l}c_1\left(\dfrac{\partial^2 w}{\partial x^2}\right)^2-c_2\left(\dfrac{\partial^2 w}{\partial x^2}\right)\cdot\left(\dfrac{1}{R}\left(\dfrac{\partial^2 w}{\partial x\partial\theta}\right)-\dfrac{\partial v}{\partial x}\right)\\ +c_3\left(\left(\dfrac{1}{R}\left(\dfrac{\partial^2 w}{\partial x\partial\theta}\right)-\dfrac{\partial v}{\partial x}\right)^2+\left(\dfrac{\partial^2 w}{\partial x^2}\right)\cdot\left(\dfrac{1}{R^2}\left(w+\dfrac{\partial^2 w}{\partial\theta^2}\right)\right)\right)\\ -c_4\left(\dfrac{1}{R^2}\left(w+\dfrac{\partial^2 w}{\partial\theta^2}\right)\right)\cdot\left(\dfrac{1}{R}\left(\dfrac{\partial^2 w}{\partial x\partial\theta}\right)-\dfrac{\partial v}{\partial x}\right)+c_5\left(\dfrac{1}{R^2}\left(w+\dfrac{\partial^2 w}{\partial\theta^2}\right)\right)^2\end{array}\right]dA-\\ \sigma_x t\iint\left[\dfrac{\partial u}{\partial x}+\dfrac{1}{2}R^2\left(\dfrac{\partial v}{\partial x}\right)^2+\dfrac{1}{2}\left(\dfrac{\partial w}{\partial x}\right)^2\right]dxRd\theta\end{array}\right] \quad (4.48)$$

4.2.4 Rayleigh-Ritz method

The Rayleigh-Ritz method was introduced by Ritz in 1908 as a generalization of a technique described by Rayleigh in 1877. The procedure is based on the Principle of Minimum Potential Energy: which states that, an elastic structure is in equilibrium if there is no change in the total potential energy of the structure when its displacement field is changed arbitrarily by small amount. At the critical load the total potential is always a minimum, which given by

$$\partial\Pi=\delta(U+V)=0 \quad (4.49)$$

4.2.5 Application to curved plate subjected to edge forces

In the case of a curved plate subjected to a uniformly compressive axial force, the Rayleigh-Ritz method may be applied to obtain an approximate value of the critical buckling load. The critical point in the application of the method is the choice of the possible admissible deformation. By assuming a

form for the buckled deformation, the obtained critical buckling load is the upper limit, since the actual deformation corresponds to that for the least resistance of the imperfect plate. However, providing the boundary conditions are satisfied and the assumed the deformation shape is physically admissible, the solution obtained is sufficiently accurate for most engineering purposes (Redshaw 1938).

To model the buckling response of a short length of a curved plate we now consider in the present study a simply supported plate on two circumferential sides at $x = 0$ and $x = L$, with one longitudinal side free and the other side clamped. The problem to be analysed is shown in Figure 4.3. Adopted herein are displacement expressions to those chosen by Redshaw to solve the elastic buckling problem of a curved plate. They are

$$w = Af(\theta)\cos\left(\frac{kz}{R}\right) \tag{4.50}$$

$$Ru = Bf(\theta)\cos\left(\frac{kz}{R}\right) \tag{4.51}$$

$$v = Cf(\theta)\sin\left(\frac{kz}{R}\right) \tag{4.52}$$

with $k = \frac{m\pi R}{L}$, for the generators subdivide into m half-waves. Function $f(\theta) = 6\phi^2\theta^2 - 4\phi\theta^3 + \theta^4$ represents approximately the form of the deflection across the panel. ϕ is the angle subtended from the free edge to the second longitudinal side where the displacement boundary conditions are for the fully clamped situation. This is the model illustrated in Figure 4.3. A, B and C in Equations (4.50) to (4.52) are arbitrary constants. Then for a critical value of

the total potential energy Π its first derivative with respect to these constants should zero.

By substituting the assumed displacement functions above into Equations (4.50) to (4.52) and then into Equation (4.48) the strain energy can be expressed as follows

$$
\begin{aligned}
U=\frac{2}{3}E_1 I\iint\Bigg[
&b_1\left(-A\frac{k}{R}\left(6\phi^2\theta^2-4\phi\hat{\theta}+\theta^4\right)\sin\left(\frac{kz}{R}\right)\right)^2\\
&+b_2\left(-A\frac{k}{R}\left(6\phi^2\theta^2-4\phi\hat{\theta}+\theta^4\right)\sin\left(\frac{kz}{R}\right)\right)\cdot\left(\frac{C}{R}\left(6\phi^2\theta^2-4\phi\hat{\theta}+\theta^4\right)\sin\left(\frac{kz}{R}\right)+\frac{B}{R}\left(12\phi^2\theta-12\phi\hat{\theta}+4\hat{\theta}^3\right)\cos\left(\frac{kz}{R}\right)\right)\\
&-b_3\left(-A\frac{k}{R}\left(6\phi^2\theta^2-4\phi\hat{\theta}+\theta^4\right)\sin\left(\frac{kz}{R}\right)\right)\cdot\left(-B\frac{k}{R}\left(6\phi^2\theta^2-4\phi\hat{\theta}+\theta^4\right)\sin\left(\frac{kz}{R}\right)+\frac{A}{R}\left(12\phi^2\theta-12\phi\hat{\theta}+4\hat{\theta}^3\right)\cos\left(\frac{kz}{R}\right)\right)\\
&+b_4\left(\frac{C}{R}\left(6\phi^2\theta^2-4\phi\hat{\theta}+\theta^4\right)\sin\left(\frac{kz}{R}\right)+\frac{B}{R}\left(12\phi^2\theta-12\phi\hat{\theta}+4\hat{\theta}^3\right)\cos\left(\frac{kz}{R}\right)\right)^2\\
&-b_5\left(\frac{C}{R}\left(6\phi^2\theta^2-4\phi\hat{\theta}+\theta^4\right)\sin\left(\frac{kz}{R}\right)+\frac{B}{R}\left(12\phi^2\theta-12\phi\hat{\theta}+4\hat{\theta}^3\right)\cos\left(\frac{kz}{R}\right)\right)\cdot\\
&\left(-B\frac{k}{R}\left(6\phi^2\theta^2-4\phi\hat{\theta}+\theta^4\right)\sin\left(\frac{kz}{R}\right)+\frac{A}{R}\left(12\phi^2\theta-12\phi\hat{\theta}+4\hat{\theta}^3\right)\cos\left(\frac{kz}{R}\right)\right)\\
&+b_6\left(-B\frac{k}{R}\left(6\phi^2\theta^2-4\phi\hat{\theta}+\theta^4\right)\sin\left(\frac{kz}{R}\right)+\frac{A}{R}\left(12\phi^2\theta-12\phi\hat{\theta}+4\hat{\theta}^3\right)\cos\left(\frac{kz}{R}\right)\right)^2
\Bigg]dA+\\
\frac{1}{2}D\iint\Bigg[
&c_1\left(-C\frac{k^2}{R^2}\left(6\phi^2\theta^2-4\phi\hat{\theta}+\theta^4\right)\sin\left(\frac{kz}{R}\right)\right)^2\\
&-c_2\left(-C\frac{k^2}{R^2}\left(6\phi^2\theta^2-4\phi\hat{\theta}+\theta^4\right)\sin\left(\frac{kz}{R}\right)\right)\cdot\left(C\frac{k}{R^2}\left(12\phi^2\theta-12\phi\hat{\theta}+4\hat{\theta}^3\right)\cos\left(\frac{kz}{R}\right)+B\frac{k}{R^2}\left(6\phi^2\theta^2-4\phi\hat{\theta}+\theta^4\right)\sin\left(\frac{kz}{R}\right)\right)\\
&+c_3\left(\left(C\frac{k}{R^2}\left(12\phi^2\theta-12\phi\hat{\theta}+4\hat{\theta}^3\right)\cos\left(\frac{kz}{R}\right)+B\frac{k}{R^2}\left(6\phi^2\theta^2-4\phi\hat{\theta}+\theta^4\right)\sin\left(\frac{kz}{R}\right)\right)^2\right.\\
&\left.-\left(C\frac{k^2}{R^2}\left(6\phi^2\theta^2-4\phi\hat{\theta}+\theta^4\right)\sin\left(\frac{kz}{R}\right)\right)\cdot\left(C\frac{1}{R^2}\left(6\phi^2\theta^2-4\phi\hat{\theta}+\theta^4\right)\sin\left(\frac{kz}{R}\right)+C\frac{1}{R^2}\left(12\phi-24\phi\theta+12\hat{\theta}^2\right)\sin\left(\frac{kz}{R}\right)\right)\right)\\
&-c_4\left(C\frac{1}{R^2}\left(6\phi^2\theta^2-4\phi\hat{\theta}+\theta^4\right)\sin\left(\frac{kz}{R}\right)+C\frac{1}{R^2}\left(12\phi-24\phi\theta+12\hat{\theta}^2\right)\sin\left(\frac{kz}{R}\right)\right)\\
&\left(C\frac{k}{R^2}\left(12\phi^2\theta-12\phi\hat{\theta}+4\hat{\theta}^3\right)\cos\left(\frac{kz}{R}\right)+B\frac{k}{R^2}\left(6\phi^2\theta^2-4\phi\hat{\theta}+\theta^4\right)\sin\left(\frac{kz}{R}\right)\right)\\
&+c_5\left(C\frac{1}{R^2}\left(6\phi^2\theta^2-4\phi\hat{\theta}+\theta^4\right)\sin\left(\frac{kz}{R}\right)+C\frac{1}{R^2}\left(12\phi-24\phi\theta+12\hat{\theta}^2\right)\sin\left(\frac{kz}{R}\right)\right)^2
\Bigg]dA
\end{aligned}
$$

The author performed hand calculation to establish the integration over the length L of the plate problem and the following expression is obtained

$$U=\frac{2}{3}E_s tR\int\left[\begin{array}{l} b_1\left(A^2\frac{k^2Lf^2(\theta)}{2R^2}\right)-b_2\left(AC\frac{kLf^2(\theta)}{2R^2}\right)-b_3\left(AB\frac{k^2Lf^2(\theta)}{2R^2}\right) \\ +b_4\left(C^2\frac{Lf^2(\theta)}{2R^2}+B^2\frac{Lf'^2(\theta)}{2R^2}\right)-b_5\left(AB\frac{Lf'^2(\theta)}{2R^2}-BC\frac{kLf^2(\theta)}{2R^2}\right) \\ +b_6\left(B^2\frac{k^2Lf^2(\theta)}{2R^2}+A^2\frac{Lf'^2(\theta)}{2R^2}\right) \end{array}\right]d\theta$$

$$+\frac{1}{2}D'R\int\left[\begin{array}{l} c_1\left(C^2\frac{k^4Lf^2(\theta)}{2R^4}\right) \\ +c_3\left(C^2\frac{k^2Lf'^2(\theta)}{2R^4}+B^2\frac{k^2Lf^2(\theta)}{2R^4}-C^2\frac{k^2Lf^2(\theta)}{2R^4}-C^2\frac{k^2Lf(\theta)f''(\theta)}{2R^4}\right) \\ -c_4\left(CB\frac{kLf^2(\theta)}{2R^4}+CB\frac{kLf(\theta)f''(\theta)}{2R^4}\right) \\ +c_5\left(C^2\frac{Lf^2(\theta)}{2R^4}+C^2\frac{Lf''^2(\theta)}{2R^4}+C^2\frac{Lf(\theta)f''(\theta)}{2R^4}\right) \end{array}\right]d\theta$$

Then by performing the integration over the circumferential direction of the element the strain energy expression is

$$U=\frac{E_s t}{3R}\left[\begin{array}{l} \frac{104}{45}k^2Lb_1\phi^9A^2-\frac{104}{45}kLb_2\phi^9AC-\frac{104}{45}k^2Lb_3\phi^9AB+\frac{104}{45}Lb_4\phi^9C^2 \\ +\frac{72}{7}Lb_4\phi^7B^2-\frac{72}{7}Lb_5\phi^7AB+\frac{104}{45}kLb_5\phi^9BC+\frac{104}{45}k^2Lb_6\phi^9B^2+\frac{72}{7}Lb_6\phi^7A^2 \end{array}\right]$$

$$+\frac{D'}{4R^3}\left[\begin{array}{l} \frac{104}{45}k^4Lc_1\phi^9C^2+\frac{72}{7}k^2Lc_3\phi^7C^2+\frac{104}{45}k^2Lc_3\phi^9B^2-\frac{104}{45}k^2Lc_3\phi^9C^2 \\ -\frac{104}{45}kLc_4\phi^9BC \\ -\frac{12}{7}kLc_4\phi^7CB+\frac{104}{45}Lc_5\phi^9C^2+\frac{144}{5}Lc_5\phi^5C^2+\frac{12}{7}Lc_5\phi^7C^2 \end{array}\right]$$

Collecting like terms the final strain energy expression is

$$U=\left[\begin{array}{l}\left(\frac{4.62E_st}{3R}k^2Lb_1\phi^9+\frac{20.58E_st}{3R}Lb_6\phi^7\right)A^2-\left(\frac{4.62E_st}{3R}k^2Lb_3\phi^9+\frac{20.58E_st}{3R}Lb_5\phi^7\right)AB\\ -\frac{4.62E_st}{3R}kLb_2\phi^9AC+\left(\frac{20.58E_st}{3R}Lb_4\phi^7+\frac{4.62E_st}{3R}k^2Lb_6\phi^9+\frac{2.31D'}{4R^3}k^2Lc_3\phi^9\right)B^2\\ +\left(\frac{4.62E_st}{3R}kLb_5\phi^9-\frac{1.71D'}{4R^3}kLc_4\phi^7-\frac{2.31D'}{4R^3}kLc_4\phi^9\right)BC\\ +\left(\begin{array}{l}\frac{4.62E_st}{3R}Lb_4\phi^9+\frac{2.31D'}{4R^3}k^4Lc_1\phi^9+\frac{10.29D'}{4R^3}k^2Lc_3\phi^7-\frac{2.31D'}{4R^3}k^2Lc_3\phi^9\\ -\frac{1.71D'}{4R^3}k^2Lc_3\phi^7+\frac{2.31D'}{4R^3}Lc_5\phi^9+\frac{28.8D'}{4R^3}Lc_5\phi^5+\frac{1.71D'}{4R^3}Lc_5\phi^7\end{array}\right)C^2\end{array}\right]$$

By substituting the assumed displacement functions Equations (4.50) to (4.52) into Equation (4.48), the work done by the compressive forces at onset of the buckling may be expressed as follows

$$V=\sigma_z t\iint\left[\begin{array}{l}-A\frac{k}{R}\left(6\phi^2\theta^2-4\phi\theta^3+\theta^4\right)\sin\left(\frac{kz}{R}\right)+\\ \frac{1}{2}\left(-B\frac{k}{R}\left(6\phi^2\theta^2-4\phi\theta^3+\theta^4\right)\sin\left(\frac{kz}{R}\right)\right)^2\\ +\frac{1}{2}\left(C\frac{k}{R}\left(6\phi^2\theta^2-4\phi\theta^3+\theta^4\right)\cos\left(\frac{kz}{R}\right)\right)^2\end{array}\right]dzRd\theta$$

By performing the integration over the length of the element, the following expression is obtained

$$V=\sigma_z tR\int\left[\frac{Lk^2}{4R^2}\left(6\phi^2\theta^2-4\phi\theta^3+\theta^5\right)^2B^2+\frac{Lk^2}{4R^2}\left(6\phi^2\theta^2-4\phi\theta^3+\theta^4\right)^2C^2\right]d\theta,$$

Then by further performing the integration over circumferential length b of the element, the following expression for the work done by the compressive forces is obtained

$$V=\frac{104}{45}\cdot\frac{\sigma_z tLk^2\phi^9}{4R}\left(B^2+C^2\right)$$

The total potential energy is given by

$$\Pi=U+V$$

For Π to have a minimum or maximum value for variations in the arbitrary constants A, B and C requires that

$$\frac{\partial \Pi}{\partial A} = \frac{\partial \Pi}{\partial B} = \frac{\partial \Pi}{\partial C} = 0 \tag{4.53}$$

The condition of Equation (4.53) gives a system of linear and homogeneous equations in the unknown arbitrary constants A, B and C. they are

$$\frac{\partial \Pi}{\partial A} = \begin{bmatrix} \left(2\frac{E_s t}{3R}k^2 Lb_1\phi^9 + \frac{924}{104}\frac{E_s t}{3R}Lb_6\phi^7\right)A \\ -\left(\frac{E_s t}{3R}k^2 Lb_3\phi^9 + \frac{462}{104}\frac{E_s t}{3R}Lb_5\phi^7\right)B \\ -\frac{E_s t}{3R}kLb_2\phi^9 C \end{bmatrix} = 0 \tag{4.54}$$

$$\frac{\partial \Pi}{\partial B} = \begin{bmatrix} \left(\frac{E_s t}{3R}k^2 Lb_3\phi^9 + \frac{462}{104}\frac{E_s t}{3R}Lb_5\phi^7\right)A \\ +\left(\frac{924}{104}\frac{E_s t}{3R}Lb_4\phi^7 + 2\frac{E_s t}{3R}k^2 Lb_6\phi^9 \right. \\ \left. +2\frac{D'}{4R^3}k^2 Lc_3\phi^9 - 2\frac{\sigma_x tLk^2\phi^9}{4R}\right)B \\ +\left(\frac{E_s t}{3R}kLb_5\phi^9 - \frac{77}{104}\frac{D'}{4R^3}kLc_4\phi^7 - \frac{D'}{4R^3}kLc_4\phi^9\right)C \end{bmatrix} = 0 \tag{4.55}$$

$$\frac{\partial \Pi}{\partial C} = \begin{bmatrix} -\frac{E_s t}{3R} kLb_2 \phi^9 A \\ +\left(\frac{E_s t}{3R} kLb_5 \phi^9 - \frac{77}{104} \frac{D'}{4R^3} kLc_4 \phi^7 - \frac{D'}{4R^3} kLc_4 \phi^9 \right) B \\ +\begin{pmatrix} 2\frac{E_s t}{3R} Lb_4 \phi^9 + 2\frac{D'}{4R^3} k^4 Lc_1 \phi^9 + \frac{924}{104} \frac{D'}{4R^3} k^2 Lc_3 \phi^7 \\ -2\frac{D'}{4R^3} k^2 Lc_3 \phi^9 + 2\frac{D'}{4R^3} Lc_5 \phi^9 + \frac{2592}{104} \frac{D'}{4R^3} Lc_5 \phi^5 \\ +\frac{154}{104} \frac{D'}{4R^3} Lc_5 \phi^7 - 2\frac{\sigma_z t L k^2 \phi^9}{4R} \end{pmatrix} C \end{bmatrix} = 0 \qquad (4.56)$$

By elimination of the arbitrary constants A, B and C from Equations (4.54) to (4.56) the following determinant in terms of b_i and c_i is obtained

$$
\begin{vmatrix}
\left(2k^2b_1\phi^2 + \frac{924}{104}b_6\right) & \left(k^2b_3\phi^2 + \frac{462}{104}b_5\right) & -kb_2\phi^2 \\
\left(k^2b_3\phi^2 + \frac{462}{104}b_5\right) & \left(\frac{924}{104}b_4 + 2k^2b_6\phi^2 + \frac{3}{2}\frac{D'}{E_stR^2}k^2c_3\phi^2 - \frac{3}{2}\frac{\sigma}{E_s}k^2\phi^2\right) & \left(kb_5\phi^2 - \frac{58}{104}\frac{D'}{E_stR^2}kc_4 - \frac{3}{4}\frac{D'}{E_stR^2}kc_4\phi^2\right) \\
-kb_2\phi^2 & \left(kb_5\phi^2 - \frac{58}{104}\frac{D'}{E_stR^2}kc_4 - \frac{3}{4}\frac{D'}{E_stR^2}kc_4\phi^2\right) & \left(2b_4\phi^2 + \frac{3}{2}\frac{D'}{E_stR^2}k^4c_1\phi^2 + \frac{693}{104}\frac{D'}{E_stR^2}k^2c_3 - \frac{3}{2}\frac{D'}{E_stR^2}k^2c_3\phi^2 + \frac{3}{2}\frac{D'}{E_stR^2}c_5\phi^2 + \frac{1944}{104}\frac{D'}{\phi^2E_stR^2}c_5 + \frac{116}{104}\frac{D'}{E_stR^2}c_5 - \frac{3}{2}\frac{\sigma}{E_s}k^2\phi^2\right)
\end{vmatrix} = 0 \qquad (4.57)
$$

In the case of 2-dimensional curved plate compressed solely in the z-direction the traction boundary conditions ($z = 0$, and $z = L$) are given by

$\sigma_x = \tau_{xz} = 0$

Therefore from Equation (4.4) the stress intensity is

$$\sigma_i = \sigma_z$$

Consequently, the plasticity coefficients b_i and c_i reduce to

$$b_1 = c_1 = \frac{1}{4} + \frac{3}{4}\frac{E_t}{E_s}$$

$$b_3 = b_5 = c_2 = c_4 = 0$$

$$b_2 = b_4 = c_3 = c_5 = 1$$

$$b_6 = \frac{1}{2}$$

Substitute the value of the plasticity coefficients b_i and c_i in Equation (4.57) yields

$$\begin{vmatrix} \left(2k^2\phi^2 c_1 + \frac{462}{104}\right) & 0 & -k\phi^2 \\ 0 & \left(\frac{924}{104} + k^2\phi^2 + \frac{3}{2}\frac{D'}{E_s tR^2}k^2\phi^2 - \frac{3}{2}\frac{\sigma_x}{E_s}k^2\phi^2\right) & 0 \\ -k\phi^2 & 0 & \left(2\phi^2 + \frac{3}{2}\frac{D'}{E_s tR^2}k^4\phi^2 c_1 + \frac{693}{104}\frac{D'}{E_s tR^2}k^2 - \frac{3}{2}\frac{D'}{E_s tR^2}k^2\phi^2 + \frac{3}{2}\frac{D'}{E_s tR^2}\phi^2 + \frac{1944}{104}\frac{D'}{\phi^2 E_s tR^2} + \frac{116}{104}\frac{D'}{E_s tR^2} - \frac{3}{2}\frac{\sigma_z}{E_s}k^2\phi^2\right) \end{vmatrix} = 0 \quad (4.58)$$

By expanding the determinant from Equation (4.58) yields

$$\left(2k^2\phi^2c_1+\frac{462}{104}\right)\left(\begin{array}{l}2\phi^2+\frac{3}{2}\frac{D'}{E_stR^2}k^4\phi^2c_1+\frac{693}{104}\frac{D'}{E_stR^2}k^2-\frac{3}{2}\frac{D'}{E_stR^2}k^2\phi^2\\+\frac{3}{2}\frac{D'}{E_stR^2}\phi^2+\frac{1944}{104}\frac{D'}{\phi^2E_stR^2}+\frac{116}{104}\frac{D'}{E_stR^2}-\frac{3}{2}\frac{\sigma_z}{E_s}k^2\phi^2\end{array}\right)-k^2\phi^4=0$$

Rearranging for σ_z gives

$$\frac{\sigma_z}{E_s}=\frac{D'}{E_stR^2}\left(k^2c_1+\frac{462}{104\phi^2}-1+\frac{1}{k^2}+\frac{1296}{104k^2\phi^4}+\frac{77}{104k^2\phi^2}\right)+\frac{4}{3k^2}-\frac{4}{3\left(2k^2c_1+\frac{462}{104\phi^2}\right)}$$

or

$$\frac{\sigma_z}{E_s}=\left[\begin{array}{l}\frac{t^2}{9R^2}\left(k^2c_1+\frac{462}{104\phi^2}-1+\frac{1}{k^2}+\frac{1296}{104k^2\phi^4}+\frac{77}{104k^2\phi^2}\right)\\+\frac{4}{3k^2}-\frac{4}{3\left(2k^2c_1+\frac{462}{104\phi^2}\right)}\end{array}\right] \qquad (4.59)$$

By noting that the arc length $b=R\phi$ and that from Redshaw (1938) the bulge distance for a curved panel of constant radius R is $d=\frac{b^2}{8R}$ approximately, then on substitution we have

$$\frac{\sigma_z}{E_s}=\frac{\pi^2t^2}{9b^2}\left(\begin{array}{l}\left(\frac{mb}{L}\right)^2c_1+\frac{462}{104\pi^2}-\frac{\phi^2}{\pi^2}+\frac{\phi^2}{\pi^2\left(\frac{m\pi R}{L}\right)^2}\\+\frac{1296}{104\pi^4}\left(\frac{L}{mb}\right)^2+\frac{77}{104\pi^2\left(\frac{m\pi R}{L}\right)^2}+\frac{768}{\pi^4}\left(\frac{d}{t}\right)^2\left(\frac{L}{mb}\right)^2\end{array}\right) \qquad (4.60)$$

On comparing Equation (4.60) to Equation (4.1), with ν = 0.5 for the inelastic condition it is seen that the terms in the bracket is for $K_{\min}$. Now let the bracket expression be set to K, so that we have

$$K=\left(\begin{array}{l}\left(\frac{mb}{L}\right)^2 c_1+\frac{462}{104\pi^2}-\frac{\phi}{\pi^2}^2+\frac{\phi^2}{\pi^2\left(\frac{m\pi R}{L}\right)^2} \\ +\frac{1296}{104\pi^4}\left(\frac{L}{mb}\right)^2+\frac{77}{104\pi^2\left(\frac{m\pi R}{L}\right)^2}+\frac{768}{\pi^4}\left(\frac{d}{t}\right)^2\left(\frac{L}{mb}\right)^2\end{array}\right) \tag{4.61}$$

Substitute for $\frac{L}{mb}$ by Q and by neglecting the terms, which have relatively small values and which when summed are insignificant the following expression for K is obtained

$$K=Q^{-2}c_1+\frac{462}{104\pi^2}+\frac{1296}{104\pi^4}Q^2+\frac{768}{\pi^4}\left(\frac{d}{t}\right)^2Q^2 \tag{4.62}$$

For σ_z in Equation (4.60) to be a minimum K must be a minimum, and this condition is given by

$$\frac{dK}{dQ}=0 \tag{4.63}$$

Therefore we have that

$$K_{\min}=\frac{1}{\pi^2}\left[2c_1^{\frac{1}{2}}\left(\frac{162}{13}+768\left(\frac{d}{t}\right)^2\right)^{\frac{1}{2}}+\frac{462}{104}\right] \tag{4.64}$$

From which the inelastic critical buckling stress, $\bar{\sigma}_{cr}$, is given by

$$\bar{\sigma}_{cr}=\frac{E_s t^2}{9b^2}\left[2c_1^{\frac{1}{2}}\left(\frac{162}{13}+768\left(\frac{d}{t}\right)^2\right)^{\frac{1}{2}}+\frac{462}{104}\right] \tag{4.65}$$

or

$$\bar{\sigma}_{cr}=\frac{E_s}{12(1-\nu^2)}\left(\frac{t}{b}\right)^2\left[2c_1^{\frac{1}{2}}\left(\frac{162}{13}+768\left(\frac{d}{t}\right)^2\right)^{\frac{1}{2}}+\frac{462}{104}\right]$$

When compared with the elastic solution in Equation (4.67) it is seen that the main changes is secant modulus instead of Young's modulus and plasticity coefficients c_1.

4.3 Development of the plasticity reduction factor for curved plate element

The development of an expression for plasticity reduction factor, which is defined below, is based on a bifurcation in the equilibrium equation, and the assumption that instability of the thin-walled section takes place entirely in the plastic regime. Its formulation will assume also that Poisson's ratio is 0.5, due the incompressibility condition. The plasticity reduction factor is the number by which the critical buckling stress computed for the elastic case must be multiplied to give the critical stress for the plastic case. It can expressed by

$$\overline{\eta} = \frac{\overline{\sigma}_{cr}}{\sigma_{cr}} \tag{4.66}$$

in which σ_{cr} is the elastic critical stress of the same curved plate under axial compression. For the elastic case Redshaw (1938) obtained the following expression for the critical buckling stress

$$\sigma_{cr} = \frac{E}{12(1-\nu^2)}\left(\frac{t}{b}\right)^2\left[2\left(\frac{162}{13}+768\left(\frac{d}{t}\right)^2\right)^{\frac{1}{2}}+\left(\frac{135}{91}\right)(6-7\nu)\right] \tag{4.67}$$

Redshaw states that Equation (4.67) is valid providing the limiting value of the ratio $\frac{d}{t} \leq \frac{\pi^2}{4}\left[\frac{1}{3(1-\nu^2)}\right]^{\frac{1}{2}}$. For the elastic case he assumed $\nu = 0.3$ so $\frac{d}{t} \leq 1.5$ whereas for the plastic case $\frac{d}{t} \leq 1.64$ by assumption that $\nu = 0.5$.

In calculating the plasticity reduction factor the author applies Stowell technique, with the critical stress computed on the assumption of perfect elasticity and with $\nu = 0.5$ instead of $\nu = 0.3$. This gives from Equation (4.67) the solution

$$\sigma_{cr} = \frac{Et^2}{9b^2}\left[2\left(\frac{162}{13} + 768(1.64)^2\right)^{\frac{1}{2}} + \left(\frac{135}{91}\right)\cdot 2.5\right]$$

$$\sigma_{cr} = \frac{Et^2}{9b^2}[94.9] \qquad (4.68)$$

After substituting into Equation (4.66) the inelastic critical stress from Equation (4.65) and the elastic equivalent from Equation (4.68) the plasticity reduction factor is given by

$$\overline{\eta} = \frac{E_s}{E}\left(0.04 + 0.96\sqrt{\frac{1}{4} + \frac{3}{4}\frac{E_t}{E_s}}\right) \qquad (4.69)$$

This new factor will be used in Section 6.3.2 to establish the prediction of inelastic critical load for ε-section.

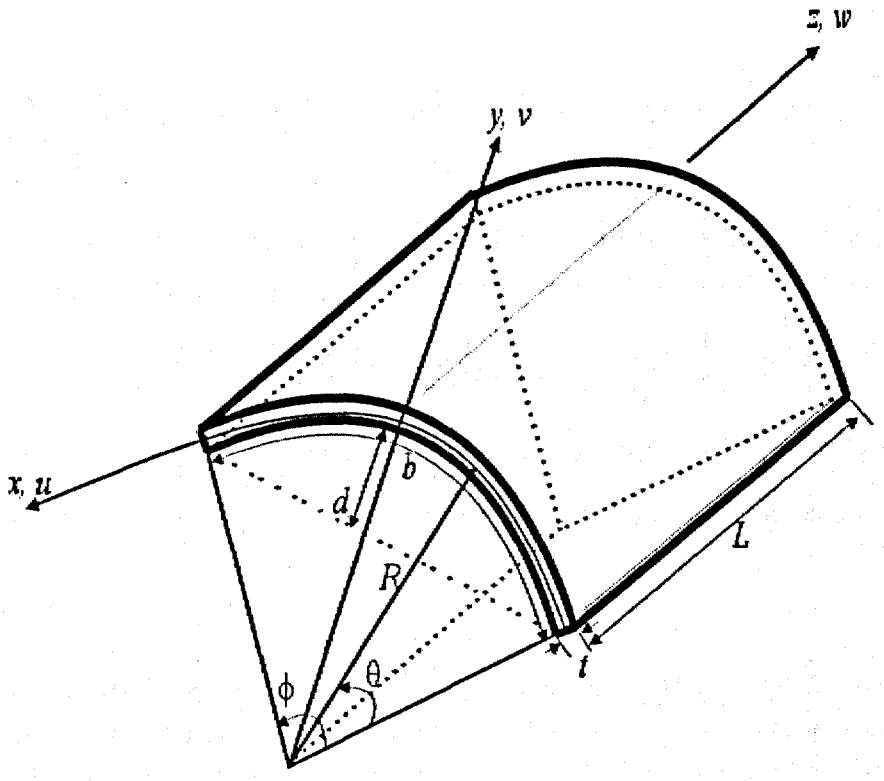

Figure 4.1. Curved plate geometry and displacements components.

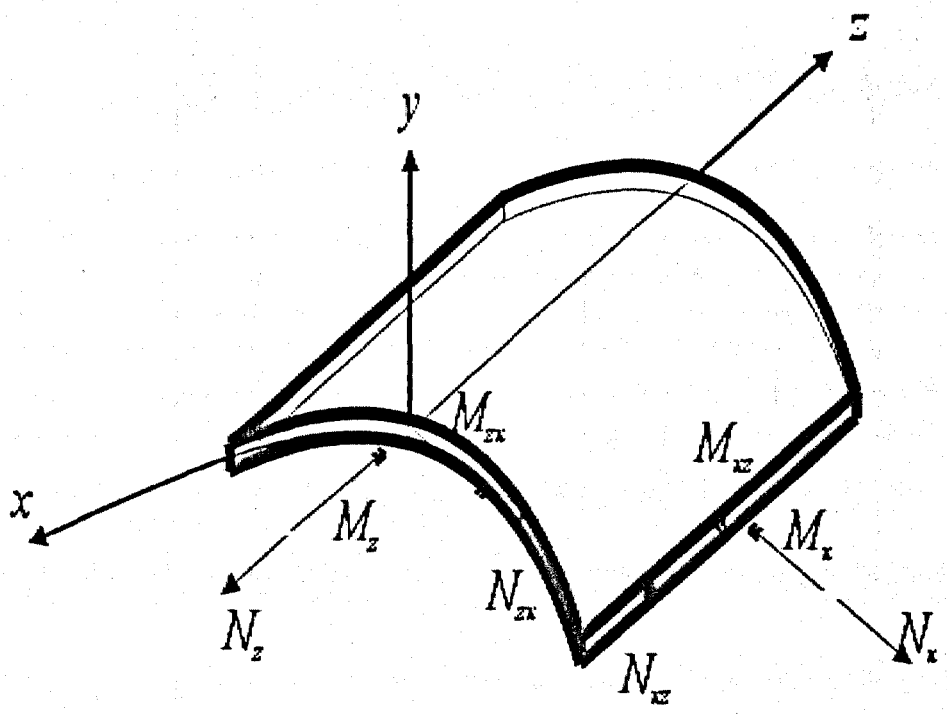

Figure 4.2. Curved plate moment and force intensities.

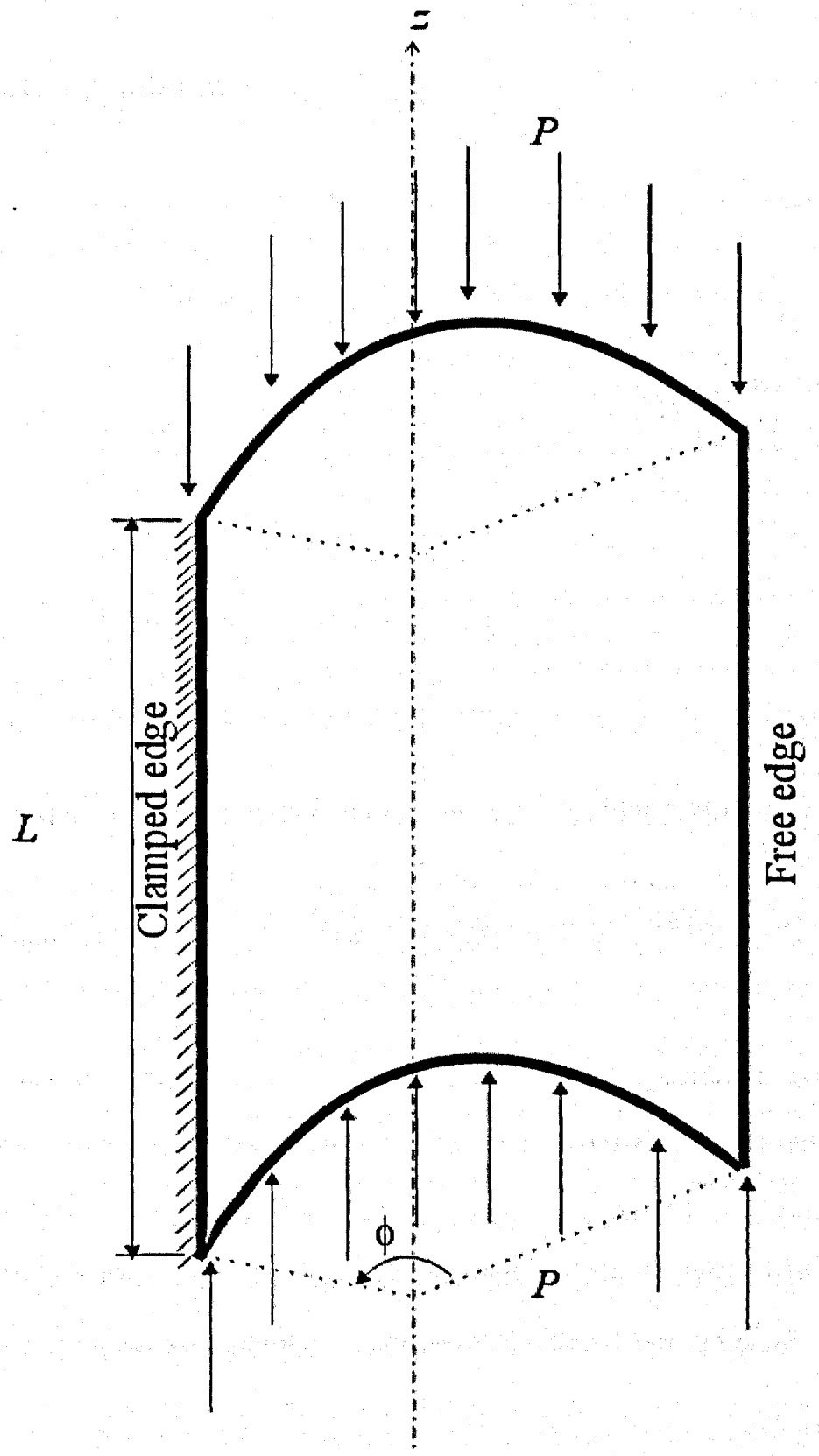

Figure 4.3. Curved plate under axial compression force.

Chapter 5 Experimental Method for Characterisation of Stub and Stud ε-columns

5.1 Introduction

As described in Chapter 3 open cross-section, thin-walled, cold-formed column members have at least three competing modes of buckling failure local, distortional and overall. Although the local and overall flexural modes will be examined by way of physical testing, the main objective of the research is to develop a consistently accurate and practical method of determining the ultimate carrying capacity of ε-section stud columns, which fail by a mode of overall flexural buckling.

The buckling and post-buckling of columns with standard cold-formed shapes has been studied extensively, and key papers reporting experimental investigations are by Azhari, and Bradford (1993), Rasmussen and Trahair (1994), Popovic *et al.* (1999), Cheng *et al.* (2003). Furthermore, design guidance for such shapes are available in national standard codes of practice. However, the provisions contained in part 5 of BS 5950:1998 cannot be directly applied to predict the resistance of ε-shaped columns. The clauses are based on the members comprising flat plate elements, with certain geometric arrangements. Clauses in Section 10 of the same code of practice do allow for the characterisation of any cross-sectioned thin-walled steel component by physical testing. The author will present results from series of full-sized tests in accordance with this section of the British Standard. A total of 62 tests were conducted on ε-columns having the two

wall thicknesses of 1.5 and 2 mm. All ε-sections had the major- and minor-axis dimensions of 100 mm and 43 mm, as shown in Figure 5.1. Tensile coupon testing was conducted on 6 specimens cut from an ε-section to characterise the steel's properties. Stub column tests were conducted on 8 specimens of length 200 mm. six of the short columns were tested without strain gauges and two had strains gauges mounted around the perimeter at mid-height, to investigate the change in strain profile under local failure behaviour. Stud column tests were conducted on 54 long columns specimens at the single column length of 2.7 m, which corresponds to the typical column height in a modular 'picture' frame (see Figure 2.5).

5.2 Tensile coupon tests

Six tensile coupon specimens were prepared in the School of Engineering. The measured specimen dimensions are 1.5 mm thickness by 5 mm width by 50 mm length. Specimens were cut so that their longitudinal axis was parallel to the direction of the final rolling. The specimens were not flatten and so possessed the curvature of the ε-section. The tensile coupon testing is to determine the yield stress, Y_s, tensile strength U_s, initial Young's modulus (E) and the percentage elongation e_u.

Testing was carried out under normal ambient room conditions. Load was applied under stroke control at a constant rate of 3 mm/min, using a 100 kN Testometric testing machine. The machine is a computer-controlled universal materials-testing machine using Testometric's software running under the Windows operating system. Test setups are fully configurable and simply

controlled by using the standard PC serial interface to generate load-stroke plots. The 100 kN load cell is calibrated annually by Central Calibration Services.

5.3 Stub column tests

5.3.1 Introduction

Although thin-walled columns can be susceptible to local buckling at relatively low stress, they do possess post-local-buckling strength, and this property has been thoroughly investigated by Hancock (2003), Schafer (2002), and Ioannidis *et al.* (1999). The post-buckling strength of a concentrically loaded column depends mainly on the slenderness ratio (i.e. the width-to-thickness ratio) of the individual plate elements that form the section's shape. If the slenderness ratio of an element is larger than the corresponding critical slenderness ratio, it will buckle locally prior to yielding, and thus becomes only partially effective. The post-local-buckling strength may be considered by adopting the effective-width concept as introduced by van Karman *et al.* (1932) and given by Equation (3.5). On the other hand if the element is stocky the local buckling may occur at relatively high mean stress levels and the failure is referred to as crippling failure (Singer *et al* 1998).

5.3.2 Preparation of specimens

The eight stub column specimens of 200 mm length were prepared from 1.5 mm thick ε-section at the Market Harborough works of Modula 2000 Ltd., and were delivered, to the Structures Laboratories in the School of Engineering.

Figure 5.2 shows two of the specimens. The specimens are labelled as S1-S8, with S for the stub length situation.

Two of eight specimens S7 and S8 were tested with strain gauges located at different positions, as shown in Figure 5.3. All specimens have been carefully inspected for imperfections and flatness of the end surfaces and it is believed to be within the tolerances of erection criterion (L/1000).

5.3.3 Test procedure

Tests were carried out using 40-ton Amsler universal testing machine, with the flat-ended specimens bearing directly on the rigid loading plates. The type of loading test is a strength test to determine the load-carrying capacity. A photo of the full test rig with specimen S7 is shown in Figure 5.4. In each test, two displacement transducers were used for measuring the relative axial shortening displacement between the rigid base and crosshead and, the mid-height lateral deflections for flexure about the minor axes. A 150 kN (15 tonnes) load cell is used to measure the compressive force. The load cell is placed on a rigid steel base plate of the Amsler machine. The base and top arrangements of the test rig are shown in Figure 5.4. Except for the axial movement of the crosshead there are no other free degrees-of-freedom in the strength test.

Using two steel spreader plates at top and bottom of the specimen ensures the uniform distribution of the applied load. Each of the spreader plates is marked to enable it to either mate with the bearing surface of the load cell at

the bottom or with the crosshead of the Amsler testing machine at the top. To position a stub column relative to the spreader plate's centreline offsets at a predetermined distance from the centreline are drawn onto the spreader plates so that the centroid of the 1.5 mm thick ε-section (see Figure 5.1) is aligned with the centroid of the load cell and testing machine.

5.3.4 Instrumentation

The 15 tonnes load cell was calibrated by Mr Colin Banks (Civil Engineering Technician). To measure displacements, two 25 mm HS25 strain-gauge displacement transducers, supplied by Welwyn Strain Measurement, are used. These can be seen in Figure 5.4. These two transducers are connected to a Solartron 3531D Orion data logger (serial No. 100582, certificate of calibration to the original manufacture's specification) and were calibrated by Mr Banks, using dimensioned gauges from a Mitutoyo MFG Gage block set. The block set has calibration certification to Grade II. 10 mm long strain gauges of post-yield type YL-10 (Tokyo Sokki Kenkujo Co. Ltd.) are placed positioned around specimen to measure the longitudinal direct strains under compression. The sixteen gauges are located as shown in Figure 5.3. It can be seen that gauges Nos 1 to10 are at the mid-length of the specimen and 1 to 8, which were positioned at 1.5 mm apart are there to measure the strain profile in one half of the single-symmetric ε-section. Gauges Nos 9 and 10 are mounted symmetrically about the minor-axis with 4 and 1 and are there to establish how different the strain distribution might be in the two halves. Stain gauges are connected to the Orion data logger.

5.3.5 Loading and measurements

The rate of load application is such that the specimen's behaviour could be considered to be quasi-static. The tests are performed under load control. The load is applied in increments of 5 kN and the test terminated when the column fails. Once the maximum load is attained the specimen is unloaded. Measurements of the compression load, two displacement and strain-gauge readings are taken in real time using a Solartron 3531D Orion data logger. The load is taken to the nearest 0.05 kN, the displacement to the nearest 0.01 mm and strain to ±5 με. Readings are taken after sufficient time, after each load increment, to allow the test specimen to reach what the author considered to be stationary equilibrium. After each increment, the test specimen is carefully examined for signs of excessive deformation, rupture, yielding, local or overall buckling.

5.4 Stud column testing

5.4.1 Introduction

Physical tests are to be conducted, in accordance with Section 10 of BS 5950:1998, on stud columns to determine the axial load capacities of ε-shaped sections, taking into account the influence of restraints afforded by in-service boundary conditions. Presented in this thesis are component test results for 54 stud columns having the two wall thicknesses of 1.5 and 2 mm. All ε-sections had the major- and minor-axis dimensions of 100 mm and 43 mm. Testing was conducted at the single unbraced column length of 2.7 m, which corresponds to the typical column height in a modular 'picture' frame.

5.4.2 Preparation of specimens

The 54 stud-column specimens were prepared at the Market Harborough works of Modula 2000 Ltd., and were delivered, to the Structures Laboratories in the School of Engineering. Specimens were prepared to the engineering drawings given in Figures 5.6 (a) to (e).

Figure 5.1 shows the cross-section of the 100x43x1.5 mm ε-section without stiffener brackets and when the wall thickness is 1.5 mm. Figure 5.7 shows such a plain ε-section with reusable end plates for concentric loading. Modula 2000 Ltd. provided these specific reusable end-plate fixtures that simulate the "real panel" displacement boundary conditions. These plates are 150 mm square and 12 mm thick. The 54 specimens involve nine column types in batches of six specimens. The six specimens are numbered from 1 to 6. Figures 5.6(a) to (e) show the nine column-type differences. The six types with labels WU104 to WU109 (where pair of labels are given, for example WU104 + WU105, the first is for the ε-section of 1.5 mm wall thickness and the second is for the higher thickness of 2.0 mm) have three different intermediate bracing stiffener/bracket arrangements, for the two ε-section wall thicknesses. All six types have at the top and the bottom, a 300 mm long stiffener bracket. Details are given in Figures 5.6(a) to (c).

This series of 54 tests also involved three column types (WU110 to WU112) where the open ε-section is fully enclosed. Details of the three column types with a closed cross-section are shown in Figures 5.6(d) and (e). For types WU110 and WU111 the ε-section is enclosed with curved close fitting plates

(labelled stiffener brackets in Figure 5.6(d)) of CR4 grade steel, having 110 mm arc length and 1.5 mm thickness. In type WU112 the continuous enclosure (Figure 5.6(e)) is by a 100x40x1.5 mm^3 C-section of S350 grade steel.

The stiffener and bracing brackets, curved enclosure plates and the C-section are connected to the ε-section using 6x15 mm^2 MIG plug welds, which are spaced every 255 mm. However, when a stiffener is butted against a stiffener or bracket the centre-to-centre spacing of the plug welds is lower at 50 mm.

Using CAD software Peter Dann Ltd. have calculated the nominal sectional properties for the five column cross-sections, ignoring the discontinuous brackets and stiffeners in columns WU104 to WU109. Table 5.1 presents the column height (L), and the sectional properties of the cross-sectional area (A), the second moment of area about the major axis (I_x), the second moment of area about the minor-axis (I_y), the minor axis radius of gyration (r_y). In the last column the slenderness ratio (λ) is given, for an effective length L_E = 1.0L. Table 5.2 presents mechanical properties to the CR4 and S350 grade of steel from Table 31 of EN 10147: 2000.

To check the magnitude of the initial geometrical imperfection due to minor-axis out-of-straightness, measurements of geometry were conducted on specimens chosen randomly. This was done by laying a specimen down on a flat steel table and taking, at 100 mm intervals along the specimen's 2.7 m

length, relative height measurements using a dial gauge reading to 0.01 mm. The measured camber is found to be negligible, ranging from 0.0 to a maximum of 0.6 mm, or $L/4500$. Note that a practical erection criterion for structural steelwork is that a column is allowed a 'lack of straightness' tolerance of $L/1000$. The stud ε-columns of types WU104 to WU112 therefore surpass this erection criterion and for practical proposes they can be considered to be straight members.

Table 5.1. Geometric properties of stud column ε-sections.

Stud column type (1)	Length, L (mm) (2)	Thickness, t (mm) (3)	Area, A (mm^2) (4)	I_x 10^4 (mm^4) (5)	I_y 10^4 (mm^4) (6)	Radius of gyration ($r_y = \sqrt{I_y/A}$) (7)	Slendern -ess ratio ($\lambda = L/r$) (8)
WU104	2700	2.00	436	61.3	9.61	14.9	182
WU105	2700	1.50	330	39.2	7.47	15.1	179
WU110	2700	2.00	627	73.4	15.8	15.9	170
WU111	2700	1.50	520	61.2	13.2	15.9	170
WU112	2700	2.00	717	97.7	18.6	16.1	168

Table 5.2. Nominal steel mechanical properties.

Steel grade EN 10147: 2000 (1)	Modulus of elasticity E (kN/mm^2) (2)	Yield strength Y_s (N/mm^2) (3)	Ultimate tensile Us strength (N/mm^2) (4)	Ultimate elongation (mm) (5)
CR4	174	205	326	36
S350	205	350	420	--

5.4.3 Test procedure

The test procedure is in accordance with Section 10 "*Loading Tests*" in BS 5950:1998 part 5. The type of loading test is a component test to determine the load-carrying capacity (see Clause 10.7). Herein the failure criterion for

the test is based on the specimen having a minor-axis or major-axis mid-height (maximum) lateral displacement of 9 mm (i.e. column height/300). For the column types tested the limiting deflection is always that due to minor-axis flexure.

A sketch of the full test rig is shown in Figure 5.8(a). In each test, three displacements are measured. These are the axial shortening (in z-direction) and, at mid-height, the lateral deflections for column flexure about the major and minor axes (in the x- and y-directions, respectively). In Figure 5.8(a) the positive directions for the three orthogonal displacements are defined. The photograph in Figure 5.8(b) shows a specimen with the two orthogonal displacement transducers placed at mid-height. With respect to Figure 5.8(a), the image in Figure 5.8(b) is taken on the other side of the column. The author uses a 120 kN (12 tonnes) load cell. The base plate for locating the load cell is placed on the concrete strong floor without any bedding material to 'pack-out' gaps. The base and top arrangements to the test rig are shown in Figures 5.7, 5.10 and 5.11. Except for the axial movement of the jack there are no other free degrees-of-freedom in the strength test.

To transfer load into a column Figures 5.10 and 5.11 show that there are two steel spreader plates at top and bottom connected to the reusable end plates shown in Figure 5.7. The four mating plates have squared sides of 150 mm and a thickness of 15 mm. Close to the corners there are four 18 mm diameter holes, for connecting bolts of M12 size. A spreader plate has a recess that allows it to either mate with the bearing surface of the load cell at

the bottom or with the hydraulic jack at the top. To position a specimen relative to the spreader plates there are the two reusable end plates, which have similar dimensions and corner holes. These are shown in Figure 5.7. Welded to the end plates are two circular tubes of 35 mm diameter and 65 mm height. They are positioned at equidistance from the plate's centre and are fabricated to slot directly into the ε-section. On assembling a spreader plate and end plate there is slack available in this loading fixture, via the four corner bolt holes (see Figure 5.10), to facilitate the adjustment of the specimen's vertical positioning that will align the load path for concentric loading. To connect the lower loading fixture to the load cell there is a hole of 8 mm diameter in the spreader plate that mates with a central boss on the load cell. Depending on the column type, this hole is offset at a predetermined distance from the top plate's centreline so that the centroid of the non-symmetry ε-column is aligned with the centroid of the load cell.

Using a plumb line the centre of the load cell and centre of the jack's piston are aligned and the bolts on the test rig are tightened to securely fix them in position. A specimen is then slotted over the tubes of the load transfer fixtures and by careful positioning of the column; the line-of-action of the compression load can be located through the nominal centroid axis of the ε-column specimen.

5.4.4 Instrumentation

The 12 tonne load cell was calibrated by Mr Colin Banks (Civil Engineering Technician) using a 100 kN Testometric testing machine (UKAS certificate of

calibration No. 05960 issued by Central Calibration). To measure the column's displacements, as shown in Figure 5.8(a), three 25 mm HS25 strain-gauge displacement transducers, supplied by Welwyn Strain Measurement, are used. These can be seen in Figures 5.8(b) and 5.11. One gauge measured the axial shortening displacement, and the other two measured the mid-height minor-axis lateral deflections.

Four strain gauges are mounted within the upper quarter length of the column for obtaining the point of zero curvature and hence the actual column effective length for stud columns. Two specimens of type WU104 were tested with strain-gauge type FLA-6 (Tokyo Sokki Kenkujo Co. Ltd.), while the remaining 50 specimens were without.

The three transducers and the four strain gauges are connected to the Orion data logger.

5.4.5 Loading sequence

The rate of load application is such that the specimen's behaviour could be considered to be quasi-static. The tests are performed under stroke control. Initially, load is applied in increments of 5 kN. When the minor axis lateral deflection is observed to be tending towards 9 mm the control of the increasing load is established by controlling the next increment of the higher lateral deflection. Once the maximum load is attained the specimen is unloaded.

5.4.6 Measurements

Measurements of the compression load, the three displacements and the four strain-gauge readings are taken in real time using the Orion data logger. The load is taken to the nearest 0.05 kN and the displacement to the nearest 0.01 mm. Readings are taken after sufficient time, after each load increment, to allow the test specimen to reach, what the author considered to be stationary equilibrium.

After each increment, the test specimen is carefully examined for signs of excessive deformation, rupture, yielding, local or overall buckling.

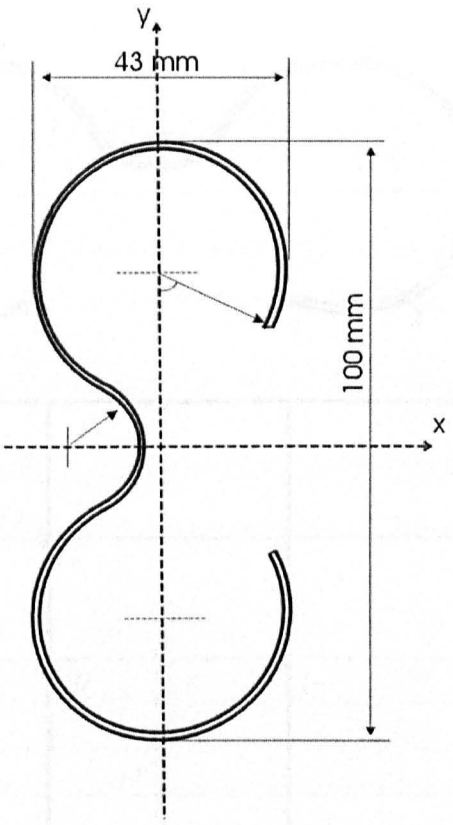

Figure 5.1. Cross-section of ε-column with the major axis (x-x) the horizontal plane through the centre of the cross-section.

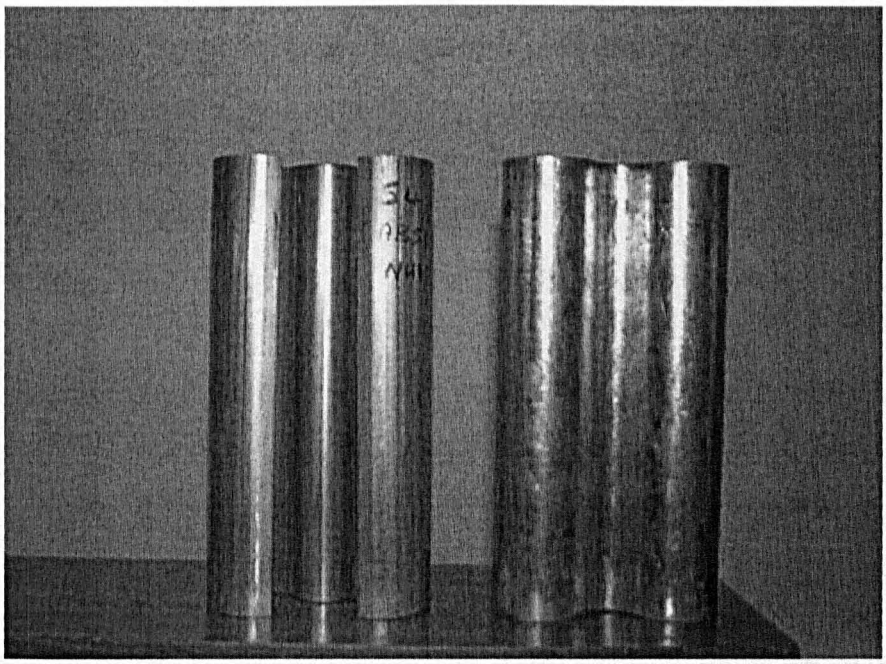

Figure 5.2. Stub column specimens.

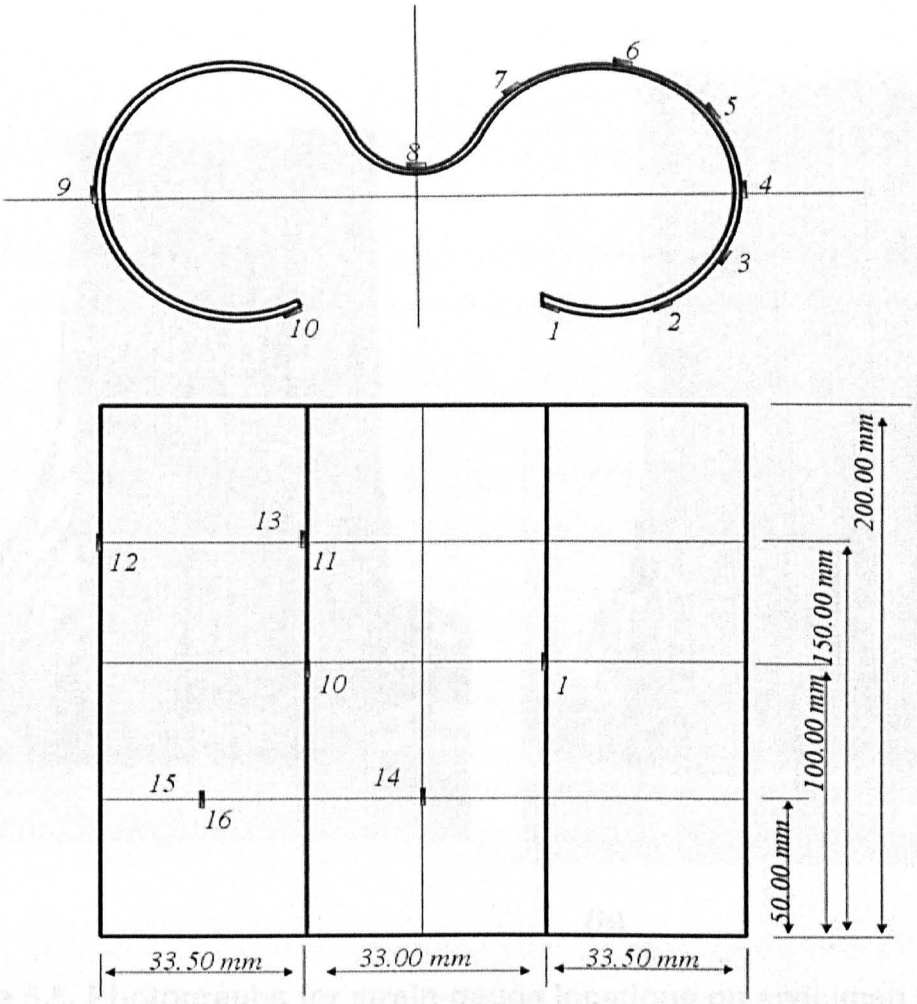

Figure 5.3. Strain gauges locations on specimens S7 and S8.

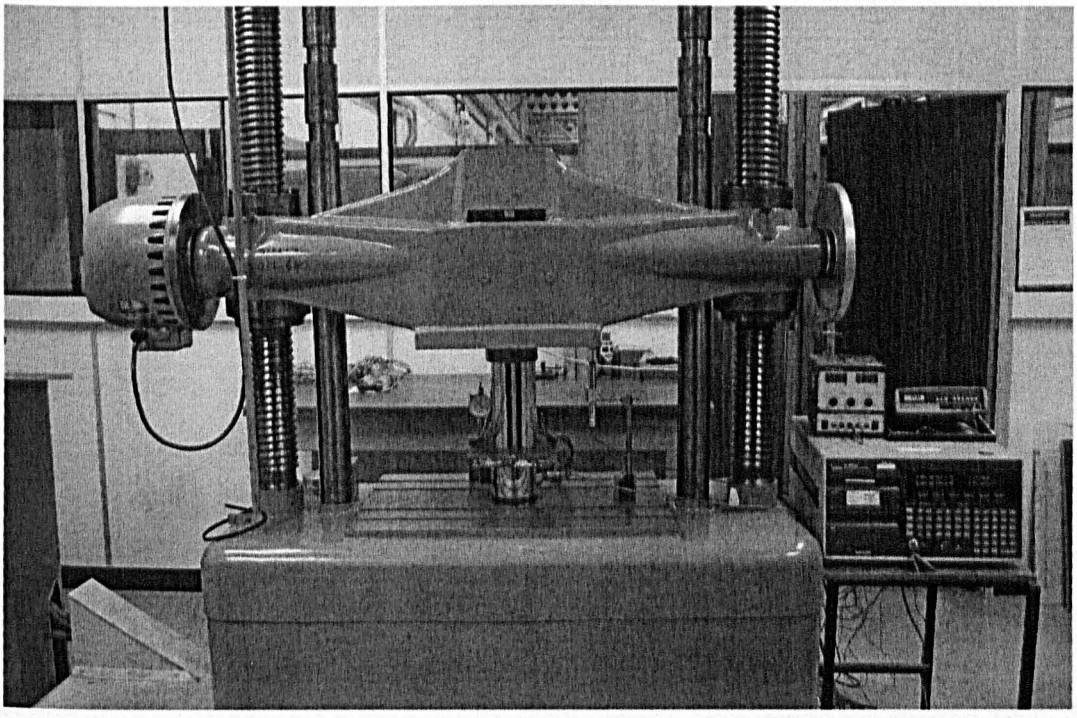

Figure 5.4. Local buckling test arrangement with specimen S7.

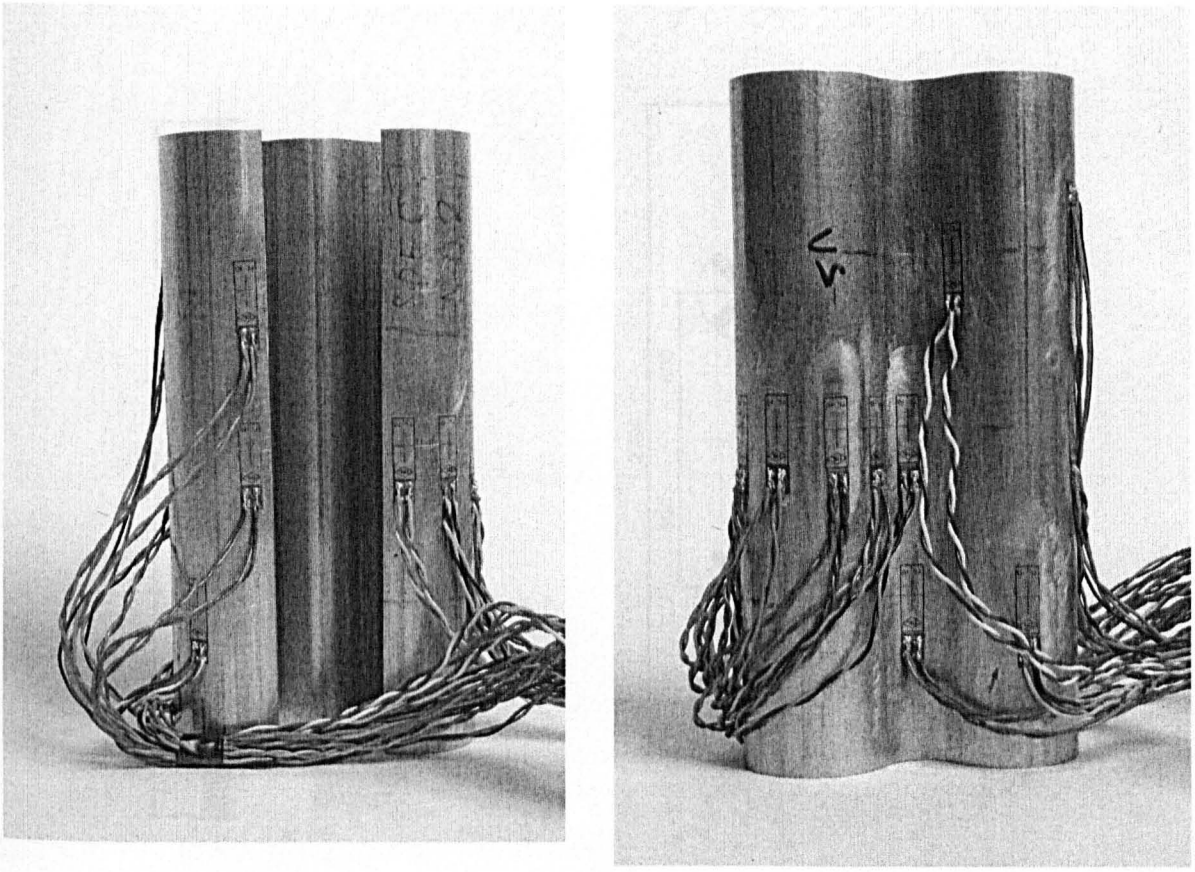

(a) (b)

Figure 5.5. Photographs for strain-gauge locations on specimen S7 (a) front view, (b) back view.

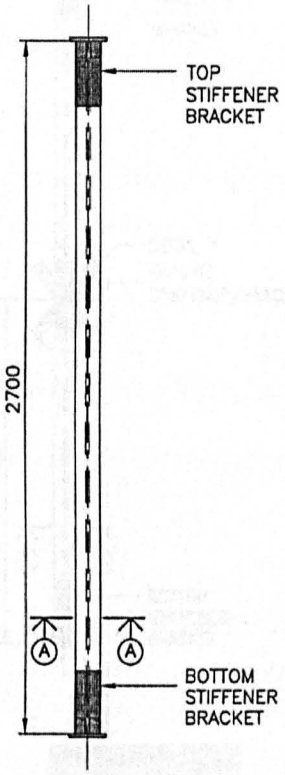

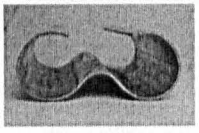

SECTION A-A

(a)

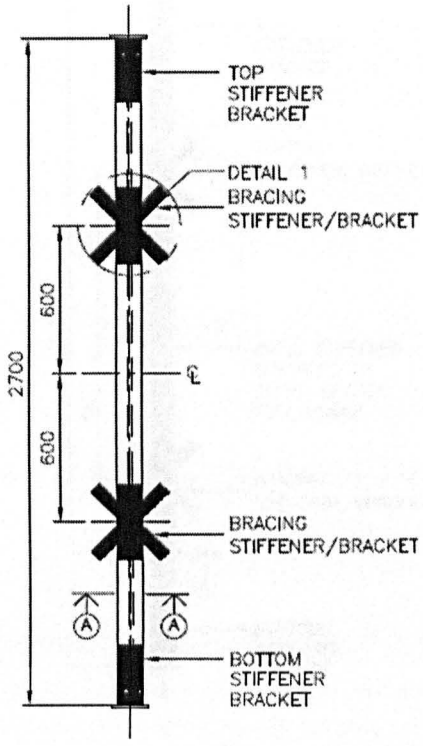

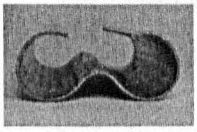

SECTION A-A

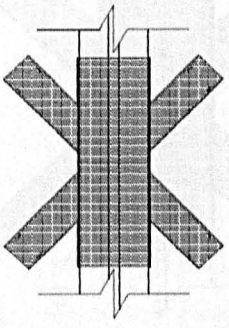

DETAIL 1

(b)

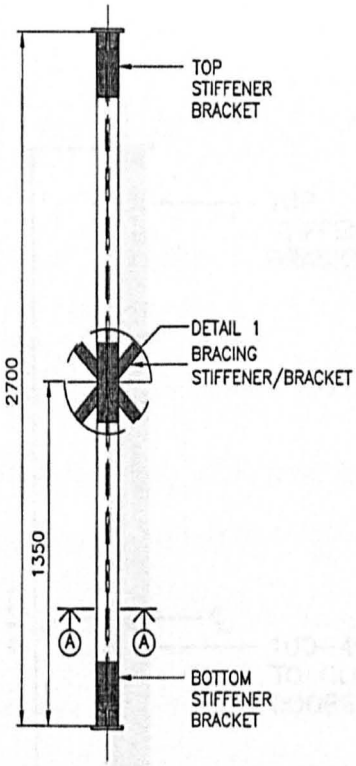

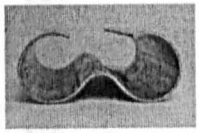

SECTION A-A

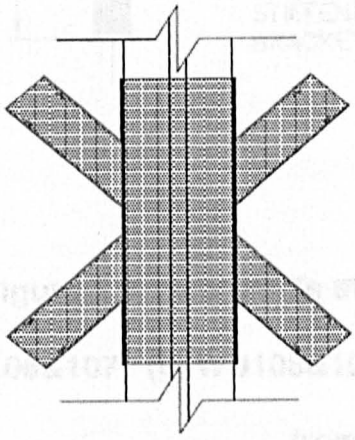

DETAIL 1

(c)

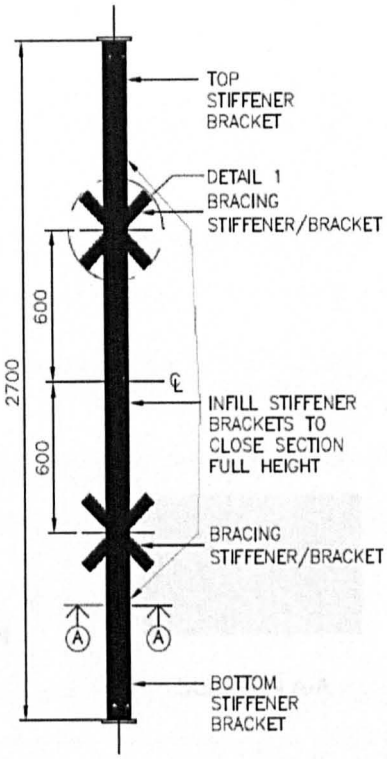

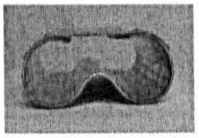

SECTION A-A

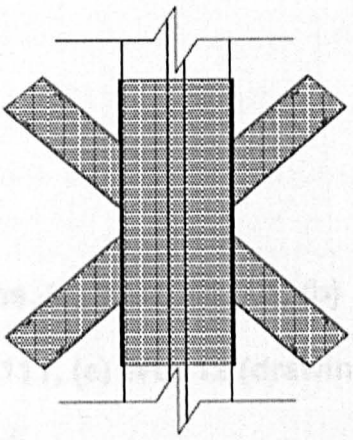

DETAIL 1

(d)

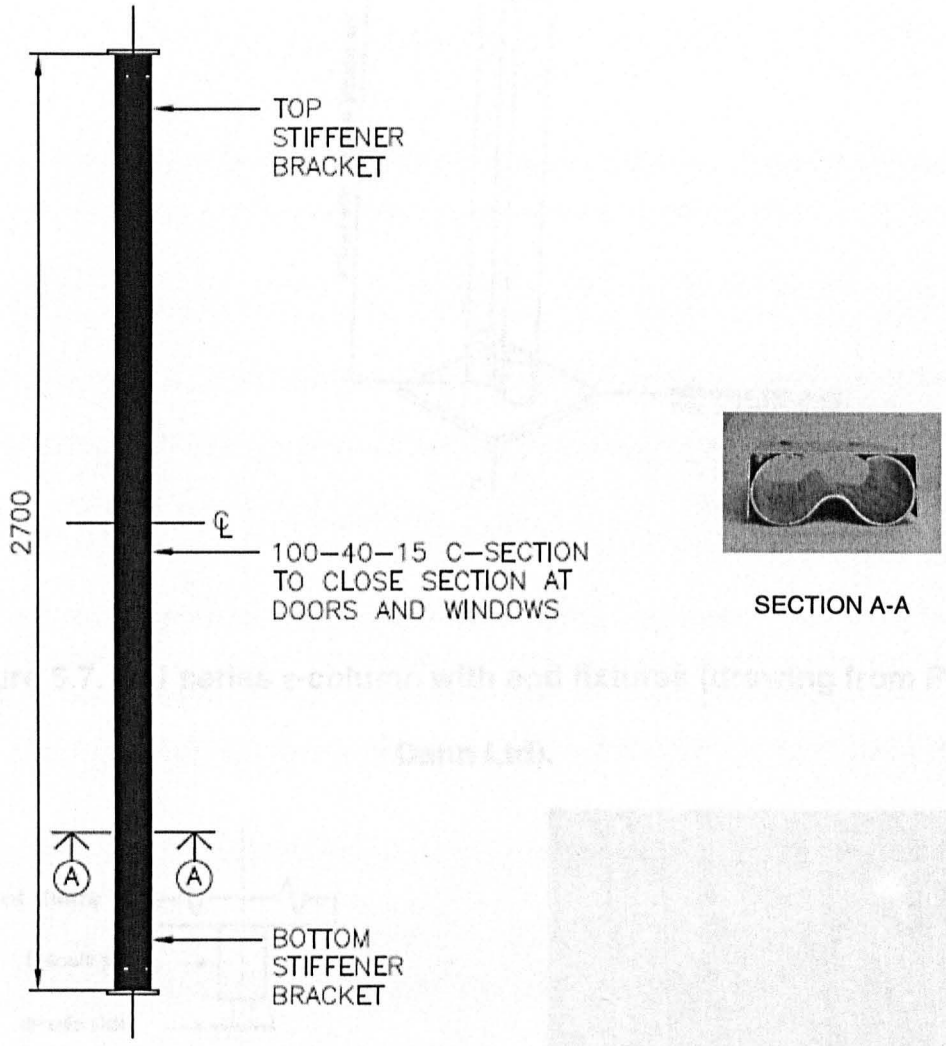

(e)

Figure 5.6. ε-column's stiffener locations, (a) WU104&105, (b) WU106&107, (c) WU108&109, (d) WU110&111, (e) WU112 (drawings from Peter Dann Ltd).

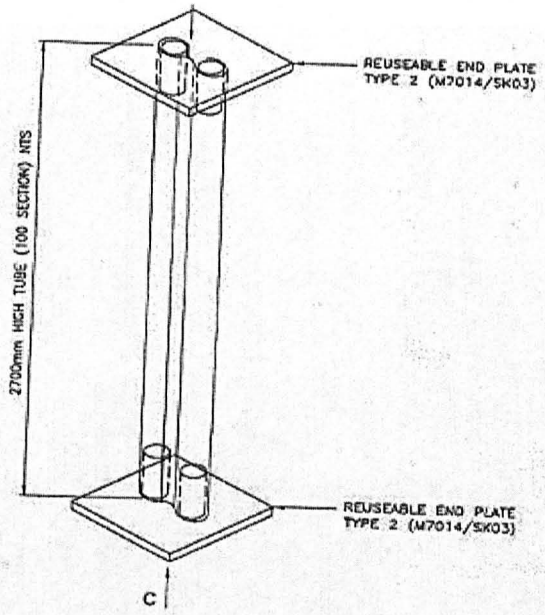

Figure 5.7. WU series ε-column with end fixtures (drawing from Peter Dann Ltd).

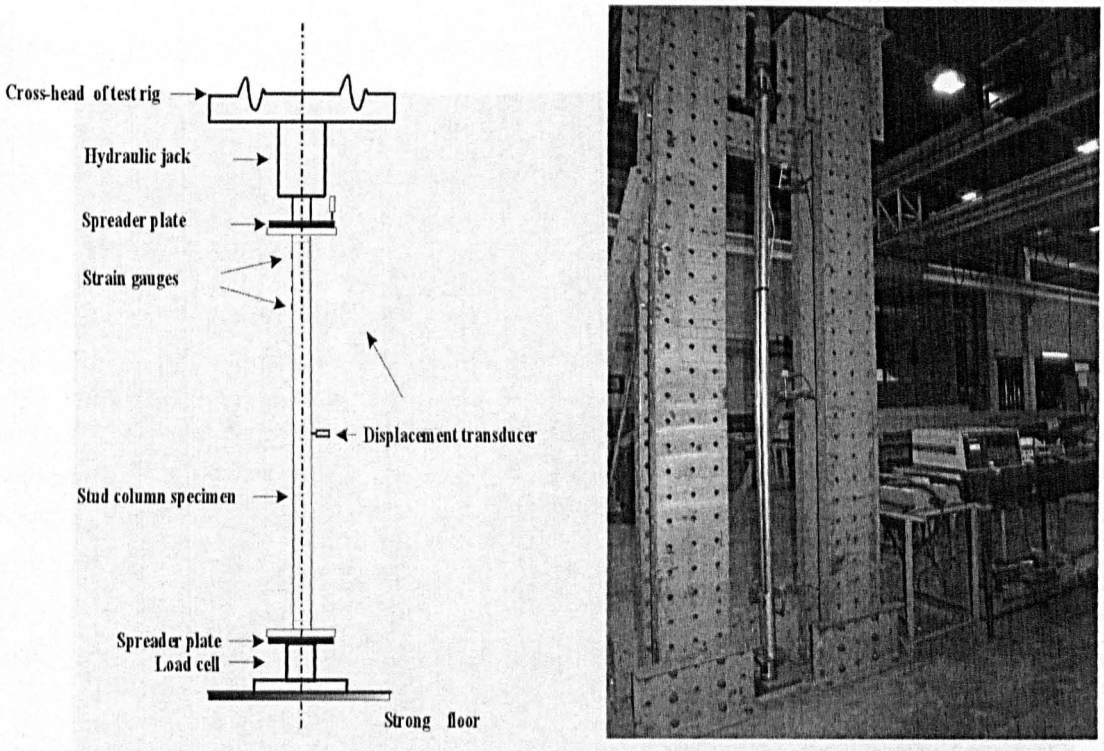

(a) (b)

Figure 5.8.Test rig, (a) Schematic of test rig, (b) Test rig with 2.7 m stud column ready for testing.

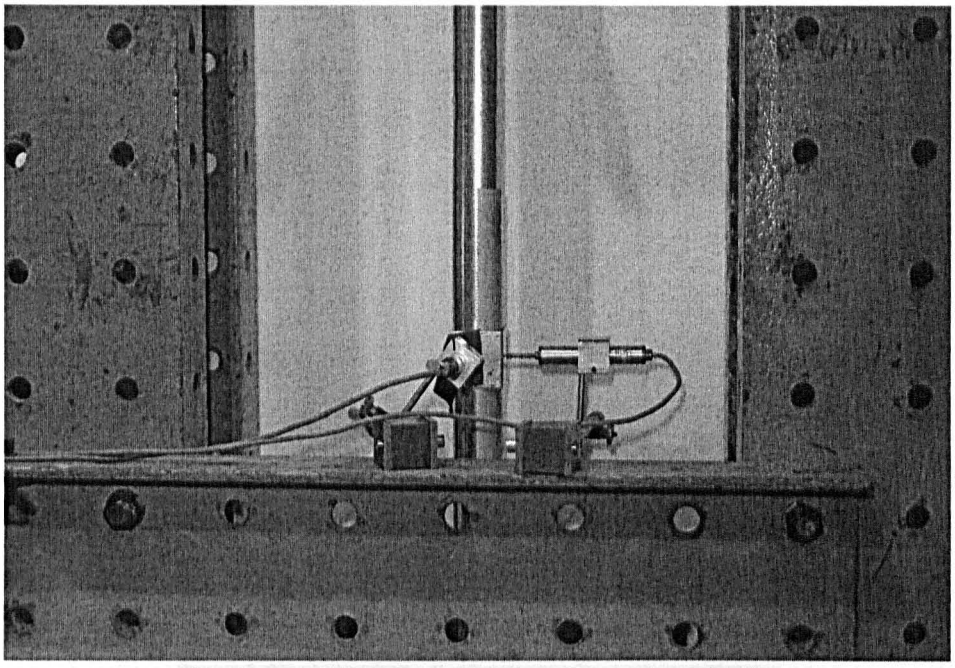

Figure 5.9. Displacement transducers at mid-length to measure lateral deflection in the major x- and minor z-direction.

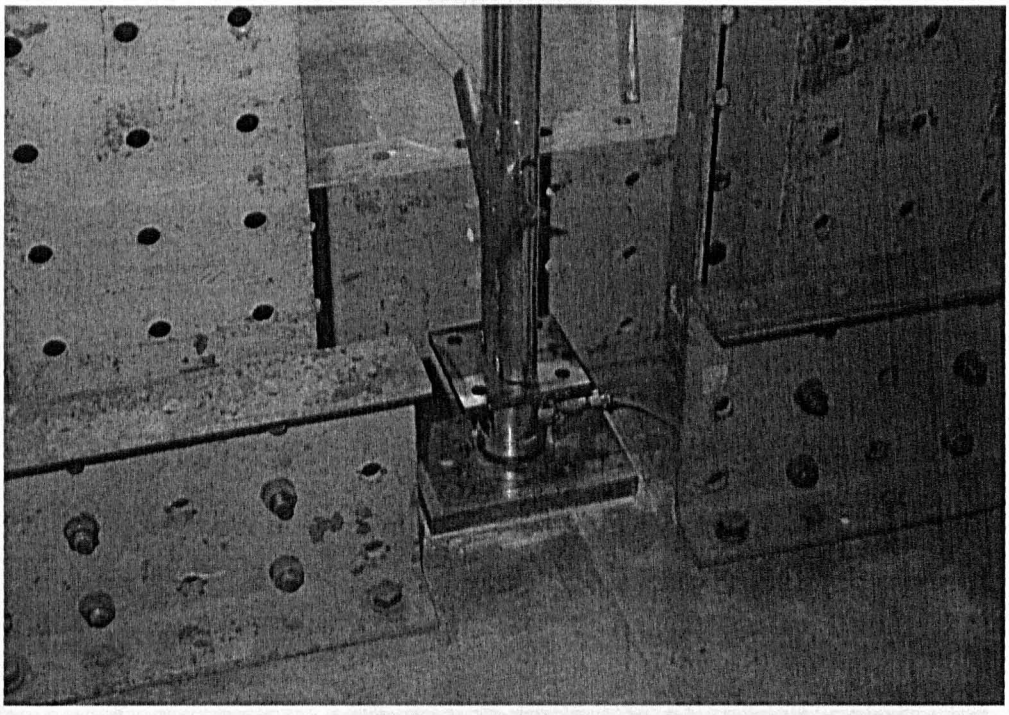

Figure 5.10. Base fixture and 120 kN load cell.

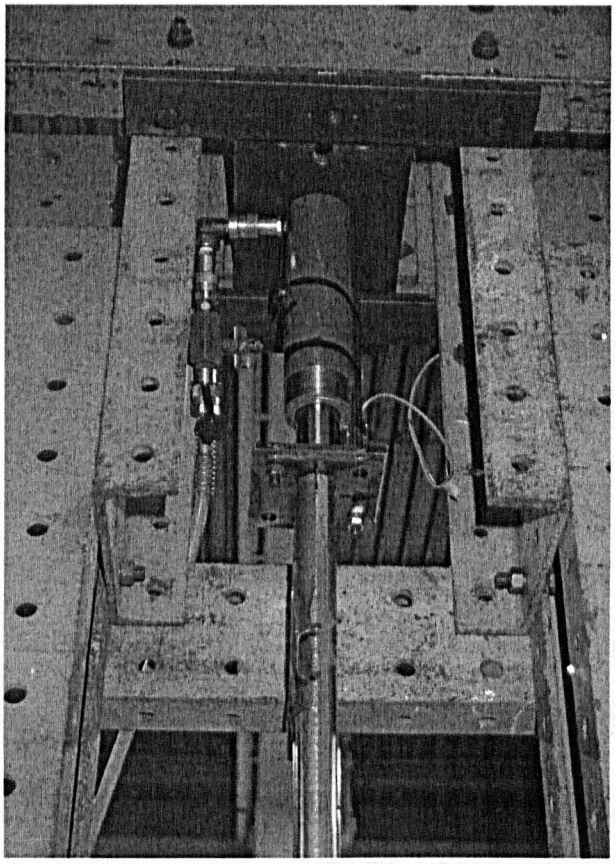

Figure 5.11. Top fixture, load jack and axial displacement transducer.

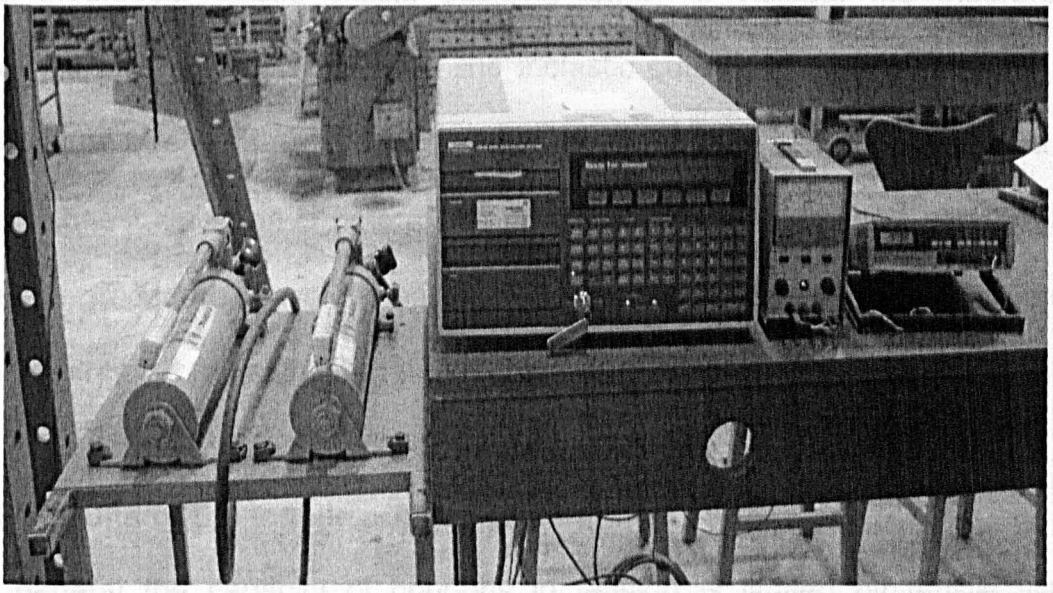

Figure 5.12. Hydraulic Jacks and data logger.

Chapter 6 Stub Column Study with 1.5 mm thick ε-section

6.1 Introduction

A number of axial compression tests were carried out on short "stub" columns of the 1.5 mm thick ε-section to determine its load distribution and resistance at failure. To characterise the steel material a small series of tensile coupon tests were performed to determine the actual mechanical properties, after the ε-section had been shaped by the cold-forming process. The results of the tensile coupon tests are used to determine the yield stress, Y_s, the 0.2% proof stress, $\sigma_{0.2}$, the ultimate tensile strength, U_s, the initial Young's modulus (E), the secant modulus (E_s), and the tangent modulus (E_t). These mechanical properties were required by the author to obtain, using the stub-column test results and theory in Chapter 4, the ε-section's plasticity reduction factor. This new plasticity reduction factor is needed to get a value for the theoretical inelastic critical buckling load multiplying it by the value of the theoretical elastic critical buckling load. To validate the theoretical findings experimental values for the inelastic critical stress are used. From the failure stress established by way of the experiments the effective area of the thinnest ε-section is determined. This effective area is to be used in the design procedure, development from Section 6 of BS5950-5:1998, for stud columns of 2.7 m height.

6.2 Results of the tensile coupon tests

In general the capacity of coupons in tension is limited by tensile yield strength, Y_s, or ultimate strength, U_s. To investigate the buckling resistance of

the stub columns it is necessary to know the strengths and moduli of elasticity of the cold-formed steel. This will ensure that representative material property values can be used in Section 6.3.2, which will present the theoretical derivations for the inelastic critical buckling stress. A total of 6 specimens were tested under axial tension using the test set-up and test procedure detailed in Section 5.2

A typical stress v strain relationship is plotted in Figure 6.1. It was obtained from loading a coupon of only 5 mm width because it is cut from a ε-section with continuous curvature. In the figure the solid line curve is the average curve from the results of six specimens. As can be seen from the average curve the cold-formed steel may be assumed to behave in a perfect linear elastic behaviour, up to the point of first yield, at a stress of 355 N/mm^2. Before this first yield point the material's response to direct stress can be determined using elastic theory. This is not valid once the specimen yields and the steel undergoes plastic deformation and strain hardening. When the yielding of a material shows an absence of a sharply defined yield point, there is the need for design to define an equivalent yield point. The generally accepted approach is to adopt the stress at 0.2% plastic strain, i.e. the 0.2% proof stress. From the average curve in Figure 6.1 the value of $\sigma_{0.2}$, is determined to be 490 N/mm^2. As is well known, the Young's modulus is obtained from the stress v strain relationship by estimating an initial gradient to the elastic portion of the stress-strain curve. From the average specimen curve in Figure 6.1 the estimated average value of the Young's modulus is

204 GPa (or kN/mm^2) (with Standard Deviation (SD) of 16.1) and (Coefficient of Variation (CoV) of 7.9%).

For the author's theoretical study to follow in Section 6.3.2, the material behaviour, beyond the elastic range, can be represented by the model derived by Ramberg and Osgood (1943). Their model gives the following expression to the shape of the stress-strain curve in the strain-hardening region.

$$\varepsilon = \frac{\sigma}{E} + \varepsilon_p \left(\frac{\sigma}{\sigma_p} \right)^n \tag{6.1}$$

In Equation (6.1) the variables ε_p and σ_p are the proof strain and proof stress, typically the stress taken at 0.2% strain, and constant n defines the shape of the curve at its knee, with a value of 25 being typical for a cold-formed structural grade steel (Bradford 1994). After substitution in Equation (6.1) for $\varepsilon_p = 0.002$ and $n = 25$, the Ramberg and Osgood expression becomes

$$\varepsilon = \frac{\sigma}{E} + 0.002 \left(\frac{\sigma}{\sigma_p} \right)^{25} \tag{6.2}$$

In Table 6.1 the nominal and experimental average values of the mechanical properties are presented in columns 1 to 7. To show the difference between nominal and measured values columns 8 to 10 give property ratios. The closer to 1 these ratios the close the two values are. The nominal values are taken from Table 31 of EN 10147: 2000 and are those recommended to be used in design, if the actual characteristic values for the steel are unknown. The data in the table show that there is a very good agreement between the nominal and coupon values for the yield strength and the modulus of

elasticity. In the case of the ultimate tensile strength the coupon value is about 30% higher, and this, following Yu (1973), may be attributed to a strength enhancement from the cold-forming process.

The experimental results in Table 6.1 were used in Equation (6.2) to create the semi-empirical stress-strain curve given in Figure 6.1 by the dashed line. The two curves in the figure show that the Ramberg and Osgood expression can be used to describe the steel's response to tensile stress, in a very reasonable manner. By assuming the same outcome if the stress is compressive we can use Equation (6.2) to establish the prediction of the tangent modulus.

Table 6.1 Mechanical properties to the steel in the ε-section of 1.5 mm thick

Nominal values taken from EN 10147: 2000			Average experimental values from coupon tests				Property ratios		
1	2	3	4	5	6	7	8	9	10
Y_{snom} N/mm^2	$U_{s.nom}$ N/mm^2	E_{nom} kN/mm^2	Y_s N/mm^2	$\sigma_{0.2}$ N/mm^2	U_s N/mm^2	E kN/mm^2	$\frac{Y_s}{Y_{s.nom}}$	$\frac{U_s}{U_{s.nom}}$	$\frac{E}{E_{nom}}$
350	420	205	355	490	546	204	1.01	1.3	0.99

In order to evaluate the plasticity reduction factor, for the ε-section, it is necessary to have values to the other two moduli of elasticity. The tangent modulus, E_t, which is the slope of the tangent to the stress-strain curve at any value of stress (Giroud 1994), is obtained on differentiating the Ramberg and Osgood expression. So from Equation (6.2) we obtain

$$E_t = \frac{d\sigma}{d\varepsilon} = \frac{Y_s E}{Y_s + 0.002En\left(\frac{\sigma}{Y_s}\right)^{n-1}} \tag{6.3}$$

The secant modulus, which is the gradient of the straight line between a point under consideration and the origin, is simply obtained from

$$E_s = \frac{\sigma}{\varepsilon} \tag{6.4}$$

where in Equation (6.4) σ and ε are the stress and strain at any point along the stress-strain curve (see Figure 6.1).

Table 6.2 presents these moduli at different stress levels on using Equations (6.1), (6.3) and (6.4). The four stress levels are given in column 1 of the table. Up to the first yield point level, at 355 N/mm^2, the secant and tangent modulus can be assumed to be equivalent to the Young's Modulus of elasticity, whose value is in column 2. Beyond this stress level the secant and tangent modulus values in columns 3 and 4 in Table 6.2 can be seen to reduce, increasingly so as the stress approaches U_s.

Table 6.2: Moduli of steel determined at different stress levels

1	2	3	4
σ (N/mm^2)	E (kN/mm^2)	E_s (kN/mm^2)	E_t (kN/mm^2)
355 (Y_s)	204	204	204
418	------	200	140
447	------	187	61.9
470 (U_s)	------	157	23.6
490	------	111	9.35

6.3 Analysis of stub column testing

Thin-walled members under compression are liable to encounter geometrical instability as they may develop a failure mode either by local elastic buckling or by a local plastic mechanism. Both of these local modes must be considered when determining the member's behaviour (Mahendran 1997). There are different scenarios that can be used in estimating the ultimate resistance of stub columns. Murray (1984) used the method of intersection of elastic and rigid plastic curves to estimate the ultimate load. His rigid-plastic curve was based on the observed local plastic mechanism, whilst the elastic curve was developed from simple elastic analysis. The method favoured by Parks and Yu (1989) uses the tangent modulus approach to theoretically predict the inelastic buckling of a curved plate element, which is curved only in the plane normal to the direction of axial compression. For the purpose of determining the ultimate load capacity of the ε-section short column the effective modulus approach is adopted by the author. A total of 8 specimens were tested under axial compression using the test set-up and test procedure detailed in Section 5.3.

Figure 6.2 shows an axial shortening versus compression load curve for a 1.5 mm thick ε-section stub column of height 200 mm. By examining the response of the 8 specimens tested it can be observed that they failed at mean uniform stress level of 344 N/mm^2. This corresponds to a load of 113.5 kN, and is where the experimental curve in Figure 6.2 begins to depart from the elastic curve, given by ($\delta = \frac{\sigma_i \cdot L}{E}$). This point on the curve may be considered as the point where the steel first reaches yield. By referring to

Figure 6.1 for the coupon testing, the yield stress of the actual steel is 355 N/mm^2. It is therefore found that there is a good agreement with the average stub-column value at onset of yielding.

Departure from an elastic behaviour increases with increased loading, until the column's resistance reaches a maximum load of 147 kN (with Standard Deviation (SD) of 2.8) and (Coefficient of Variation (CoV) of 1.9%). This ultimate state is equivalent to an average stress of 447 N/mm^2, which is assumed to be constant over the 330 mm^2 cross-sectional area of the ε-section. Compared to the U_s of 546 N/mm from coupon testing, the stub-columns have an ultimate failure strength that is 22% lower. This may be interpreted as the stub columns experiencing failure by inelastic instability, rather than by material crushing. Elastic theory is able to predict the stress level, up to the point of first yield, and can be used to define the load at which the yield initiates. And as can be observed from the mean curve in Figure 6.2 the stub columns possess 30% extra post-yield strength.

Typical readings from a longitudinal strain gauge No 8 of specimen S7 with load are given as diamond symbols in Figure 6.3. This reflects the similar stub-column behaviour, during a strength test, as shown in Figure 6.2 for the axial shortening response.

Figures 6.4(a) to 6.4(h) show a post-test photograph for each of the 8 stub columns. It is evident from these photos that all specimens experience failure by localised buckling phenomena. A localised buckling mode is known to be

a first interaction mode, which may occur prior to the overall buckling of the member. Once a localised buckling pattern occurs, the short column's post-buckling behaviour is characterised by large local out-of-the-plane displacements with the steel deforming in the inelastic range. This response of the thin-walled ε-section produces plastic folding, and the member ultimately fails by a plastic mechanism. Such behaviour can be seen in the severely deformed configurations of the 8 stub columns in Figures 6.4(a) to 6.4(h). This post-buckling deformation has been found by Ungureanu and Dubina (2004) to be specific to cold-formed steel stub columns.

Figure 6.5 shows the variation in strain profiles around the outer side of specimen S7, at mid-height, and at the compressive stress levels of 170, 344, 418 and 447 N/mm^2. Due to the symmetry in the ε-section about the major axis, only half of it is considered in creating the plot in Figure 6.5. The location of the eight strain gauges is shown in Figure 6.6. As can be seen in the figure, the strain profile will show a fairly constant compressive stress over the cross-sectional area, while this stress does not exceed 344 N/mm^2. But when the load increases the average compressive stress to 418 N/mm^2 there is a noticeable change in shape of the strain profile, indicating the initiation of local inelastic buckling. This change from the uniform profile continues to gradually increase and reaches a maximum at a stress level of 447 N/mm^2. This state indicates the specimen has now lost complete stability, and it can be assumed that this stress is that for the resistance of the stub column.

A flat thin-walled plate element under edge compression buckles in such way that there can be only one half-wave in the perpendicular direction and several half-waves in the direction of compression (Timoshenko and Gere 1961). Figure 6.5 clearly shows the strain profile for the ε-section having a buckling shape of two-and-half half-wavelengths. Based on this observed failure mechanism regime we can for this analysis consider the ε-section to consist of two outer flanges and central web as shown in Figure 6.7. The author observes from the strain profiles in Figure 6.5 that, in the direction perpendicular to the applied load, each of the "flanges" buckles in one half-wavelength and the "web" into three half-wavelengths.

6.3.1 Plasticity reduction factor, $\overline{\eta}$, for curved element

When instability in the section initiates at a compressive stress above the elastic range we know that elastic theory can no longer be used to predict the critical buckling load. Stowell (1948) proposed a method for handling this situation by retaining the formula derived for the elastic situation and finding an effective, or reduced modulus of elasticity that gave the correct prediction for the inelastic situation when inserted into these formulae. The author in Section 4.3 adopts this approach for developing the new expression of plasticity reduction factor, $\overline{\eta}$, Equation (4.69), that can be linked directly to the flange element in the curved ε-section.

By using the steel's mechanical properties listed in Table 6.2 $\overline{\eta}$ is computed for the ε-section of 1.5 mm wall thickness. Figure 6.8 presents the characteristic for $\overline{\eta}$ as a function of compressive stress. It is noted that,

when the critical stress is equal or lower than the yield stress (Y_s = 355 N/mm^2), the value of $\overline{\eta}$ is 1.0, and the failure is governed by the elastic critical buckling stress that can be obtained from applying elastic theory. As long as the critical stress exceeds the yield value, the plasticity reduction factor is found to decrease, approaching zero limit as the critical stress tends towards the ultimate strength for the steel. This later state may be interpreted as the material strength governing failure when the critical stress approaches U_s. Between the bounds of the elastic stability and "crushing" strength failures the inelastic stability failure lies.

6.3.2 Prediction of Inelastic critical load for ε-section

Inelastic critical buckling load for the ε-section stub column is predicted using the element-by-element method of Parks and Yu (1989). In their approach the failure of any element of the member signifies failure of the whole member. Based on the assumption in Section 6.3 that the ε-section consists of two flanges and a web elements, and according to the Parks and Yu hypothesis, then only the inelastic critical buckling stress for the flange element shown in Figure 6.9 needs to be considered.

The analytical prediction for the local buckling resistance of curved plate elements under compressive action is a complex task. Redshaw (1938) developed the following expression for curved plates with constant radius of curvature, based on the classical energy approach, which is used to predict the elastic critical buckling stress σ_{cr}

$$\sigma_{cr} = \frac{E}{6(1-\nu^2)}\left[\left(12(1-\nu^2)\left(\frac{t}{R}\right)^2 + \left(\frac{\pi t}{b}\right)^4\right)^{\frac{1}{2}} + \left(\frac{\pi t}{b}\right)^2\right] \tag{6.5}$$

In Equation (6.5) the geometrical variables t, b and R define the shape of curved plate element (see Figure 6.9) and v is Poisson's ratio.

Sechler and Dunn (1942) showed that Equation (6.5) could be expressed in terms of a flat plate and a cylindrical shell buckling stresses as

$$\left(\frac{\sigma_{cr}}{E}\right)_{sc} = \left(\left(\frac{\sigma_{cr}}{E}\right)_c^2 + \frac{1}{4}\left(\frac{\sigma_{cr}}{E}\right)_f^2\right)^{\frac{1}{2}} + \frac{1}{2}\left(\frac{\sigma_{cr}}{E}\right)_f \tag{6.6}$$

where $\left(\frac{\sigma_{cr}}{E}\right)_{sc}$ is buckling stress ratio of a simply supported curved element subjected to uniform compression, $\left(\frac{\sigma_{cr}}{E}\right)_c$ is buckling stress ratio of a cylinder with the same *R/t* ratio as curved element, and $\left(\frac{\sigma_{cr}}{E}\right)_f$ is buckling stress ratio of a simply supported flat plate with same *t/b* ratio as the curved element.

Later Parks and Yu (1989) modified Equation (6.6) assuming v to be 0.3, and replacing the theoretical value of buckling stress ratio of the cylinder $\left(\frac{\sigma_{cr}}{E}\right)_c = 0.6\frac{t}{R}$ with a reduced empirical relationship $\left(\frac{\sigma_{cr}}{E}\right)_c = 0.25\frac{t}{R}$, based on the results of the stiffened curved element tests. The Parks and Yu expression is

$$\left(\frac{\sigma_{cr}}{E}\right)_{sc} = \left(0.0625\left(\frac{t}{R}\right)^2 + 3.267\left(\frac{t}{b}\right)^4\right)^{\frac{1}{2}} + 1.807\left(\frac{t}{b}\right)^2 \tag{6.7}$$

A further modification can be made to Equation (6.7) to account for the work of Seide and Weingarten (1961) (Calladine 1983) that recommends we should replace R in the expression of buckling stress ratio of the cylinder $\left(\frac{\sigma_{cr}}{E}\right)_c = 0.6\frac{t}{R}$ by $\overline{R}$ a radius of curvature of the deformed cross-section at the point where the compressive stress is greatest as a criterion of local buckling for curved arc of steadily increasing curvature. This lead to

$$\left(\frac{\sigma_{cr}}{E}\right)_{sc} = \left(0.0625\left(\frac{t}{\overline{R}}\right)^2 + 3.267\left(\frac{t}{b}\right)^4\right)^{\frac{1}{2}} + 1.807\left(\frac{t}{b}\right)^2 \qquad (6.8)$$

Equation (6.8) is used by the author to cope with the complexity of the shape of the ε-section. For a section with a wall thickness t of 1.5 mm, the mid-plane radius R is 20.75 mm, and the length of the flange $b = R\phi$ is 43 mm. This modelling case is illustrated in Figure 6.9. Based on the assumed local buckling failure pattern shown in Figure 6.6 the angle ϕ to the flange element is taken to be 120° and $\overline{R}$ is 50 mm (the distance from the centriod to the outer side of the flange) now from Equation (6.8), the elastic critical stress of the assumed flange is predicted to be σ_{cr} = 890 N/mm^2.

By using the moduli of elasticity from Table 6.2, which corresponds to the ultimate failure load of the stub column 447 N/mm^2 and Equation (4.69), the plasticity reduction factor, $\overline{\eta}$, is calculated to be 0.62. Consequently, the theoretical inelastic critical stress given by $\overline{\sigma}_{cr} = \overline{\eta}\sigma_{cr}$ is predicted to be 552 N/mm^2. In Section 6.3 we found that, for the stub columns tested, the mean stress level at inelastic buckling failure is 418 N/mm^2. As a result of this, the ratio of the tested-to-theoretical stresses for the inelastic buckling is 0.76.

The ultimate failure load for the stub ε-column is then obtained by multiplying the theoretical $\overline{\sigma}_{cr}$ by the section's effective area, A_{eff}.

A summary of the stub column's inelastic critical buckling stress results is given in Table 6.3, together with the ratio of the experimentally determined value $\overline{\sigma}_{cr}^{eaxp}$ and the theoretically determined value $\overline{\sigma}_{cr}$. The correlation between theory and practice is considered to be acceptable.

Table 6.3. Summary of inelastic critical buckling stresses from experiments and theory.

1	2	3
$\overline{\sigma}_{cr}^{eaxp}$	$\overline{\sigma}_{cr}$	$\frac{\overline{\sigma}_{cr}^{eaxp}}{\overline{\sigma}_{cr}}$
418	552	0.76

6.3.3 Effective area, A_{eff}

It is well established that, in some cases, flat plates under compression stress, will develop additional load-carrying capacity. This is commonly known as the post-buckling strength and is found to be a function of the plate's slenderness. For "slender" flat plates the ultimate stress may well be several times the critical buckling stress. When buckling occurs there is a redistribution of the stress field across the width of the plate. This redistribution is the basis for the effective width concept presented in Section

3.3. This leads to the thin-walled plate having an effective area, A_{eff}, which is given by tb_{eff}.

Based on the unified theory of plastic buckling by Stowell (1948), Hopperstad, Lagseth and Tryland (1999) developed, for the inelastic buckling situation, a simple theory for the effective width. They assumed that once inelastic buckling had occurred, a continuous reduction in b_{eff} would take place in the plate. The ultimate load is reached when the decrease in b_{eff} is found to be more rapid than the increase in the flow stress σ_{eff} due to strain hardening, over the effective area. During this process the part of the flat plate associated with A_{eff} remains stable (i.e., undeformed out-of-the-plane), and carries the entire compressive load. For this situation the effective width can be expressed by

$$\frac{b_{eff}}{b} = \sqrt{\overline{\eta}\frac{\sigma_{cr}}{\sigma_{eff}}} \qquad \text{for} \qquad \bar{\varepsilon} \geq \bar{\varepsilon}_{cr} \tag{6.9}$$

where $\bar{\varepsilon}_{cr}$ is the limit of the plastic strain. By substituting into Equation (6.9) the plasticity reduction factor $\overline{\eta}$ given by Equation (4.69), the elastic critical stress given by Equation (6.8), and the proof stress, $\sigma_{0.2}$, of 490 N/mm^2 for the effective stress σ_{eff} the ratio of the effective width (b_{eff}) to the total width (b) is calculated to be 1. On taking in Equation (6.9) the experimental stress of 418 N/mm^2 to be σ_{eff} the b_{eff}/b ratio is found to be greater than 1. These determined effective width ratios suggest to the author that the ε-section, even with its lowest practical wall thickness of 1.5 mm, can be classified as a "stocky" section, with respect to failure by local buckling. Moreover, the study has shown that the full cross-sectional area of the section may be considered

to be effective in the elastic design calculations in accordance to Section 6 of BS5950-5:1998, since local instability failure has been found to occur in the inelastic range. It is therefore proposed that the expression for the effective area of the ε-sections is

$$A_{\text{eff}} = A. \tag{6.10}$$

In Equation (6.10) A is for the cross-sectional area as given in Table 5.1 of the current (ε-section) of size 100x43 mm.

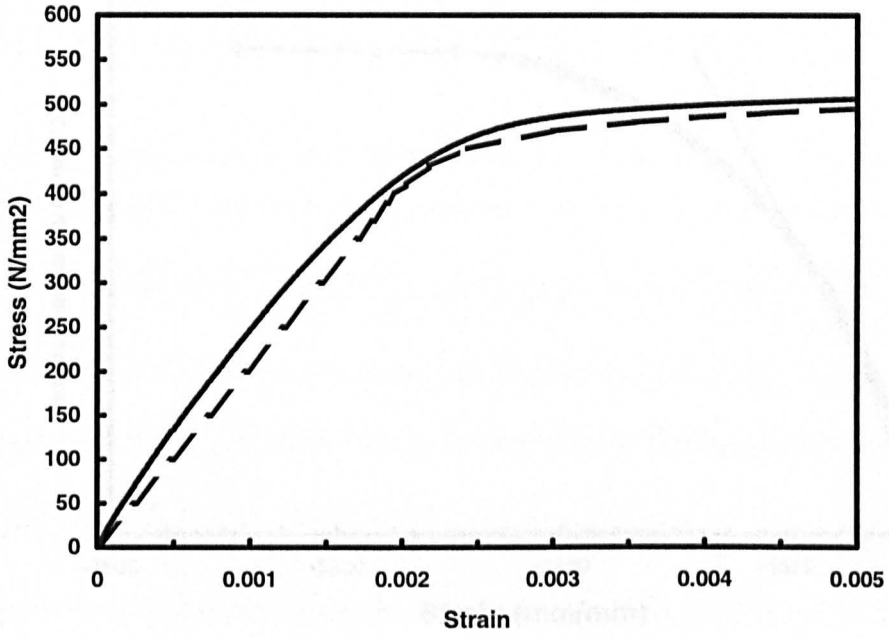

Figure 6.1. Tensile stress v strain curve for ε-section steel, from coupon ———, from Equation (6.2) — — - .

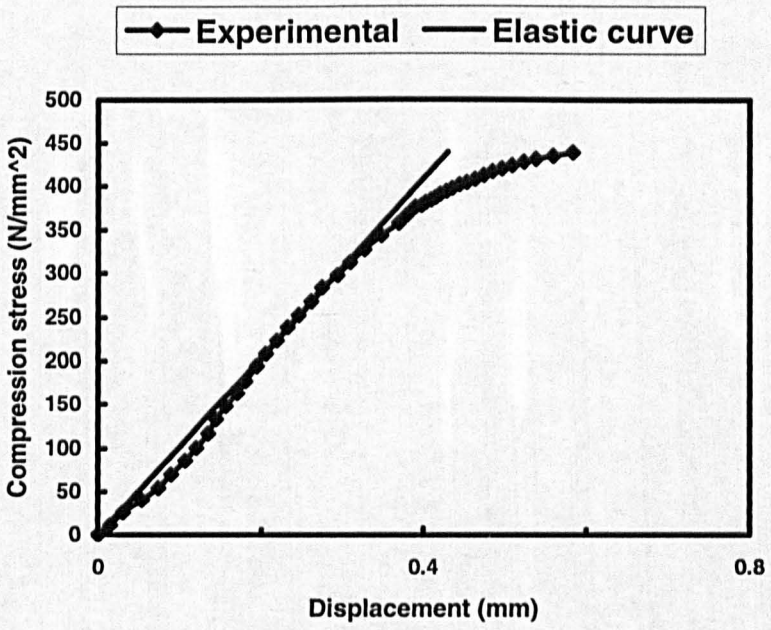

Figure 6.2. Mean axial shortening versus compression stress from 8 stub columns of the 1.5 mm ε-section at a height of 200 mm.

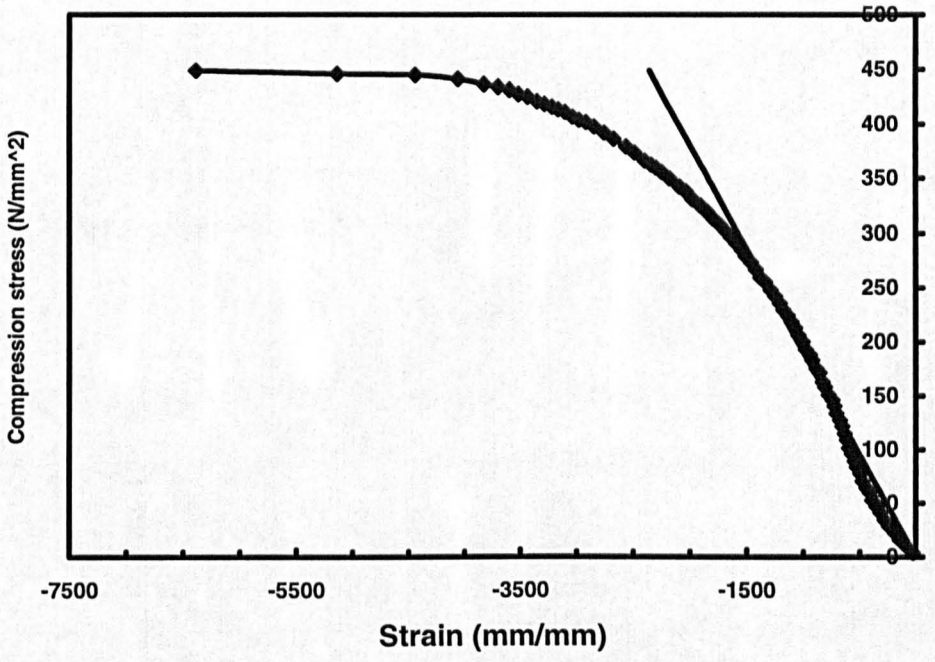

Figure 6.3. Axial strain from gauge No. 8 versus compression stress from stub column S7 of the 1.5 mm ε-section at a height of 200 mm.

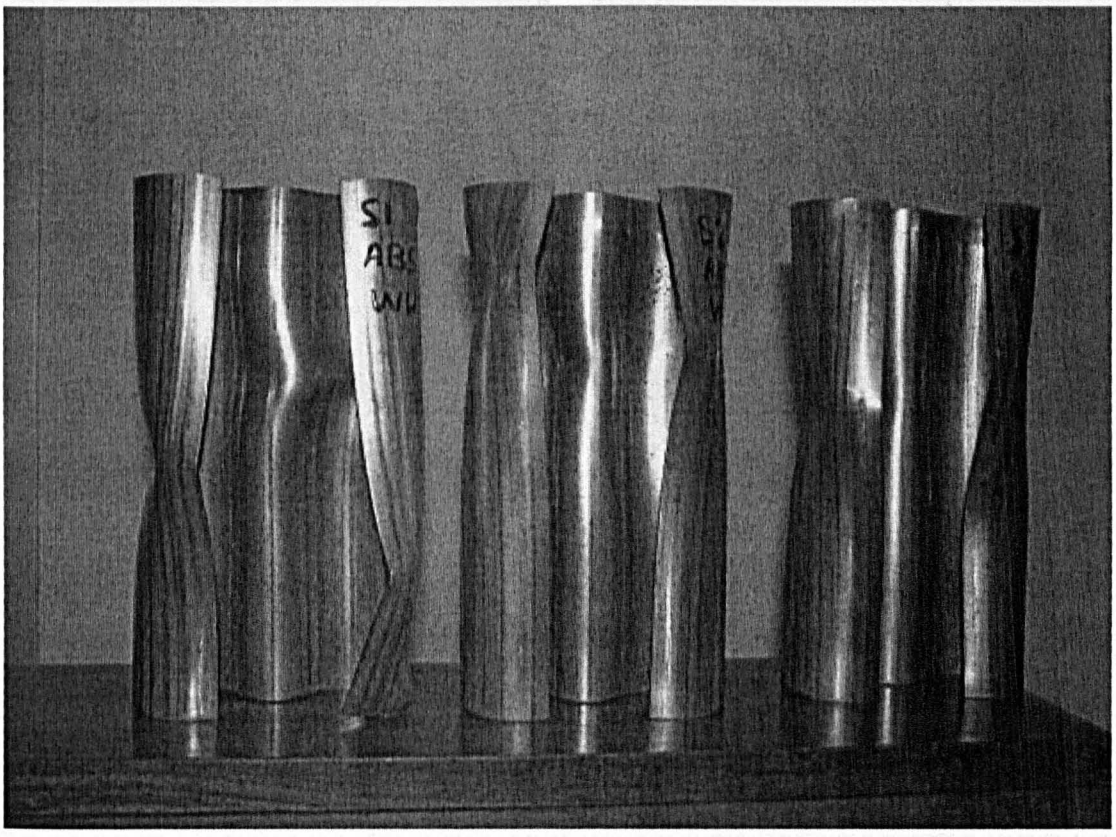

(a) Specimen, S1 (b) Specimen, S2 (c) Specimen, S3

(d) Specimen, S4 (e) Specimen, S5 (f) Specimen, S6

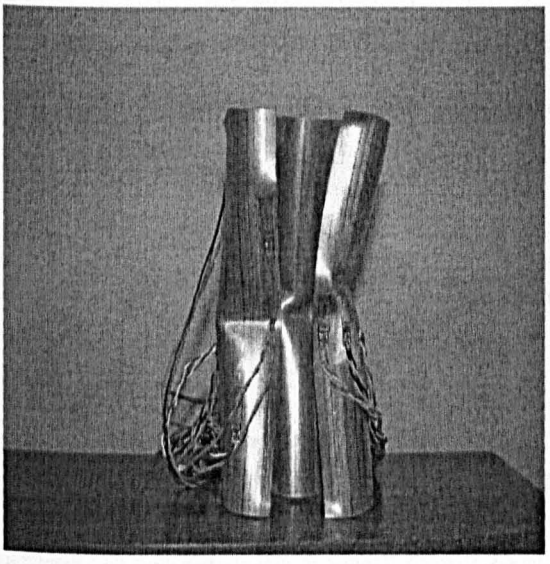

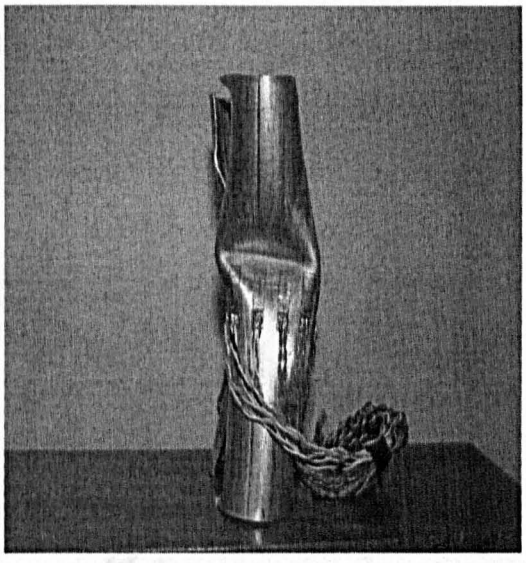

(g) Specimen, S7 (h) Specimen, S8

Figure 6.4. Post-test deformations of stub specimens S1 to S8.

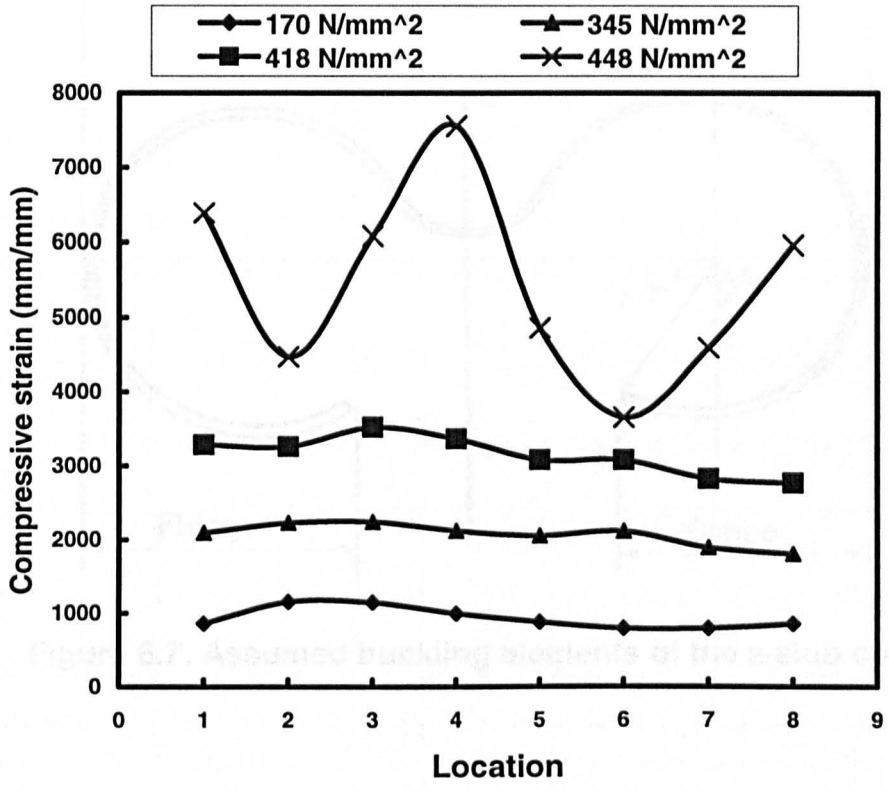

Figure 6.5. Strain profiles at mid height for different axial compressive stress levels, using stub-column specimen.

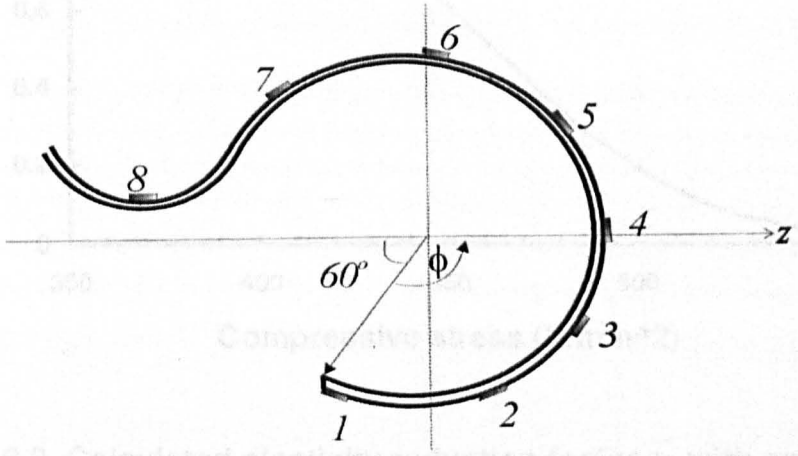

Figure 6.6. Locations of strain gauges Nos. 1 to 8 at the mid-height for stub column specimens S7 and S8.

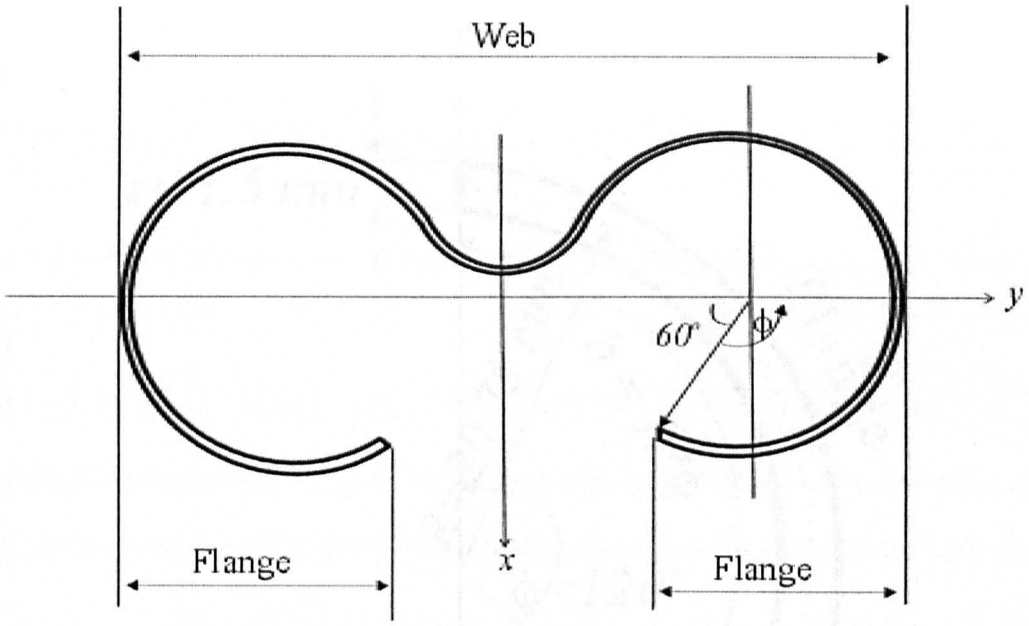

Figure 6.7. Assumed buckling elements of the ε-stub column.

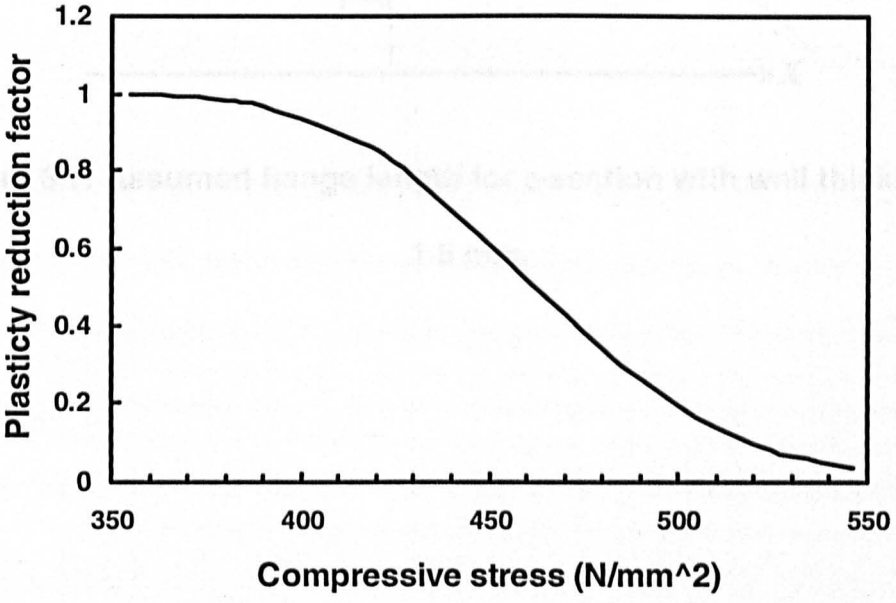

Figure 6.8. Calculated plasticity reduction factor $\bar{\eta}$ with compressive stress for the 1.5 mm ε-section.

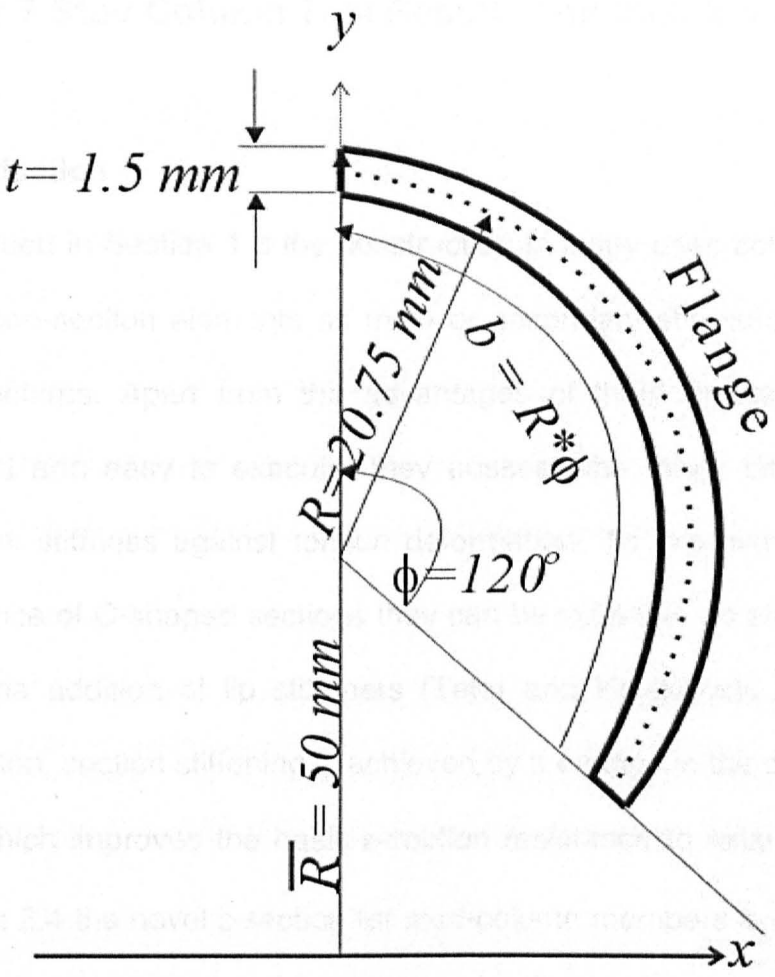

Figure 6.9. Assumed flange length for ε-section with wall thickness of 1.5 mm.

Chapter 7 Stud Column Test Results and their Evaluation

7.1 Introduction

As described in Section 1.3 the construction industry uses cold-formed thin-walled open-section elements as main or secondary structural members in steel structures. Apart from the advantages of their application, such as lightweight and easy to execute, they possess the major disadvantage of having low stiffness against torsion deformation. To improve the structural performance of C-shaped sections they can be stiffened, as shown in Figure 2.2, by the addition of lip stiffeners (Teter and Kolakowski 2004). In this investigation, section stiffening is achieved by a change in the cross-sectional shape, which improves the basic ε-section resistance to axial compression. In Section 2.4 the novel ε-section for stud-column members is detailed. Such members are of S350 structural grade steel with the wall thicknesses of 1.5 and 2 mm. As Figure 2.4 shows the section has a major- and minor-axis dimension of 100 mm and 43 mm, respectively. The open ε-section is stiffened by the addition of bracket stiffeners. Figures 5.6(a) to 5.6 (d) show the various stiffener brackets and enclosure combinations of CR4 steel of 1.5 mm thickness that are used to make the nine different columns types (with labels WU104 to WU112). The exception to using the CR4 grade of steel is the 100x40x1.5 C-section of grade S350 steel, which is used to fully enclose the ε-section in column type WU112.

Details of the test procedure used in each component test are given in Chapter 5. In what follows an evaluation and analysis of the test results is

given in the context of providing technical information for the recommendation of design guidance for 2.7 m stud columns of ε-sections.

The new experimental results are compared to buckling resistances under axial load, predicted in accordance with Clause 6.2.3 in BS5950-5:1998. This is used to show that, providing ε-columns continue to be made with tight tolerances, their design capacity, based on a mid-height lateral displacement of 9 mm (length/300), is often 20 to 40% higher than that predicted by Clause 6.2.3, assuming failure by flexural buckling with an effective length of 0.85. In all 54 tests the observed mode of failure was minor-axis flexure, leading to buckling failure, this can be seen in Figure 7.1. After the test load had been removed a visual inspection was carried out on each of the columns. It was observed that the specimens had not experienced any permanent lateral deformation or twisting deformations, showing that the behaviour to maximum load had been elastic and reversible.

7.2 Test results for stud columns

Typical continuous load-displacement curves from the 54 tests are plotted in Figures 7.2 to 7.10. The load is axial compression and the displacement is the minor-axis lateral deflection at the column's mid-height. There is one plot for each of the nine different ε-column types, identified by type labels WU104 to WU112. These plots are for the average value of the six specimens for each column type. The full set of 54 load-displacement plots is given in Appendix A. Presented in Figures 7.12 to 7.15 are comparisons of the load-displacement characteristics given by the nine types of ε-column. All plots

have the same scale on their lateral displacement axis (± 15 mm), but the load scale, in kN, changes. The load scale's upper limit depended on the resistance of the column type tested. As a failure criterion, a 9 mm (length/300) displacement limit is given by the dashed vertical lines in Figures 7.2 to 7.10 for both the positive and negative directions of mid-height lateral deflection. The characteristics shape of the load displacement plots in figures 7.2 to 7.10 show that as soon as the axial load is increased the lateral deflection will start to create so-called elastic-plastic curve. The theoretical Euler critical buckling load cannot be estimated directly from the test data because of the presence of initial imperfections. The influence of geometrical imperfection is described in Section 3.2.2.

Table 7.1 summarizes the salient strength test results. In the table, the first and second column entries give the column type and the specimen number, as defined in Section 5.4.2. Column entries three to five give the results of the strength load (P_{str}) (for a 9 mm minor-axis lateral deflection), the mean strength load $P_{str.mn}$ and its Standard Deviation (SD) and Coefficient of Variation (CoV) %.

Table 7.1. Fifty-four concentric full length ε-column test results.

ε-column type (1)	Spec. No. (2)	Strength test load results (kN)		
		Strength load P_{str} (3)	$P_{str.mn}$ SD (CoV %) (4)	Mean strength load, $P_{str.mn}$ (5)
WU104 *Figure 5.6(a)*	1	52.00	1.33 (2.5)	53.8
	2	55.00		
	3	53.00		
	4	55.50		
	5	53.00		
	6	54.00		
WU105 *Figure 5.6(a)*	1	44.00	2.30 (5.1)	44.7
	2	48.60		
	3	45.00		
	4	45.50		
	5	43.00		
	6	42.00		
WU106 *Figure 5.6(b)*	1	56.50	1.68 (3.0)	55.0
	2	55.00		
	3	53.80		
	4	55.50		
	5	57.00		
	6	52.50		
WU107 *Figure 5.6(b)*	1	43.50	0.94 (2.2)	42.6
	2	42.50		
	3	42.30		
	4	41.50		
	5	44.00		
	6	42.00		
WU108 *Figure 5.6(c)*	1	53.00	0.75 (1.4)	53.66
	2	54.00		
	3	54.00		
	4	52.50		
	5	54.50		
	6	54.00		

Table 7.1. Fifty-four concentric full length ε-column test results.

ε-column type (1)	Spec. No. (2)	Strength test load results (kN)		
		Strength load P_{str} (3)	$P_{str.mn}$ SD (CoV %) (4)	Mean strength load, $P_{str.mn}$ (5)
WU109 *Figure 5.6(c)*	1	45.00	0.93 (2.1)	44.3
	2	45.50		
	3	43.00		
	4	44.50		
	5	44.50		
	6	43.00		
WU110 *Figure 5.6(d)*	1	80.00	1.55 (2.0)	79.0
	2	79.00		
	3	80.00		
	4	80.00		
	5	79.00		
	6	76.00		
WU111 *Figure 5.6(d)*	1	58.50	1.07 (1.9)	57.4
	2	59.00		
	3	56.50		
	4	56.50		
	5	**48.00**[1]		
	6	57.00		
WU112 *Figure 5.6(e)*	1	103.0	2.23 (2.2)	100
	2	97.00		
	3	100.0		
	4	99.00		
	5	101.0		
	6	90.00		

After completing the component test with specimen WU111-5, it was observed that a strength load of 48.0 kN (given in bold font in Table 7.1) is

26% lower than the lowest of the previous four tests. This prompted an inspection of the test rig to identify the problem. It was discovered that the end moment had been sufficient to cause a permanent deformation in the threaded stud connecting the jack to the base plate (see Figure 5.10). This single lower strength value brings into question the measured resistances of specimens Nos. 1 to 4 of WU111 column type. The damaged base plate was replaced with one fabricated to be fit for purpose, and so the resistance of the sixth WU111 specimen was unaffected by the test-rig problem. As this specimen gave a similar resistance to Nos. 1 to 4 the author has not rejected the four strength results that were obtained prior to knowing that a base plate in the test rig (Figure 5.8) was damaged.

7.2.1 Effective length of ε-columns

In obtaining the solution to the ordinary differential equation that governs column behaviour different end boundary conditions have to be considered. The expression for elastic critical buckling load (P_E) by Euler is for the situation of simply supported ends. His expression can be made more general by introducing the effective length (L_E) concept, so that $P_E = \pi^2 \frac{EI}{L_E^2}$, and L_E is used rather than the actual column length, L. L_E is defined as the distance between the points of contra-flexure, giving $L_E = kL$, with k the effective length factor, that is 0.5 for the perfectly fixed-ended and 1.0 for perfectly pin-ended cases. In practice, the end conditions are neither fully fixed nor fully pinned. Normally there is a certain degree of rotational restraint at the ends (Jones et al. 1983). For this semi-rigid condition the effective length factor k shall lie between its upper and lower bound values and this is

why Table 9 of BS 5950-5: 1998 gives k = 0.85 for compression members effectively held in position at both ends and restrained in direction at one or both ends.

To predict the actual L_E for the ε-columns, the experimentally determined distribution for the flexural stress is analysed. At any section along the specimen there is a combination of a mean axial compressive stress $\sigma_c = \frac{P}{A}$ and maximum compressive bending stress $\sigma_f = \frac{My_f}{I}$, which corresponds to moment $M = P\delta$, where δ is the mid-height deflection. This gives a total compressive stress of $\sigma_t = \sigma_f + \sigma_c$. Hence the flexural stress is $\sigma_f = \sigma_t - \frac{P}{A}$, and at the point of zero curvature its value is zero. To establish where along the length of the column this, readings are taken from strain gauges at several different distances from the top of WU105 specimen. This process is shown in Figure 7.11(a) at a P of 44 kN, and using the theoretical treatment just given the flexural stresses values at these locations are calculated and plotted in Figure 7.11(b). From the curve in this figure, the point of contra-flexure is estimated to be at 0.257 m, from an end support. This distance gives us an effective length of 0.81L, where L is 2.7m. This experimentally-derived value of L_E is assumed by the author to be the actual L_E when predicting later in this chapter the load capacity (resistance) of all the nine ε-column types.

7.2.2 Effect on buckling resistance of intermediate stiffening

Figure 7.12 was constructed to show plots of mean load (from six specimens) against lateral deflection for the three column types WU104, WU106 and WU 108, having a ε-section of 2 mm wall thickness. The difference between these three stud columns is that WU104 has no intermediate bracing stiffeners (see Figure 5.6(a)), WU106 has two bracing stiffeners of length 300 mm, at ±600 mm from the mid-height position (see Figure 5.6(c)), while WU108 has a single bracing stiffener of length 300 mm at the mid-height position (see Figure 5.6(e)).

From Table 7.1 the mean strength loads ($P_{str.mn}$) for the three column types are 53.8 kN (with Standard Deviation (SD) of 1.33 kN), 55.0 kN (SD of 1.68 kN) and 53.7 kN (SD of 0.75 kN), respectively. There is small variation in mean strength loads ($P_{str.mn}$), with the maximum Coefficient of Variation (CoV) of 2.5%, and CoV for the three means of 1.3%.

Figure 7.13 shows the mean load-displacement curves for the column types WU105 (Figure 7.5(a)), WU107 (Figure 7.5(b)), and WU109 (Figure 7.5(c) that are equivalent to types WU104, WU106, and WU108, respectively, except that the wall thickness is 0.5 mm lower, at 1.5 mm. As Table 7.1 presents, these smaller cross-sectional area specimens gave, respectively, mean strength loads ($P_{str.mn}$) of 44.7 kN (SD of 2.3 kN), 42.6 kN (SD of 0.94 kN) and 44.3 kN (SD of 0.93 kN). Again there is a small difference in three mean values, as given by a CoV of only 2.5%.

By using the t and F statistical tests it should be feasible to show that the each of the two groups of three specimens can be said to belong to a single population. In other words, it is the author's belief that the ε-column minor-axis buckling resistance is independent of the presence and number of intermediate bracing stiffeners.

7.2.3 Influence on buckling resistance of the wall thickness

In Figure 7.14 typical load-displacement plots for column types WU104 (wall thickness is 2 mm) and WU105 (1.5 mm) are presented. The only difference between these two column types is the wall thickness. An increase in this thickness of 0.5 mm results in a strength load increase of about 20%. This is lower than the 29% increase that is theoretically predicted, solely on assuming Euler buckling and the increase in the second moment of area about the minor-axis (I_y). Sectional properties are given in column six of Table 5.1.

7.2.4 Influence on buckling resistance of the cross-section configuration

Figure 7.15 presents typical load-displacement curves for the column types WU104, WU105, WU110, WU111, and WU112. The first two of these five columns have two stiffeners of length 300 mm at the ends of specimen. Over a length of 2.1 m the ε-section is, therefore, fully open. The last three column types all have the ε-sections that are fully enclosed along the 2.7 m length. The curves in the figure show that the general characteristic shape of the

load-displacement response from the five column types is similar. On evaluating the resistances of paired columns, that have the same ε-section thickness with fully enclosed or fully opened ε-sections, it is found to increase by 46% for WU110 over WU104, and by 28% for WU111 over WU105.

The significant difference in the percentage increases between the two-paired equivalents might be attributed to the experimental problem that occurred when testing the batch of six WU111 specimens. This problem, and how it was removed has been discussed previously in Section 7.2.

For WU112 columns, when a C-section of 1.5 mm thick is used to fully enclose the open-section, the strength load is found to be 85% higher than if the 2 mm thick ε-section has top and bottom stiffener brackets and intermediate stiffener brackets too. This increase is similar to the calculated increase in minor-axis second moment of area of 93%. These sectional properties for WU104 and WU112 column types are given in Table 5.1.

7.2.5 The overall effective load eccentricity in the series of ε-column tests

It will be instructive to show theoretically how the test results differ from the theoretical bifurcation response, because the presence of inherent imperfections in the test arrangement leads to an overall effective load eccentricity (Mottram, Brown and Anderson 2003). Simple and approximate analytical treatment of the problem can be achieved by considering the response of the two simple beam-column problems shown in Figures 7.16(a)

and 7.16(b). In both situations the member is assumed to be straight (i.e. there is no out-of-straightness) when the axial compression load P is zero. For the eccentrically loaded situation shown in Figure 7.16(a) the Euler-Bernoulli behaviour for small deflections, gives the differential equation

$$EIy'' + P \cdot (y + e) = 0 \qquad (7.1)$$

In Equation (7.1), I can be either I_x or I_y, depending on the action of moment Pe. By solving this equation, it can be shown that the increase in mid-height lateral displacement δ_e with axial compression P, is given by (Mottram et al. 2003)

$$\delta_e = e\left(\sec\left(\frac{\pi}{2}\sqrt{\frac{P}{P_E}}\right) - 1\right) \qquad (7.2)$$

Where e is the load eccentricity (taken to be the same at both ends), and P_E is the critical Euler buckling load for a pinned-pinned column ($=\frac{\pi^2 EI}{L^2}$, with effective length $L_E = L$). Equation (7.2) shows that, as soon as the axial compression increases, the lateral deflection will start to grow. This is what is found during the column tests, and is seen in the load-displacement curves plotted in Figures 7.2 to 7.10.

However, in the series of column tests under evaluation, the ends of the specimens are not pinned, as the displacement boundary conditions are closer to the clamped-clamped situation. We have already established that the end conditions are for an effective length of about $0.81L$.

Figure 7.16(b) shows the situation when the same member has no axial load and end moments M_o (= $M_{A\theta A}$= $M_{B\theta B}$) which are equal to Pe and acting in the opposite sense to the end moments, of magnitude, Pe in Figure 7.16(a). For the fixed-fixed end condition, Fertis (1996) determined an expression for the mid-height displacement for the situation in Figure 7.16 (b). It is

$$\delta_{MA\theta A} = \frac{M_0}{P_{cr}}\left(1-\cos\frac{2\pi x}{L}\right) \qquad (7.3)$$

Where in Equation (7.3), P_{cr} is the critical Euler critical buckling load given by $\frac{4\pi^2 EI}{L^2}$ for the fixed end condition (i.e., with $L_E = 0.5L$). After substitution in this equation for Pe, as the fixed end moment M_0, and combining Equations (7.2) and (7.3), an estimate for the total mid-height displacement of a beam-column element with clamped-clamped ends (θ_A = -θ_B = 0) and a load eccentricity e is given by

$$\delta_e - \delta_{MA\theta A} = e\left(\sec\left(\frac{\pi}{2}\sqrt{\frac{P}{P_E}}\right)-1-\frac{P}{P_{cr}}\left(1-\cos\frac{2\pi x}{L}\right)\right) \qquad (7.4)$$

By using Equation (7.4) to fit the load-displacement plots we can obtain an estimate to the overall effective load eccentricity e.

In Table 7.2, the fourth column gives the strength ratio of $P_{str.mn}/P_{cr}$ using the buckling loads given in columns two and three, and the measured mid-height lateral deflection when the strength test was terminated. This shows that the mean experimental buckling load is between 0.39 and 0.55 of the upper bound column resistance, had the column ends been fully-fixed, which they were not. Using the simple and approximate theoretical treatment Equation (7.4) an estimate of this eccentricity (e) for five ε-type columns is given in the

sixth column of Table 7.2. This approximate procedure indicates that e lies somewhere in the range from 2.0 to 2.5 mm, and that the overall effective load eccentricity appears to be independent of having the ε-section fully-opened or fully-enclosed. It is observed that the presence of the inherent imperfections in testing has introduced an overall load eccentricity when the column load is supposed to be concentric. Although small, at maximum 1/1080th of column length, its influence on the flexural response, about the minor-axis, will reduce the measured buckling resistance from the Euler value by an amount that cannot be readily quantified.

Table 7.2. Column failure loads and overall effective load eccentricities.

ε-column type	Critical Euler buckling load, P_{cr}[1]	Mean strength load, $P_{str.mn}$	$P_{str.mn}/P_E$	Minor-axis lateral displacement (mm)	Overall load eccentricity from Equation (7.4) (mm)
(1)	(2)	(3)	(4)	(5)	(6)
WU104	106	53.8	0.50	8.9	2.4
WU105	82.0	44.7	0.55	8.9	2.5
WU110	175	79.0	0.45	10.3	2.3
WU111	146	57.4	0.39	8.2	2.0
WU112	206	100	0.49	8.4	2.4

Notes: 1. P_{cr} is critical Euler buckling load for a fixed-fixed column, and is given by $\frac{4\pi^2 EI}{L_E^2}$.

7.2.6 ε-column design strengths

Columns of light gauge steel can failure either by crushing (a plastic strength mode) or by buckling (an elastic or inelastic stability mode). The structural

design of steel cold-formed members is strongly dependent on their stability and the torsional behaviour. Thin-walled open cross-sectional members under compression load are susceptible to different instability modes of failure, such as local, global or the modal interaction of local and global. In obtaining expressions that give the ultimate load of such column member there are many factors that influence its carrying capacity. These factors involve local bucking effects, boundary conditions, imperfections and flexural-torsional buckling.

The intervention of the local plate-buckling mode has been considered in Section 6.3.3, by using the traditional effective-width approach, which permits the reduction of the ultimate load by means of an experimentally calibrated approximate formulation, such as the effective area. In the case of ε-columns, of thickness 1.5 mm and higher, the cross-sectional area has been shown in Section 6.3.3 to be fully effective, so long as the predicted local buckling is above the elastic range (i.e. when the section experiences inelastic local buckling). The actual effective length of a stud column has been predicted in Section 6.2.1 to be $0.81L$. Section 7.2.5 has used the test results to establish the overall effective load eccentricities (e) that are given in the sixth column of Table 7.2. By visual inspection of the deformation in the strength tests the author considers the torsional flexural deformation to be negligible for the ε-columns having a length of 2.7 m. What the author did observe were the columns failing in pure flexural buckling about the minor axis. It can be seen in Figure 7.1 that under severe lateral deformation, the column does not experience any twisting deformation.

For sections that are symmetrical about a single axis and which are subjected to torsional-flexural instability, the buckling resistance P_c', according to Clause 6.2.3 of BS5950-5: 1998 is given by

$$P_c' = \frac{M_c P_c}{M_c + P_c e_s} \tag{7.5}$$

In which M_c is the moment capacity of the section determined in accordance with Clause 5.2.2, and e_s is the distance between the geometric neutral axis of the gross cross-section and that of the effective cross-section. This distance can be assumed to be zero, as the gross cross-section is considered to be fully effective within the elastic range. Now Equation (7.5) reduces to $P_c' = P_c$, with P_c the buckling resistance under axial load, determined in accordance with Clause 6.2.3, from

$$P_c = \frac{P_E P_{cs}}{\phi + \sqrt{\phi^2 - P_E P_{cs}}} \tag{7.6}$$

and

$$\phi = \frac{P_{cs} + (1+\eta)P_E}{2}. \tag{7.7}$$

In Equations (7.6) and (7.7) P_{cs} is the short strut capacity, given by $P_{cs} = Y_s A$, on the basis of full section yielding, P_E is the Euler critical buckling load ($= \frac{\pi^2 E I_y}{L_E^2}$), and η is the Perry coefficient for $\frac{L_E}{r} \le 20$, $\eta = 0$, and for $\frac{L_E}{r} > 20$,

$$\eta = 0.002\left(\frac{L_E}{r} - 20\right).$$

In the other hand the design capacity of the tested specimens, in accordance with Clause 10.8.3.1, is given by the expression

$$design\ capacity = K_t * \left[\frac{mean\ test\ result}{R_s} \right] \tag{7.8}$$

in which R_s is the relative strength coefficient, determined in accordance to Clause 10.4, and assume to be 1.2. K_t is a statistical coefficient that should not be > 1.0.

Table 7.3 summarizes the columns strength results. In the table, the first column entries give the column type, as defined in Section 5.4.2. Column entries two and three give the results of the mean strength load $P_{str.mn}$, and the design capacity, $P_{d.cap}$, load using the test results and Equation (7.8) of Clause 10.8.3.1. The next two columns give the theoretical values for the critical Euler buckling load ($P_E = \frac{\pi^2 E I_y}{L_E^2}$), and the design buckling resistance load $P_{c.nom}$, using nominal measured properties and Equation (7.6) of Clause 6.2.3. For the theoretical Euler load calculations (column entry 4 in the table) the effective length L_E is $0.81L$. This value is same as that determined from testing and can be assumed to be representative of the rotational stiffness due to the spot welded end-connections to the ε-columns in modular and panel construction (see Figure 2.5). The sectional properties used to determine the theoretical buckling loads are given in Table 5.1 and the steel properties are given in Table 5.2. The last column in Table 7.3 presents the ratio of the design capacity determined from the strength testing (Clause

10.8.3.1) to the design load derived using Clause 6.2.3 and the measured properties.

Table 7.3. ε-column strength test and theoretical results.

ε-column type	Strength test load results (kN)		Theoretical strength load (kN)		Load ratio
	Mean strength load, $P_{str.mn}$	Design capacity Clause, $P_{d.cap}$, 10.8.3.1	Euler critical buckling load, P_E,	Buckling resistance, $P_{c.nom}$, Clause 6.2.3	(3)/(5)
(1)	(2)	(3)	(4)	(5)	(6)
WU 104	53.8	44.8	36.9	34.1	1.3
WU 105	44.7	36.3	28.7	26.4	1.38
WU 106	55.0	45.9	36.9	34.1	1.35
WU 107	42.6	35.5	28.7	26.4	1.35
WU 108	53.7	44.7	36.9	34.1	1.31
WU 109	44.3	36.9	28.7	26.4	1.4
WU 110	79.0	65.8	60.6	55.5	1.19
WU 111	57.4	47.8	50.6	46.3	1.03
WU 112	100	83.3	71.4	65.3	1.28

Using the procedure in Clause 10.8.3.1 and Equation (7.8), the design capacities from the strength testing are determined to be 44.8, 45.9 and 44.7 kN for column types WU104, WU106 and WU108, respectively. By using the calculation procedure in Clause 6.2.3 and Equations. (7.5) to (7.7), the design buckling resistance (P_c) for these three column types is 34.1 kN. As the load ratio in column six of Table 7.3 shows there is, up to, a 35% increase in the load capacity if the design load, for the ε-column with 2 mm wall thickness, is determined from the physical test results.

Again using the procedure in Clause 10.8.3.1, the design capacities from the strength testing are 36.3, 35.5 and 36.9 kN for column types WU105, WU107 and WU109, respectively. By following Clause 6.2.3 the value of P_c is 26.4 kN. As the load ratios for these column types in Table 3 show there is about a 40% increase in the design load capacity when the data from testing are used rather than the universal design procedure of Clause 6.2.3. This increase in capacity, for the 1.5 mm ε–section, is slightly higher than for the group of three column types with the 2 mm wall thickness.

We shall now consider the strengths of the three column types WU110 to WU112, where the open ε-section is fully enclosed, either with a close-fitting 1.5 mm shaped plate sections (WU110 and WU111) or with a C-section, whose flanges surround and contact the ε-section. Column types WU110 and WU111 have plate enclosures that are shown in Figure 5.6(d) as stiffener brackets. The difference between these two types is that the ε-section wall thickness is 2 mm in WU110 and 1.5 mm in WU111. The six WU110 columns gave a mean strength load ($P_{str.mn}$) of 79 kN. Using Clause 10.8.3.1 and Equation (7.8), the design load capacity from this physical testing is 65.8 kN, while Clause 6.2.3 gives a calculated design buckling strength of 55.5 kN. For this column type there is a 19% increase in the design resistance if the test data are used. The smaller sized columns of type WU111 gave a $P_{str.mn}$, neglecting specimen No. 5, of 57.4 kN and a design load by Clause 10.8.3.1 of 47.8 kN. From Clause 6.2.3 the design buckling resistance is determined to be 46.3 kN. The increase in using the test data to establish the design load

for this column type is now only 3%. This is much lower than for the other column types, and might have been due to a load fixture problem with the test rig, as explained in Section 7.2.

Figure 5.6(e) is for column type WU112, which has a 2 mm thick ε-section fully enclosed by a 100x40x1.5 mm C-section. The batch of six specimens gave a mean strength load of 100 kN. The design load capacity from these results is 83.3 kN and the value of P_c is calculated from Equations. (7.5) to (7.7) to be 65.3 kN. These values give a 28% increase in the design load capacity, if the test results are used to establish this design value.

Presented in Table 7.4 is a summary of the ε-column strength results obtained by different methods, and their ratios. In the table column one gives the ε-column types. Entries in columns two to five give, for the five column types, $P_{str.mn}$, $P_{d.cap}$, the buckling resistance load $P_{c.exp}$, using the test results and Clause 6.2.3 and $P_{c.nom}$. Columns entries six to eight present the ratios of the design capacities, obtained using the three approaches provided by way of the clauses in BS5950:5:1998, to the experimental mean strength load ($P_{str.mn}$).

Table 7.4. Column resistances based on the series of ε-column tests.

ε-column type	Mean strength load, $P_{str.mn}$ (kN)	Design capacity, Clause 10.8.3.1 $P_{d.cap}$ (kN)	Buckling resistance Clause 6.2.3 $P_{c.exp}$ (kN)	Buckling resistance Clause 6.2.3 $P_{c.nom}$ (kN)	$P_{d.cap}/P_{str.mn}$	$P_{c.exp}/P_{str.mn}$	$P_{c.nom}/P_{str.mn}$
(1)	(2)	(3)	(4)	(5)	(6)	(7)	(8)
WU104	53.8	44.8	38.3	34.1	0.83	0.71	0.63
WU105	44.7	36.3	29.7	26.4	0.81	0.66	0.59
WU110	79.0	65.5	62.5	55.5	0.83	0.79	0.70
WU111	57.4	47.8	52.2	46.3	0.83	0.91	0.81
WU112	100	83.1	73.6	65.3	0.83	0.74	0.65

When Clause 10.8.3.1 is used to obtain the design loads, as given in the third column in Table 7.4, they are about 83% of the mean value obtained experimentally. In the case of adopting the universal design procedure in Clause 6.2.3, and using the experimentally estimated values to ε-column properties, the predicted strengths, in the fourth column of Table 7.4, range from 66% to 91% of $P_{str.mn}$. When the same procedure in Clause 6.2.3 is followed, but now using nominal values for the properties, the predicted strengths, in the fifth column of Table 7.4, range from 59% to 81% of $P_{str.mn}$. These tabulated results show that there is about a 12% increase in the predicted design strengths of the ε-columns when measured properties are used with Clause 6.2.3.

Table 7.5. Perry coefficient based on the series of ε-column tests.

ε-column type (1)	Effective length factor (k) (2)	Effective length L_E (mm) (3)	Slenderness ratio ($\lambda_y = L_E/r_y$) (4)	Perry coefficient in BS5950:5-1998 (5)
WU104	0.81	2187	147	0.254
WU105	0.81	2187	145	0.250

The presence of the overall effective load eccentricity is also reflected in a high value for the Perry coefficient, η, as its value is zero for perfect case which appears in Equation (7.7). Its values for the two fully-opened ε-columns are given in column five of Table 7.5 that obtained using Equation (7.6) and test values of P_c. These coefficients are obtained using Clause 6.2.3 and the experimentally determined effective length (L_E) given in column three of Table 7.5. The appropriate effective length factor (k), in column two, is the experimentally-derived value of 0.81, which is from Section 7.2.1.

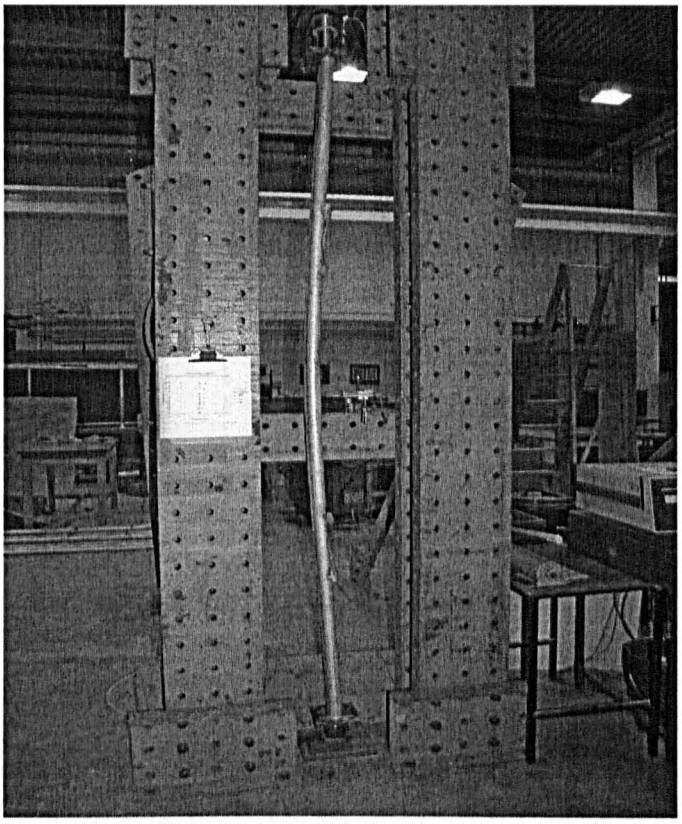

Figure 7.1. Typical specimen deformation at maximum test load.

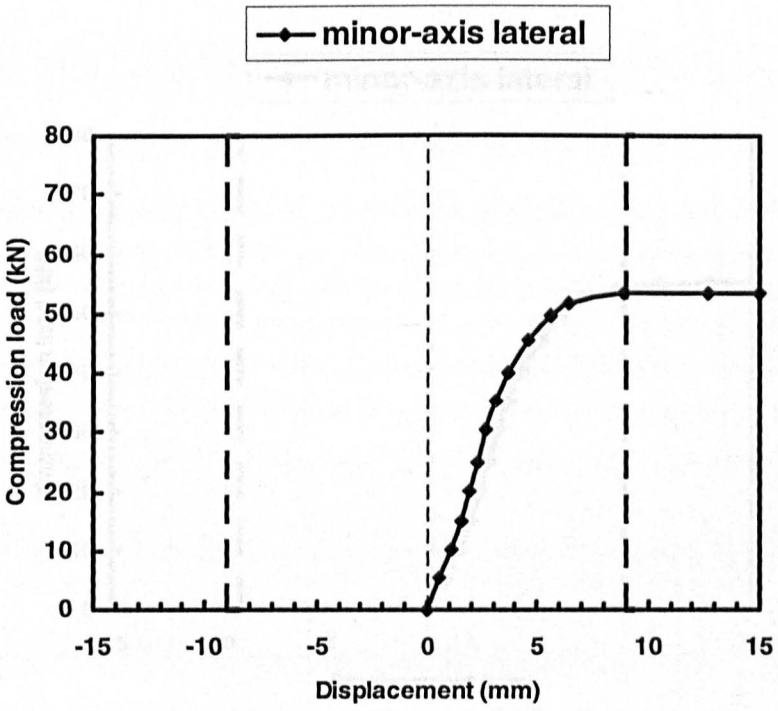

Figure 7.2. Load-displacement curve for column of type WU104.

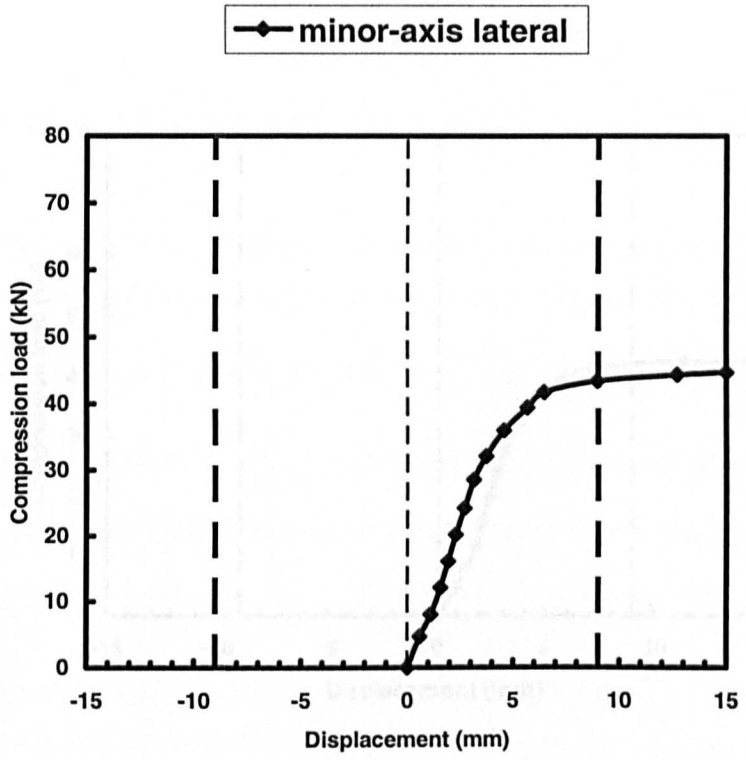

Figure 7.3. Load-displacement curve for column of type WU105.

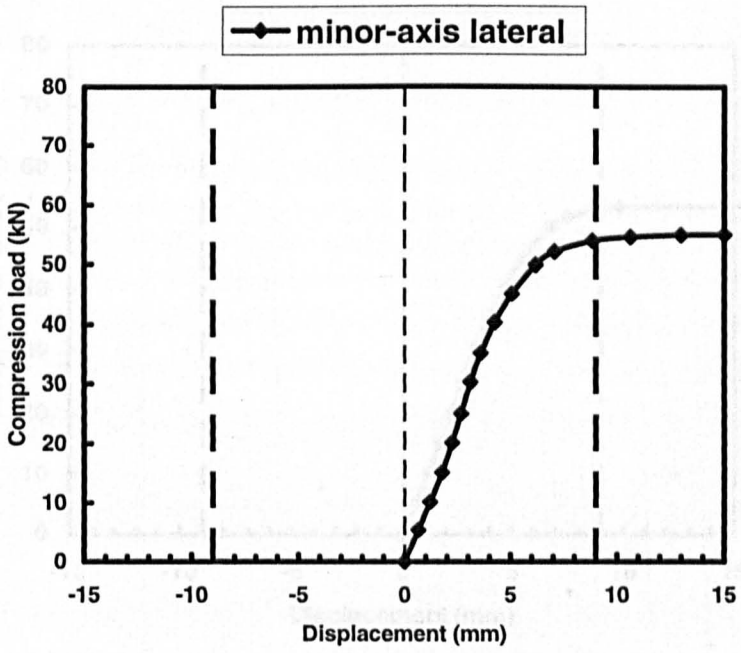

Figure 7.4. Load-displacement curve for column of type WU106.

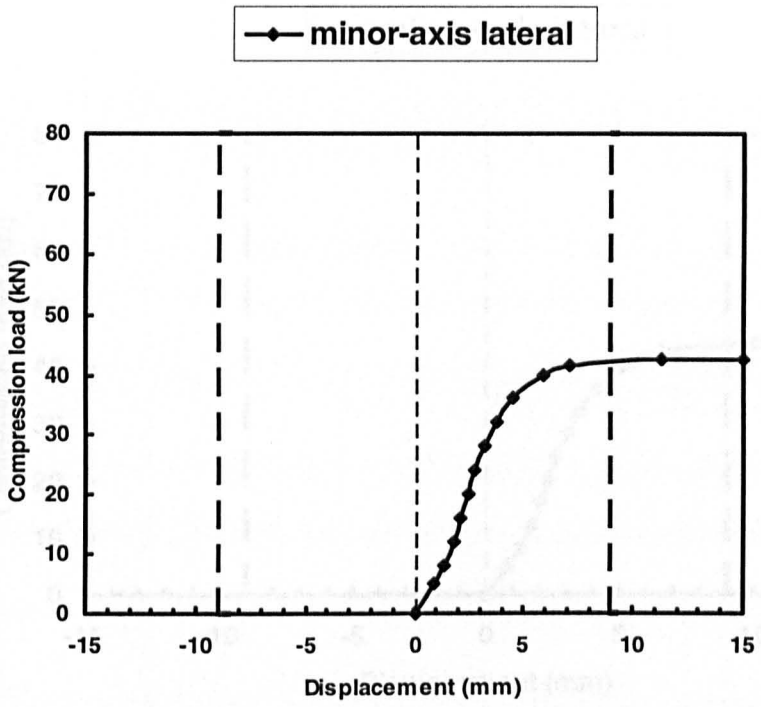

Figure 7.5. Load-displacement curve for column of type WU107.

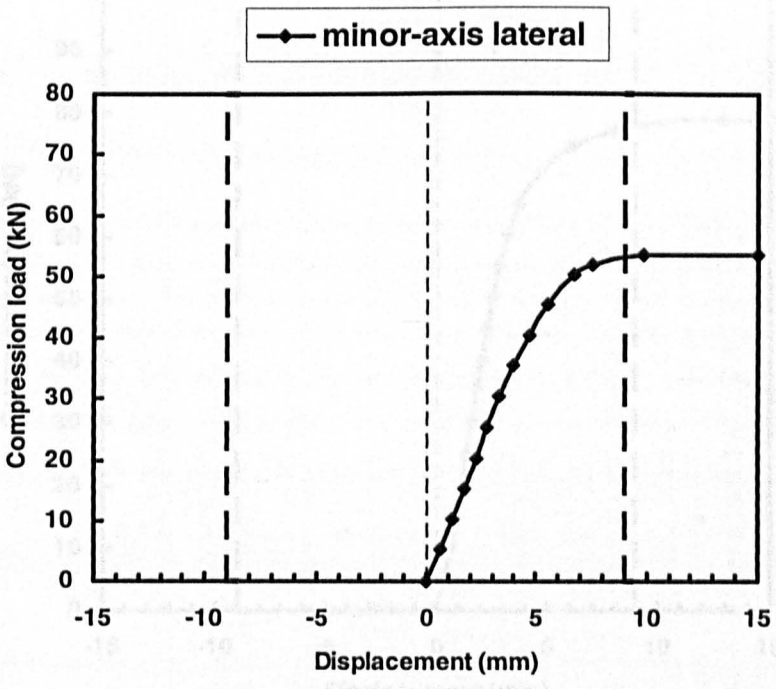

Figure 7.6. Load-displacement curve for column of type WU108.

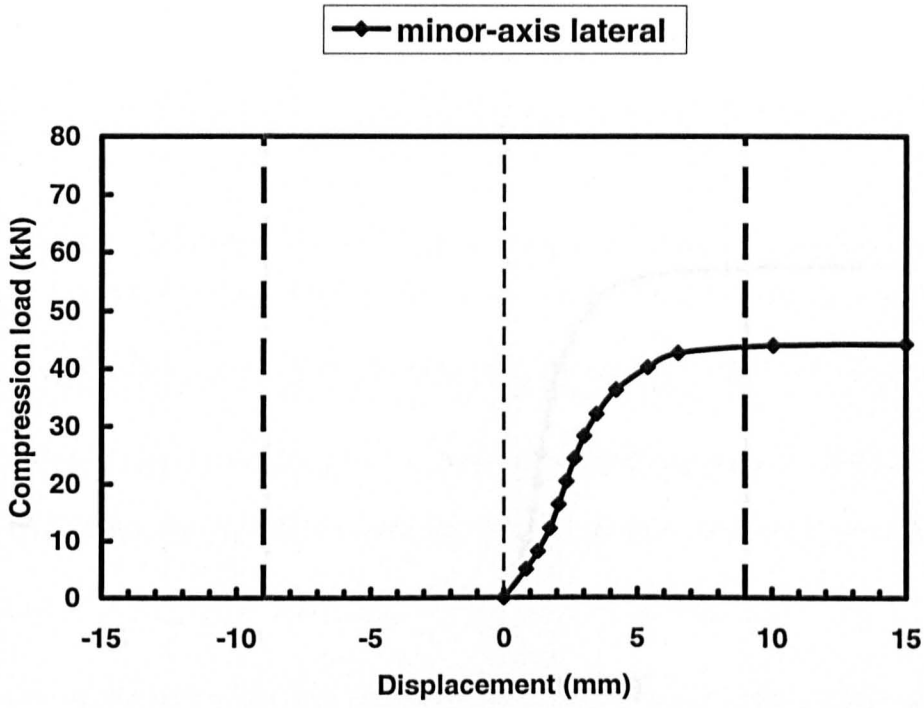

Figure 7.7. Load-displacement curve for column of type WU109.

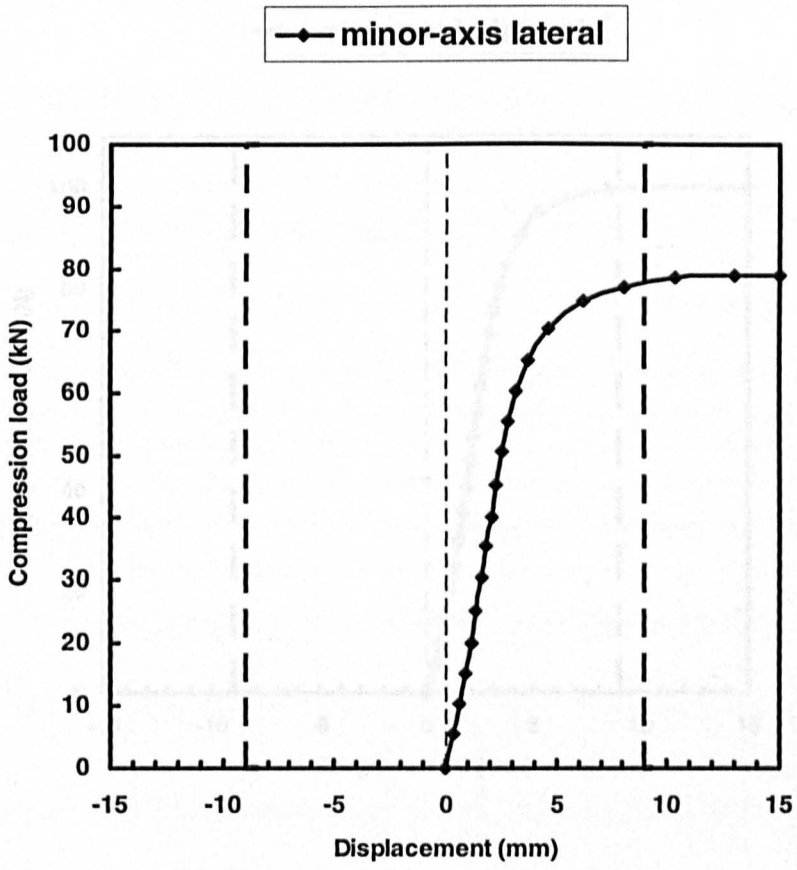

Figure 7.8. Load-displacement curve for column of type WU110.

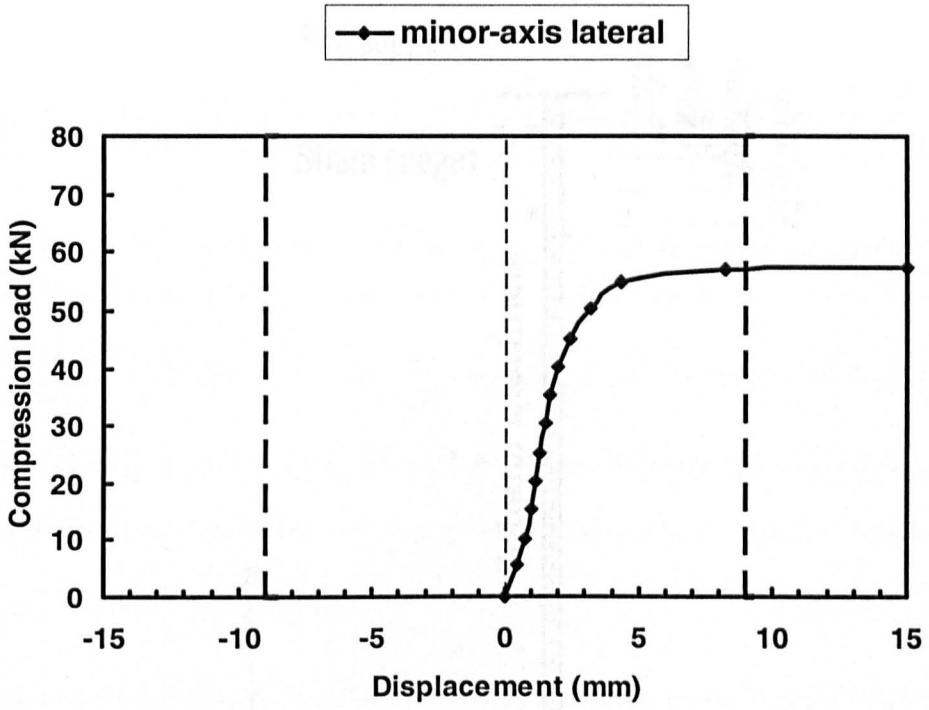

Figure 7.9. Load-displacement curve for column of type WU111.

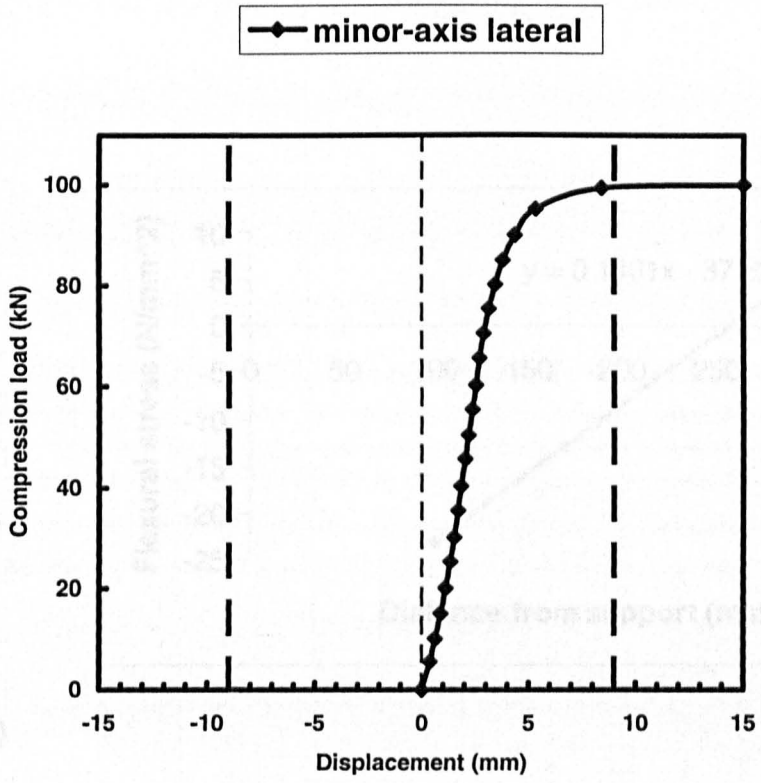

Figure 7.10. Load-displacement curve for column of type WU112.

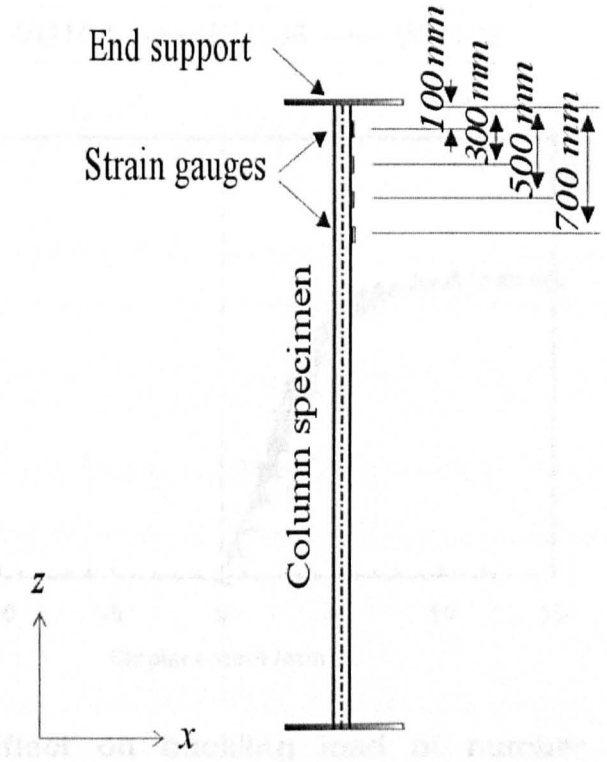

(a)

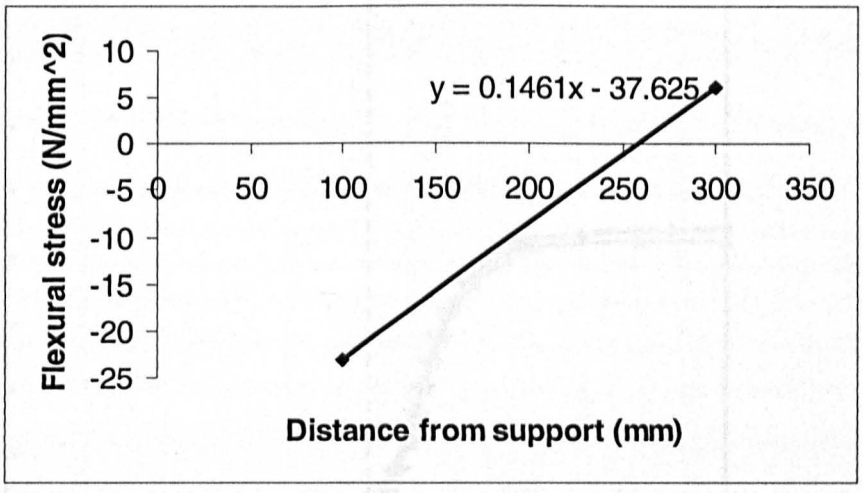

(b)

Figure 7.11 Determination of the point of zero curvature, (a) Locations of the strain gauges, (b) Location of the point of zero curvature from the ends of a ε-column.

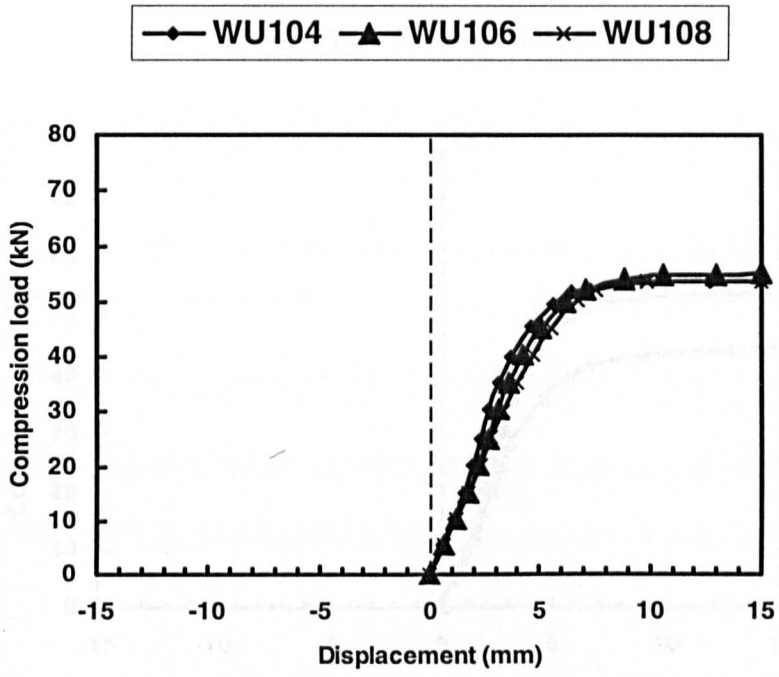

Figure 7.12. Effect on buckling load of number and location of stiffeners, from testing columns of types WU104, WU106 and WU108.

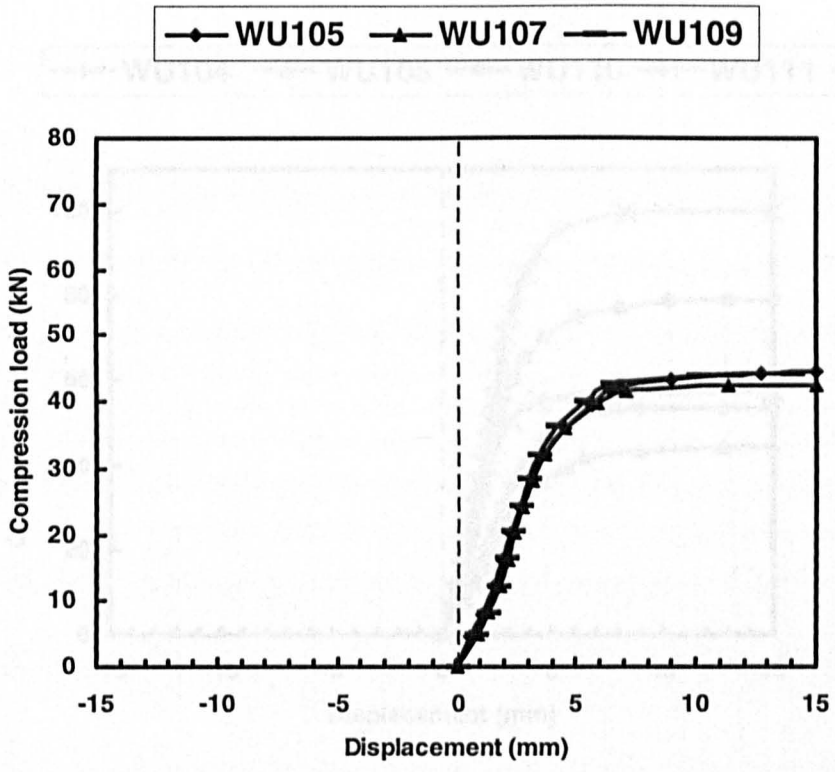

Figure 7.13. Effect on buckling load of number and location of stiffeners, from testing columns of types WU105, WU107 and WU109.

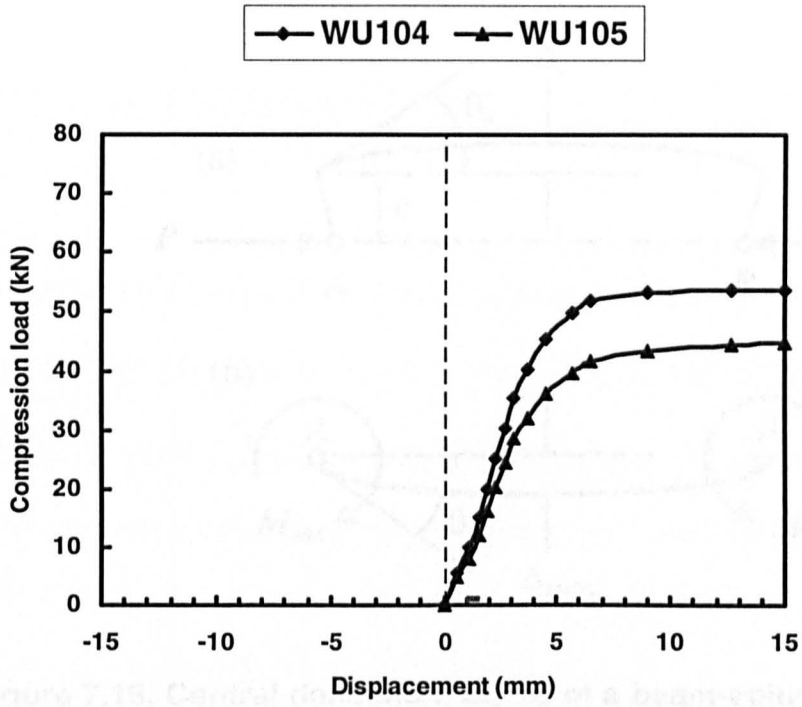

Figure 7.14. Influence on buckling resistance of ε-section wall thickness, with column type WU104 at 1.5 mm and WU105 at 2 mm.

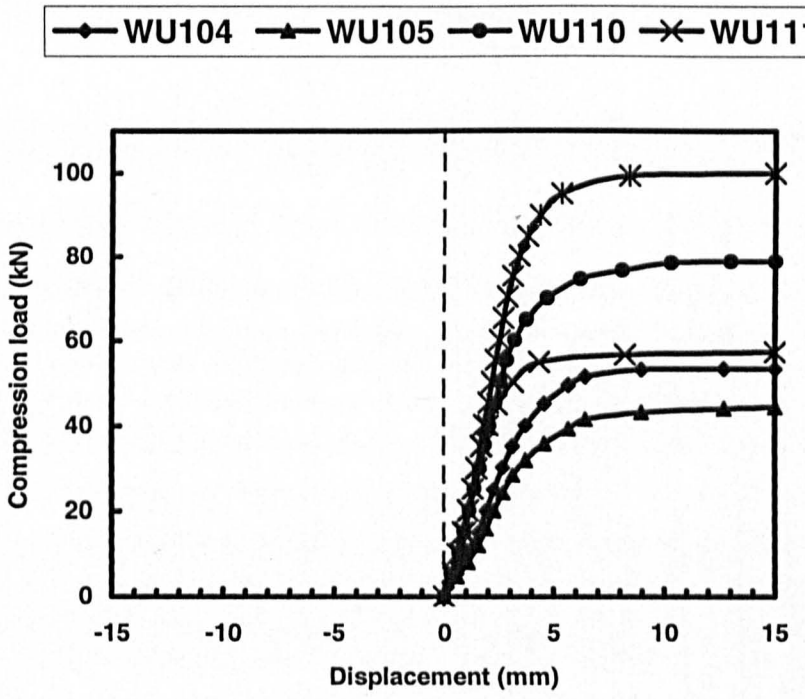

Figure 7.15. Influence on load-displacement response and buckling resistance of having ε-section fully-opened in column types WU104 and WU105 and fully-enclosed in column types WU110 to WU112.

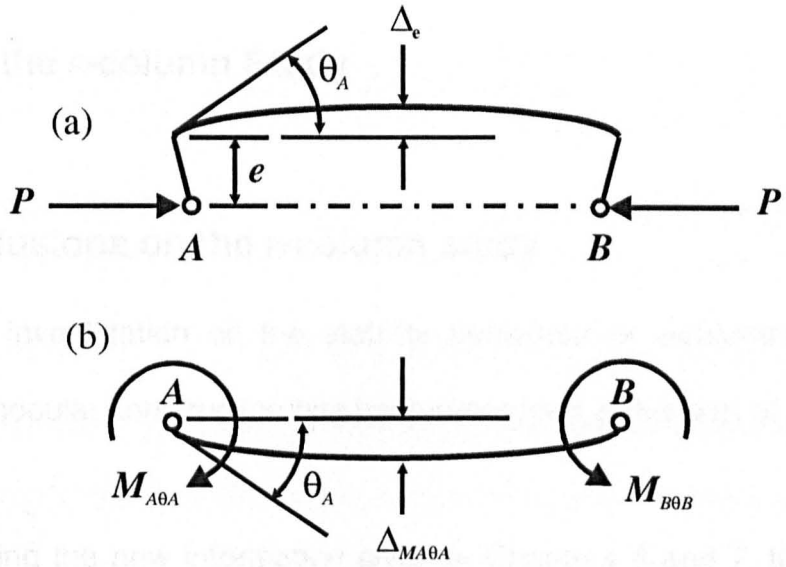

Figure 7.16. Central deflection, (a) Δ_e of a beam-column member due to load eccentricity, (b) $\Delta_{MA\theta A}$ of a beam-column member, without axial compression, due to equal end-moments.

Chapter 8 Conclusions and Recommendations for Further Work on the ε-column Study

8.1 Conclusions on the ε-column study

A detailed investigation on the stability behaviour of ε-columns of 2.7 m length for modular construction has been presented in this part of the thesis.

On evaluating the new information given in Chapters 6 and 7, the following findings and conclusions can be made:

(a) In order to predict, the critical load for local buckling of ε-columns the author has developed a new plasticity reduction factor for the complex curved cross-sectional shape. This new factor enables the prediction of the critical local buckling load of ε-stub that occurs in the inelastic regime.

(b) Using coupon test results the actual stress against strain relationship for the steel in the ε-sections was established, and need to determine for the inelastic local buckling analysis the initial Young's modulus, the secant modulus, and the tangent modulus.

(c) Stub column failure loads from physical testing confirmed the theoretical work showing that the critical buckling load for the local mode does occurs in the plastic region. From this finding with the ε-section of lowest wall thickness (i.e. 1.5 mm) it can be said that there is no reduction in the column strength due to local instability, since it cannot happen in the elastic range. It can therefore be concluded that when designing ε-columns of 2.7 m length the engineer can consider the gross area of the

section to be the effective area. This is often not the case when if steel section has the conventional shapes shown in BS5950-5: 1998. These generally comprise an assembly of flat plates and the finding show why the curve ε-shape is a more optimal use of thin-gauge steel.

(d) By inspecting the strain profile at failure in the stub ε-column, the inelastic buckling shape is observed to be in the form of two-and-half half-wavelengths. From this information the author proposes that the failed ε-section under compression can be considered to consist of two outer flanges and central web elements. Based on this assumption the critical local buckling load of the flange component was theoretically predicted and this is considered to be the failure load of the 1.5 mm thick stub ε-column.

(e) Conventional single symmetry open-section members of flat-plate elements are recognised to have a relatively low resistance to torsion. BS5950-5: 1998 accounts for this fact by including a reduction term in the expressions to calculate column strength. Since the author did not observe the loaded ε-columns experiencing any twisting deformation, it is concluded that torsional-flexural instability can be ignored in the design of ε-columns of 2.7 m height. Designers therefore need not have to account for the movement of the effective neutral axis in accordance to clause 6.2.4 in BS5950-5: 1998.

(f) For simplicity in design calculations the column's connections are modelled as either pinned or fixed. In reality, the end conditions do provide a degree of rotational restraint. For the test fixtures used in the series of strength test the effective length factor was estimated to be 0.81, by applying the technique of obtaining the point of contra-flexure. It is believed that this value is able to represent the actual effective length in practice (see Figure 2.5 for how a modular unit might be constructed). This, and finding (g) means that the column design capacities determined from testing can be used in design practice.

(g) The ε-column specimens were found to have an out-of-straightness imperfection ranging from 0.0 to 0.6 mm over the 2.7 m length. Given that the maximum is only $L/4500$ compared to the $L/1000$ for design criterion in BS5950-1 we can conclude that ε-members can be considered to be straight. By using a simple structural analysis the overall load eccentricity in the test programme was estimated to be between 2.0 and 2.5 mm, and this appears to be independent of having the ε-section open or enclosed. The presence of an overall load eccentricity caused the test strength loads to be lower than had the resultant force acted through the centroid of the section. Since a load eccentricity is very probable in practice the test results reported in this thesis will inherently allow for this strength reduction.

(h) By using the 54 new strength test results it has been shown that the column design capacities are higher than those predicted using Clause 6.2.3 in BS5950-5: 1998 for the Euler buckling mode of failure and an

effective length of 0.81. This will remain valid providing ε-sections continues to be made with tight tolerances.

(i) To develop modular frames of minimum weight and fabrication cost will require ε-sections of a variety of cross-sectional sizes. Nine different types of ε-columns have been investigated so far. The results for the five sections of 2.0 mm wall thickness and for the four sections of 1.5 mm thickness have shown that:

- there is no significant strength increase by having intermediate bracing stiffeners.
- by increasing the wall thickness from 1.5 mm to 2 mm column strength increases by 20%, and this corresponds to the change in minor-axis second moment of area.
- by enclosing the open ε-sections of 2 mm and 1.5 mm wall thicknesses, the resistances increases by 46% and 28%, respectively.
- by further increasing column stiffness by way of including a continuous stiffener of C-section, the buckling resistance is increased by 85%.

(j) Finally, this study on ε-columns for modular construction has shown that column design by Clause 6.2.3 is going to be acceptable as long as the deliverables of the author's research are taken into account.

8.2 Recommendations for further work

The findings in this part of the thesis show that the ε-section shape for cold-formed sections will, for the same weight of steel, increase the torsional stiffness and the resistance to concentric compressive load. It can be anticipated that the rapid and continuing advances in materials science and production technologies will give us additional performance improvements and reduced costs through the optimization process. Regardless of the current advantages that can be achieved by using ε-sections in Modern Methods of Construction further investigations are needed. They should include studies on the successful integration of ε-section columns with other building components, such as beams, joints and bracing system. A key aspect to future research must be the development of a comprehensive understanding of constructionability needs, specifications and design rules that facilitate fabrication, erection and future maintenance.

The author recommends the following six topics for further work:

- Although in Chapter 4 a new theoretical treatment for the inelastic critical buckling load of curved-plate element is presented, and used to determine loads for ε-sections, its validation still requires a carefully conducted series of physical tests that satisfy the theoretical specified boundary conditions.
- Based on a measured stress distribution profile at the mid-height plane of a stub ε-column the buckling form at failure was assumed. The author then assumed that the classification of the 1.5 mm thick ε-section made it consist of two-flanges and one-web components. More

physical tests are required to justify this classification of how the ε-section behaves under compressive load.

- In practice the shear force to be transferred from beams to columns are eccentric (i.e. applied at an offset to the supporting column). It is essential, to represent what happens in practice, for there to be a characterisation of ε-columns under eccentric loading.
- Evidence from the stud column tests shows that the end fixity in the test arrangement is neither pinned nor fixed (i.e. some degree of connection stiffness exists that is insufficient to develop full continuity BS5950-5: 1998). To confirm this finding a study on the end fixity factor in modular units is required. This is also needed in order to avoid any adverse affects to other components in the structural system.
- To develop strut curves the characterisation of concentrically loaded ε-columns is required over the full range of lengths.
- Thin-walled steel sections have been utilized as primary members in the form of stud column, roof trusses and floor joists to carry compression, tension and bending forces. For ε-sections to have a universal application as members in MMC it is going to be necessary to investigate their structural performance for their utilisation as beam and truss members.

Chapter 9 Analysis of Frames of Fibre Reinforced Polymer Sections

9.1 Introduction

A FRP composite is a combination of a polymer resin (or plastic) based matrix and a reinforcing system in the form of high-strength fibres. The resin is often a polyester, vinyl ester or epoxy and the fibres can be of glass, aramid, or carbon. The resin protects the fibres, maintains their alignment, and distributes the loads evenly among them. There are a number of processing methods to make products such as reinforcing rods, strengthening strips or plates, and structural shapes and systems for the construction sector (Hollaway and Head 2001).

According to Ludovico (2002) the automotive industry first introduced FRPs into vehicle bodies in the early 1950s. Because these materials have desirable characteristics research went into improving the materials and their manufacturing processes. This effort in the 1950s and 1960s led to the development of new manufacturing methods, such as pultrusion, resin transfer moulding, and filament winding. Their development can be seen to have helped to advance composite technology into new markets.

The aerospace industry first began to use FRPs in pressure vessels, containers, and other non-structural aircraft components. By the 1990s the

aircraft sector were starting to use FRPs in primary load-bearing structures. The application FRPs in the construction sector can be seen to have been slower and only gathered pace in the 1980s, after the first road bridges were strengthened using carbon FRP plates (Hollaway and Head 2001). Today we observe that major new application areas for FRPs are for infrastructure, industrial facilities, and offshore exploration and production. Figure 9.1(a) show the West Mill Bridge in Oxfordshire, which has a Pultruded FRP deck (ASSET) produced by Fiberline Composites A/S of Denmark. The handrails, and the girders on which the ASSET deck is supported are also of pultruded shapes. Figure 9.1(b) shows the Dubai international Airport Terminal Interior upgrading, which involved the fabrication and installation of wall façades fabricated of hand lay-up FRP material.

9.2 Pultruded structural shapes and systems

Of particular interest in the field of civil engineering are Pultruded FRP shapes and systems in which the polymer-based matrix is reinforced by fibres, often glass, by a process called pultrusion. Standard pultruded shapes are used as primary load-bearing members in trusses and braced framed structures, with bolting being the preferred method of connection (Turvey 2002). Figure 9.2 shows some standard and non-standard PFRP products. Combining such standard and non-standard shapes we produce an efficient form of construction systems.

9.3 The pultrusion process

The pultrusion process is shown schematically in Figure 9.3. FRPs are typically organized in a laminate structure, such that each lamina (or ply) can

contain an arrangement of unidirectional fibres or woven fibre fabrics embedded within a thin layer of light polymer matrix material. In the pultrusion process the "virgin" fibre reinforcement is pulled through a resin impregnation bath to coat it with the matrix. Typically the fibres are E-glass type. It should be noted that the matrix comprises a polymer resin, filler (e.g. clay) and other additives (such as colourant, fire retardant, die releasing agent). This uncured composite material is then pulled through perform plates to begin to form the fibre and matrix structure, and finally through a heated die (150 °C) to cure the matrix. A cured solid product of the desired shape exits the die at a rate of about 1 to 3 metres per minute. The name of the process comes from it having a set of pullers that pull the pultrudate through the machine. The final stage is to cut the shape into predetermined lengths, which is often set at 6 m. As has already been mentioned standard shapes are stocked by the major pultruders, and, to aid design engineers, these manufacturers provide their own design manuals. The available guidance for design includes manuals from Fiberline Composites A/S (Anon 1995), Strongwell (Anon 1989), and Creative Pultrusions (Anon 1999)

Pultruded Fibre Reinforced Plastic (PFRP) composites are used as structural members in civil engineering construction as lighter, more durable alternatives to steel and concrete elements (Bank and Mosallam 1991). The tensile and compressive strengths of the PFRP material are > 200 MPa along a section's length and about half this stress in the perpendicular directions. Under short-term loading the material can be taken to be linear elastic to failure. Structural failure of members and frames will be

characterised by excessive deflection or by an instability mode. Yielding, which is associated with material rupture is an uncommon failure mode for stressed PFRP members (Mottram *et al.* 2003).

For standard pultruded sections of I- and H-shapes the full-section longitudinal modulus in flexure is about 20-24 GPa (E) (Anon 1989) and the full-section in-plane shear modulus is about 4 GPa (G) (Mottram 2004).

9.4 Uses of FRPs in civil engineering

There are three broad divisions into which applications of FRP in civil engineering can be classified and these are for new build, repair and rehabilitation applications, and architectural applications. New build such as bridges and buildings executed of PFRP shapes and systems have demonstrated exceptional durability, and effective resistance to effects of environmental exposure (Keller 2003, Bank 2006).

The biggest usage of FRPs in the construction sector is for retrofitting and strengthening of existing structures, which on assessment by structural engineers are found in need of such maintenance. As Hollaway and Head (2001) present there are a number of advantages to adhesively bonding FRPs to deteriorated or under-strengthened structures that makes these materials the first choice. Another retrofitting approach that is used by several companies is to wrap damaged bridge piers to improve their structural integrity.

9.5 Merits and drawback

Along with FRPs' high relative strength properties, the most relevant merits for their use in construction are lightweight, excellent durability and corrosion resistance. Other merits for new build and retrofitting and repair are: a longer life cycles, a reduced maintenance cost, an increased site productivity and efficiencies in initial project and whole-life cost. Other features that provide reasons for their choices are: ease of installation, electromagnetic neutrality, excellent fatigue behaviour, and potential fire resistance. Furthermore, their high strength-to-weight ratio is of significant benefit for a member in supporting higher live loads since dead weight does not contribute significantly to the loading.

However, like all structural materials, FRP has drawbacks that create some hesitancy for structural engineers to use them widely. The factors that can limit their exploitation are the high cost of the FRP itself, its brittle behaviour, its susceptibility to deformation under long-term loads, photo-degradation (from exposure to light), temperature and moisture effects, lack of design codes, and most importantly, lack of awareness and historical precedent. A number of these drawbacks are receding with time as the technology and know-how matures and we continue to get positive feedback from assessing prototype structures that have been in use for more than decade (Hollaway and Head 2001, Keller 2003).

9.6 Frame analysis

The design of framed structures requires sizing and determination of the internal equilibrium forces in their components, and to justify that the

structure is economical and safe in terms of strength and stability under the specified design loads. The first step in designing structures is the analysis to calculate deflections and the member and joints actions. The common types of frame analysis for buildings are first-order elastic, second-order elastic, first-order inelastic and second-order inelastic. The basic distinctions between these methods of analysis are whether equilibrium is satisfied on the undeformed or deformed geometry of the structure, and whether member plastification is considered. Design standards for steel structures generally treat frame stability through strength and stability criteria for beam-columns (Galambos 1998).

Many methods can be followed to obtain a determination of the elastic critical load of framed structures (Chan and Chui 2000, Chen and Lui 1991, Galambos 1998, Ghali and Neville 1997). These include the differential equation method that give exact values of critical loads, and energy methods that provide an approximate solution by way of matrix stiffness and the finite element method.

Of these, the stiffness method is an efficient way to solve models for frame structures. It is a powerful analytical method and has been applied in numerous engineering fields, such as solid mechanics and fluid mechanics (Ghali and Neville 1997). The stages in the stiffness method for buckling analysis can be given as follows:

- The frame is subdivided at nodal points into a series of discrete line-elements (for the structural members).

- For each of these "beam-column" elements the terms in the element stiffness matrix are calculated using member and material properties.
- The element stiffness matrices are assembled to form the governing global stiffness matrix, when multiplied by the vector for nodal displacements will give the nodal forces.
- The displacement boundary conditions are applying to obtain the reduced matrix, which is then inverted.
- This new matrix is multiplying by the vector of forces associated with the unknown degrees of freedom to determine the unknown displacements at the nodes.
- Back substitution for these nodal displacements into the governing equations enables the analysis to calculate element stresses and strains, and restraint actions for the reaction forces.

9.7 In-house frame analysis software called sframe

in 1998 Zheng received a PhD from the University of Warwick for research on PFRP frames. As part of his research he formulated and wrote a plane-frame analysis tool with the specific aim of analysing the behaviour of shear-flexible frames. His software, called sframe, was written in the C language for the Unix operating system environment. Zheng's coding was developed with the intention of incorporating modelling features that are relevant to the practical applications of Pultruded and other FRP shapes in frameworks. It therefore included shear-flexible elements, second-order shear-deformable effects and semi-rigid joint action. The version of sframe by Zheng could only calculate the frame deformation and member forces. It is to be noted that

Zheng developed his own shear flexible stability function for the second-order P-Δ effects and that his supervisor Dr Mottram later found that their expression were wrong.

The author's work, to be reported in Chapters 10 to 12, has been to further the sframe code so that it can be used also to determine the elastic critical load for overall frame stability. This information can then be used to predict the effective length factors for the column members. Nonlinearities due to elastic force-displacement laws are taken into account using the correct shear flexible stability functions that are given in Al-Sarraf (1986). It was intended to provide an improved sframe code that gives an easy-to-use tool for tackling the difficult problem of incremental nonlinear structural analysis of shear-flexible frames. The main emphasis has been placed on the needs of engineering practice.

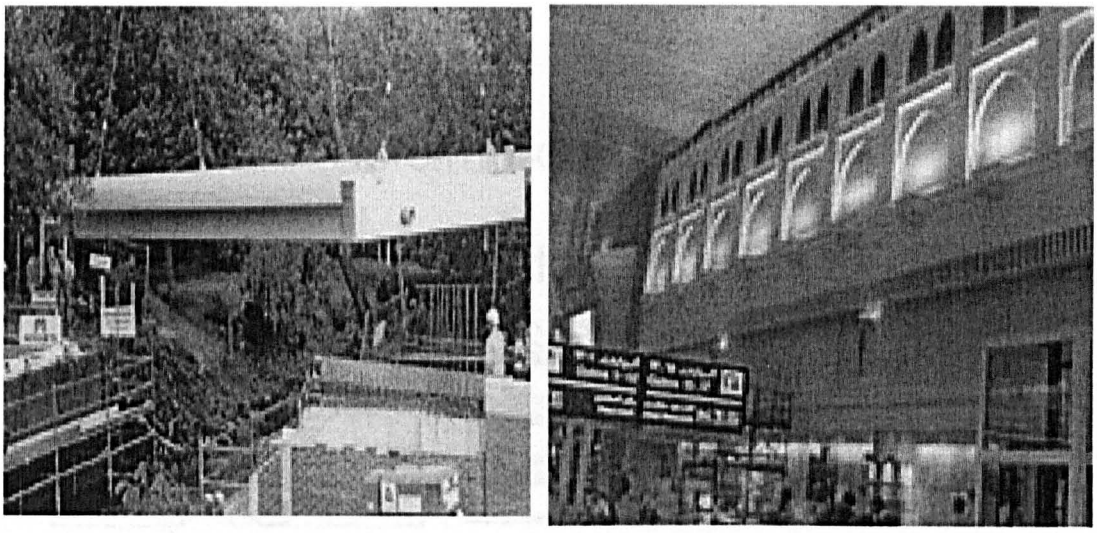

Figure 9.1. Application of FRPs in civil engineering. (a) West Mill Bridge in Oxfordshire, UK (b) Wall façade fabricated from FRP at Dubai International airport.

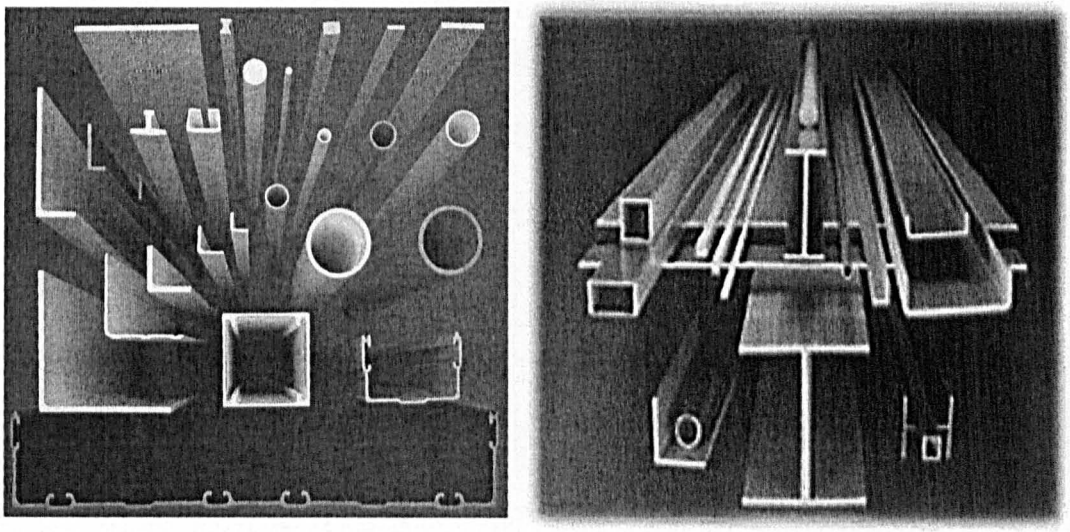

Figure 9.2. Standard and non-standard PFRP sections (from Strongwell, web site).

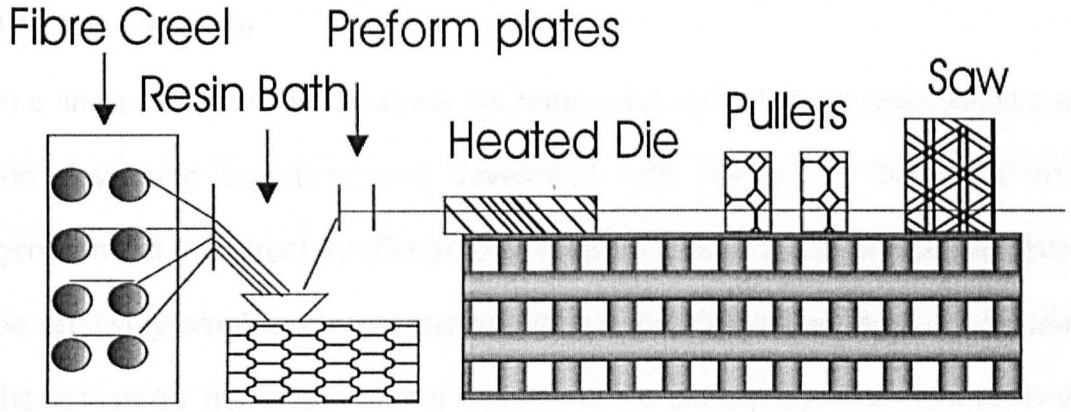

Figure 9.3. Schematic diagram showing the salient stages in the pultrusion process.

Chapter 10 Elastic Critical Load of Framed Structures

10.1 Introduction

In a linear or first-order analysis the material is modelled as linear-elastic and the governing equations are developed with respect to the undeformed geometry of the structure (Galambos 1998). The overall deformations have to be relatively small such that the resulting elastic displacements do not affect the assumed geometry of the structure. Consequently, the destabilization effect of any axial compressive force in the members is ignored and so this type of analysis cannot predict the structure's critical buckling load. In order to obtain more realistic analysis for the design of multi-storey structures it is necessary to consider the influence of geometrical effects on internal forces, caused by displacements and deflections of construction and its members. In a second-order analysis the material is still linear-elastic, but the change in geometry of the structure, for example due to side-sway Δ (as shown in Figure 10.1), is accounted for. Now when developing the governing force equilibrium equations reference is made to the current deformed configuration of the structure. The destabilizing effect of axial compression in members is accounted for, thereby, enabling the non-linear analysis to calculate the elastic critical buckling load.

For investigation of the second-order effect Figure 10.1 shows a simple frame for sway and no-sway examples. For the frame in Figure 10.1(a) a first-order analysis under gravity loads will yield bending moments in the beam equal to those for a simple span condition with zero moments in the

column. Equilibrium of the deflected shape requires large moments in the beam and non-zero moments in the column. These additional moments are due primarily to the P-Δ effect, where Δ is the lateral drift of the frame and P is the total axial load. For the frame in Figure 10.1(b), where side-sway is prevented, second-order moments are created in the beam and column arising from lateral deflection δ along the column. The additional moment in the column is equal to the column axial load P times the deflection δ, hence the name P-δ effect Galambos (1998).

The research reported in this part of the thesis addresses the topic of the theoretical analysis for the instability loading of framed structures (such as one shown in Figure 10.2) made of FRP components, and, in particular, frames with members manufactured by the pultrusion process. The mechanical properties of FRPs as presented in Section 9.3 can be greatly different from those for conventional construction materials, and their relative values are not that well known to the practicing engineer and infrastructure systems planner. This suggest that there is a need to develop new design tools, in the form of guidelines and criteria, which are consistent with the characteristics of this new category of structural material. Despite the current similarity in construction of PFRP frames (Anon 1989, Anon 1995, Anon 1999) with conventional steelwork (Owens *et al.* 1994) there has been limited computational modelling to analyse PFRP frame behaviour.

Many researchers have studied the components of PFRP frame as isolated elements (beams, columns and connections). For information on the

behaviour of PFRP beam members one can refer to the papers by Brooks and Turvey (1995), Turvey (1997) and Davalos and Qiao (1999). Regarding papers on research for the behaviour of PFRP column members, one should mention those by Zureick and Scott (1997), Lane and Mottram (2002) and Mottram (2004). On the important topic of joints between PFRP members and their structural properties the reader is directed to the research described in Bank *et al.* (1990), Mottram and Zheng (1999), and Turvey and Cooper (2000). But little work has been done so far on the behaviour of the entire PFRP frame structure as a whole. Mosallam (1990) conducted analytical and experimental investigations for both the time-independent and time-dependent response of a full-scale frame structure constructed entirely from PFRP sections. Mosallam concluded that the semi-rigid action of beam-to-column connection is a controlling factor regarding the overall behaviour of PFRP frame structures, and needs to be considered. Zheng (1998), not only characterised a number of beam-to-column joint arrangements, he also developed an analytical method to predict the static response of linear elastic plane frames. Moreover, he formulated new but incorrect shear-flexible stability functions to take account of the second-order P-Δ effects when the members are shear flexible. Flowing analysed PFRP frames to determine deformation and internal forces it was a logical step to want to develop the theoretical treatment to enable the elastic critical buckling load for overall frame instability to be established.

This chapter outlines the theoretical development of the approach that the author has introduced into the sframe coding so that it now predicts the

overall elastic critical buckling load for FRP plane framed structures. The analysis takes into account the following physical attributes of FRP frames:

- Shear-flexible element
- Semi-rigid joint action
- Shear-flexible stability functions.

Each of these attributes will be discussed further, with a presentation of how they are mathematically modelled in Sections 10.2 and 10.3.

10.2 The stability concept of structures

The stability of a structural member under compression action can be studied by using the same theory to investigate the stability of the equilibrium configuration of a rigid body system (Timoshenko and Gere 1963). Stability can be regarded as an equilibrium curve for the structural system; in this curve any point representing equilibrium values of load and deflection in a coordinate system. The equilibrium of any point on the curve is stable if, at that point, either the total potential energy of the system is locally a minimum or the system is liable to return to its current equilibrium state, when slightly disturbed. If the total potential energy is not a minimum at that point the system might either be in a condition of neutral equilibrium or instability. The value of the loading at the limit of stable equilibrium is referred to as critical buckling load. After the critical load has been achieved any equilibrium configuration of the system will be unstable, and as the structure deforms non-proportionally its stiffness reduces with change in geometry without the need for a further load increase. Instability may be considered as a deteriorating stiffness phenomenon of the structure Chan and Chui (2000).

Instability of frames can occur in the overall system or in some of its members where compression stresses exist. Before computational methods were in common use, the British Code of practices (BS 449-2: and BS 5950-1: 2000) tackled the stability of steel columns by an approximation to the value of the effective length factor. Tabulated values ranging between 0.5 and 2.0 depend upon whether the column ends are effectively held in position and restrained in direction. By reviewing the effective-length concept, Wood (1974) concluded that one of the uncertainties lies in being able to specify the effective lengths of continuous columns. Then he emphasised that to design for the limit-state of collapse it is essential to consider the overall frame instability since the effective lengths that are based on local restraints are not accurate enough for this situation.

With the universal availability of computing software and hardware during the 1980s the analysis of overall frame structures to determine their elastic critical buckling loads was recognized as being a more reliable approach to design steelwork against instability (Dowling *et al.* 1988).

It is within the context of the issues presented in Section 10.1 and the historical development of the analysis methods used to design steel frames that a computational tool for the instability analysis of plane frames of FRP members is desirable. The following Sub-sections in this Section explain the modelling approach in the static analysis code sframe that was written by Zheng (1998) and how the author modified it to calculate the theoretical loading for failure by bifurcation buckling.

10.2.1 Element shear deformation

For the structural analysis in this thesis the matrix stiffness method is adopted. The slope-deflection equations, which relate slope and sway at the ends of a member to the moments and shears at the ends, play an important role in the method's development. For the beam-column element Figure 10.3 shows the nodal forces and nodal displacements that are used in the slope-deflection equations.

The mechanical properties of advanced polymeric composites (Hollaway and Head 2001) depend on many variables, such as manufacturing process and the fibre/matrix combination and arrangement. As discussed in Chapter 1, members of FRP can have a moduli ratio (E/G) that is many times higher than for the same member of an isotropic material (Bank and Bednarczyk 1988, Mottram and Aberle 2002). This fact informs us that the deformation of an element of FRP will need to include the effect of the shearing force action. The consequence is that, shear deformation will be analysed and as we shall see in Chapter 11 its presence reduces the critical buckling load. Conservative design of FRP frames against overall buckling failure therefore requires the effect of shear deformation to be included, both for member deformation and for its influence on second-order effect via the stability functions.

Lets consider the element in Figure 10.3, where the two end moments M_1 and M_2 are different. The constant shear force along the element of length l is therefore given by $V = -(M_1 + M_2)/l$. This shear force produces additional

deformation (Mottram and Aberle 2002) to that caused by the action of the bending moment distribution. This deformation is in the form of an anticlockwise rotation (in the opposite sense to the rotation due to the action of a positive moment) that has a constant value along the element's length. And this rotation gives a slope of magnitude equal to the shear strain at the centroid of the cross-section, and which can be expressed by (Timoshenko and Gere 1972)

$$\frac{dy_s}{dx} = \frac{\tau_{xy}}{G} = \frac{\beta \overline{V}}{AG}, \tag{10.1}$$

in which, y_s is the deflection due shear, $\overline{V}$ is the shear force, A is the cross-sectional area and G is the shear modulus of the member. β is the shear correction factor, whose presence allows for the non-uniform shear stress over the section (Timoshenko and Gere 1972).

For the general beam-column element shown in Figure 10.4 the development of the set of slope-deflection equations for the case of the shear-flexible member are presented in Zheng (1998), and can be written in matrix form as

$$\begin{Bmatrix} \overline{U}_1^e \\ \overline{V}_1^e \\ \overline{M}_1^e \\ \overline{U}_2^e \\ \overline{V}_2^e \\ \overline{M}_2^e \end{Bmatrix} = \begin{bmatrix} \frac{EA}{l} & 0 & 0 & -\frac{EA}{l} & 0 & 0 \\ 0 & \frac{1}{l(\nu+\psi)} & \frac{1}{2(\nu+\psi)} & 0 & -\frac{1}{l(\nu+\psi)} & \frac{1}{2(\nu+\psi)} \\ 0 & \frac{1}{2(\nu+\psi)} & \frac{\left(\frac{l^2}{3}+\psi EI\right)}{l(\nu+\psi)} & 0 & -\frac{1}{2(\nu+\psi)} & \frac{\left(\frac{l^2}{6}-\psi EI\right)}{l(\nu+\psi)} \\ -\frac{EA}{l} & 0 & 0 & \frac{EA}{l} & 0 & 0 \\ 0 & -\frac{1}{l(\nu+\psi)} & -\frac{1}{2(\nu+\psi)} & 0 & \frac{2}{l\left(\nu+\frac{\psi}{2}\right)} & -\frac{1}{2(\nu+\psi)} \\ 0 & \frac{1}{2(\nu+\psi)} & \frac{\left(\frac{l^2}{6}-\psi EI\right)}{l(\nu+\psi)} & 0 & -\frac{1}{2(\nu+\psi)} & \frac{\left(\frac{l^2}{3}+\psi EI\right)}{l(\nu+\psi)} \end{bmatrix} \begin{Bmatrix} \overline{u}_1^e \\ \overline{v}_1^e \\ \overline{\theta}_1^e \\ \overline{u}_2^e \\ \overline{v}_2^e \\ \overline{\theta}_2^e \end{Bmatrix}, \quad (10.2)$$

where $\nu = \frac{l^2}{12EI}$ and $\psi = \frac{\beta}{GA}$, E is the member's longitudinal modulus of elasticity and I is the second moment of area. $\overline{U}_1^e$ and $\overline{U}_2^e$ are the member end axial forces, $\overline{V}_1^e$ and $\overline{V}_2^e$ are the member end shear forces, $\overline{M}_1^e$ and $\overline{M}_2^e$ are the member end-moments, $\overline{u}_1^e$ and $\overline{u}_2^e$ are the member end axial displacements, $\overline{v}_1^e$ and $\overline{v}_2^e$ are the member's end sways, and $\overline{\theta}_1^e$ and $\overline{\theta}_2^e$ are the member's end rotations.

In the linear analysis method the equations of equilibrium in Equation (10.2) are based on the undeformed frame geometry that exists before load application. In compact format Equation (10.2) for the element, e, can be rewritten as

$$\{\overline{\mathrm{F}}\}^{(e)} = [\overline{\mathrm{k}}]^{(e)}\{\overline{\delta}\}^{(e)} \quad (10.3)$$

where $[\overline{k}]^{(e)}$ is the element stiffness matrix, $\{\overline{\delta}\}^{(e)}$ is the vector for the element's nodal displacements.

10.2.2 Shear-stiff stability functions for isotropic elements

Two methods often employed to capture second-order behaviour in the element stiffness relationships are referred to as the stability-function and geometric approaches (Galambos 1998). It is relevant to understanding shear-flexible stability functions to introduce the functions for elements that are shear stiff (that is ratio E/G tending to zero). In the linear analysis method of Section 10.2.1 all members in the framework are consider as beam elements that are subjected to flexure only. The effect of axial force on changing beam-column element's stiffness is ignored. In 1956 Livesley developed set of shear-stiff stability functions in order to account for the second-order effect (P-Δ) when members are of isotropic material (the aim of his work was to develop a computer calculation method for the analysis of steel frames).

For the general shear-stiff beam-column element shown in Figure 10.4, the 6x6 elastic element stiffness matrix presented by Livesley in 1956 is

$$[\bar{\mathbf{k}}]^{(e)} = \begin{bmatrix} \frac{EA}{l} & 0 & 0 & -\frac{EA}{l} & 0 & 0 \\ 0 & \frac{12EI}{l^3}\phi_5 & -\frac{6EI}{l^2}\phi_2 & 0 & -\frac{12EI}{l^3}\phi_5 & -\frac{6EI}{l^2}\phi_2 \\ 0 & -\frac{6EI}{l^2}\phi_2 & \frac{4EI}{l}\phi_3 & 0 & \frac{6EI}{l^2}\phi_2 & \frac{2EI}{l}\phi_4 \\ -\frac{EA}{l} & 0 & 0 & \frac{EA}{l} & 0 & 0 \\ 0 & -\frac{12EI}{l^3}\phi_5 & \frac{6EI}{l^2}\phi_2 & 0 & \frac{12EI}{l^3}\phi_5 & \frac{6EI}{l^2}\phi_2 \\ 0 & -\frac{6EI}{l^2}\phi_2 & \frac{2EI}{l}\phi_4 & 0 & \frac{6EI}{l^2}\phi_2 & \frac{4EI}{l}\phi_3 \end{bmatrix} \qquad (10.4)$$

where the ϕs (i = 1 to 5) are the Livesley shear-stiff stability functions. Now we find that the element stiffness matrix $[\bar{k}]^{(e)}$ is function of axial force, that is $[\bar{k}\{P\}]^{(e)}$. It is to be noted that Equation (10.4) is in a format ready to be coded for analysis by the matrix stiffness method.

10.2.3 Shear-flexible stability functions for FRP elements

FRP members, such as standard pultruded shapes, for framed structures are recognized to be shear deformable, and accounting for the influence of shearing on the element's response is therefore desirable. To facilitate the prediction of the elastic critical buckling load of frames with shear-flexible members Al-Sarraf (1986) modified shear-stiff stiffness factor s and shear-stiff carry-over factor c. His work considered the shear-deformation effect by introducing a shear-flexible parameter μ, which is defined by

$$\mu = \frac{\beta P_E}{GA} = \frac{\beta \pi^2}{\left(\frac{l}{r}\right)^2} \frac{E}{G} \tag{10.5}$$

with r the radius of gyration ($r = \sqrt{I/A}$) and l/r the slenderness ratio for the element. The other variables have been defined and it can be observed that μ is dependent of geometrical and material properties.

In order to modify the stiffness matrix in Zheng's sframe code, which had his, incorrectly derived, shear-flexible stability functions, the author formulated shear-flexible ϕ_i functions, based on Al-Sarraf's shear-flexible stiffness factor $\bar{s}$ and shear-flexible carry-over factor $\bar{c}$. In this sub-section, a brief

description of the development of the new shear-flexible ϕ_i functions is presented.

The basic differential equation for the shear-flexible element, according to Timoshenko and Gere (1972), is

$$\frac{d^2y}{dx^2} = -\frac{M}{EI} + \frac{\beta}{AG}\frac{d\overline{V}}{dx} \tag{10.6}$$

In Equation (10.6) y is the vertical deflection and x is the distance along the element from its left-hand end. Lets now consider the beam-column element shown in Figure 10.5 where the relative end sway Δ is zero. The bending moment M_x and corresponding shear force $\overline{V}_x$ at a distance x from end 1 are

$$M_x = \left(1-\frac{x}{l}\right)M_1 - \frac{x}{l}M_2 + Py \tag{10.7}$$

$$\overline{V}_x = -\left(\frac{M_1+M_2}{l}\right) + P\frac{dy}{dx} \tag{10.8}$$

By substituting the Equations (10.7) and (10.8) into Equation (10.6), and replacing axial force P by ρP_E, the beam-column curvature expression yields

$$\zeta\frac{d^2y}{dx^2} + \frac{\rho P_E}{EI}y = \frac{1}{EI}\left[M_1\left(\frac{x}{l}-1\right) + M_2\left(\frac{x}{l}\right)\right], \tag{10.9}$$

Parameter $\zeta = 1-\mu\rho$ and P_E is the critical Euler buckling load for the element with an effective length factor of 1.0. The general solution to Equation (10.9) is

$$y = c_1\sin\pi\sqrt{\overline{\rho}}\,\frac{x}{l} + c_2\cos\pi\sqrt{\overline{\rho}}\,\frac{x}{l} + \frac{M_1}{\rho P_E}\left(\frac{x}{l}-1\right) + \frac{M_2}{\rho P_E}\left(\frac{x}{l}\right) \tag{10.10}$$

Where c_1 and c_2 are constants of integration and parameter $\overline{\rho} = \frac{\rho}{\zeta}$.

The relationship between the end-moments and end-rotations (structurally relevant) can be written as

$$M_1 = k(\bar{s}\theta_1 + \bar{s}\bar{c}\theta_2) \tag{10.11}$$

$$M_2 = k(\bar{s}\bar{c}\theta_1 + \bar{s}\theta_2) \tag{10.12}$$

in which $\bar{s}$ is the shear-flexible stiffness factor and $\bar{c}$ is the shear-flexible carry-over factor.

By substitution for the end-moments M_1 and M_2 in Equation (10.10), and applying the boundary conditions, the solution for $\bar{s}$ and $\bar{c}$ yields expressions

$$\bar{s} = \frac{\bar{\alpha}(1 - 2\zeta\bar{\alpha}\cot 2\bar{\alpha})}{\tan\bar{\alpha} - \zeta\bar{\alpha}} \tag{10.13}$$

and

$$\bar{c} = \frac{2\zeta\bar{\alpha} - \sin 2\bar{\alpha}}{\sin 2\bar{\alpha} - 2\zeta\bar{\alpha}\cos 2\bar{\alpha}} \tag{10.14}$$

where $\bar{\alpha} = 0.5\pi\sqrt{\bar{\rho}}$. Because $\bar{s}$ and $\bar{c}$ are dependent on the shear-flexibility parameter μ their values are dependent on the geometric and material properties of the element.

A set of non-linear shear-flexible equations for the general beam-column member, shown in Figure 10.4, can now be develop in a similar manner as in the pure rotation case in Figure 10.5, and they are.

$$M_{12} = k\left(\bar{s}\theta_1 + \bar{s}\bar{c}\theta_2 - \bar{s}(1+\bar{c})\frac{\Delta}{l}\right) \tag{10.15}$$

$$M_{21} = k\left(\bar{s}\bar{c}\theta_1 + \bar{s}\theta_2 - \bar{s}(1+\bar{c})\frac{\Delta}{l}\right) \tag{10.16}$$

$$\overline{V} = \frac{k}{L}\left(\bar{s}(1+\bar{c})\theta_1 + \bar{s}(1+\bar{c})\theta_2 - 2\overline{A}\frac{\Delta}{l}\right) \tag{10.17}$$

Parameter $\overline{A}$ in Equation (10.17) is defined as $\bar{s}(1+\bar{c}) - 0.5\pi^2\overline{\rho}$.

In terms of $\bar{\phi}_1$ the shear-flexible stiffness factors are given by

$$\bar{s} = \frac{\zeta\bar{\alpha}^2 + \bar{\phi}_1 - \eta\bar{\phi}_1^2}{1-\zeta\bar{\phi}_1} \tag{10.18}$$

and

$$\bar{c} = \frac{1}{\bar{s}}\left(\frac{\zeta\bar{\alpha}^2 - \bar{\phi}_1 + \eta\bar{\phi}_1^2}{1-\zeta\bar{\phi}_1}\right) \tag{10.19}$$

$\bar{\phi}_1 = \bar{\alpha}\cot\bar{\alpha}$ and is the author's first shear-flexible $\bar{\phi}_i$ function. In order to construct the stiffness matrix (as in Equation (10.2)) for the shear-flexible beam-column element another four shear-flexible phi functions ($\bar{\phi}_i$ (i = 2 to 5)) were formulated by the author, and their expressions are:

$$\bar{\phi}_2 = \frac{\beta\bar{\alpha}^2}{3(1-\beta\bar{\phi}_1)} \tag{10.20}$$

$$\bar{\phi}_3 = \frac{3\bar{\phi}_2 + \bar{\phi}_1}{4} \tag{10.21}$$

$$\bar{\phi}_4 = \frac{3\bar{\phi}_2 - \bar{\phi}_1}{2} \tag{10.22}$$

$$\bar{\phi}_5 = \bar{\phi}_1\bar{\phi}_2 \tag{10.23}$$

The workings to the derivation of the $\bar{\phi}_i$ functions are to be found in Appendix B. It will be observed that the shear-flexible phi functions have the same format as the shear-stiff phi functions.

The modified 6x6 elastic element stiffness matrix of the general shear-flexible beam-column is now given by

$$\left[\bar{k}\right]^{(e)} = \begin{bmatrix} \frac{EA}{l} & 0 & 0 & -\frac{EA}{l} & 0 & 0 \\ 0 & \frac{12EI}{l^3}\bar{\phi}_5 & -\frac{6EI}{l^2}\bar{\phi}_2 & 0 & -\frac{12EI}{l^3}\bar{\phi}_5 & -\frac{6EI}{l^2}\bar{\phi}_2 \\ 0 & -\frac{6EI}{l^2}\bar{\phi}_2 & \frac{4EI}{l}\bar{\phi}_3 & 0 & \frac{6EI}{l^2}\bar{\phi}_2 & \frac{2EI}{l}\bar{\phi}_4 \\ -\frac{EA}{l} & 0 & 0 & \frac{EA}{l} & 0 & 0 \\ 0 & -\frac{12EI}{l^3}\bar{\phi}_5 & \frac{6EI}{l^2}\bar{\phi}_2 & 0 & \frac{12EI}{l^3}\bar{\phi}_5 & \frac{6EI}{l^2}\bar{\phi}_2 \\ 0 & -\frac{6EI}{l^2}\bar{\phi}_2 & \frac{2EI}{l}\bar{\phi}_4 & 0 & \frac{6EI}{l^2}\bar{\phi}_2 & \frac{4EI}{l}\bar{\phi}_3 \end{bmatrix} \qquad (10.24)$$

And this is the element stiffness matrix that is in the sframe code. The form of the element stiffness matrix in Equation (10.24) is ready for coding and with standard matrix stiffness analysis procedures it is straightforward to establish the overall stiffness matrix for any plane frame.

10.2.4 Verification of developed $\bar{\phi}_i$ functions

The influence of the shear-flexible parameter μ on the shear-flexible $\bar{\phi}_1$ function is shown graphically in Figure 10.6. $\bar{\phi}_1$ is plotted for different values of μ against the non-dimensional elastic critical Euler buckling load ratio ρ. At $\rho = 0$ (i.e. a zero axial force), the value of $\bar{\phi}_1$ function is unity and the terms in Equation (10.24) for the element stiffness matrix restore their linear form. As ρ increases from zero, and is positive for compressive axial force, the value of the $\bar{\phi}_1$ function decreases gradually from one to zero, the later value is for onset of instability. If the axial force is tensile there is a stiffening effect given by a negative ρ, and so the value of $\bar{\phi}_1$ is > 1.0.

It is worthwhile to observe the effect of μ on the critical buckling load for an element with simply supported ends and subjected to only axial compression (there are no end moments (i.e. $M_1 = M_2 = 0$)). Let us consider the curve for the shear-stiff case (μ is zero) given in Figure 10.6 by the upper solid line. It gives $\rho = 1$ for the onset of instability and so the critical load is the Euler value ($\frac{\pi^2 EI}{l^2}$). When the member is shear-flexible and μ is equal 0.1, the curve for $\overline{\phi}_1$ in Figure 10.6 is given by the bottom solid line. Now the onset of instability will occur when $\rho = 0.85$. This informs us that for the shear-flexible situation the elastic critical buckling load is lower than the shear-stiff Euler value.

10.3 Semi-rigid joint action in frame analysis

Connections are the components that form the frame's joints to connect the members together and through which forces and moments are transmitted. Depending on the member arrangements there is a variety of joint configurations, such as single-sided or double-sided, and beam splices etc. Figure 10.7 shows the connection detailing for four joint configurations between beam and column members that could be use with pultruded structural shapes. The main method of connecting the components to fabricate the joint is by bolting. To further enhance the initial rotational stiffness in PFRP joints adhesive bonding can be used (Mottram 1996). A number of researchers have used full-sized physical tests to determine the moment rotation characteristics of PFRP joint configurations and these studies have been reviewed by Turvey and Cooper (2004).

It is current practice when designing steel framed structures to assume that joints are either ideally pinned or ideally rigid (BS 5950-1: 2000). The rigid-case assumption implies that the joint possesses a very high rotational stiffness in comparison with the flexural stiffness of the connected members, and is capable of transmitting the moments without any relative rotational deformation between the connected members. This is illustrated in Figure 10.8(a). In the case of the pinned assumption the joint's rotational stiffness is taken to be very small such that they cannot be a transfer of moments between the connected members. The deformation of the beam members is shown in Figure 10.8(b). The actual joint behaviour will, of course, fall between these two bounds to given us semi-rigid joint action. At a given stage of loading, if the joint has rotation θ and the semi-rigid connection gives a rotation represented by ϕ, as illustrated in Figure 10.8(c) (Anderson *et al.* 1993). For a realistic, and perhaps more economical, frame design it would be advantageous in the analysis to include the true moment-rotation response of the joints, as shown in Figure 10.9, which is neither parallel to the moment-axis (i.e. rigid connection) nor the rotation-axis (i.e. pinned connection) but lies in between (i.e. semi-rigid connection).

To rely on conventional steel practice and to design pultruded frames as braced, with simple connections, might not produce the optimum solution (Bass and Mottram 1994, Mosallam 1994, Mottram 1996, Turvey and Cooper 1996, and Mottram and Zheng 1996). This became the additional stiffness to the frame from semi-rigid action will either reduce the member sizes or increase the capacity of load for the limit states. It is therefore necessary

when determining the overall instability of framed structures to include the M-ϕ characteristics of the joints.

The application of computer simulation has permitted more refined and accurate representation of the joint behaviour to be included in the analysis. Zheng (1998) used the hybrid element concept shown in Figure 10.10 to model semi-rigid joint action in his programme sframe. To minimize the need for computing resources, the semi-rigid joint is treated as a spring, which has no physical length, and attached to the beam-column element while the other side represents the node to the element, which appears in the frame model. It is assumed that only its rotational degree of freedom is relevant in the numerical analysis, and by employing this assumption the number of terms in the element's stiffness matrix remains unchanged. To take account of semi-rigid action in sframe the analysis proceeds by modifying the loading side of the governing matrix equation. To follow next is a brief description of the mathematical treatment to include the semi-rigid action in the frame analysis.

The end rotation of a member with a semi-rigid action is partly due to the rotation of the joint θ and partly due to rotation of the connection ϕ. Consequently, the deformation and stresses of this member which can be treated as the results of two systems of loads acting on it. These are due to the actual loads applied and the extra loads due the to semi-rigid rotations $\bar{\phi}_1^e$ and $\bar{\phi}_2^e$ as nodes 1 and 2.

Using $\{\bar{F}\}^e$ to represent the forces vector for the member and $\{\bar{\delta}\}^e$ to represent the joint displacement vector, the relationship between member end-forces and displacement is written as Zheng (1998).

$$\{\bar{F}\}^{(e)} = [\bar{k}]^{(e)}\{\bar{\delta}\}^{(e)} + \{\bar{F}_s\}^{(e)} \tag{10.25}$$

where

$$\{\bar{F}\}^{(e)} = \begin{Bmatrix} \bar{U}_1^e \\ \bar{V}_1^e \\ \bar{M}_1^e \\ \bar{U}_2^e \\ \bar{V}_2^e \\ \bar{M}_2^e \end{Bmatrix}; \quad \{\bar{\delta}\}^{(e)} = \begin{Bmatrix} \bar{u}_1^e \\ \bar{v}_1^e \\ \bar{\theta}_1^e \\ \bar{u}_2^e \\ \bar{v}_2^e \\ \bar{\theta}_2^e \end{Bmatrix}; \quad \{\bar{F}_s\}^{(e)} = \begin{Bmatrix} 0 \\ -\frac{6EI}{l^2}\left(\bar{\phi}_1^e + \bar{\phi}_2^e\right) \\ \frac{EL}{l}\left(4\bar{\phi}_1^e + 2\bar{\phi}_2^e\right) \\ 0 \\ \frac{6EI}{l^2}\left(\bar{\phi}_1^e + \bar{\phi}_2^e\right) \\ \frac{EI}{l}\left(2\bar{\phi}_1^e + 4\bar{\phi}_2^e\right) \end{Bmatrix}$$

It can be seen that the right hand side of Equation (10.25) consists of two parts. Its first part represents the relationship of the end forces to the displacement of a member in a plane frame that has rigid joints at both ends. The second part to Equation (10.25) gives the influence on forces of the relative joint rotation from the semi-rigid action.

10.4 Analysis for the elastic critical buckling load of frames

As has been discussed previously, FRP members are characterized by their high strength-to-modulus and high longitudinal-to-shear modulus ratios. This means members and structures are most susceptible to failure by a buckling instability. The author therefore modified the coding to the static version (Zheng 1998) of sframe so that the analysis tool would also determine the elastic critical buckling load for the modelled frame problem.

Stability of an elastic framed structure may be explained by considering its change of stiffness with increasing load. The overall stiffness matrix for the stable frame has the property of positive definiteness, whereas, at its stability limit, its "stiffness" vanishes. Consequently, the stability of the frame can be "measured" by the value to the determinant of the overall stiffness matrix. It can be noted that, by involving the shear-flexible stability functions (ϕ_i) in the analysis, allowance is made of the destabilising effect from the presence of axial compression in the shear-flexible members.

For nodal force equilibrium, the internal forces, **F,** should balance the applied loads, **P**. The matrix relationship between nodal forces and displacements, δ, in the overall system is defined by

$$\{P\} = [K]\{\delta\} \tag{10.26}$$

This system of equations is then solved analytically to obtain the nodal displacements corresponding to equilibrium with a set of external forces.

For the non-linear analysis Equation (10.26) can be rewritten as

$$\{\mathbf{P}\} = [\mathbf{K}\{\mathbf{P}\}]\{\delta\} \tag{10.27}$$

$\mathbf{K(P)}$ implies that the overall stiffness matrix $\mathbf{K}$ is a function of the current values in the load vector $\mathbf{P}$. If the nodal forces are known, the terms of $\mathbf{K(P)}$ can be calculated via the ϕ_i functions, and Equation (10.27) solved for nodal displacements (deflections and rotations), by way of

$$\{\delta\} = [\mathbf{K}\{\mathbf{P}\}]^{-1}\{\mathbf{P}\} \tag{10.28}$$

For a given set of loads there is, as from the linear static analysis, a unique set of nodal displacements. This will always be the true as long as the frame remains in stable equilibrium. If the loading causes the structure to be in a state of neutral equilibrium, where many deformation configurations are possible, there is no uniqueness for the relationship between loads and frame deformation. Although Equation (10.27) now exists, Equation (10.28) does not, and this is only possible if the overall stiffness matrix $\mathbf{K(P)}$ is singular (Coates *et al.* 1994). The singularity of $\mathbf{K(P)}$ is equivalent to the structure's overall stiffness being zero.

A test for the singularity of $\mathbf{K(P)}$ will be a check for stability, since if it is calculated not to be zero and remains positive definite the structure can be said to be in a stable state. The frame will be on the boundary of instability when the matrix is singular. The system will become unstable when it has no overall stiffness and no additional load is required to induce a buckling mode shape. Mathematically a null load vector gives this situation and so joint equilibrium is defined by

$$[\mathbf{K}]\{\delta\} = \{\mathbf{0}\} \tag{10.29}$$

For the non-trivial solution to Equation (10.29) the displacement vector δ cannot have all entries equal to zero, the determinant $\mathbf{K}$ must be zero. Thus for the condition of instability of the structure the following should be hold

$$|\mathbf{K}| = 0 \tag{10.30}$$

The elastic response of the structure is governed by Equation (10.4), or more precisely, by Equation (10.27). The use of $\mathbf{K}(\lambda\mathbf{P})$ implies that $\mathbf{K}$ is a function of the applied load $\lambda\mathbf{P}$, where λ is the critical load factor that multiplies the initial loads in vector $\mathbf{P}$ to give their magnitudes when instability occurs. To determine the value of λ the mathematical problem is linearized by carrying out a double iterative process. The outer iterative loop has λ increasing in a step-by-step manner and the singularity of $\mathbf{K}(\lambda\mathbf{P})$ is checked. At each of the outer-loop load levels there is an inner iterative loop using the Newton-Raphson's technique, prior to the singularity check, to find the correct values to the axial forces in the members. This non-linear solution procedure is repeatedly until the analysis gives a consistent set of nodal displacements that satisfy the equilibrium of the nodes (or members) in their current deformed positions. The number of iterations required depends on how near the structure is to instability and how good is the modeller's initial estimate to the loading values that will cause instability.

The singularity of a matrix can be checked by a number of algorithms. The one chosen by the author is to examine the value of the determinant of the overall stiffness matrix to find out what loading causes it to be zero. Coates *et at.* (1994) inform us that the mathematical situation for a singularity cannot be exactly obtained, and so in practice it is not be feasible to calculate the value of λ that gives the "exact" singularity state. Instability, using the sframe analysis, is therefore flagged only when the sign of the determinant becomes negative, as this corresponds to a state of unstable equilibrium. By imposing a tolerance on the incremental change to λ a more accurate value to the

critical λ is obtained by linear interpolation between values that fall either side of the required critical value.

10.5 Summary for the sframe analysis tool

The author, using the approach described in Section 10.4, has modified the sframe coding by Zheng (1998) so that it can be used to predict the elastic critical buckling load of shear-flexible plane frames. In Section 10.1 the development of the shear-flexible beam-column element for member representation has been presented. As explained in Sections 10.2 and 10.3 this analysis tool is able to account for non-linear response through second-order P-Δ effects and shear-flexible stability functions. To give the analysis tool further capability Section 10.3 introduces how it accounts for the non-linear moment-rotation behaviour due to semi-rigid joint action that is found in practice (Turvey and Cooper 2004). It is to be noted that sframe does not include any material non-linearity since the FRP materials that would be used in frame construction will be linear elastic to material yield (i.e. when there is rupture).

A specific data file has to be prepared in order to run the complied C sframe source (sframe.c). Details on how to prepare a data file and the execution of the analysis tool are to be found in Appendix C.

In the next chapter the srfame analysis tool will be used to show the influence of shear-flexibility, with and without semi-rigid joint action, on changing the buckling loads to small number of example frame problems. The study to be

presented is preliminary in nature and can be used to identify what will be required for a comprehensive numerical analysis to fully understand the instability of plane frames with shear-flexible members.

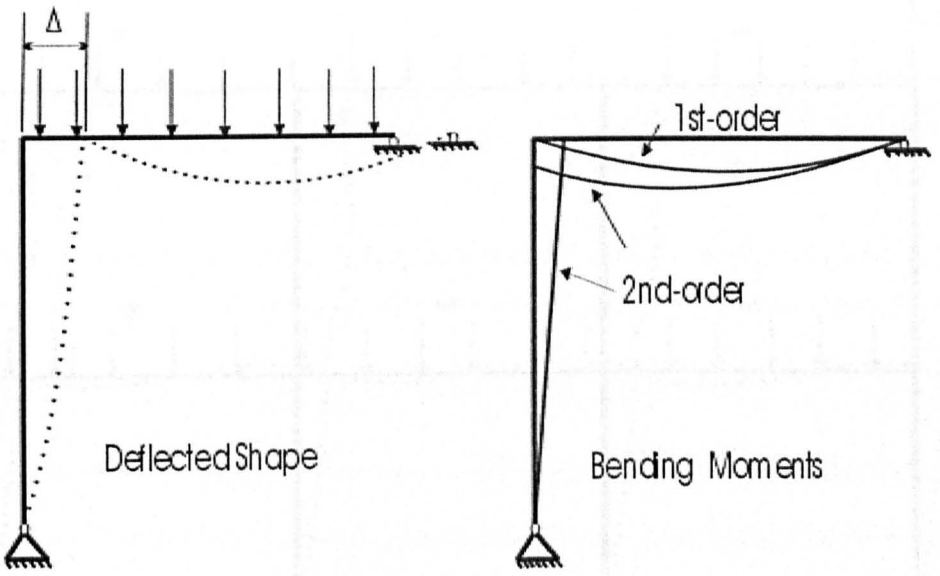

(a)

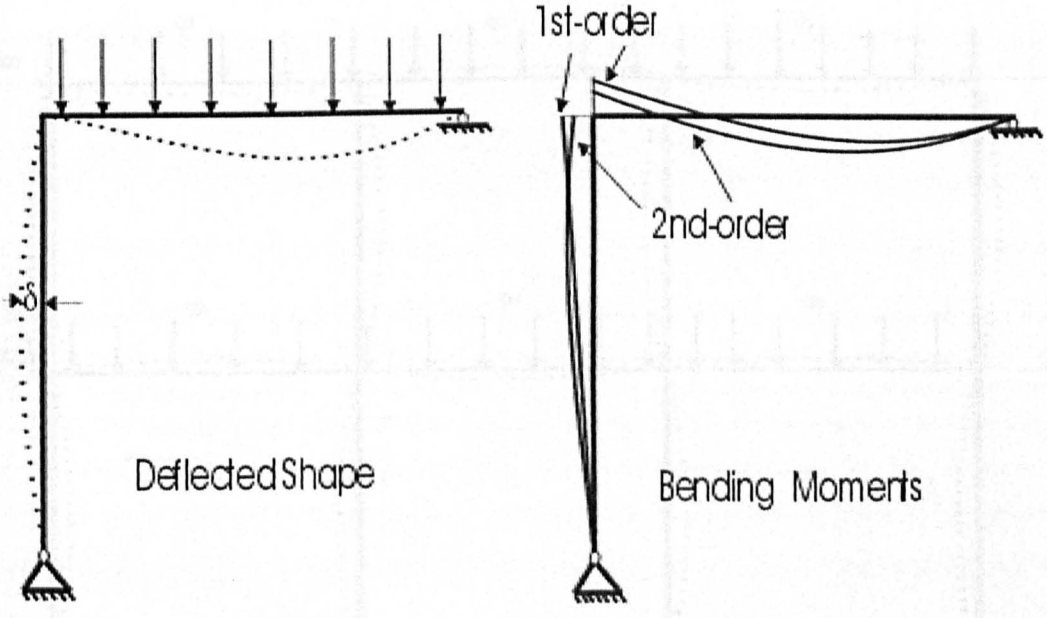

(b)

Figure 10.1. Second-order P-Δ and P-δ moments, (a) Sway permitted, (b) Sway restrained (Galambos 1998).

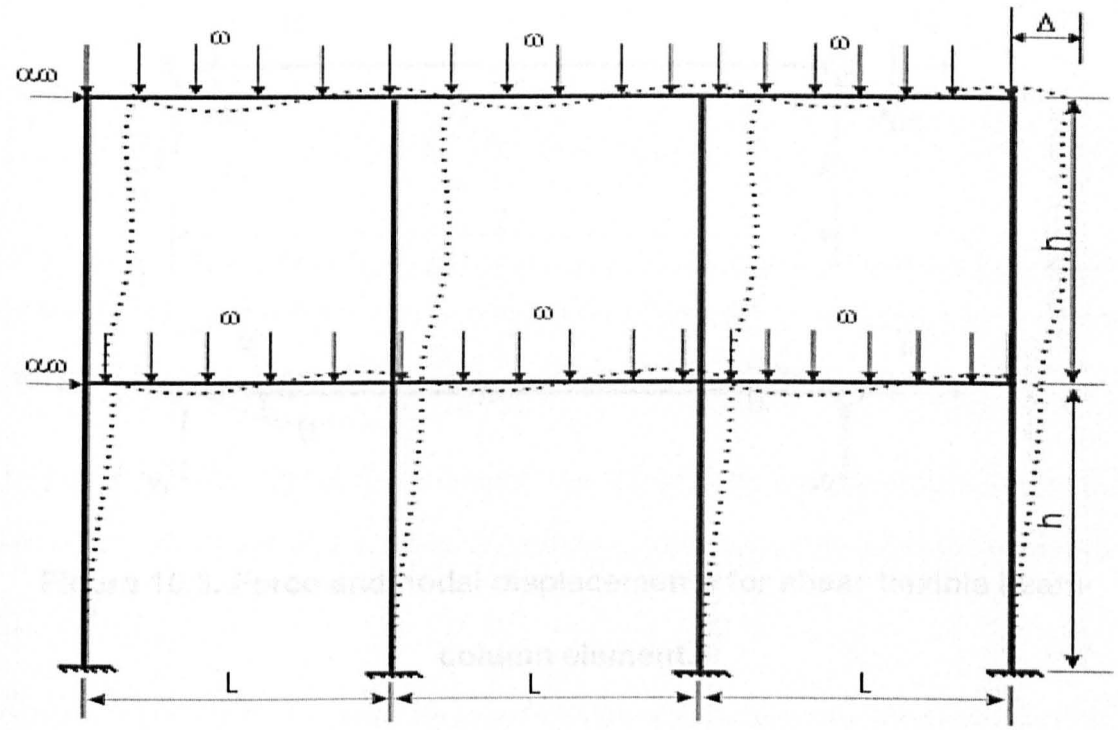

(a)

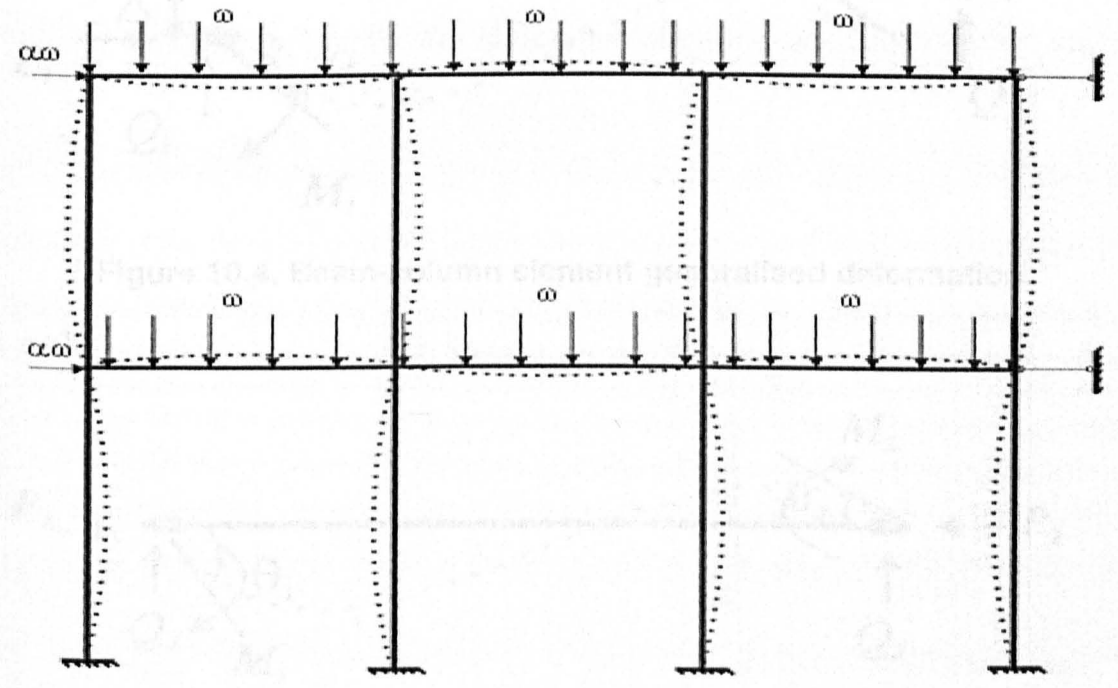

(b)

Figure 10.2. Frame deformation shapes, (a) side-sway frame, (b) no-side-sway frame.

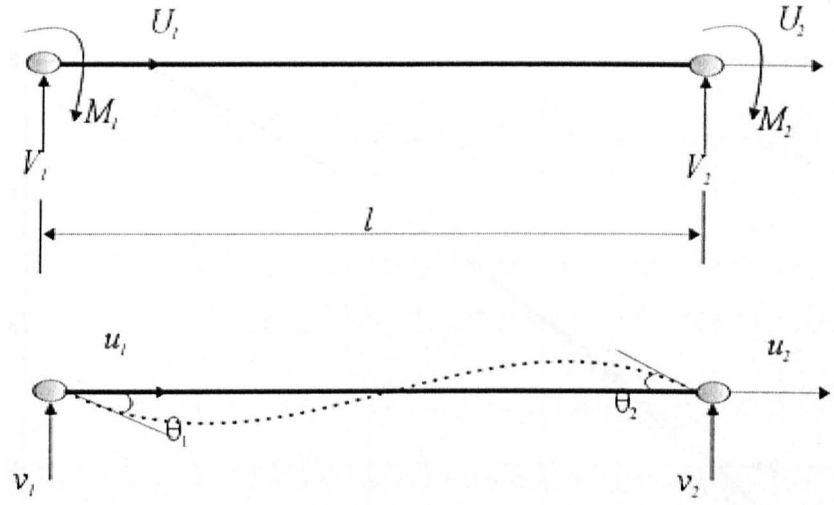

Figure 10.3. Force and nodal displacements for shear-flexible beam-column element.

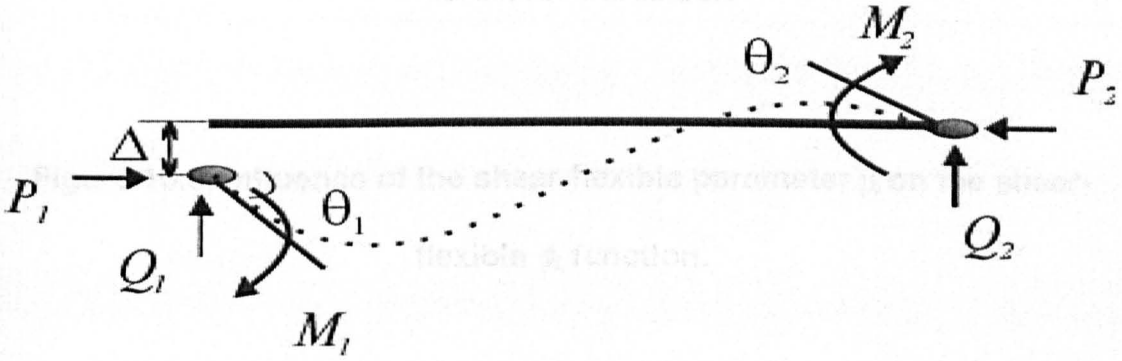

Figure 10.4. Beam-column element generalised deformation.

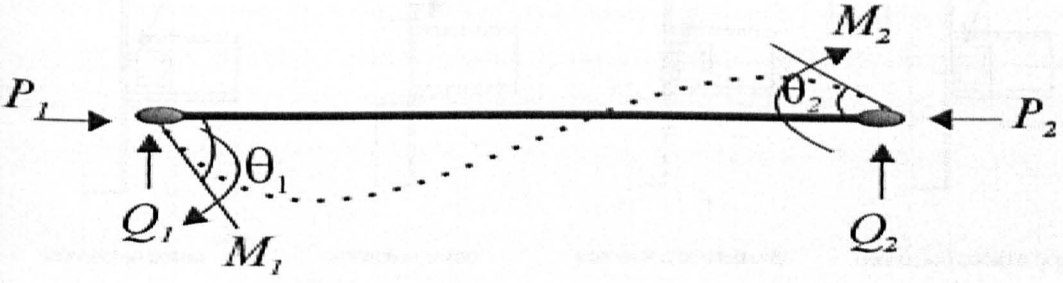

Figure 10.5. Beam-column element subjected to end rotations and no sway.

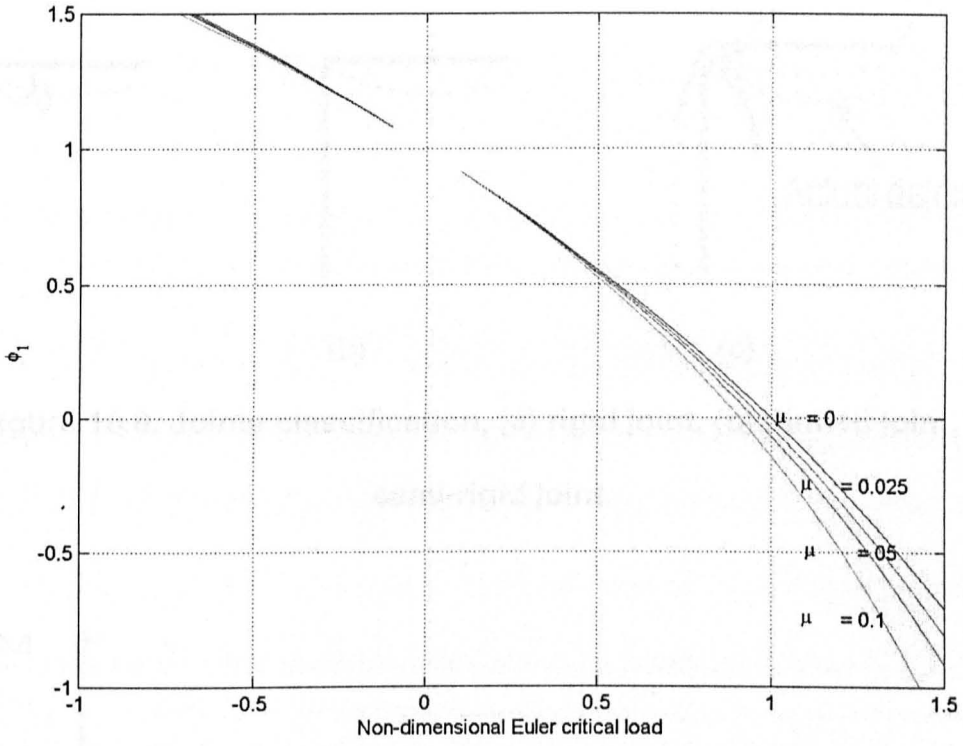

Figure 10.6. Influence of the shear-flexible parameter μ on the shear-flexible ϕ_1 function.

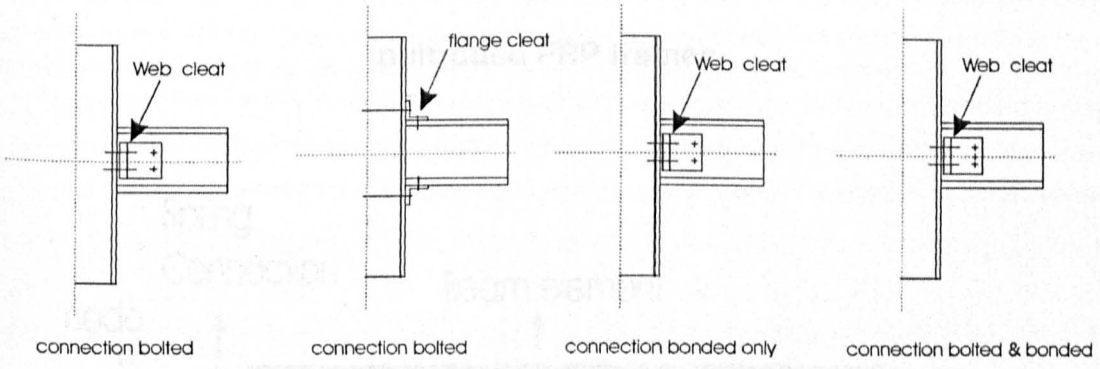

Figure 10.7. Typical connections details for joints in pultruded FRP frames (Mottram 1994).

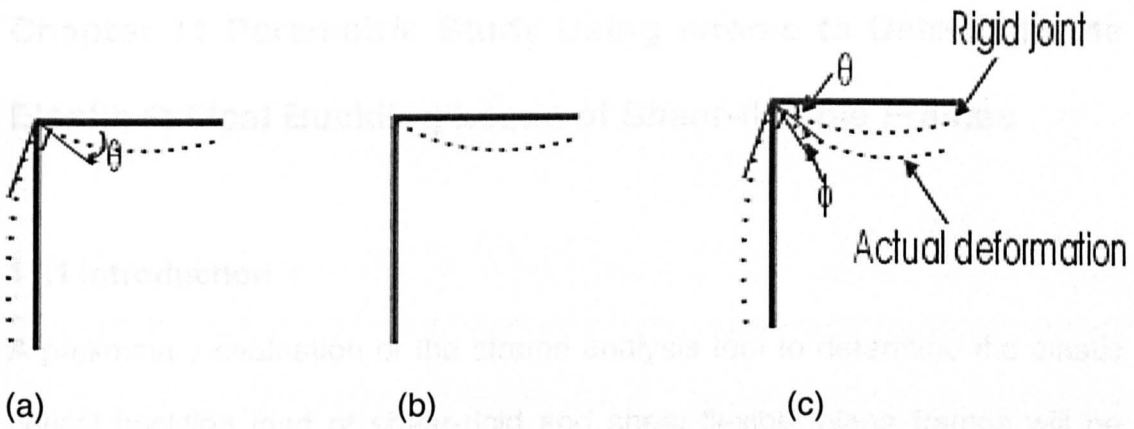

Figure 10.8. Joints classification, (a) rigid joint, (b) pinned joint, (c) semi-rigid joint.

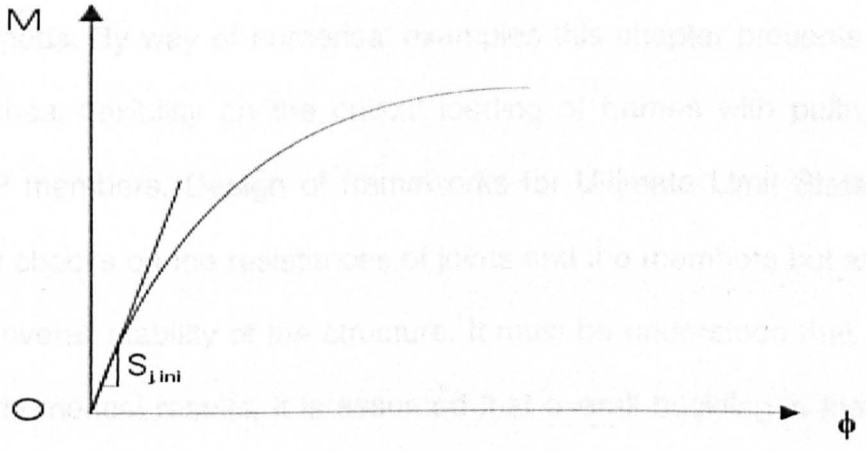

Figure 10.9. Moment-rotation curve for semi-rigid connection in pultruded FRP frames.

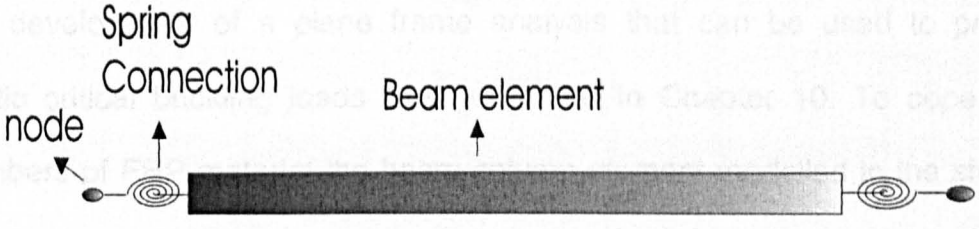

Figure 10.10. The hybrid element comprising beam-column element with end rotational springs to simulate semi-rigid joint action.

Chapter 11 Parametric Study Using sframe to Determine the Elastic Critical Buckling Loads of Shear-flexible Frames

11.1 Introduction

A preliminary evaluation of the sframe analysis tool to determine the elastic critical buckling load of shear-rigid and shear-flexible plane frames will be demonstrated by several example problems. The numerical results from sframe will, when they are available, be compared with results from other researchers, who solved the same simple problems using different analytical methods. By way of numerical examples this chapter presents the influence of shear-flexibility on the critical loading of frames with pultruded or other FRP members. Design of frameworks for Ultimate Limit State requires not only checks on the resistances of joints and the members but also checks for the overall stability of the structure. It must be understood that, in presenting the numerical results, it is assumed that overall buckling is the first mode of ultimate failure and that all over possible modes have been suppressed. This important assumption on the validity of what is to follow is one aspect for which further work is necessary.

The development of a plane frame analysis that can be used to predict elastic critical buckling loads was presented in Chapter 10. To cope with members of FRP material the beam-column element modelled in the sframe code is shear-flexible. As discussed in the previous chapter, the analysis accounts for second-order P-Δ effects by the inclusion of shear-flexible

stability phi functions, and semi-rigid action by the inclusion of the non-linear moment-rotation characteristics of the joints.

The results presented in Sections 11.2 to 11.5 will be the elastic critical buckling loads using four problem configurations. The geometry for these simple frames is conveniently based on a standard PFRP section size, which is used for beam and column members in real frames (Anon 1995, Turvey 2002). It is to be noted that, for the first time, this study evaluates the combined influence of semi-rigid joint action and material shear-flexibility on the critical buckling load of elastic framed structures.

11.2 Portal frames with shear-rigid members and rigid joints

To validate the computational approach presented in Section 10.4 the author uses established results for the elastic critical loads to two portal frame problems with isotropic 'shear-rigid' members. Figures 11.1(a) and (b) presents two simple portal frames of height 400 cm and width 400 cm. The members are given the geometric properties of a 20.3x20.3x0.953 cm^3 wide flange pultruded off-the-shelf shape (Anon 1989 and Anon 1999). Flexure is for bending about a member's major axis. For this wide-flange section the nominal major second moment of area, I, is 4130 cm^4 and the nominal cross-sectional area, A, is 56.3 cm^2. In the modelling E is taken to be 20 GPa. The actual values of the members' properties are not so important as the critical load results are reported in a suitable non-dimensional form.

The four nodes and joints in both frames are numbered 1 to 4. Joints at nodes 2 and 3 are rigid, while joints 1 and 4 at the base can be fixed (FB) or pinned (PB). A single element is used for a member between two joints and its structural response is represented in sframe by Equations. (10.5) and (10.30).

Shown in Figure 11.1(a) is the portal frame loaded to excite the sway situation, while in Figure 11.1(b) it is for the no-sway situation. In the sway case the frame is subjected to two vertical point loads (P) at nodes 2 and 3, as well as a very small sway-excitation horizontal load, H, (0.001 kN) at node 2. For the no-sway case the difference is to have the excitation 'load' as very small opposing moments, M, (0.001 kNm) applied at nodes 2 and 3.

The mode shapes to the lowest elastic buckling load are given for the two frames by the dashed lines in Figures 11.1(a) and 11.1(b). It is assumed that the frame cannot deform out of the plane and so buckling about the members' minor-axes is fully restrained.

Presented in Table 11.1 are elastic critical buckling loads for the first overall buckling mode of the sway and no-sway cases, with a fixed base (FB) or a pinned base (PB). Column one in the table defines the portal frame problem, and the reference source to the other analytical result is given in column 2. Columns three and four give the results from the two theoretical approaches, with the sframe results in the fourth column. The elastic critical buckling loads are given using the non-dimensional parameter ρ_{cr}. ρ_{cr} is defined by P_{cr}/P_E,

with P_{cr} the elastic critical load and P_E the elastic Euler buckling load of the isotropic column member with an effective-length factor of 1.0. For the PFRP column member defined above the value of P_E for global buckling about the major axis is 509 kN.

Table 11.1. Comparison of elastic critical buckling loads for simple portal frame examples with shear-rigid members.

Portal Frame problem	Author	Author ρ_{cr}	sframe ρ_{cr}	Difference %
Sway with PB Figure 3.1(a)	Timoshenko and Gere (1963)	0.184	0.184	-0.10
Sway with FB Figure 3.1(a)	Chajes (1974)	0.744	0.745	0.10
No sway with PB Figure 3.1(b)	Horne and Merchant (1965)	1.285	1.283	-0.15
No sway with FB Figure 3.1(b)	Coates *et al.* (1994)	2.550	2.548	-0.10

Notes: PB is for pinned joints at the base and FB is for fixed joints at the base.

In the last column the percentage difference between the two analytical results for the four frame problems is given. Since the maximum difference is only 0.15% it can be concluded that there is an excellent agreement between the two calculated ρ_{cr}s for each of the four shear-stiff frame problems.

11.3 Shear-flexible members and rigid joints

It is feasible for frame members of FRP reinforced with advanced carbon fibres to possess elastic constants to make the ratio E/G have a value of 80 (Mottram and Aberle 2002). The higher this ratio is, the higher will be the

influence of shearing on the response of members and the framework itself. This modulus ratio for steel is only 2.6 and this low value explains why we can model the members in isotropic frames to be shear-rigid (Mottram and Aberle 2002, Horne and Merchant 1965). Members of standard Pultruded FRP shapes can have a E/G ratio in the range 5 to 10, and because the ratio is at least double that for steel the effect of the shear-flexibility on frame response needs to be known.

Al-Sarraf (1979 and 1986) theoretically investigated the stability of the sway mode (see dashed curve for mode shape) for the two-storey single-bay frame problem shown in Figure 11.2. The heights of the storeys are equal and the four columns have the same length as the two beams. The loading to this frame for ρ_{cr} was predicted when the second moment of area (I) and length (l) of all the members are constant. For convenience the six members have the same geometrical and mechanical properties as used in the portal frame examples in Section 11.2. For the frame with shear-rigid members Al-Sarraf (1979) predicted lower and upper bounds to give the critical load in the range $0.5122 < \rho_{cr} < 0.5377$. These bounds differ by only 4.9%. Later, Al-Sarraf (1986) extended his investigation to analyse the shear-flexible situation, using shear-flexible stability factors given in his paper, and by Equations. (10.14) and (10.15). To illustrate the influence of shear-flexibility on the elastic critical buckling load (now given by the non-dimensional critical load parameter $\rho_{crsh} = P_{crsh}/P_E$), the sframe generated curve is presented in Figure 11.3. The buckling load is defined by two point vertical loads of magnitude λP, located at nodes 3 and 4. To 'excite' the sway-mode a very small

horizontal load, H, (0.01 kN) is applied at node 3. The principal variable is the moduli ratio E/G ranging from 2.5 to 80. In Figure 11.3 the abscissa is given by the non-dimensional shear-flexibility parameter μ $(= \frac{\beta P_E}{GA} = \frac{\beta \pi^2 EI}{L^2 GA}$ (Equation (10.6)), is used. For this and the frame problem in Section 11.4 the shear correction factor β is 3.07. β can be taken to be the ratio of A/A_v, where A_v is the shear area. A is 5630 mm^2 and A_v is depth of H-shape times the web thickness (nominal values give 203.3x9.53 = 1936 mm^2). β is 5630/1936 = 2.91. If, however, A_v is taken as height of web times the web thickness then it is, lower, at 1745 mm^2. Now β is 5630/1745 = 3.2. Then the mean is about 3.07 and so the β in the study is acceptable.

From the plot in Figure 11.3 it is clear that as the shear-flexibility parameter μ increases (i.e., E/G increases from 2.5 to 80), the elastic critical load ρ_{crsh} reduces from 0.504 to 0.325. For this specific frame problem we observe that the elastic critical load can decrease by 35% when the members become very shear-flexible. For PFRP members with an E/G ratio lying in the range 5 and 10, instability will occur at an elastic critical load that is < 95% of the shear-rigid frame value. Although not a significant reduction, the analysis shows that the buckling load is reduced by the presence of shear deformation, and so design using the conventional shear-rigid analysis would lead to an unsafe outcome. The importance of including shear-flexibility when determining the buckling loads of framed structures of FRP has therefore been demonstrated by evaluating the results of this simple example.

11.4 Shear-rigid members and semi-rigid joint action

The real moment-rotation characteristics of beam-to-column and column-to-base joints play an important role in the overall response (Zheng 1998), and failure of frames. Here we will consider joints in a simple portal-frame problem with a constant rotational stiffness. It is noted, however, that the sframe analysis tool (see Section 10.3) can equally cope with non-linear moment-rotation characteristics (Zheng 1998, Mottram and Zheng 1999). Let the linear rotational joint stiffness be S_j and the flexural stiffness of the connected beam member be EI/l. It is to be noted that this measure of member stiffness is for the shear-rigid situation. To classify steel joints, Annex J in Eurocode 3 (BS EN 1993-1: 2005) states that the joint is rigid if the relative stiffness $(S_j l)/(EI)$ is > 8 for a braced frame and ≥ 25 for an unbraced frame. Joints are said to possess a rotational stiffness for the pinned condition when $(S_j l)/(EI) < 0.5$. If $(S_j l)/(EI)$ lies between these two boundaries the joint will contribute semi-rigid action to the shear-rigid frame's deformation.

Figure 11.4 shows an unbraced portal frame for the sway mode of failure, which for the sframe analysis has semi-rigid beam-to-column joints at nodes 2 and 3. The column-to-base joints at column ends 1 and 4 remain fixed (i.e. $S_j = \infty$). As in the previous frame problems E is taken to be 20 GPa, and since the members are shear-rigid the ratio E/G is mathematically zero. Figure 11.5 plots ρ_{cr} against $(S_j l)/(EI)$ to show the influence of the semi-rigid action on the frame's elastic critical buckling load. As $(S_j l)/(EI)$ increases from 0.29 (pinned joints) to 25 (rigid joints), so ρ_{cr} increases from 0.302 to 0.671. Over the full

range of joint stiffnesses this example shows a 122% increase in the critical load. Now, if $(S_j l)/(EI)$ increases from 25 to ∞ (for the unbraced frame), there is only another 10% increase in ρ_{cr}. This simple example emphases the findings used to prepare Annex J of Eurocode 3 that there is no practical benefit when the frame is shear-rigid on having the parameter $(S_j l)/(EI) > 25$.

11.5 Shear-flexible members and semi-rigid joint action

Using the same sway frame problem in Section 11.4 three plots in Figure 11.6 show the variation of the elastic critical load (given by ρ_{crsh}) with joint stiffness, for members having moduli ratio E/G = 6, 20 or 80 (i.e. μ = 0.083, 0.278 or 1.111). To simplify the discussion the relative stiffness ($(S_j l)/(EI)$) for joint classification will also be used when the members are shear-flexible. For the pinned-joint condition, given by $(S_j l)/(EI) < 0.5$, the relative change in ρ_{crsh} is about 4% as E/G changes from 6 to 80. This is not significant. Whereas, for the rigid-joint condition, given by $(S_j l)/(EI) = 25$, the equivalent change in the members' shear-flexibility has a greater influence on ρ_{crsh}, resulting in a 50% decrease. This can be linked to the finding by Turvey (1999) that the influence of shear-flexibility on the member's response is higher when the ends are fixed. There is also evidence in Figure 11.6 to suggest that the relative stiffness $(S_j l)/(EI)$ will, at the joint classification boundaries, be lower as the members' shear-flexibility increases and this is an important finding for when a structural Eurocode is drafted for the designed of framed structures of FRP shapes.

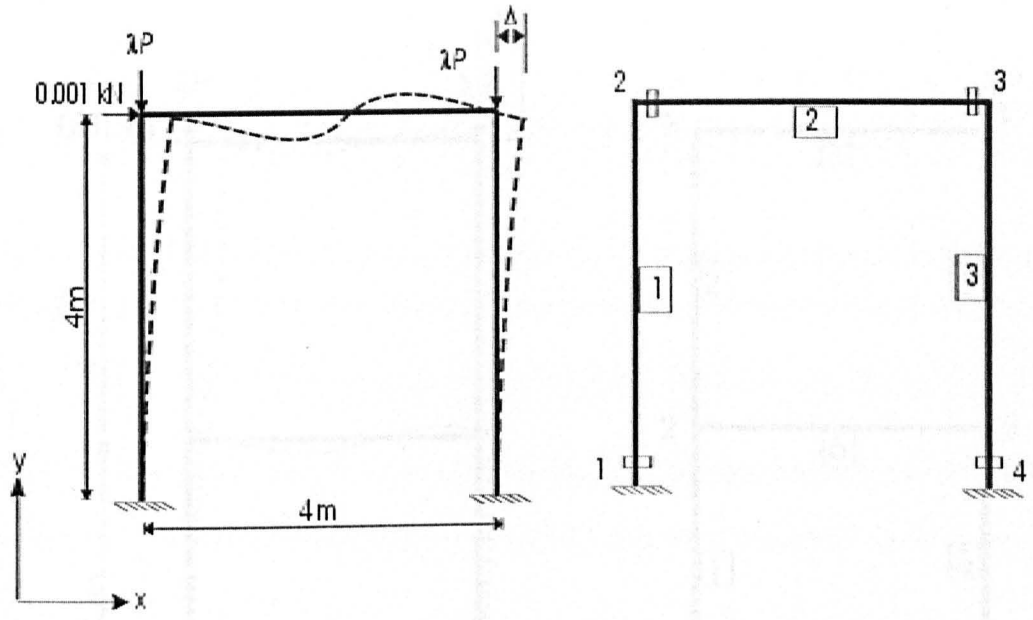

(a)

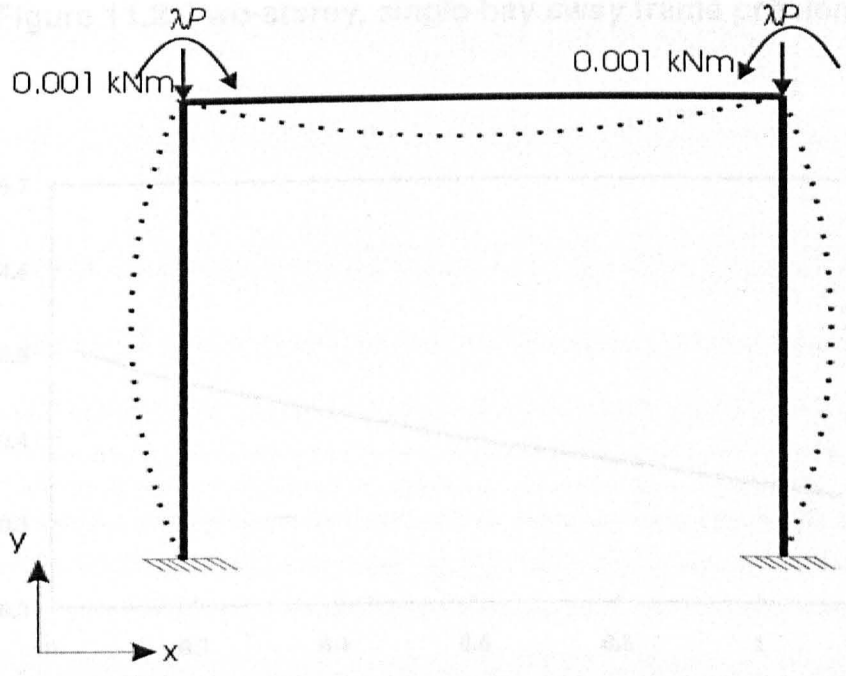

(b)

Figure 11.1. Portal frames, (a) Sway loading case, (b) No-sway loading case.

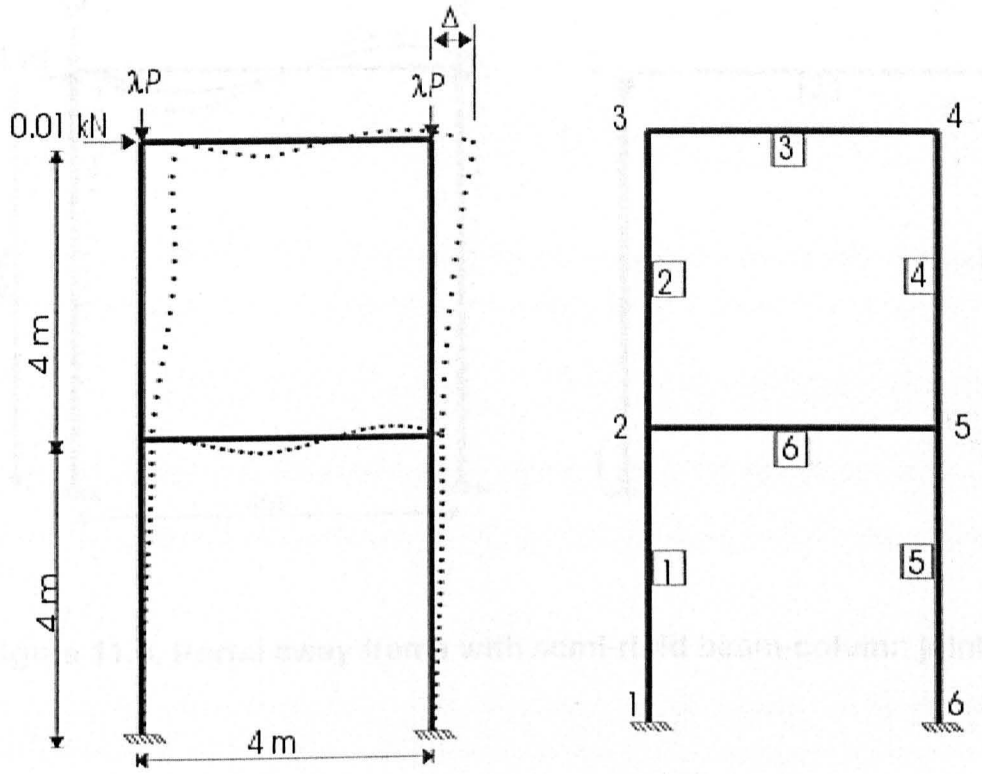

Figure 11.2. Two-storey, single-bay sway frame problem.

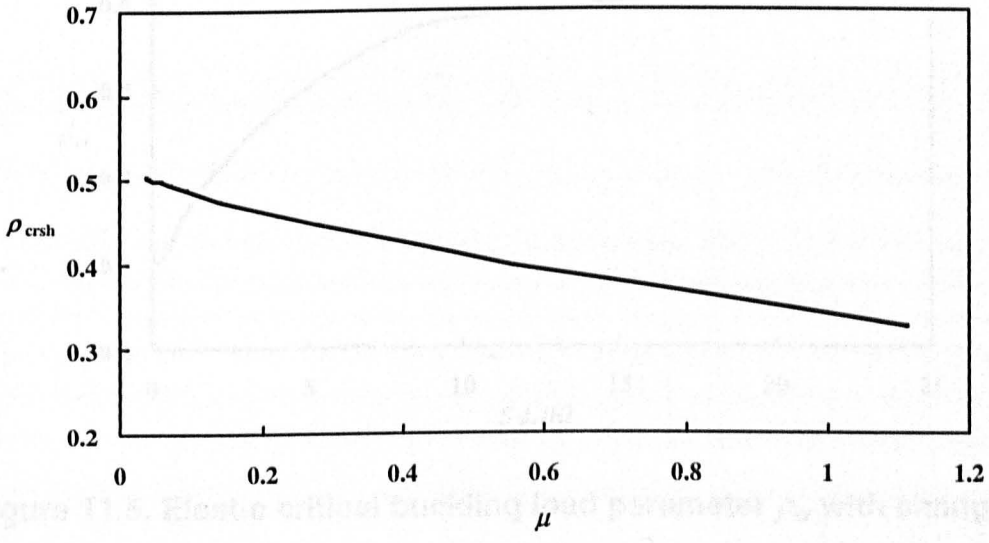

Figure 11.3. ρ_{crsh} with μ for the Al-Sarraf (1979) single-bay two-storey frame problem.

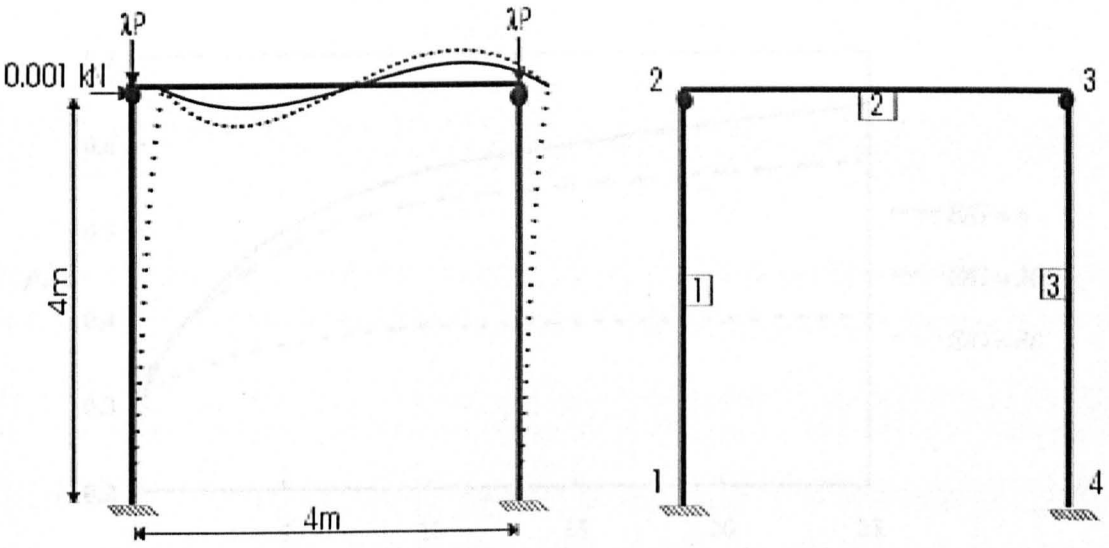

Figure 11.4. Portal sway frame with semi-rigid beam-column joints.

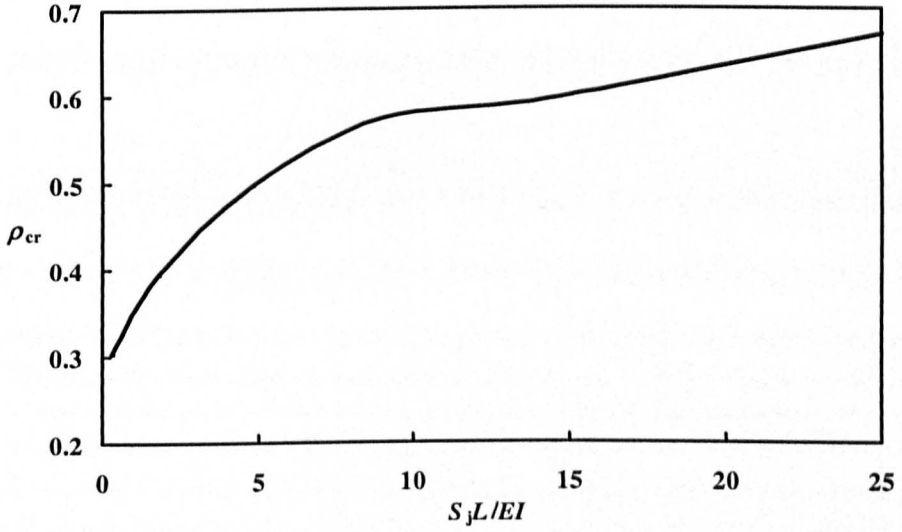

Figure 11.5. Elastic critical buckling load parameter ρ_{cr} with changing $(S_j l)/(EI)$ for a simple frame problem with shear-rigid members.

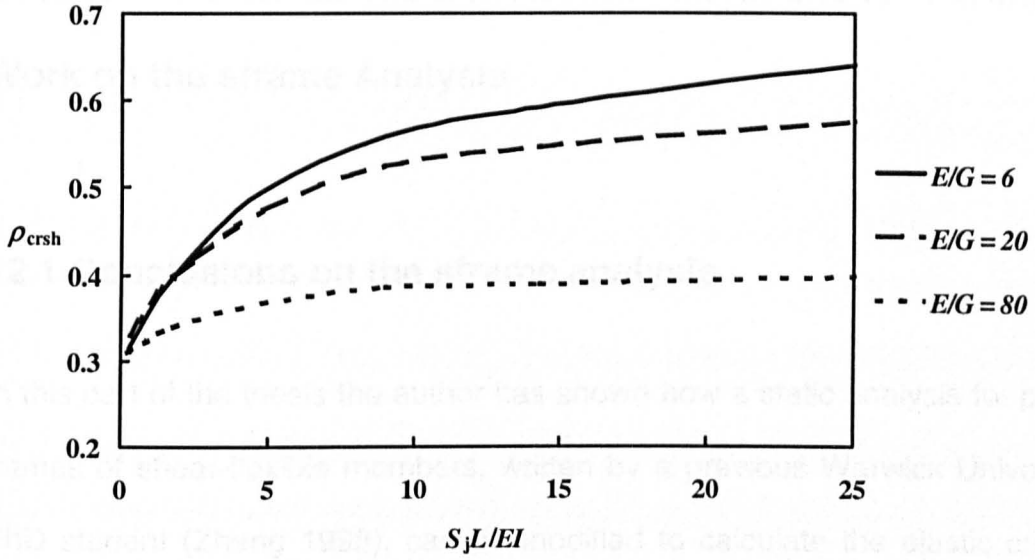

Figure 11.6. Elastic critical buckling load parameter ρ_{crsh} with changing $(S_jl)/(EI)$ and moduli ratio E/G for a simple portal-frame problem.

Chapter 12 Conclusions and Recommendations for Further Work on the sframe Analysis

12.1 Conclusions on the sframe analysis

In this part of the thesis the author has shown how a static analysis for plane frames of shear-flexible members, written by a previous Warwick University PhD student (Zheng 1998), can be modified to calculate the elastic critical buckling load for overall instability. The modified sframe programme provides a practical analysis tool that, importantly, includes non-linearity by way of second-order P-Δ effects with shear-flexible functions and semi-rigid joint action. Since a review on shear-flexible stability functions by Mottram and Aberle (2002) found that there were mistakes in the expressions for Zheng's functions, the author has successfully coded into sframe new functions that are theoretically correct. To make this modification the author has formulated shear-flexibility phi functions ($\overline{\phi}_i$ (i = 1 to 5)) based on Al-Sarraf's (1986) shear-flexible stiffness factor $\bar{s}$ and shear-flexible carry-over factor $\bar{c}$. Unlike the shear-stiff equivalent functions from Livesley (1956), it is seen that the shear-flexible phi functions are dependent of the members' geometric and material properties.

A preliminary parametric study using sframe to analyse simple plane-frame instability problems has been presented. The problems chosen have enabled an initial investigation to be made on how the elastic critical buckling load

changes due to the interaction of member shear-flexibility and semi-rigid joint action.

From the parametric study presented in Chapter 11 the following conclusions are made:

(a) It is shown that sframe can accurately predict the instability load, by way of a group of four shear-stiff portal-frame problems that have solutions to their critical loads by a different theoretical approach.

(b) By analysing a frame of two storeys and single-bay, it is shown that when the members' shear-flexibility is very high the critical load will be 35% lower than when the same members are shear-rigid. If for the same frame problem the members are of Pultruded FRP material, the buckling load is found to be 5% below the shear-rigid upper bound value.

(c) Although not a significant reduction, the study shows that the buckling load of Pultruded FRP frames is reduced by shear deformation, and so it is concluded that by using a conventional shear-rigid analysis in design, would not lead to the conservative outcome assumed by the designer.

(d) By using the Eurocode 3 joint classification scheme the joint's torsional stiffness in sframe was changed from pinned to rigid for the beam-to-column joints in a portal-frame problem. The critical-load calculations from this preliminary study show that the reduction in buckling load increases as the joint stiffness increases from the pinned to the rigid condition.

(e) The semi-rigid action results provide us with useful information regarding joint classification. Annex J of Eurocode 3 classifies a beam-to-column joint as rigid when the relative stiffness of the connection to the connected shear-rigid beam is ≥ 25. It is shown by a sframe analysis that there is no practical benefit to be gained in terms of a shear-stiff frame's resistance, to detailing a connection for a joint that is stiffer than the Eurocode lower bound for the rigid classification. Furthermore, there is evidence from the preliminary study, including semi-rigid joint action, to suggest that the relative stiffness values, at the joint classification boundaries, will be lower when the shear-flexibility of the frame's members increases. This is an important finding for when a structural Eurocode is drafted for frames of FRP materials.

(f) The importance of including shear-flexibility when determining the overall buckling loads of frame structures of FRP has therefore been demonstrated by evaluating the results of the preliminary parametric study using the sframe analysis tool. It is the author's recommendation that designers must be aware of the influence of shear-flexibility when they are analysing the overall stability of FRP structures of frame construction.

12.2 Recommendations for further work

Despite the sframe analysis tool being able to solve shear-flexible instability problems there is a need for further work. Specifically, the following recommendations for new work can be given:

- Equation (10.28) governs the elastic behaviour of the structure. In this equation the overall stiffness matrix $\mathbf{K}\{(\lambda \mathbf{P})\}$ is a function of the load vector $\{\lambda P\}$, where $\{P\}$ is the initial estimate to the applied loading that causes overall instability. The critical buckling load is then predicted by obtaining the scalar value to λ that is for the lowest buckling load. In sframe the value of load factor λ is increased manually in a step-by-step manner, and at each load increment the singularity of $\mathbf{K}\{(\lambda \mathbf{P})\}$ is checked by a trial-and-error procedure. To improve the computation, a minor modification to sframe would be to have the load factor λ increased automatically. This modification will speed up the analysis process and avoid numerical errors associated with the existing trial-and-error approach to find the critical λ.
- Currently, each new problem requires the user of sframe to generate a separate input data file. For the analysis tool to be user-friendly the code needs modifying to have an easy-to-use interface, in order to construct the data file through a few mouse clicks.

- The current output data file from sframe is in the form of a simple text format report. This may be improved by including graphically member detail reports with force/stress/deflection diagrams, etc.

- It is also essential for the sframe code to be modified to determine the load values for the development of other possible modes of failure, such as local and global member instabilities, as these might occur at a loading below that for the first overall buckling mode, which is the only failure load that is predicted by the current version of sframe.

- Mottram and Aberle (2002) have suggested that when the shear-flexibility parameter μ is > 0.025 a frame analysis should include the effect of the members' shear deformation. To confirm this as the limiting value further frame problems, covering the range of practical member arrangements and loading situations, should be analysed using the sframe analysis tool.

Appendix A Load-displacement plots

This appendix contains the full set of 54 load-displacement plots for the flexural buckling tests conducted on ε-column specimens of 2.7 m length. The plots in Figures A1 to A54 are given in order of column types WU104 to WU112. For each of the nine column types there are six specimen plots. In the plots there are two load-displacement curves for the minor axis and axial shortening deflections. All plots have the same scale on their lateral displacement axis (± 15 mm), but the load scale, in kN, changes. The upper limit on load depends on the resistance of the column type. A 9 mm (lenght/300) displacement is given for a failure criterion, by the dashed vertical lines for both the positive and negative directions of mid-height lateral displacement.

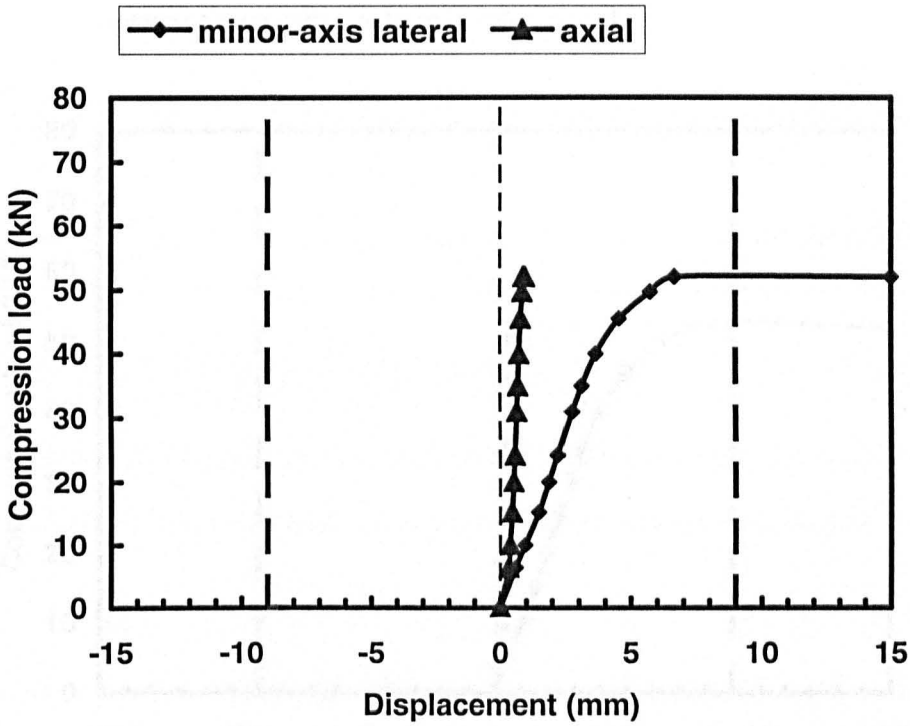

Figure A1. Load-displacement curves for WU104 specimen 1.

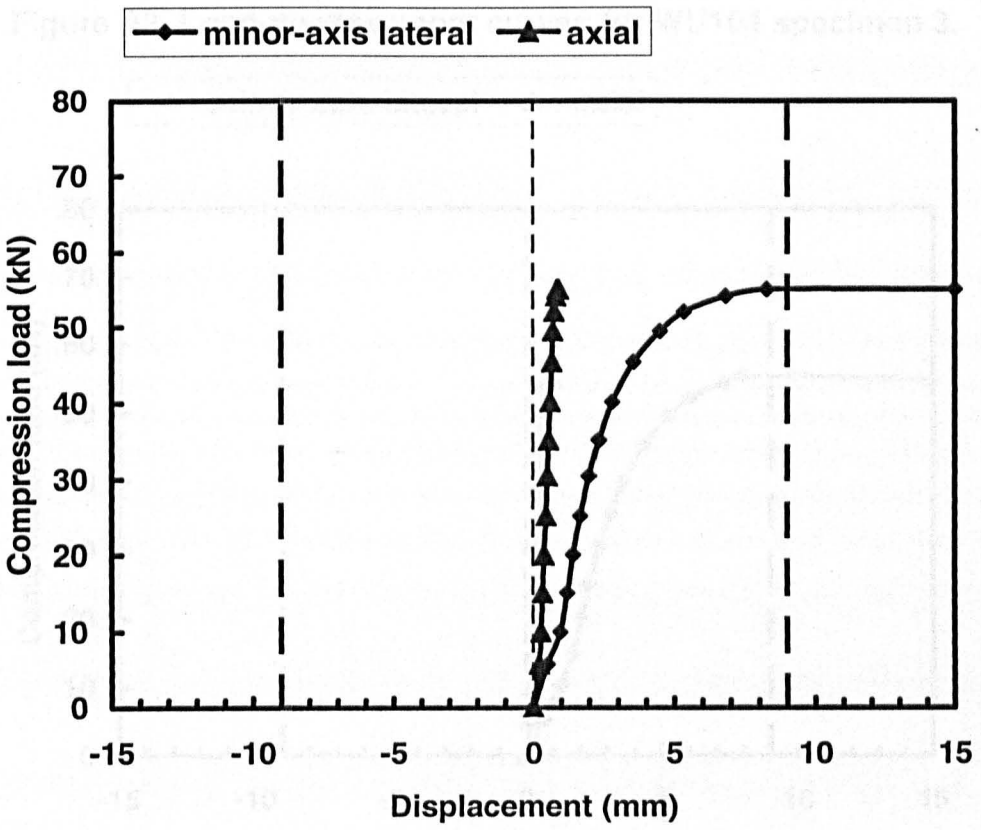

Figure A2. Load-displacement curves for WU104 specimen 2

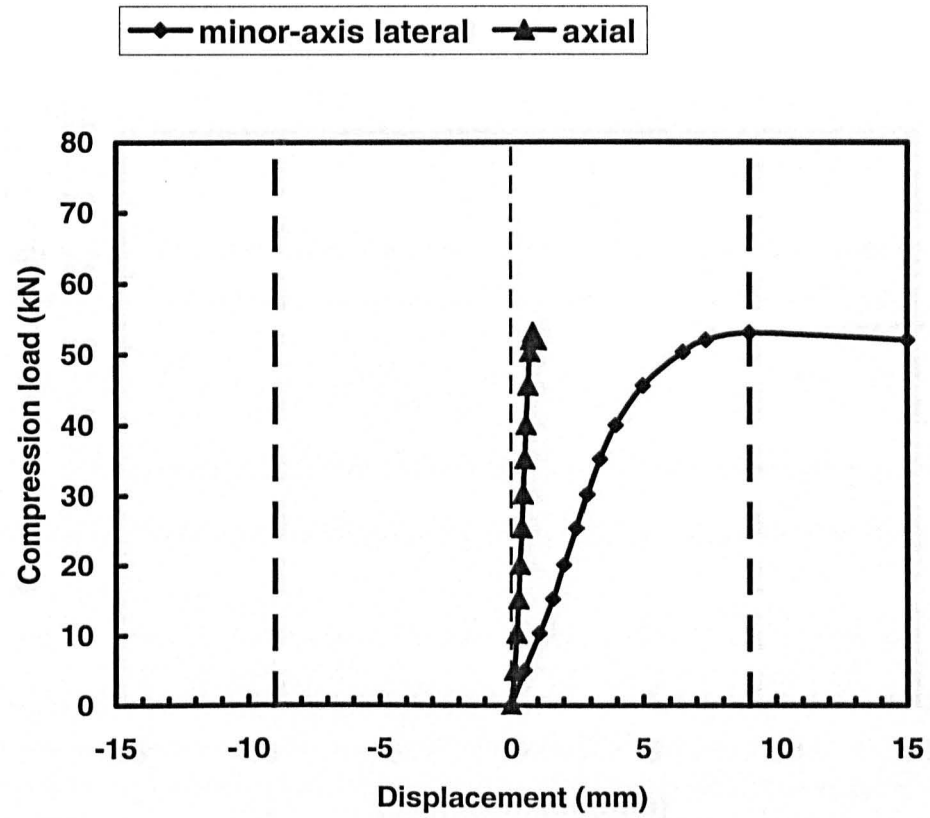

Figure A3. Load-displacement curves for WU104 specimen 3.

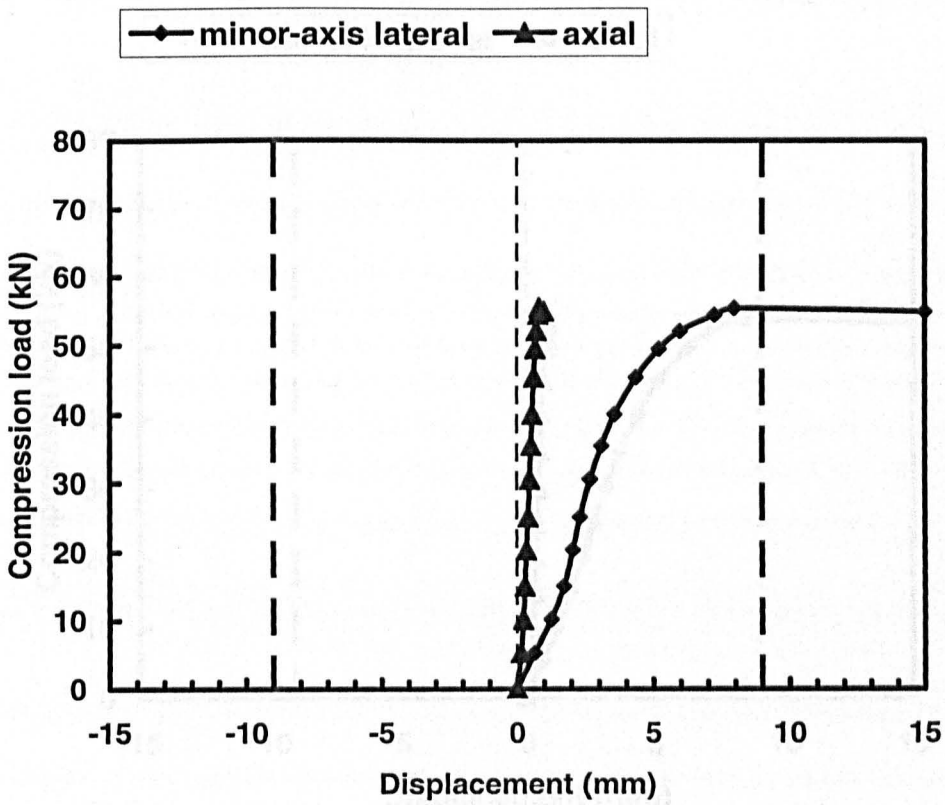

Figure A4. Load-displacement curves for WU104 specimen 4.

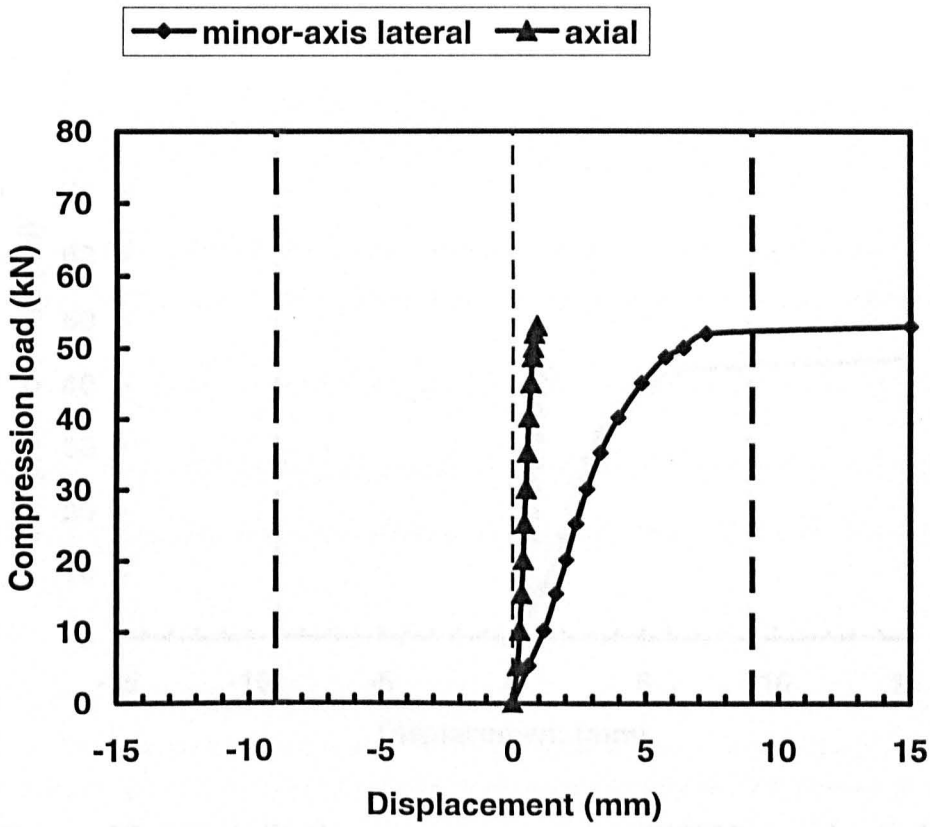

Figure A5. Load-displacement curves for WU104 specimen 5.

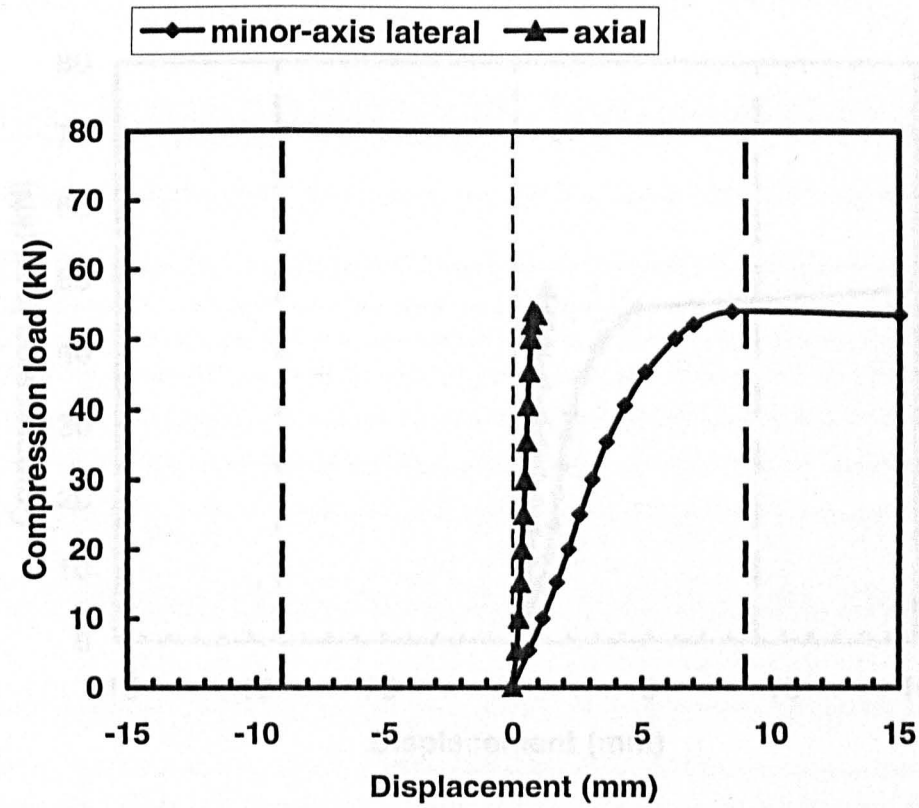

Figure A6. Load-displacement curves for WU104 specimen 6.

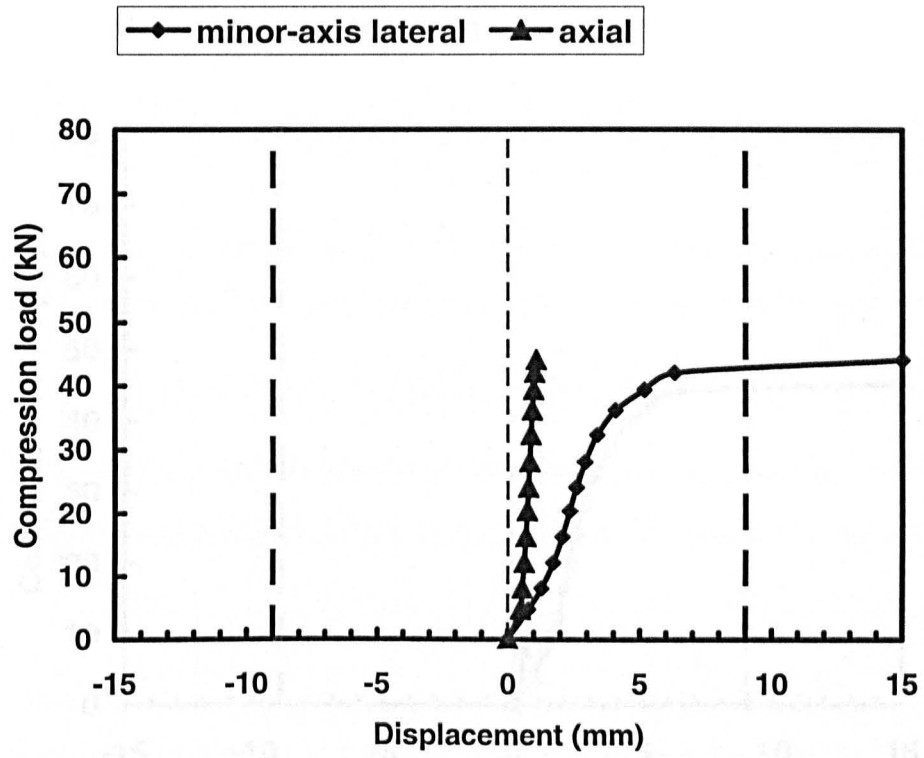

Figure A7. Load-displacement curves for WU105 specimen 1.

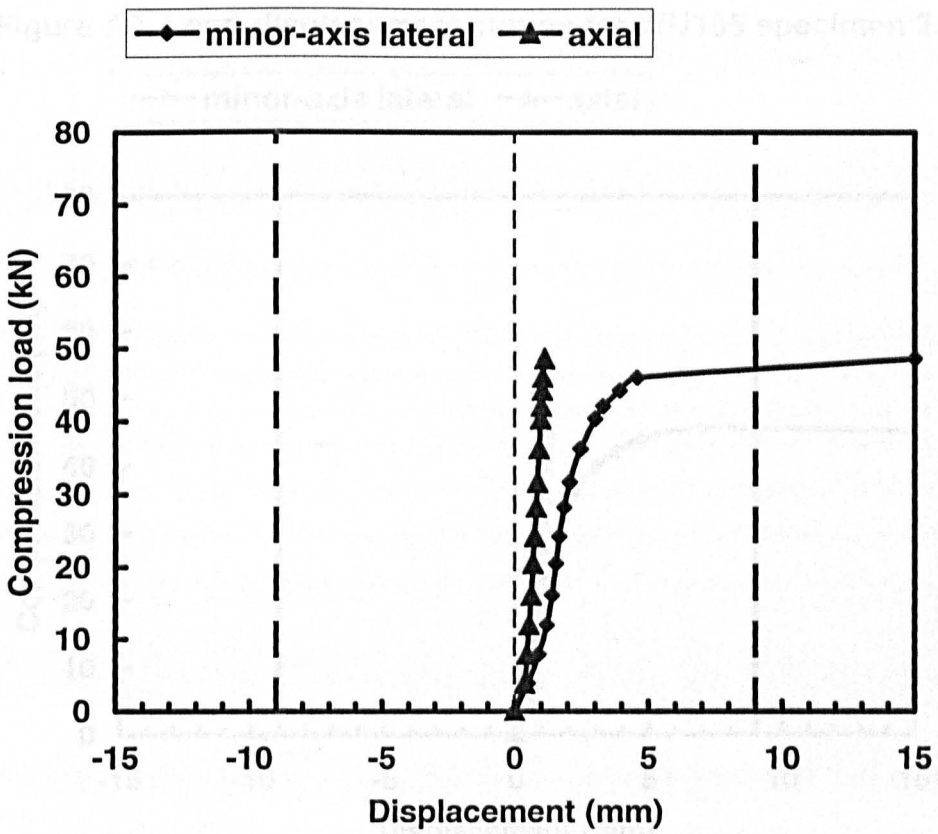

Figure A8. Load-displacement curves for WU105 column 2.

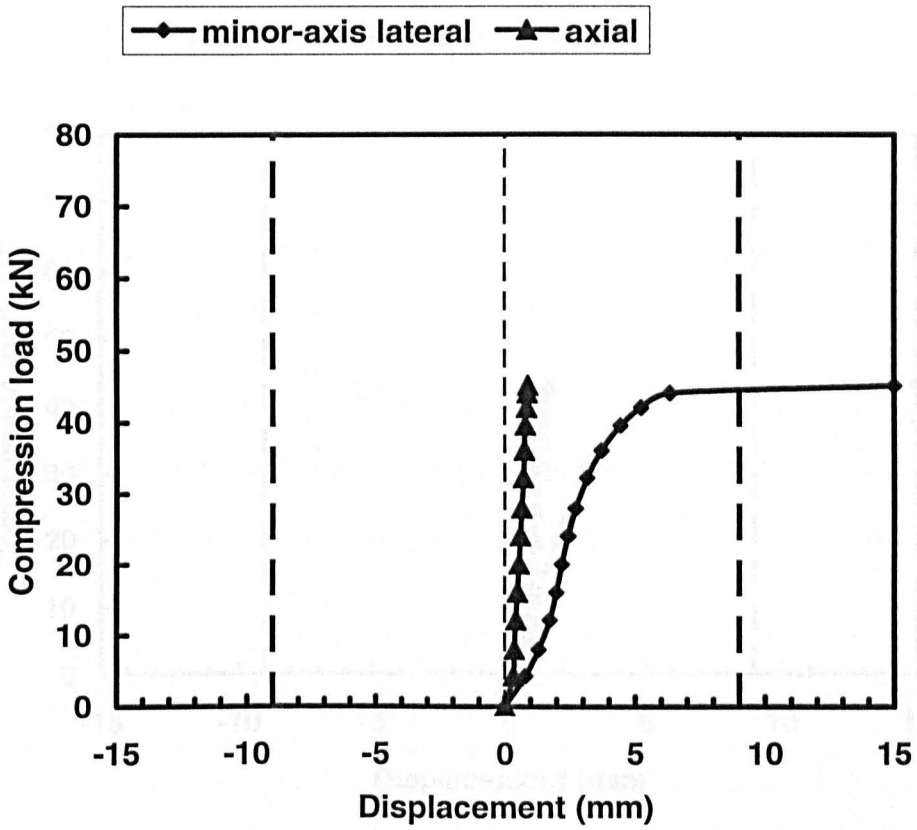

Figure A9. Load-displacement curves for WU105 specimen 3.

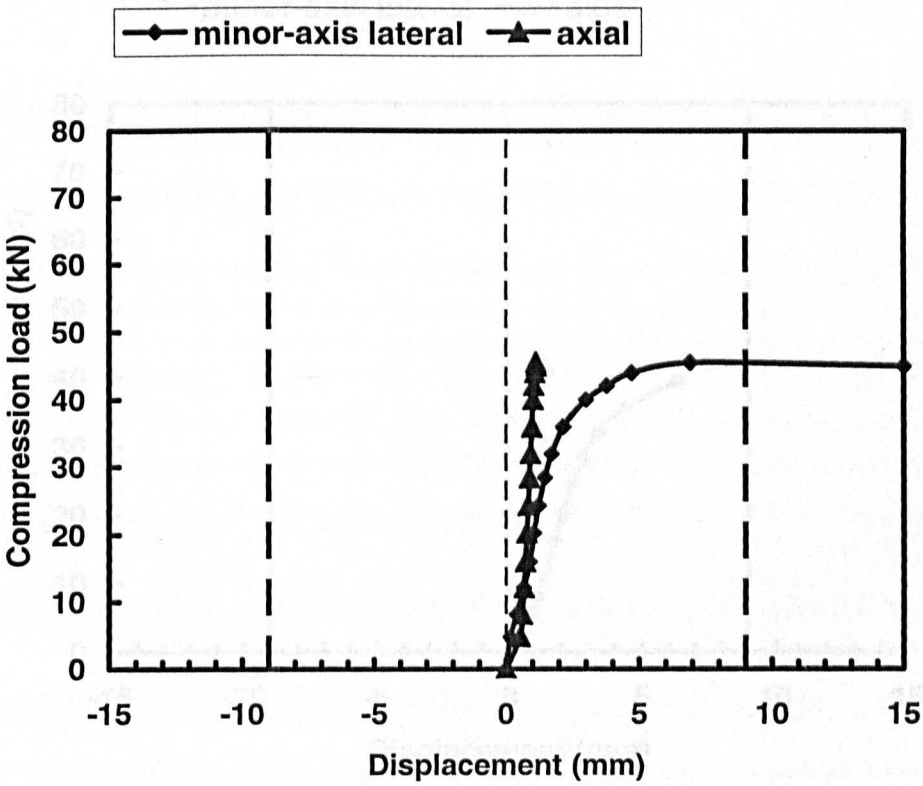

Figure A10. Load-displacement curves for WU105 specimen 4.

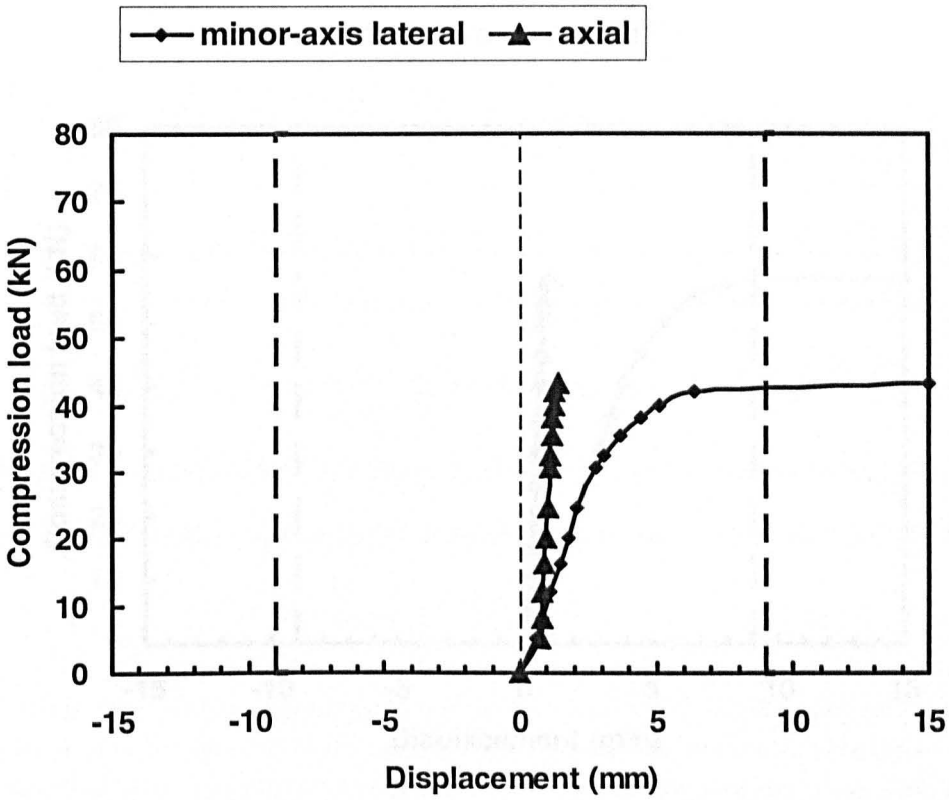

Figure A11. Load-displacement curves for WU105 specimen 5.

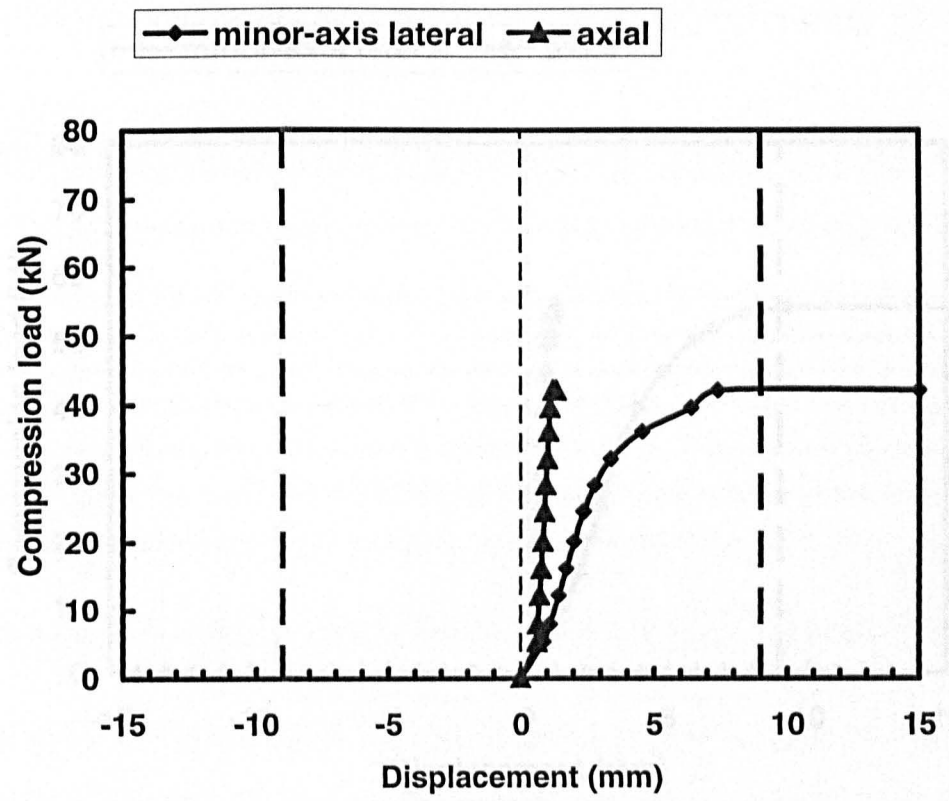

Figure A12. Load-displacement curves for WU105 specimen 6.

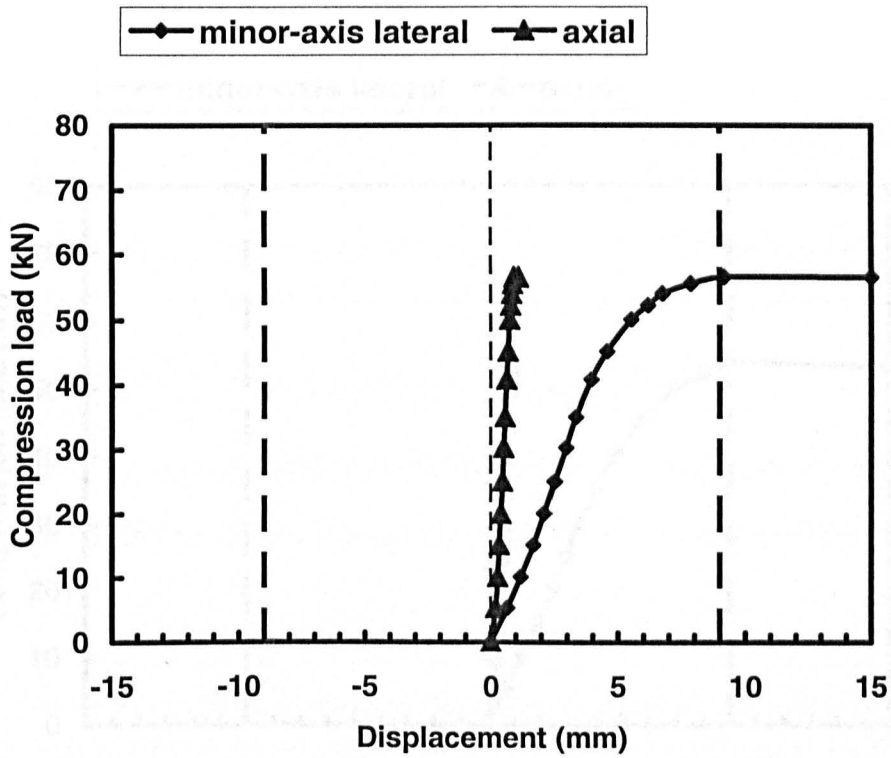

Figure A13. Load-displacement curves for WU106 specimen 1.

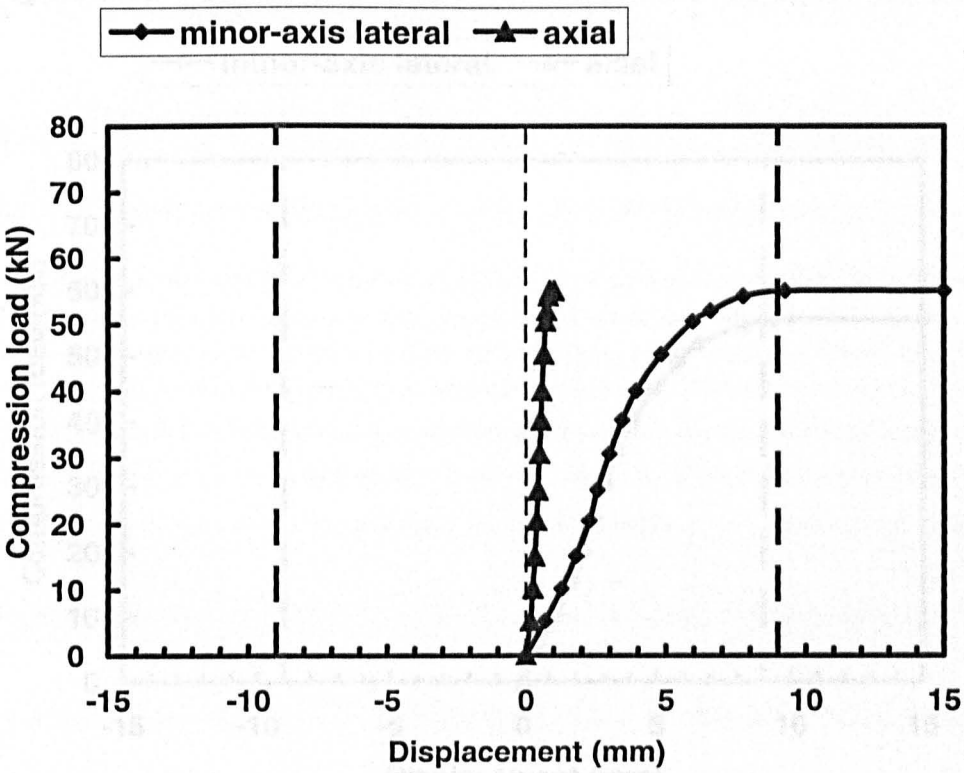

Figure A14. Load-displacement curves for WU106 specimen 2.

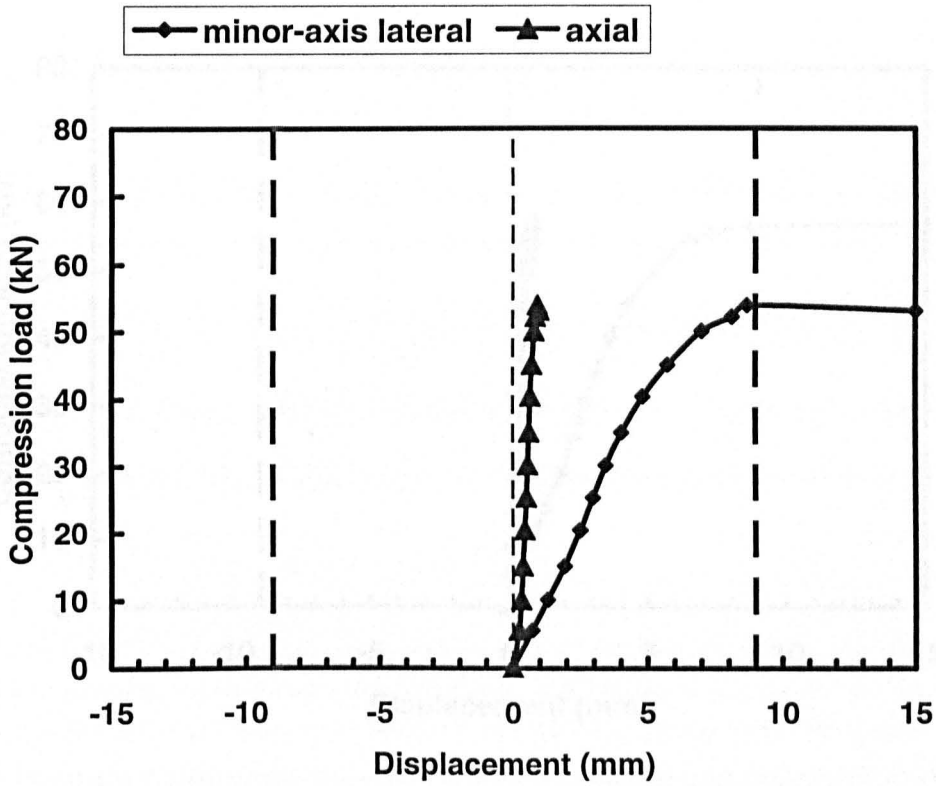

Figure A15. Load-displacement curves for WU106 specimen 3.

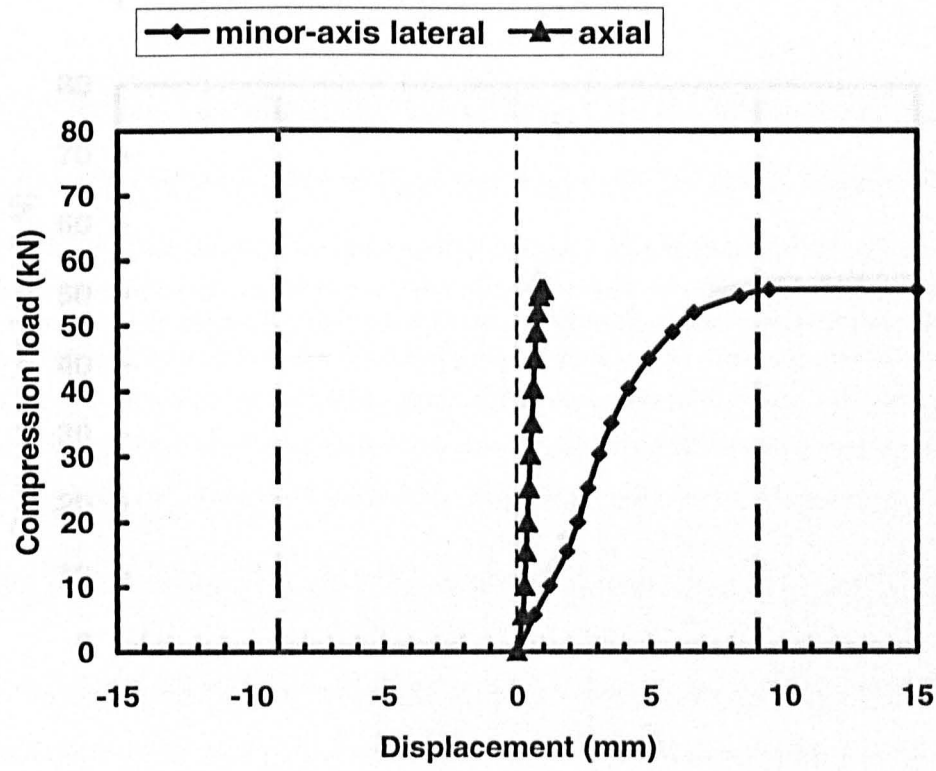

Figure A16. Load-displacement curves for WU106 specimen 4.

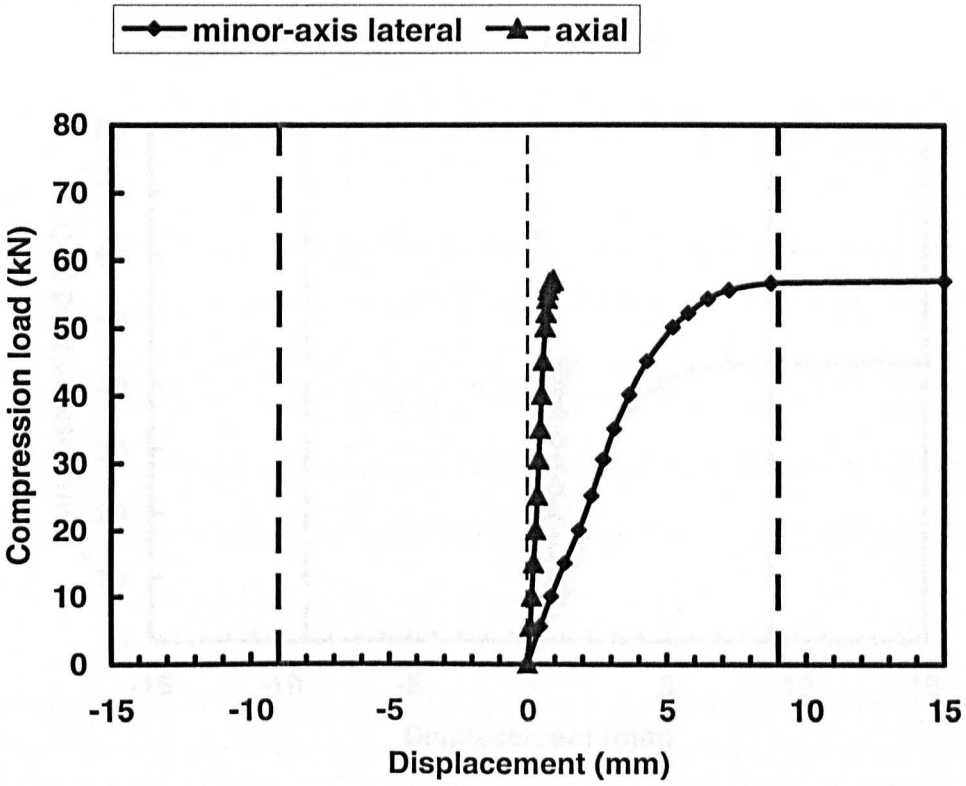

Figure A17. Load-displacement curves for WU106 specimen 5.

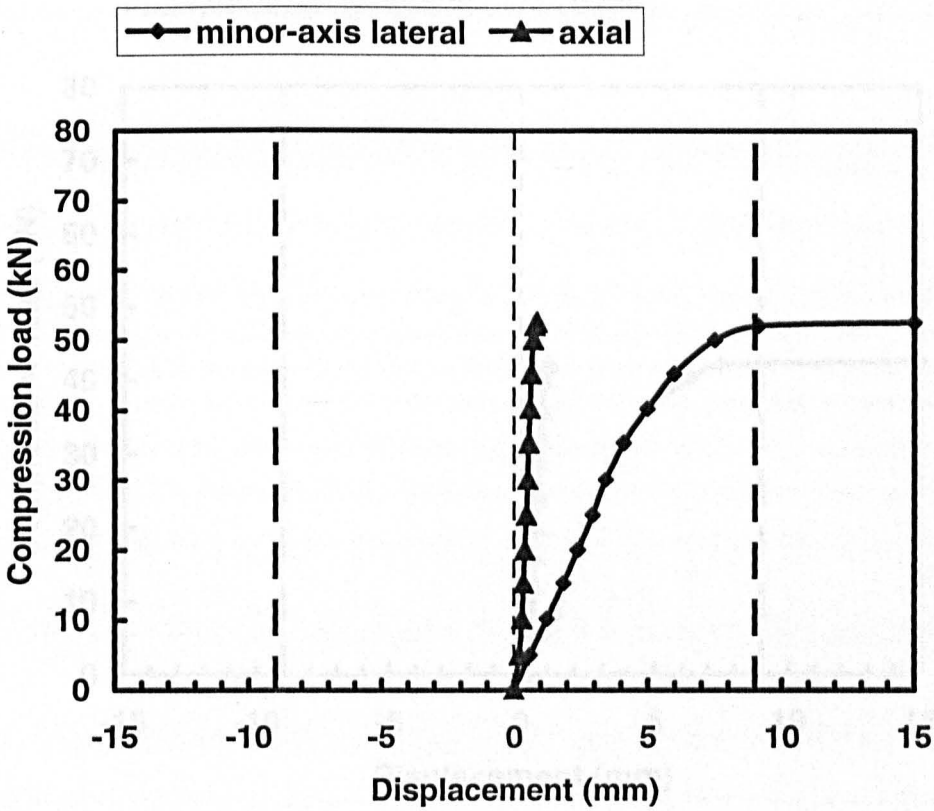

Figure A18. Load-displacement curves for WU106 specimen 6.

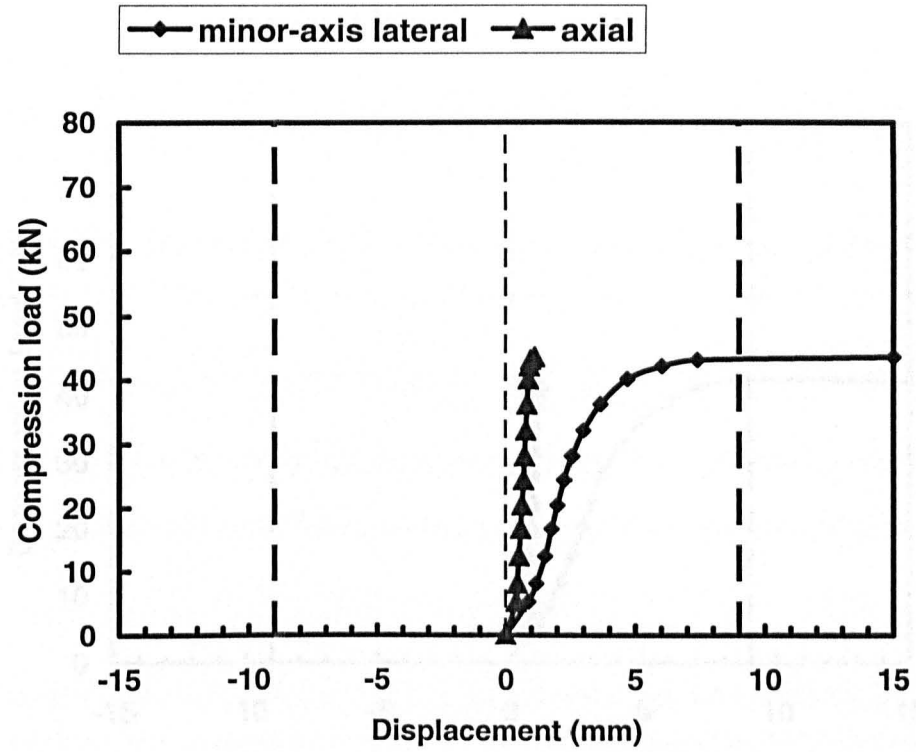

Figure A19. Load-displacement curves for WU107 specimen 1.

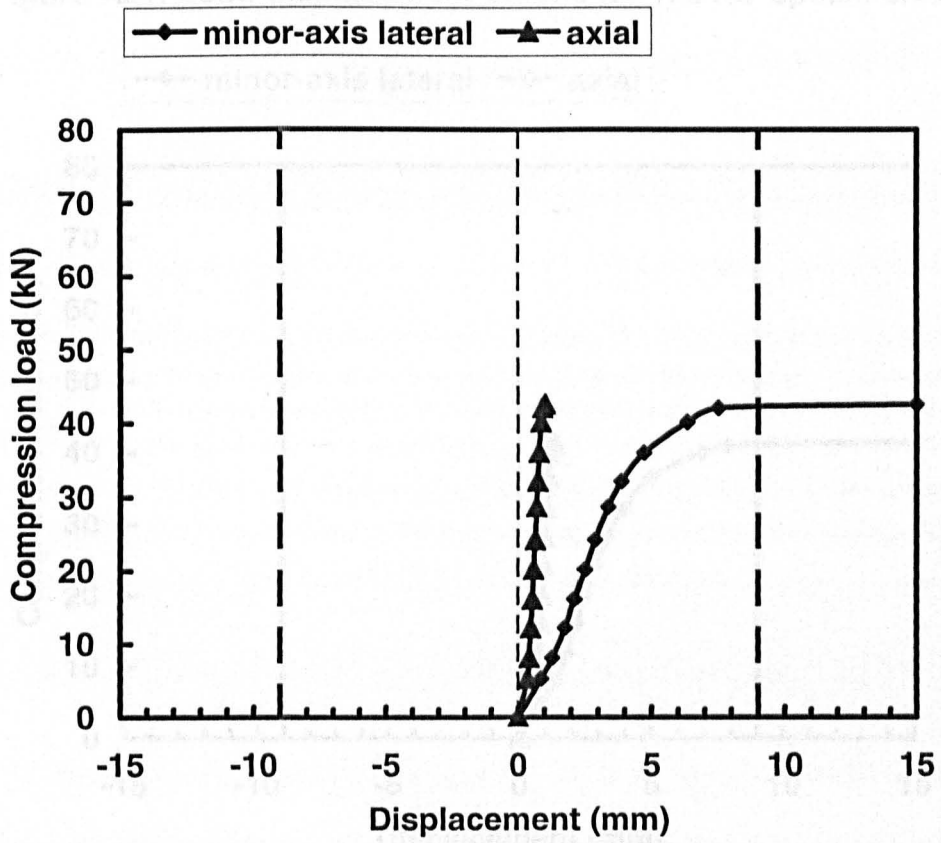

Figure A20. Load-displacement curves for WU107 specimen 2.

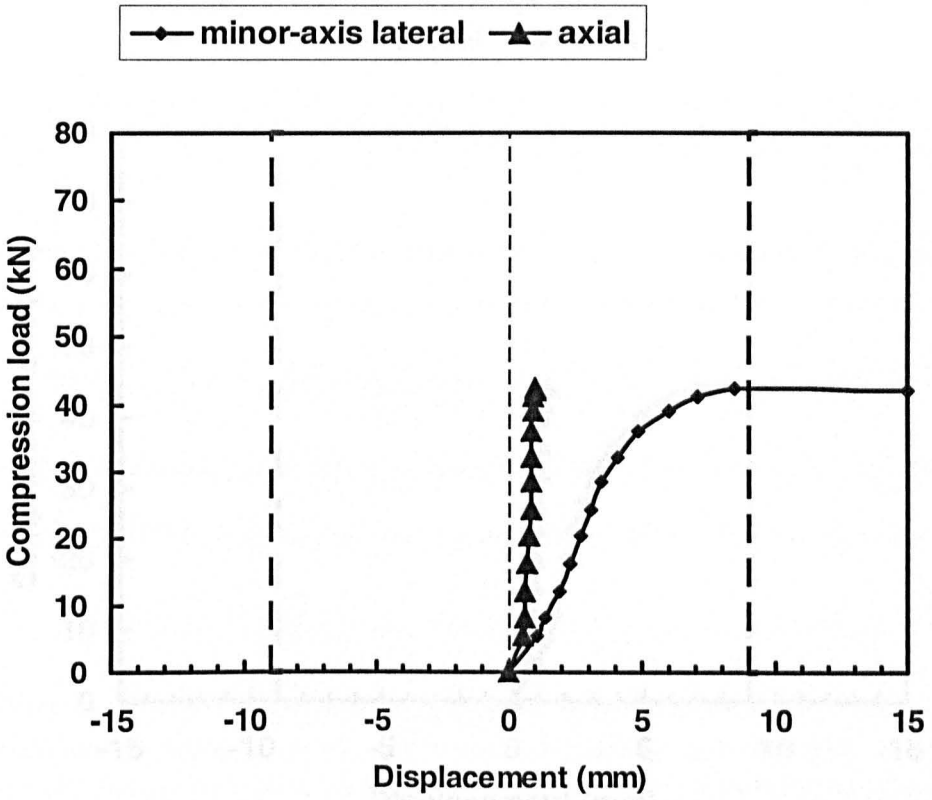

Figure A21. Load-displacement curves for WU107 specimen 3.

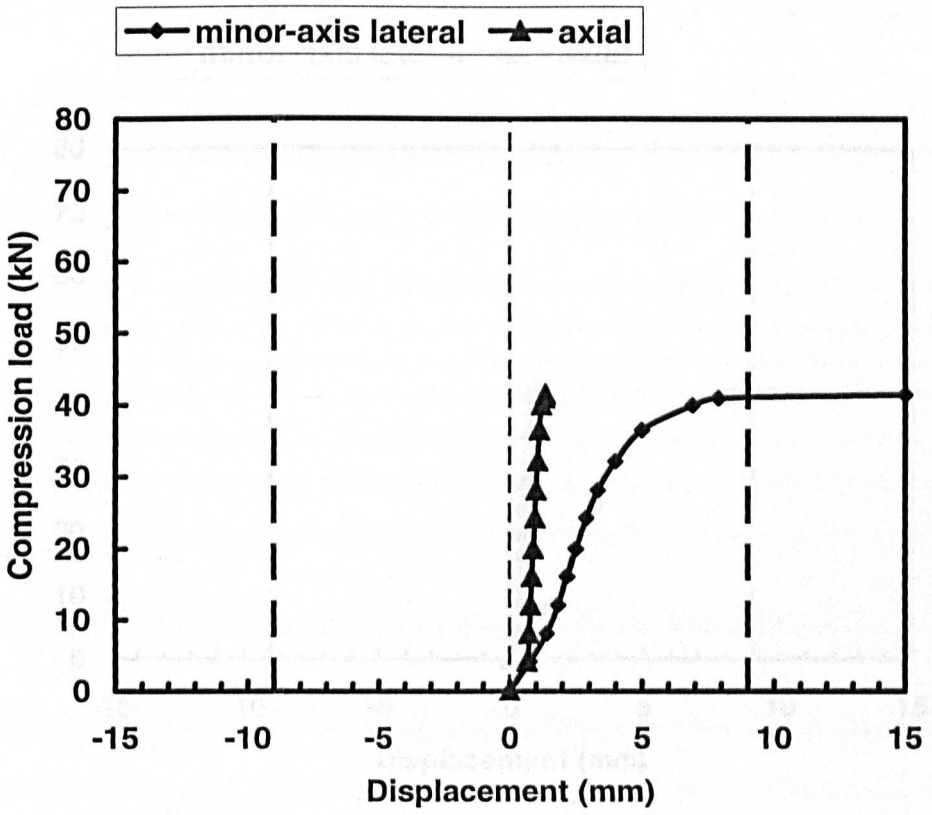

Figure A22. Load-displacement curves for WU107 specimen 4.

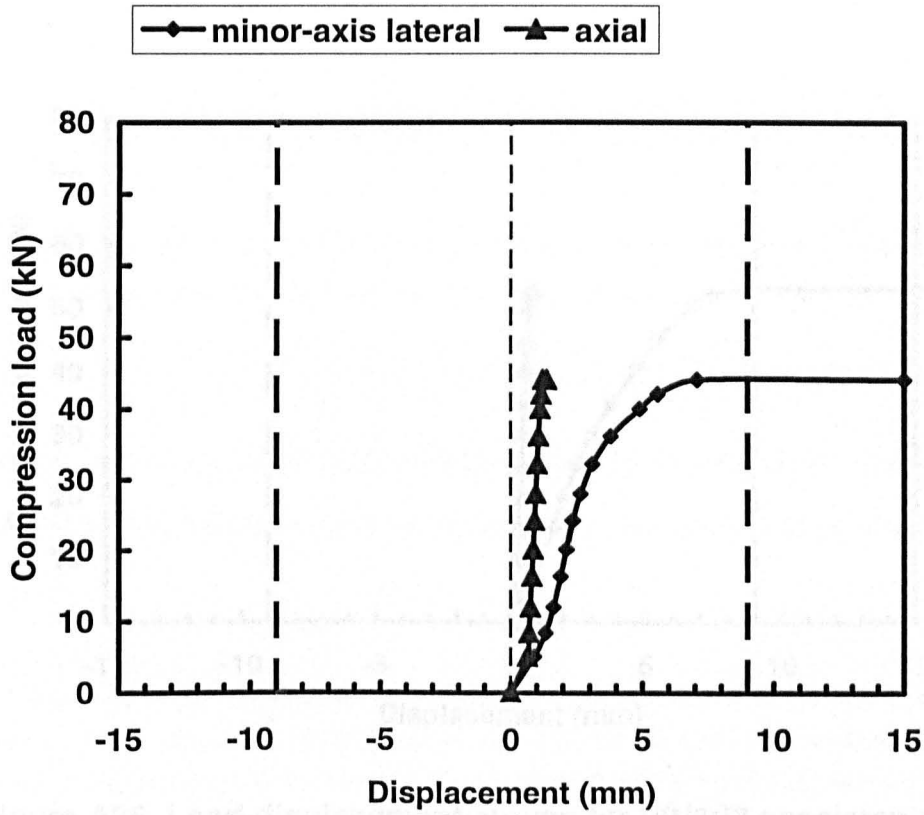

Figure A23. Load-displacement curves for WU107 specimen 5.

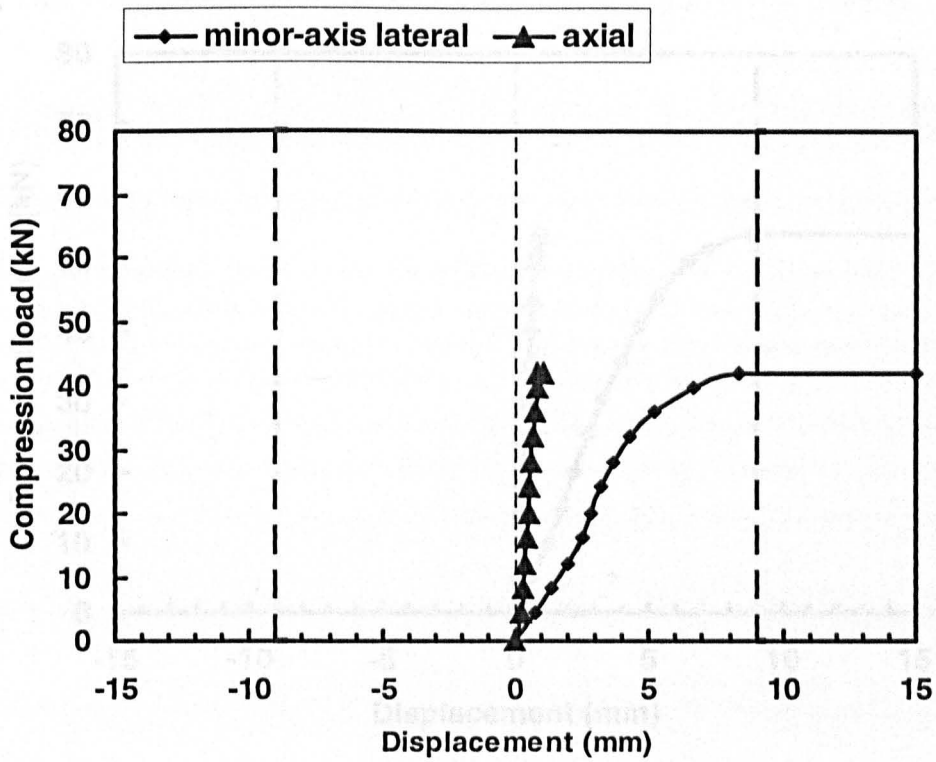

Figure A24. Load-displacement curves for WU107 specimen 6.

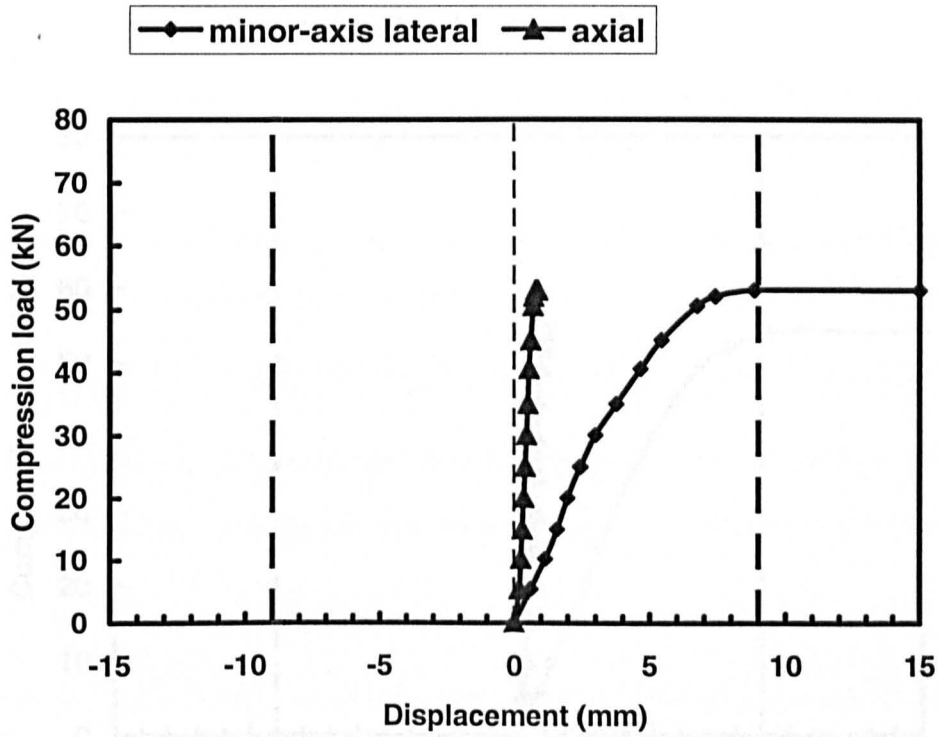

Figure A25. Load-displacement curves for WU108 specimen 1.

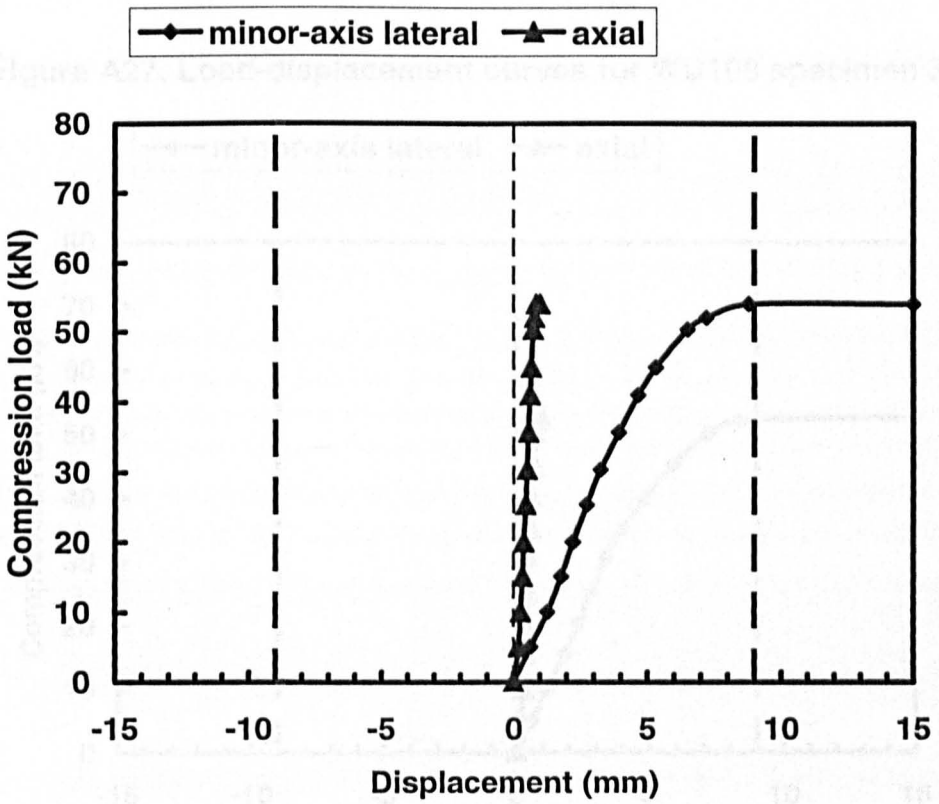

Figure A26. Load-displacement curves for WU108 specimen 2.

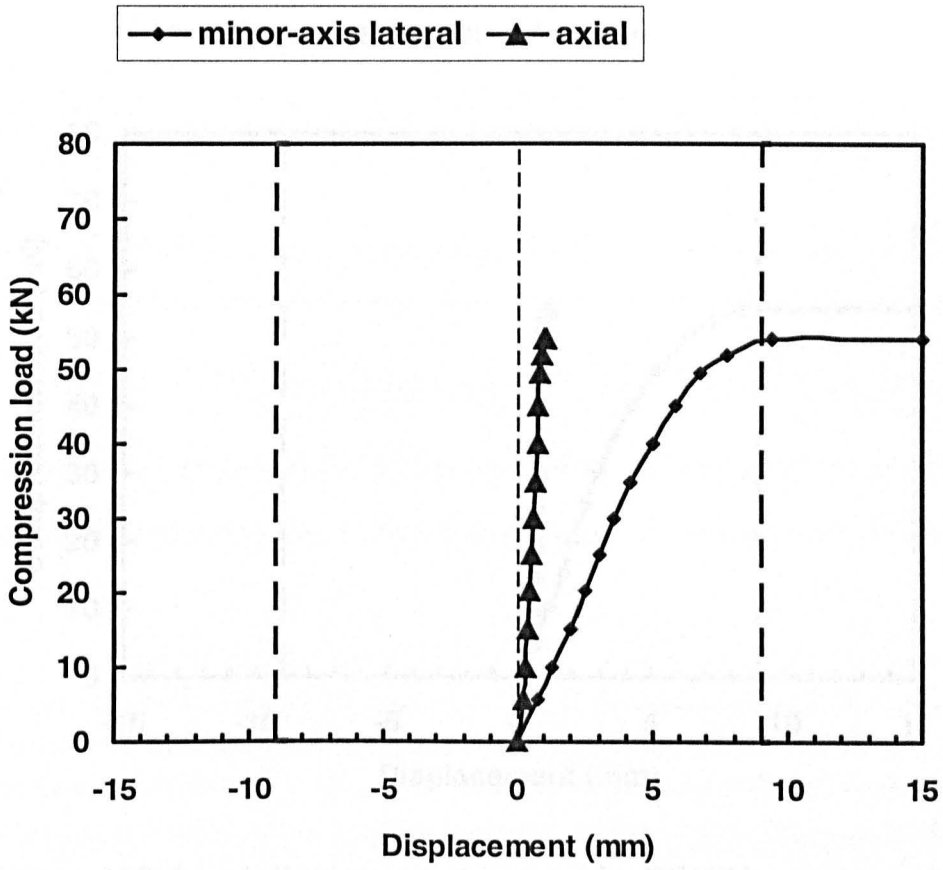

Figure A27. Load-displacement curves for WU108 specimen 3

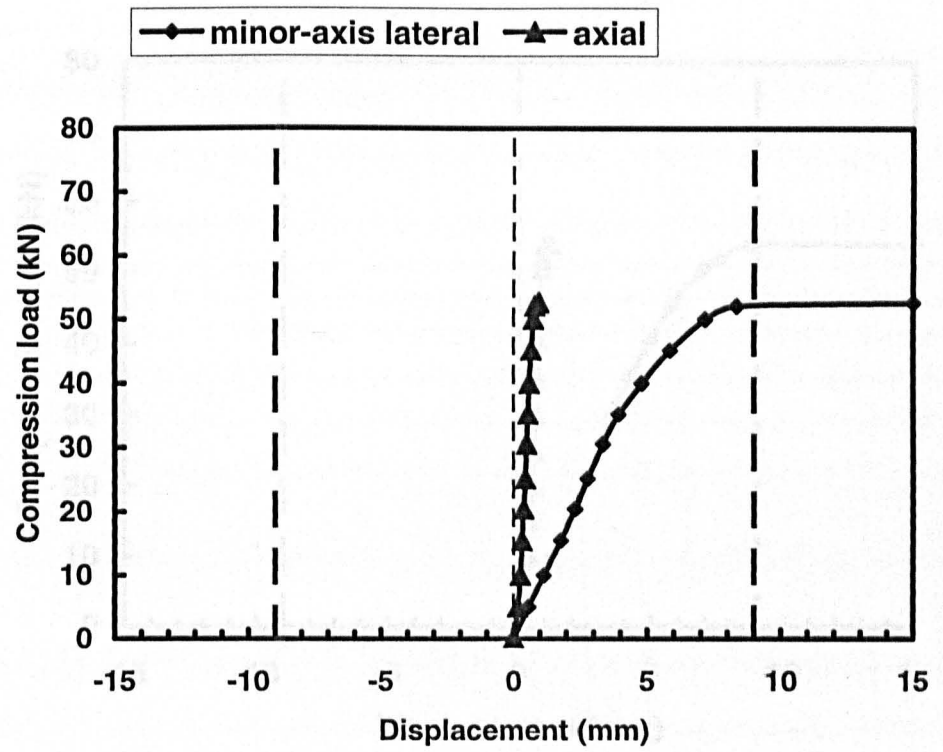

Figure A28. Load-displacement curves for WU108 specimen 4.

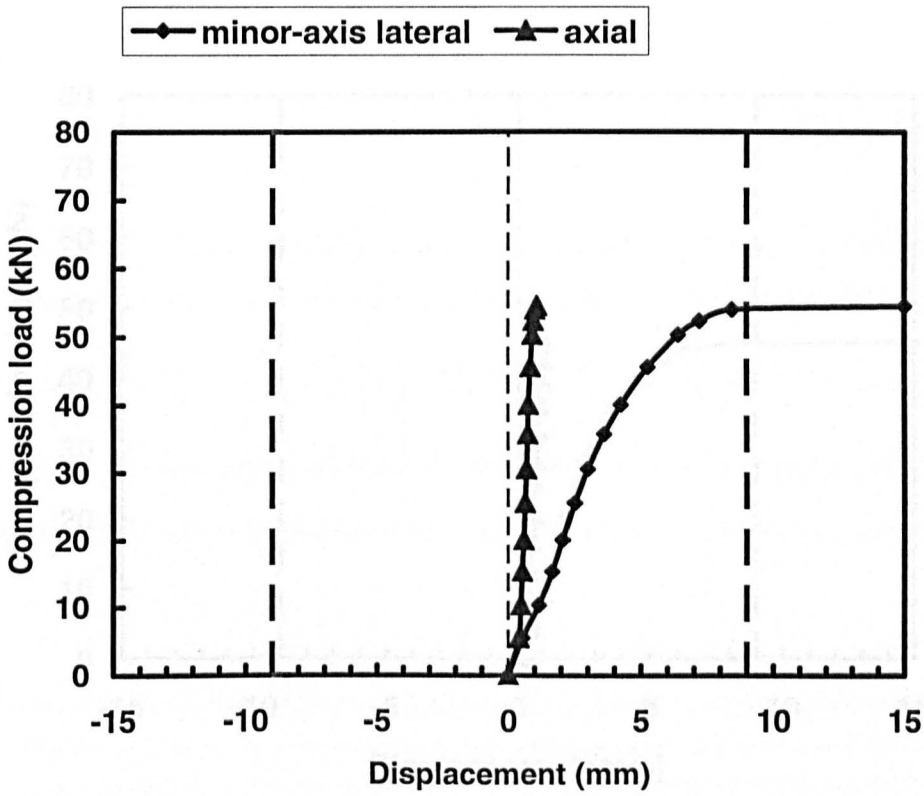

Figure A29. Load-displacement curves for WU108 specimen 5.

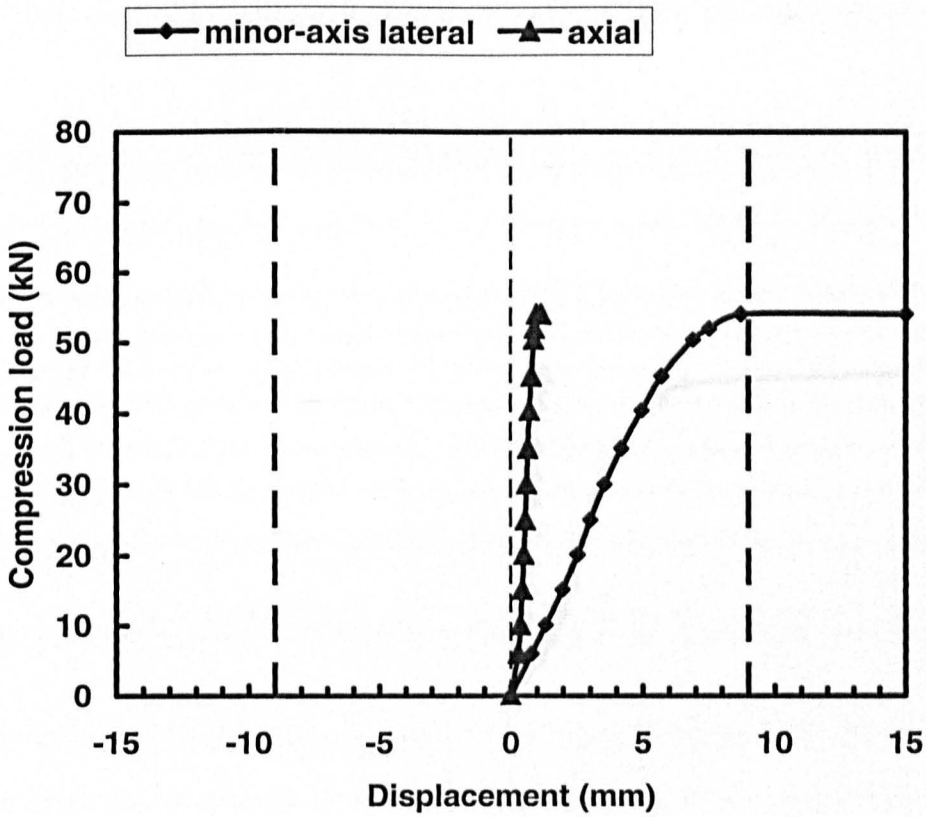

Figure A30. Load-displacement curves for WU108 specimen 6.

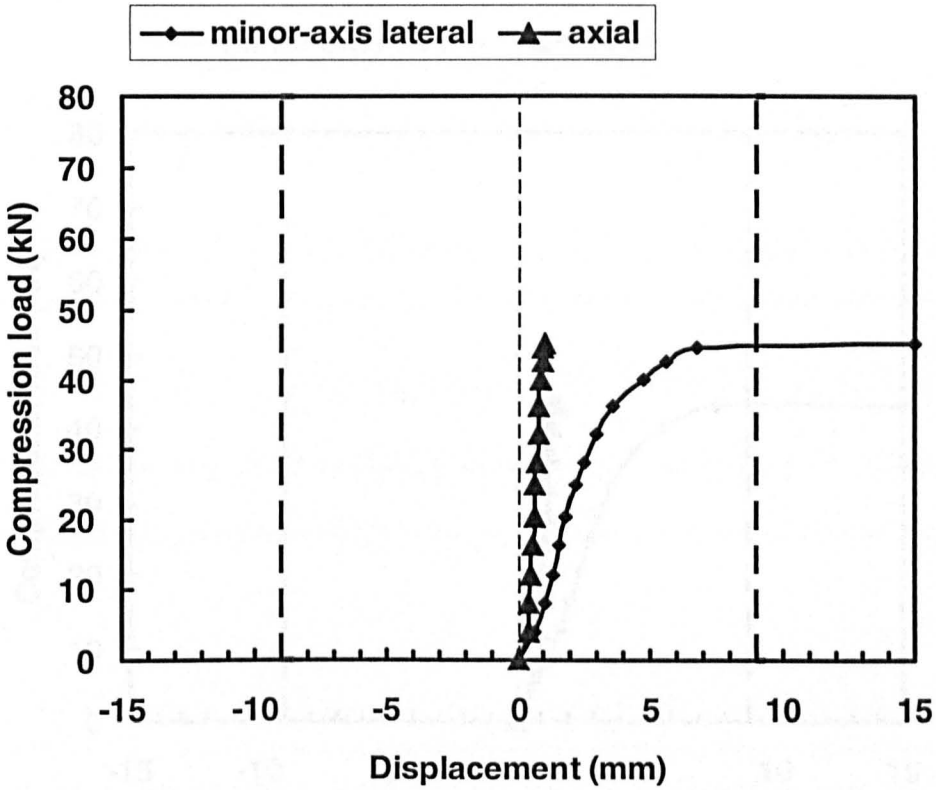

Figure A31. Load-displacement curves for WU109 specimen 1.

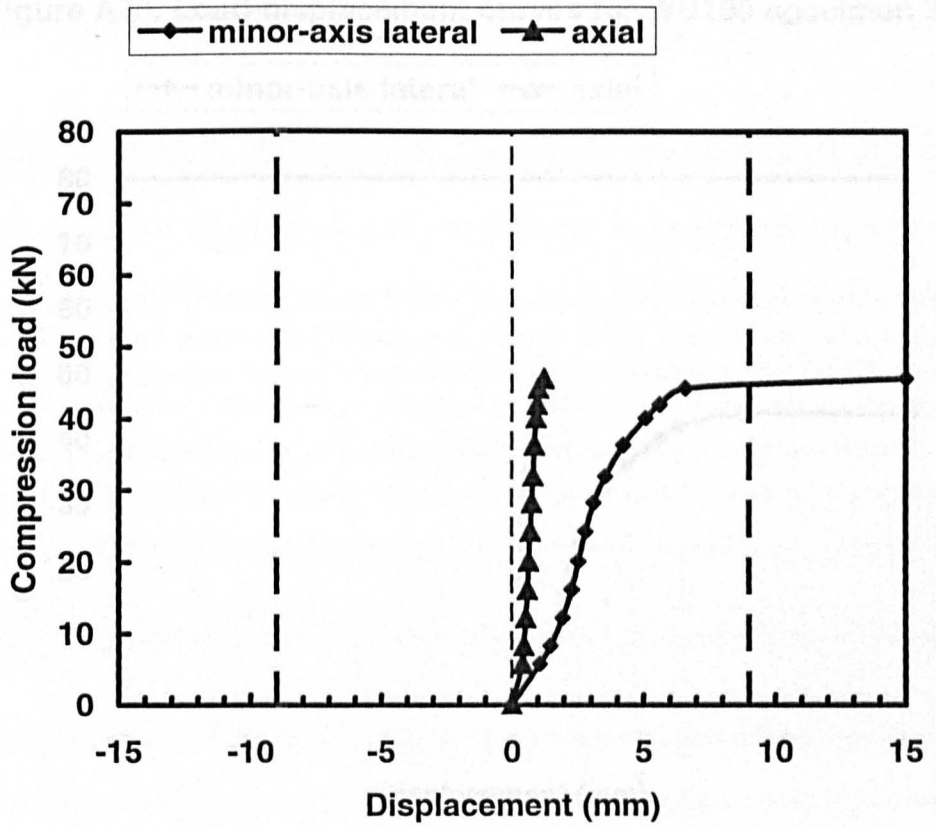

Figure A32. Load-displacement curves for WU109 specimen 2.

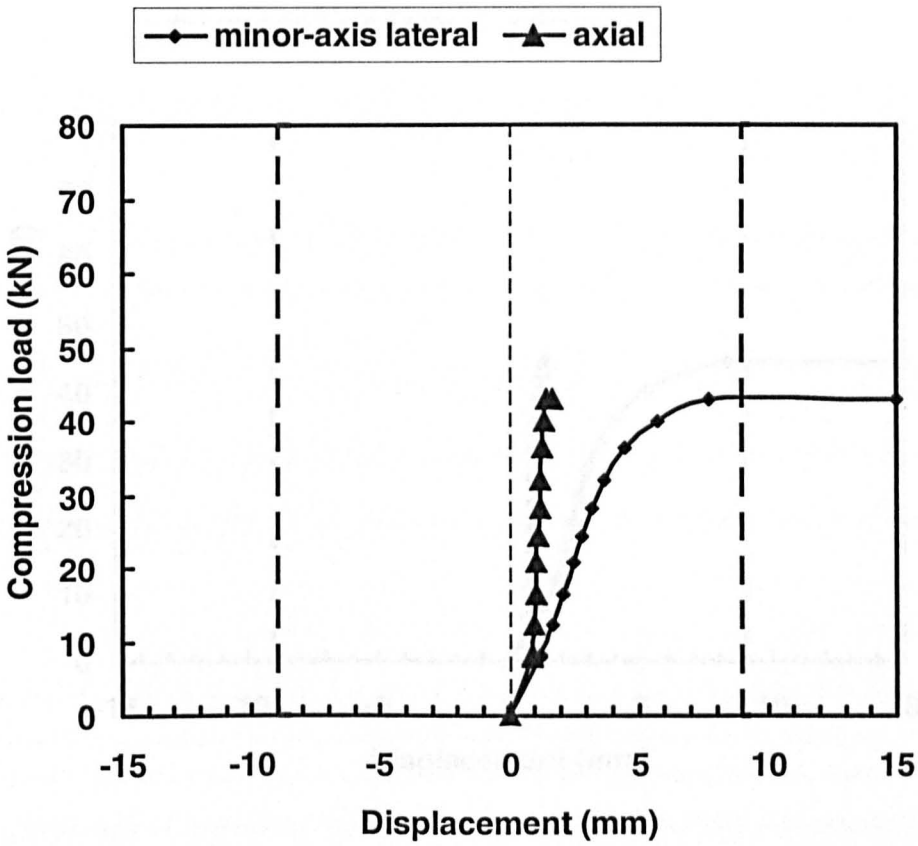

Figure A33. Load-displacement curves for WU109 specimen 3

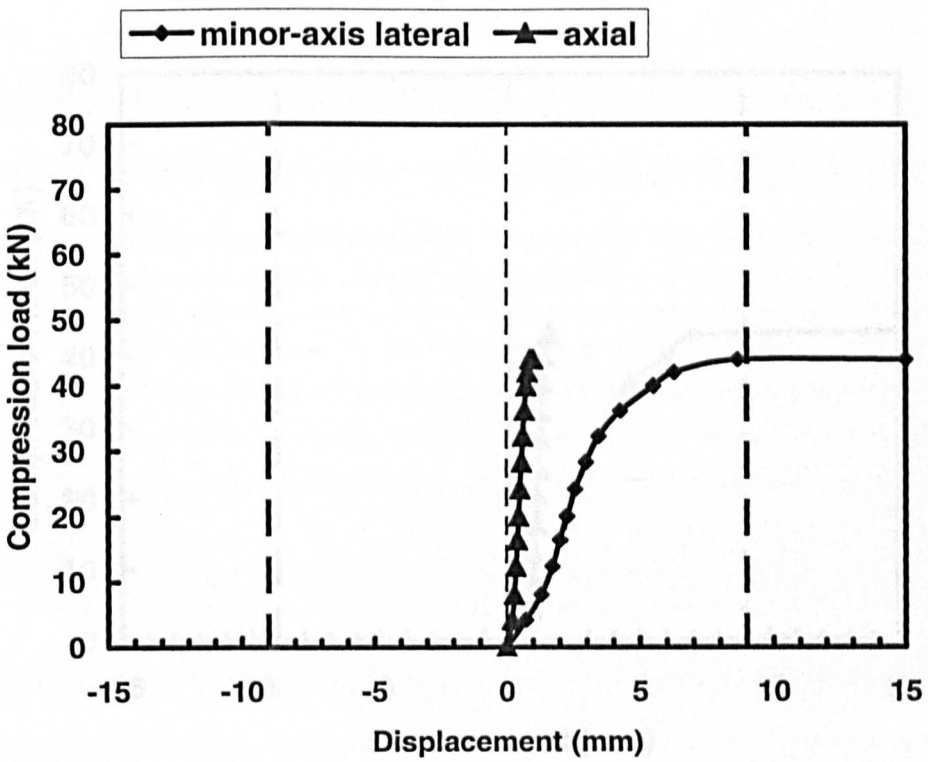

Figure A34. Load-displacement curves for WU109 specimen 4.

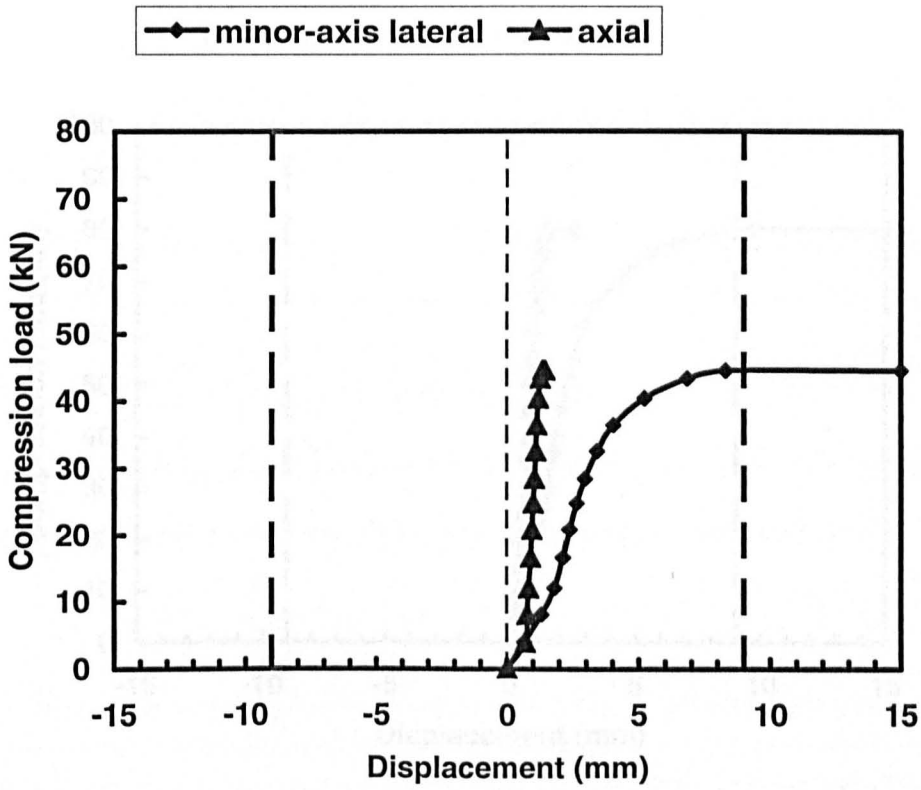

Figure A35. Load-displacement curves for WU109 specimen 5.

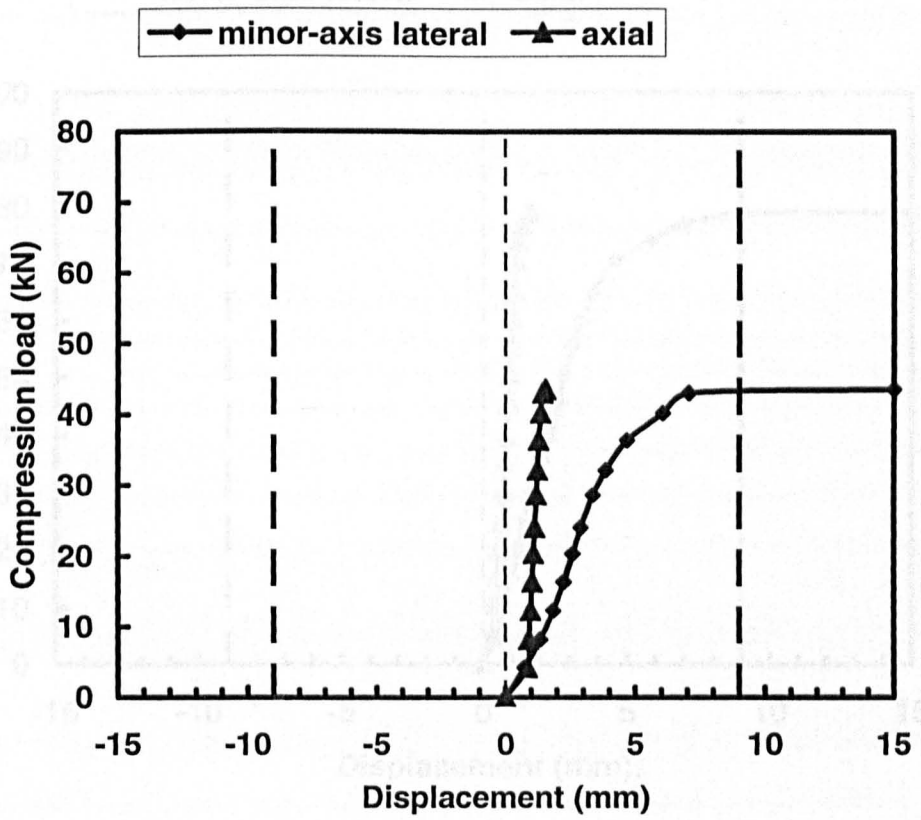

Figure A36. Load-displacement curves for WU109 specimen 6.

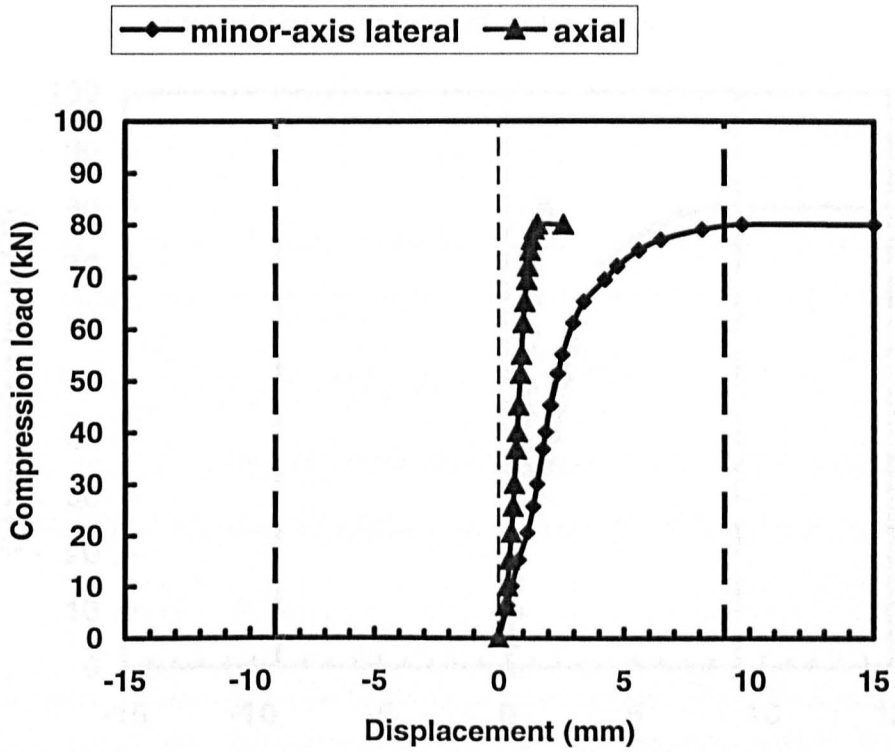

Figure A37. Load-displacement curves for WU110 specimen 1.

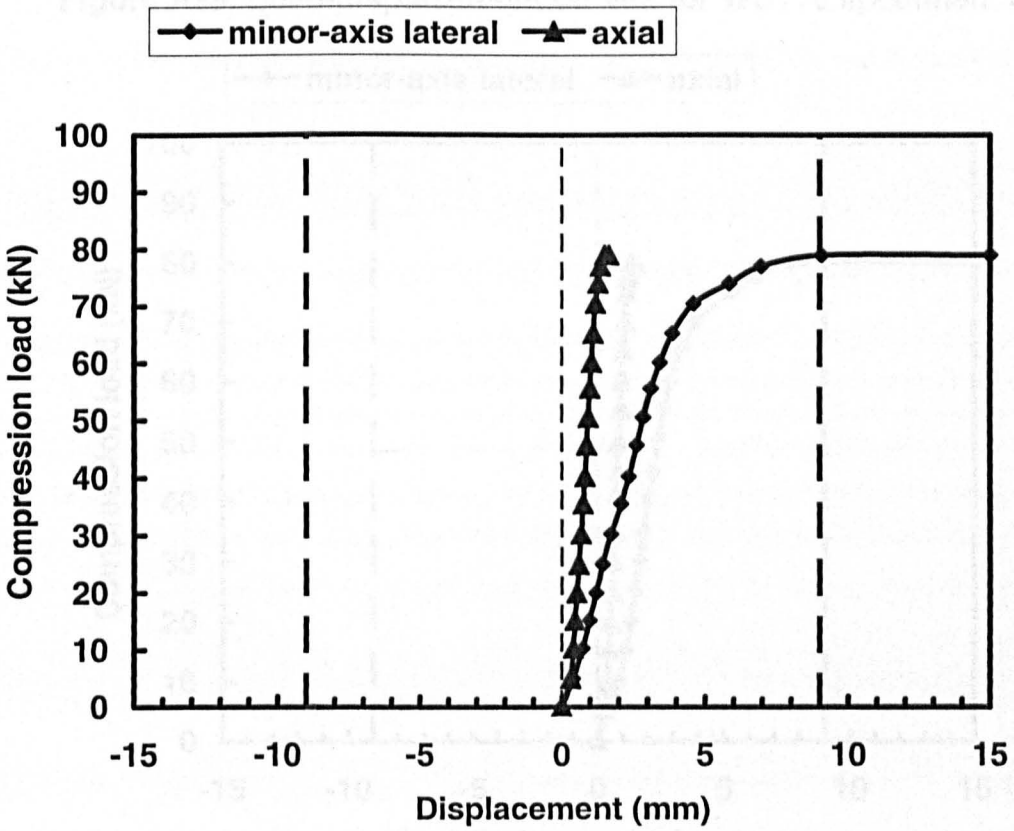

Figure A38. Load-displacement curves for WU110 specimen 2.

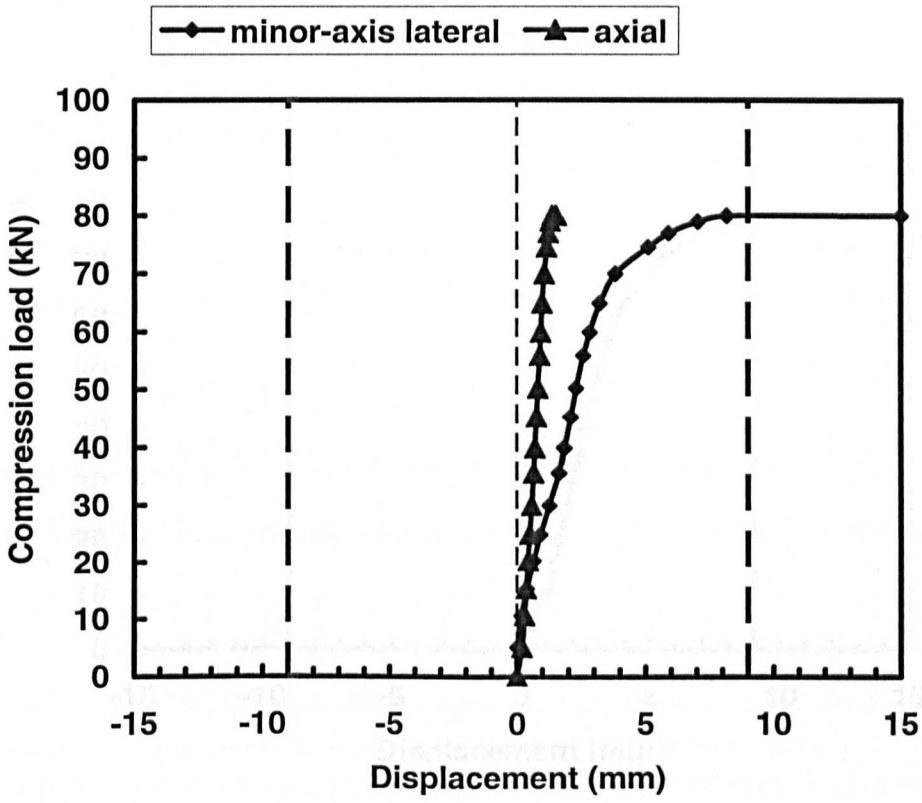

Figure A39. Load-displacement curves for WU110 specimen 3

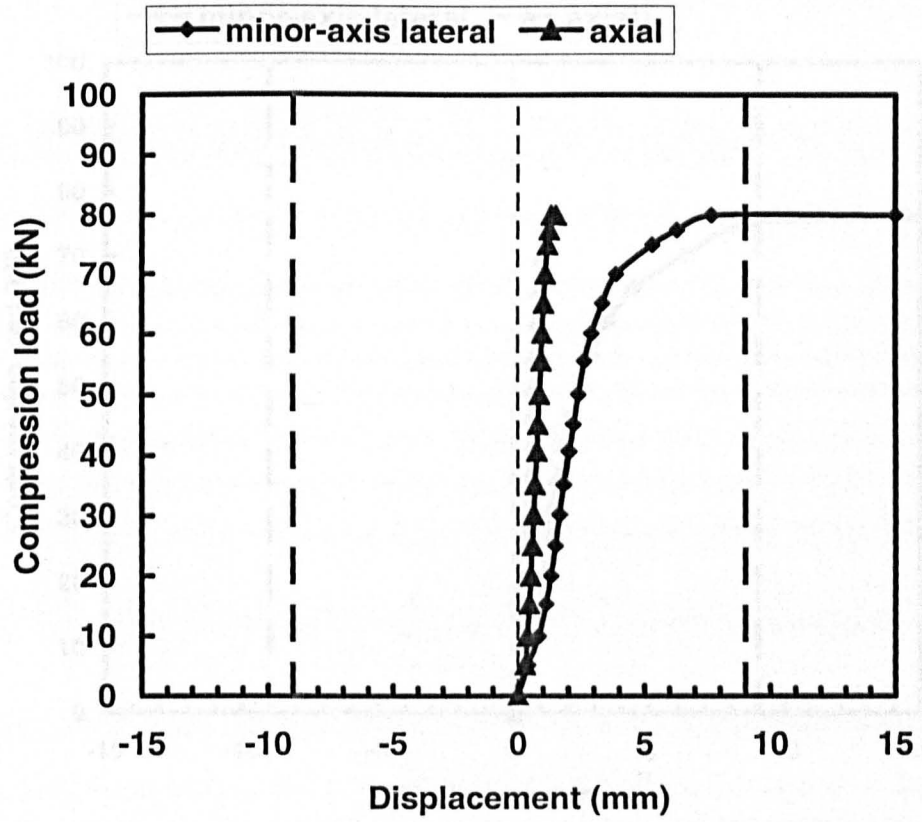

Figure A40. Load-displacement curves for WU110 specimen 4.

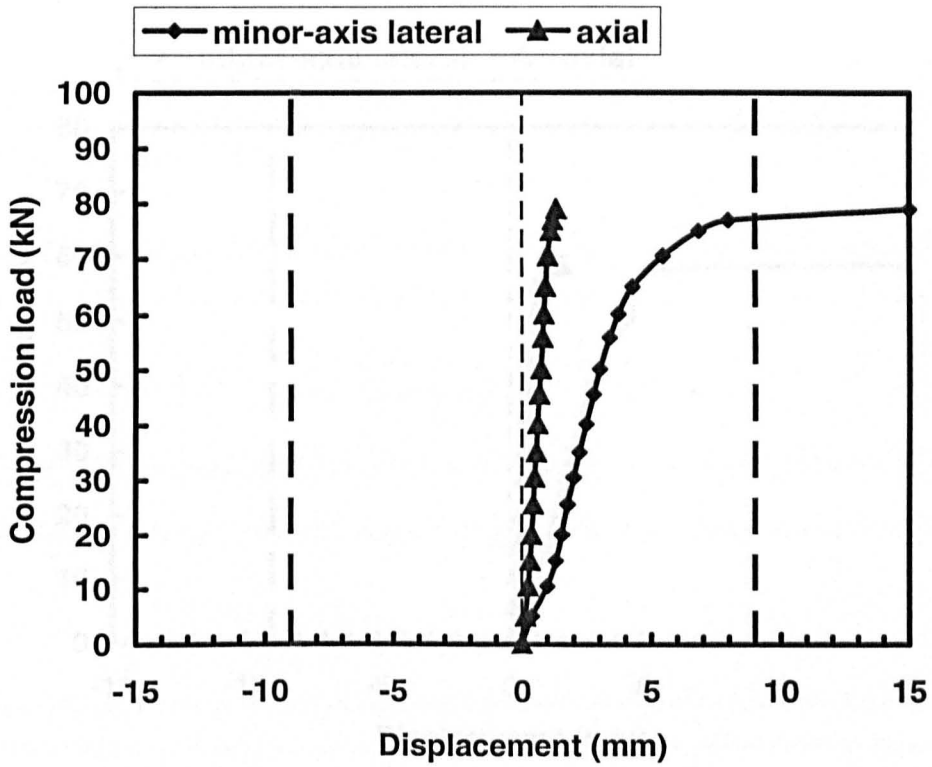

Figure A41. Load-displacement curves for WU110 specimen 5.

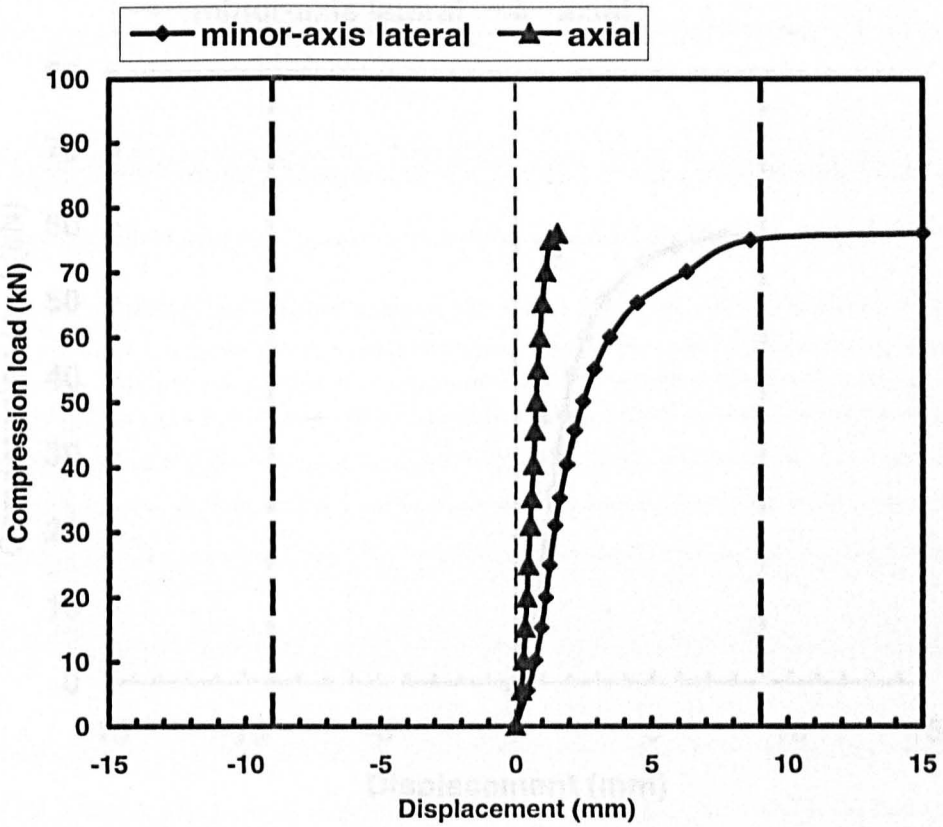

Figure A42. Load-displacement curves for WU110 specimen 6.

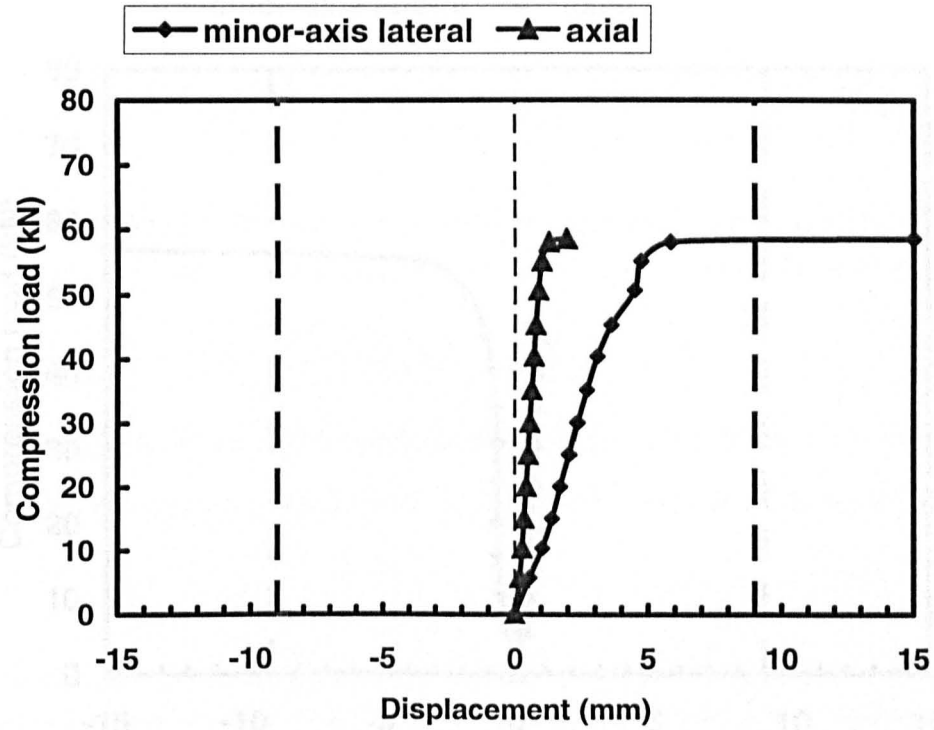

Figure A43. Load-displacement curves for WU111 specimen 1.

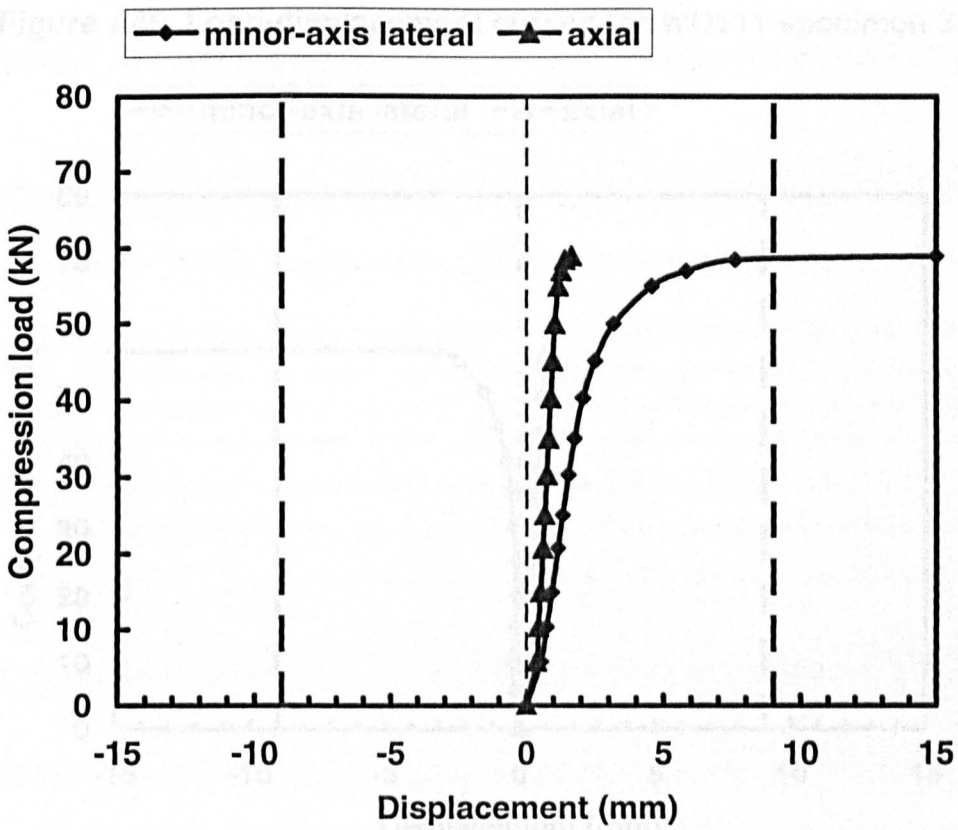

Figure A44. Load-displacement curves for WU111 specimen 2.

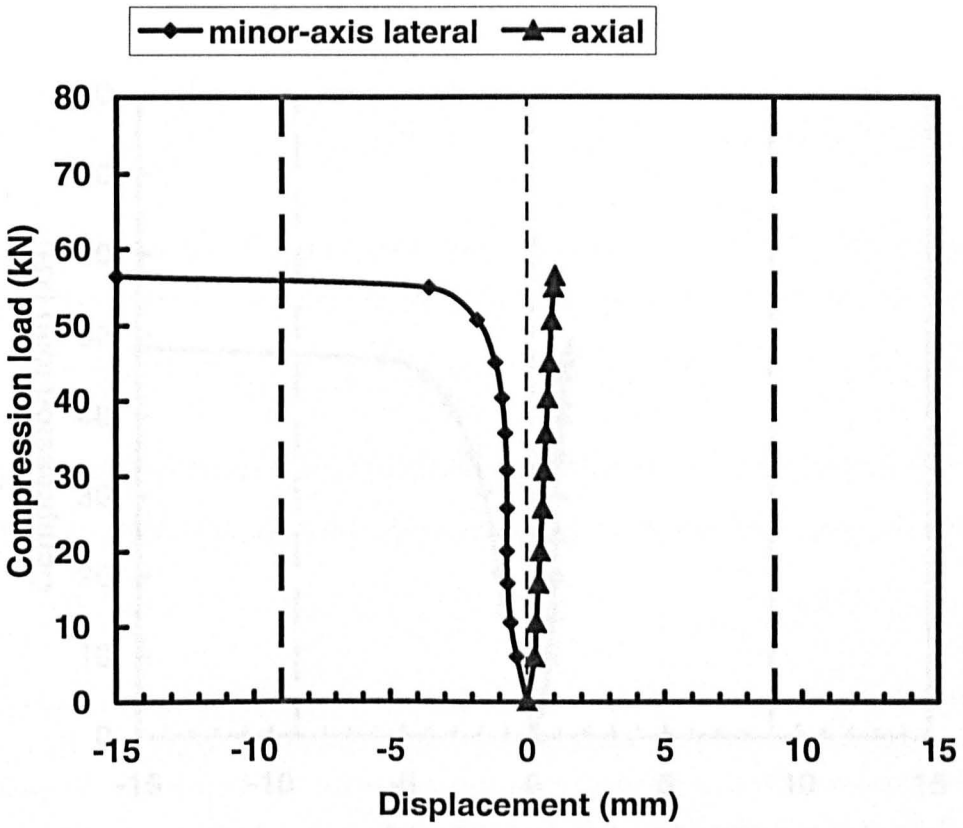

Figure A45. Load-displacement curves for WU111 specimen 3

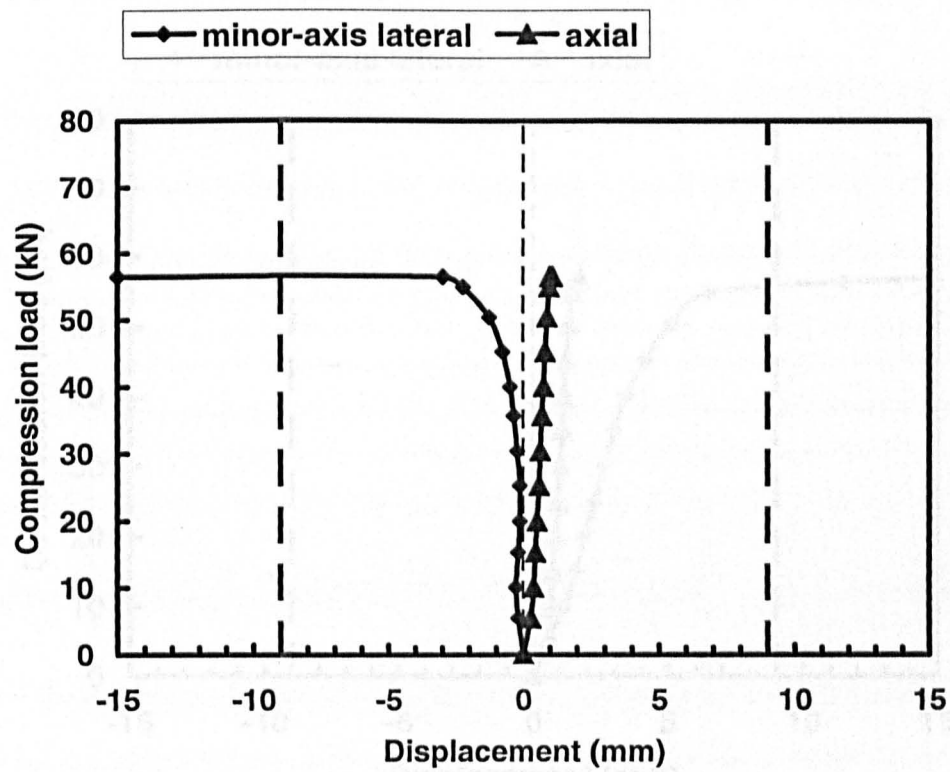

Figure A46. Load-displacement curves for WU111 specimen 4.

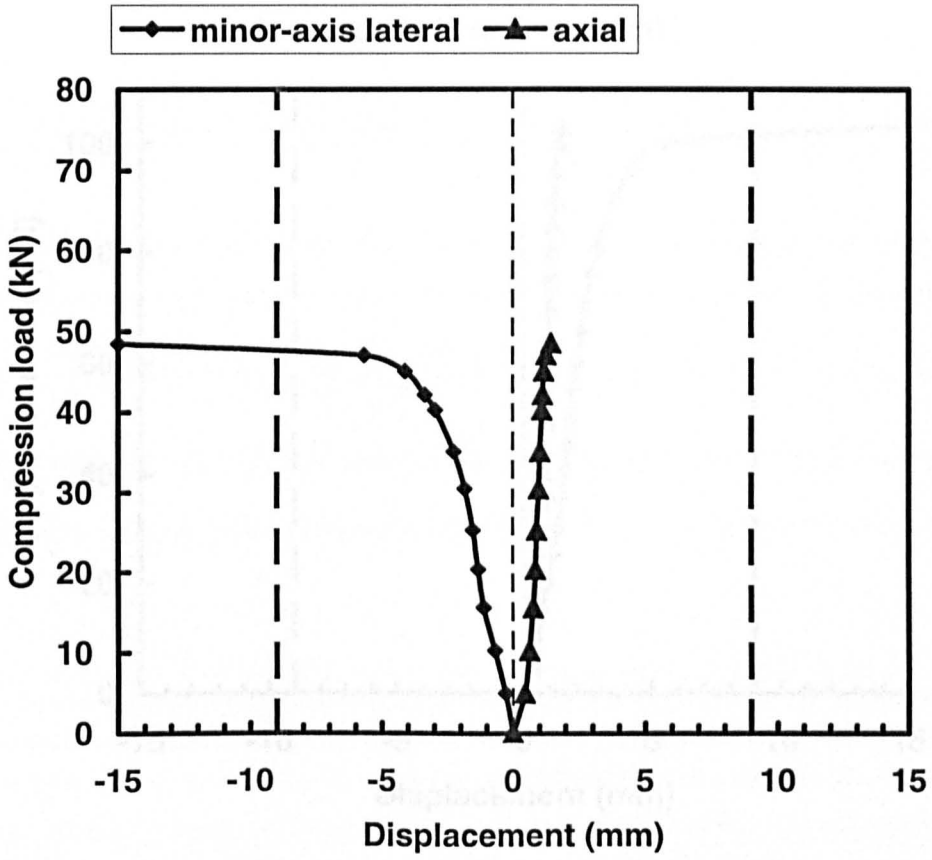

Figure A47. Load-displacement curves for WU111 specimen 5.

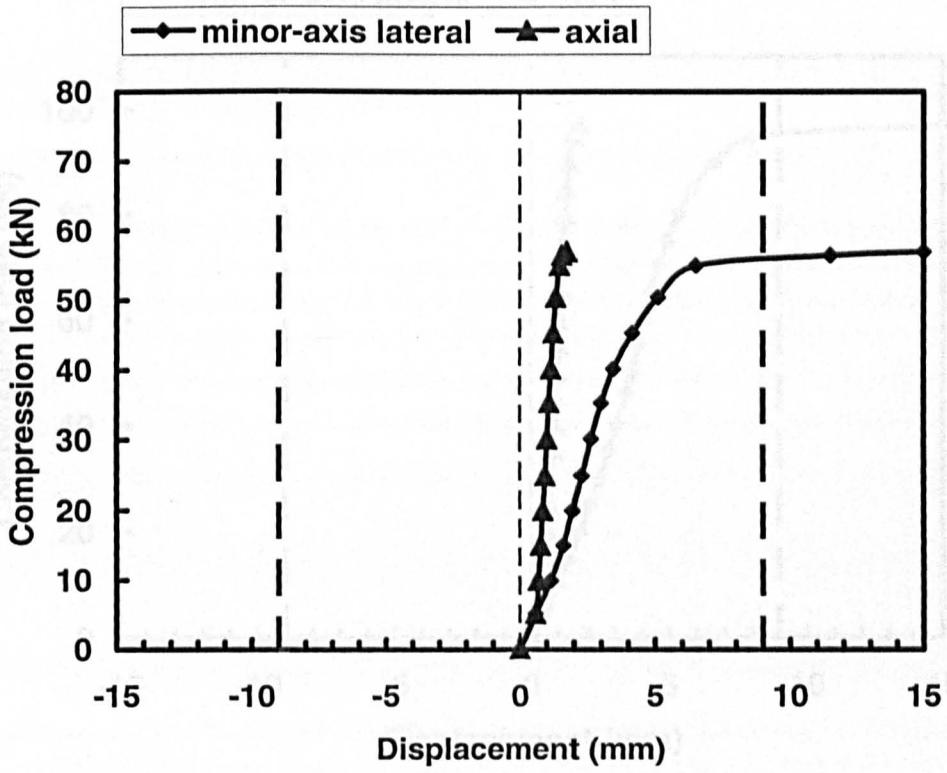

Figure A48. Load-displacement curves for WU111 specimen 6.

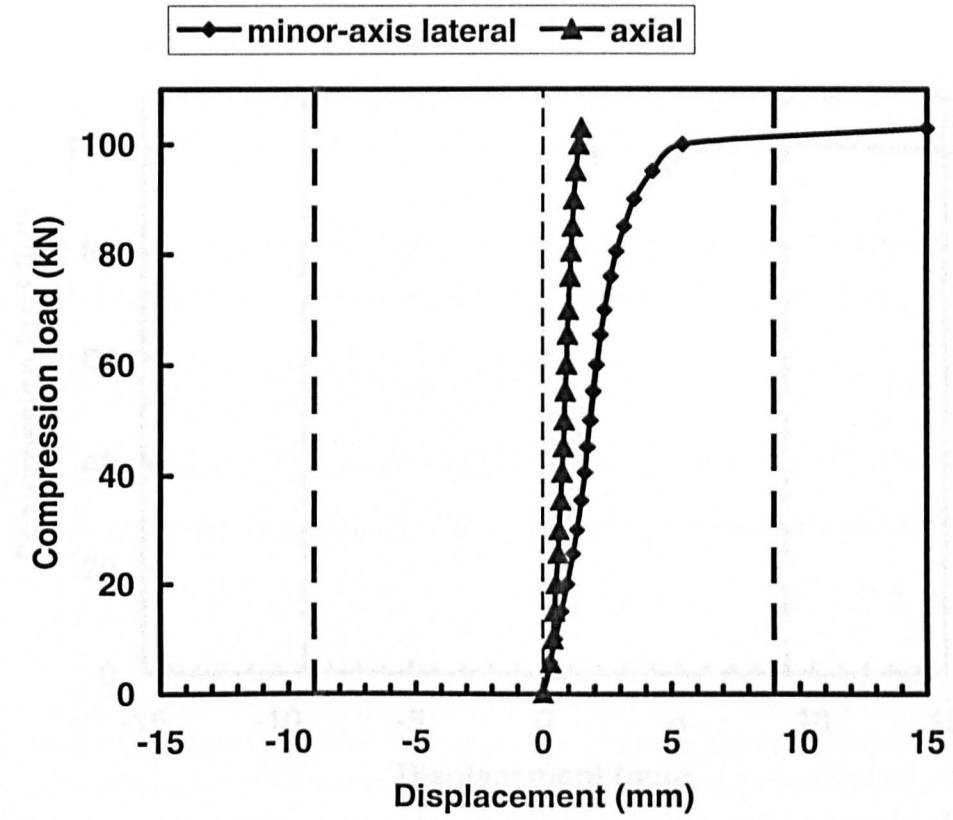

Figure A49. Load-displacement curves for WU112 specimen 1.

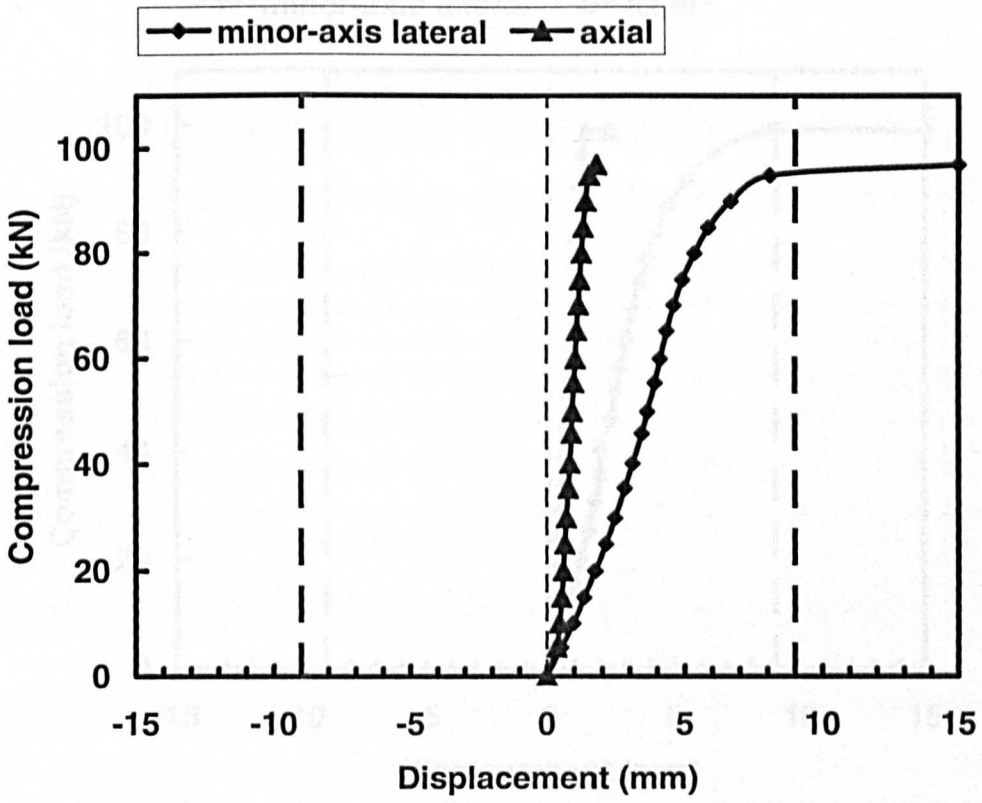

Figure A50. Load-displacement curves for WU112 specimen 2.

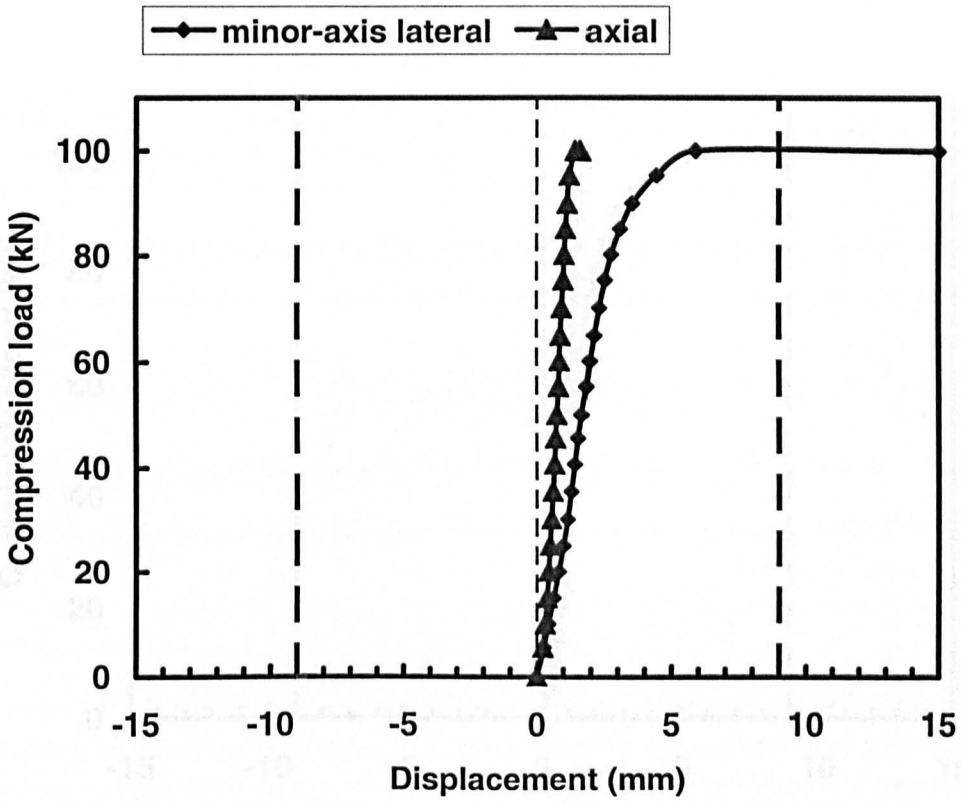

Figure A51. Load-displacement curves for WU112 specimen 3

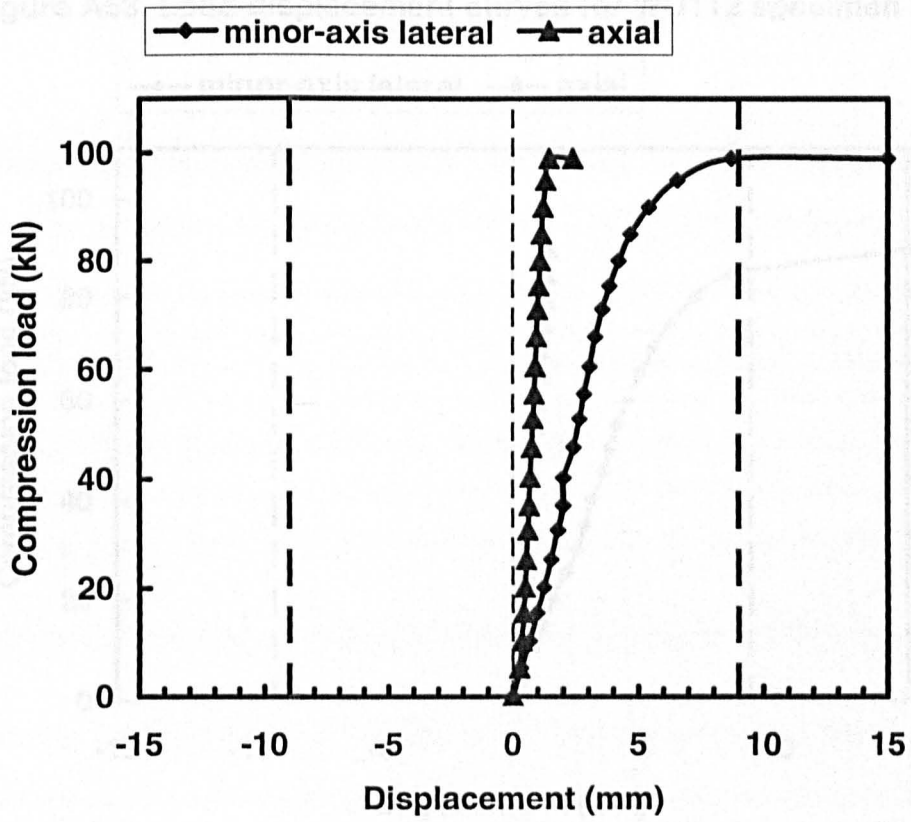

Figure A52. Load-displacement curves for WU112 specimen 4.

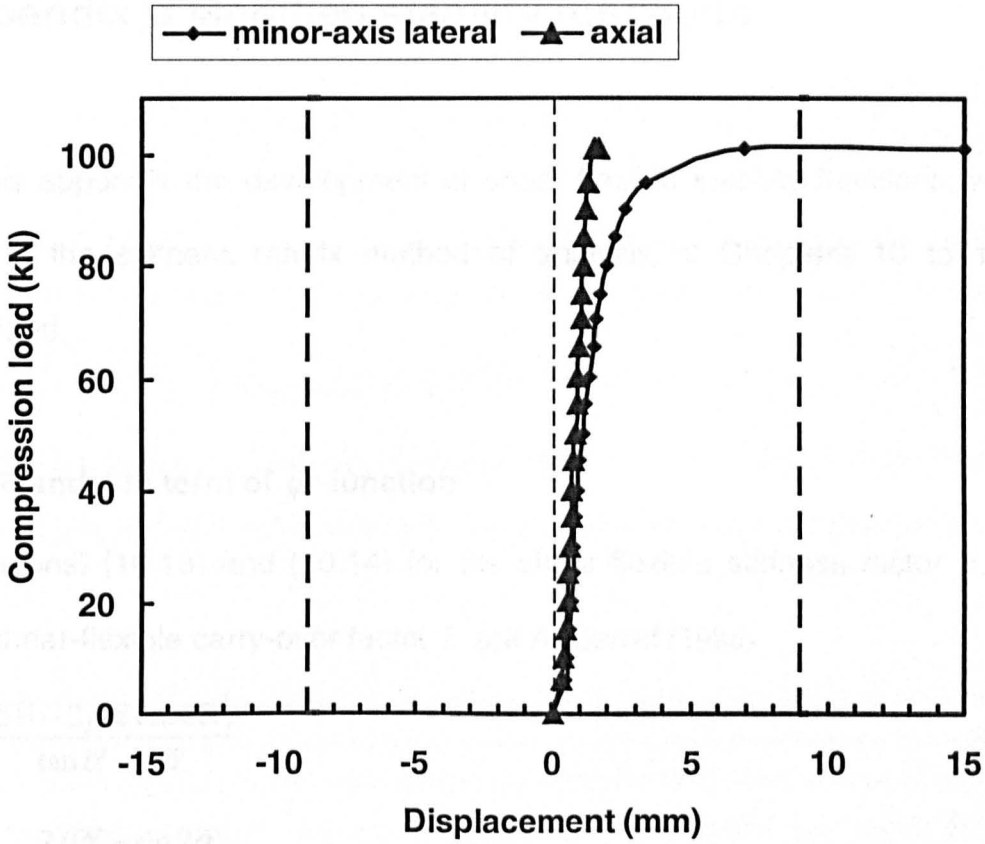

Figure A53. Load-displacement curves for WU112 specimen 5.

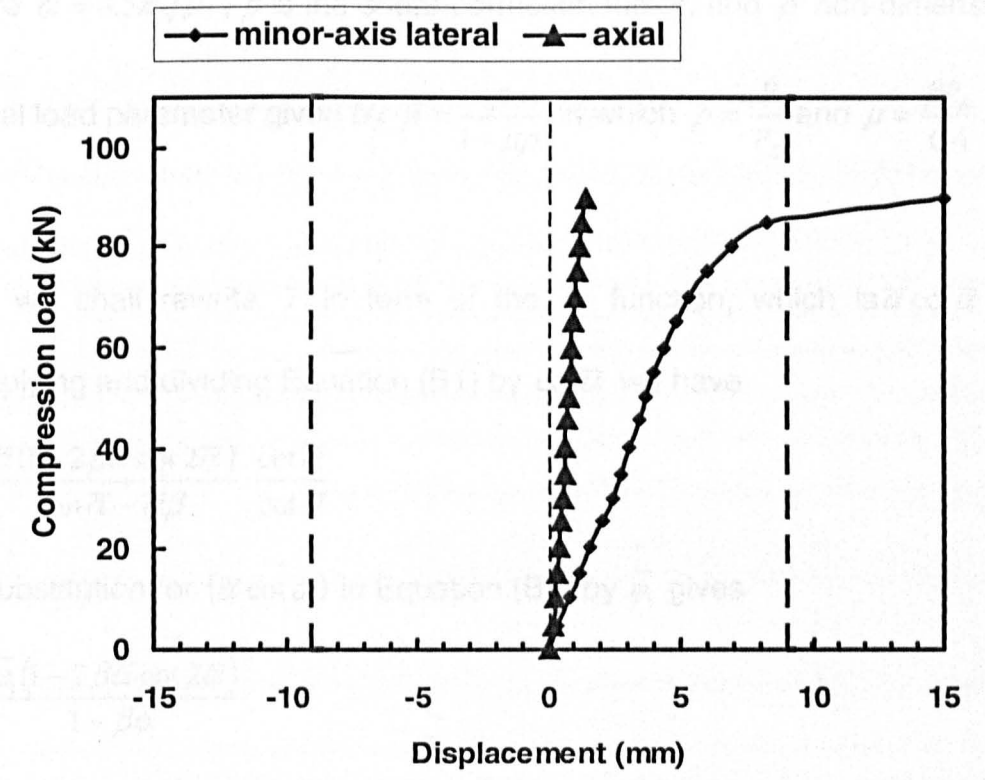

Figure A54. Load-displacement curves for WU112 specimen 6.

Appendix B Modified stability functions

In this appendix the development of shear flexible stability functions, which use in the stiffness matrix method of analysis of Chapters 10 to 12 is provided.

B.1 $\bar{s}$ and $\bar{c}$ in term of $\bar{\varphi}_1$ function

Equations. (10.13) and (10.14) for the shear-flexible stiffness factor $\bar{s}$ and the shear-flexible carry-over factor $\bar{c}$ are Al-Sarraf (1986)

$$\bar{s} = \frac{\bar{\alpha}(1 - 2\beta\bar{\alpha}\cot 2\bar{\alpha})}{\tan\bar{\alpha} - \beta\bar{\alpha}} \tag{B1}$$

$$\bar{c} = \frac{2\beta\bar{\alpha} - \sin 2\bar{\alpha}}{\sin 2\bar{\alpha} - 2\beta\bar{\alpha}\cos 2\bar{\alpha}} \tag{B2}$$

where $\bar{\alpha} = 0.5\pi\sqrt{\bar{\rho}}$, β is the shear correction factor, and $\bar{\rho}$ non-dimensional critical load parameter given by $\bar{\rho} = \frac{\rho}{1 - \mu\rho}$ in which $\rho = \frac{P}{P_E}$ and $\mu = \frac{\beta P_E}{GA}$.,

First we shall rewrite $\bar{s}$ in term of the $\bar{\phi}_1$ function, which is $\bar{\alpha}\cot\bar{\alpha}$. By multiplying and dividing Equation (B1) by $\cot\bar{\alpha}$ we have

$$\bar{s} = \frac{\bar{\alpha}(1 - 2\beta\bar{\alpha}\cot 2\bar{\alpha})}{\tan\bar{\alpha} - \bar{\alpha}\beta} \cdot \frac{\cot\bar{\alpha}}{\cot\bar{\alpha}} \tag{B3}$$

By substitution for $(\bar{\alpha}\cot\bar{\alpha})$ in Equation (B3) by $\bar{\phi}_1$ gives

$$\bar{s} = \frac{\bar{\phi}_1(1 - 2\beta\bar{\alpha}\cot 2\bar{\alpha})}{1 - \beta\bar{\phi}_1} \tag{B4}$$

$$= \frac{(\bar{\phi}_1 - 2\beta\bar{\alpha}\bar{\phi}_1\cot 2\bar{\alpha})}{1 - \beta\bar{\phi}_1} \tag{B5}$$

By substitution for $\cot 2\bar{\alpha} = \frac{1-\tan^2\bar{\alpha}}{2\tan\bar{\alpha}}$ in Equation (B5) we have

$$\bar{s} = \frac{\phi_1 - 2\bar{\alpha}\beta\bar{\phi}_1\left(\frac{1-\tan^2\bar{\alpha}}{2\tan\bar{\alpha}}\right)}{1-\beta\bar{\phi}_1} \tag{B6}$$

Butting $\cot\bar{\alpha} = \frac{1}{\tan\bar{\alpha}}$ into Equation (B6) yields

$$= \frac{\bar{\phi}_1 - 2\beta\bar{\alpha}\phi_1\left[\frac{\cot\bar{\alpha}}{2}\cdot\left(1-\frac{1}{\cot^2\bar{\alpha}}\right)\right]}{1-\beta\bar{\phi}_1} \tag{B7}$$

$$= \frac{\bar{\phi}_1 - \beta\bar{\phi}_1^2\left(1-\frac{1}{\cot^2\bar{\alpha}}\right)}{1-\beta\bar{\phi}_1} \tag{B8}$$

$$= \frac{\bar{\phi}_1 - \beta\bar{\phi}_1^2 + \beta\bar{\alpha}^2}{1-\beta\bar{\phi}_1} \tag{B9}$$

$$\bar{s} = \frac{\beta\bar{\alpha}^2 + \bar{\phi}_1 - \beta\bar{\phi}_1^2}{1-\beta\bar{\phi}_1} \tag{B10}$$

Secondly we shall rewrite $\bar{c}$ in term of the $\bar{\phi}_1$ function. By dividing all the terms in Equation (B2) by $\sin 2\bar{\alpha}$ we have

$$= \frac{\frac{2\beta\bar{\alpha}}{\sin 2\bar{\alpha}} - \frac{\sin 2\bar{\alpha}}{\sin 2\bar{\alpha}}}{\frac{\sin 2\bar{\alpha}}{\sin 2\bar{\alpha}} - \frac{2\beta\bar{\alpha}\cos 2\bar{\alpha}}{\sin 2\bar{\alpha}}} \tag{B11}$$

Substitution for $\sin 2\bar{\alpha} = 2\sin\bar{\alpha}\cos\bar{\alpha}$ in Equation (B11) lead to

$$= \frac{\frac{2\beta\bar{\alpha}}{2\sin\bar{\alpha}\cos\bar{\alpha}} - 1}{1-2\beta\bar{\alpha}\cot 2\bar{\alpha}} \tag{B12}$$

Which can be rearranged as follows

$$\bar{c} = \frac{\beta\bar{\alpha}\csc^2\bar{\alpha} - 1}{1 - 2\beta\bar{\alpha}\left(\frac{1-\tan^2\bar{\alpha}}{2\tan\alpha}\right)} \tag{B13}$$

$$= \frac{\left(\beta\bar{\alpha}\csc^2\bar{\alpha} - \cot\bar{\alpha}\right)\frac{1}{\cot\bar{\alpha}}}{1 - 2\beta\bar{\alpha}\cdot\frac{\cot\bar{\alpha}}{2}\left(1 - \frac{1}{\cot^2\alpha}\right)} \tag{B14}$$

$$= \frac{\left[\beta\bar{\alpha}\left(\cot^2\bar{\alpha}+1\right) - \cot\bar{\alpha}\right]\frac{1}{\cot\bar{\alpha}}}{1 - \beta\bar{\phi}_1\left(1 - \frac{1}{\cot^2\bar{\alpha}}\right)} \tag{B15}$$

$$= \frac{\frac{\beta\bar{\alpha}}{\cot\bar{\alpha}}\left(\cot^2\bar{\alpha}+1\right) - 1}{1 - \beta\bar{\phi}_1 + \frac{\beta\bar{\alpha}}{\cot\bar{\alpha}}} \tag{B16}$$

$$= \frac{\beta\bar{\alpha}\cot\bar{\alpha} + \frac{\beta\bar{\alpha}}{\cot\bar{\alpha}} - 1}{1 - \beta\bar{\phi}_1 + \frac{\beta\bar{\alpha}}{\cot\bar{\alpha}}} \tag{B17}$$

Substitution for $\bar{\phi}_1 = \bar{\alpha}\cot\bar{\alpha}$ and simplifying we get

$$= \frac{\beta\bar{\phi}_1^2 + \beta\bar{\alpha}^2 - \bar{\phi}_1}{\bar{\phi}_1 - \beta\bar{\phi}_1^2 + \beta\bar{\alpha}^2} \tag{B18}$$

By multiplying Equation (B18) by $1 - \beta\bar{\phi}_1$ and rearranging we will get

$$= \frac{\beta\bar{\phi}_1^2 + \beta\bar{\alpha}^2 - \bar{\phi}_1}{\frac{\left(\bar{\phi}_1 - \beta\bar{\phi}_1^2 + \beta\bar{\alpha}^2\right)}{1 - \beta\bar{\phi}_1}\cdot\left(1 - \beta\bar{\phi}_1\right)} \tag{B19}$$

$$= \frac{1}{\bar{s}}\cdot\frac{\beta\bar{\phi}_1^2 + \beta\bar{\alpha}^2 - \bar{\phi}_1}{1 - \beta\bar{\phi}_1} \tag{B20}$$

$$\bar{c} = \frac{1}{\bar{s}}\cdot\frac{\beta\bar{\alpha}^2 - \bar{\phi}_1 + \beta\bar{\phi}_1^2}{1 - \beta\bar{\phi}_1} \tag{B21}$$

B.2 Developing of the other four shear flexible stability $\bar{\varphi}_i$ functions

By using a similar expression to that presented by Meagher (1999) for the shear stiff case, the shear flexible $\bar{\phi}_2$ is given by

$$\bar{\phi}_2 = \frac{\bar{s}(1+\bar{c})}{6} \tag{B22}$$

Substituting for $\bar{s}$ and $\bar{c}$ the expressions given by Equations (B10) and (B21) respectively we obtain

$$= \frac{1}{6} \cdot \left(\frac{\beta\bar{\alpha}^2 + \bar{\phi}_1 - \beta\bar{\phi}_1^2}{1-\beta\bar{\phi}_1} \right) \cdot \left(1 + \frac{1}{\bar{s}} \cdot \frac{\beta\bar{\alpha}^2 - \bar{\phi}_1 + \beta\bar{\phi}_1^2}{1-\beta\bar{\phi}_1} \right) \tag{B23}$$

$$= \frac{1}{6} \left(\frac{\beta\bar{\alpha}^2 + \bar{\phi}_1 - \beta\bar{\phi}_1^2}{1-\beta\bar{\phi}_1} \right) \left(\frac{\beta\bar{\alpha}^2 + \bar{\phi}_1 - \beta\bar{\phi}_1^2 + \beta\bar{\alpha}^2 - \bar{\phi}_1 + \beta\bar{\phi}_1^2}{\beta\bar{\alpha}^2 + \bar{\phi}_1 - \beta\bar{\phi}_1^2} \right) \tag{B24}$$

$$= \frac{1}{6} \left(\frac{1}{1-\beta\bar{\phi}_1} \right) \cdot 2\beta\bar{\alpha}^2 \tag{B25}$$

$$\bar{\phi}_2 = \frac{\beta\bar{\alpha}^2}{3(1-\beta\bar{\phi}_1)} \tag{B26}$$

By using a similar expression to that presented by Meagher (1999) for the shear stiff case, the shear flexible $\bar{\phi}_3$ is given by

$$\bar{\phi}_3 = \frac{\bar{s}}{4} \tag{B27}$$

Substituting $\bar{s}$ we obtain

$$= \frac{1}{4} \left(\frac{\beta\bar{\alpha}^2 + \phi_1 - \beta\phi_1^2}{1-\beta\phi_1} \right) \tag{B28}$$

$$= \frac{1}{4} \left(\frac{\beta\bar{\alpha}}{1-\beta\bar{\phi}_1} + \frac{\bar{\phi}_1 - \beta\bar{\phi}_1^2}{1-\beta\bar{\phi}_1} \right) \tag{B29}$$

$$= \frac{1}{4}\left[3\bar{\phi}_2 + \bar{\phi}_1\left(\frac{1-\beta\bar{\phi}_1}{1-\beta\bar{\phi}_1}\right)\right] \tag{B30}$$

$$\bar{\phi}_3 = \frac{3\bar{\phi}_2 + \bar{\phi}_1}{4} \tag{B31}$$

As previously for $\bar{\phi}_2$ and $\bar{\phi}_3$ we use the shear stiff case given Meagher (1999) to write the shear flexible $\bar{\phi}_4$ as

$$\bar{\phi}_4 = \frac{1}{2}\bar{s}\bar{c} \tag{B32}$$

Substitution for $\bar{s}$ and $\bar{c}$, followed by rearranging

$$= \frac{1}{2}\left(\frac{\beta\bar{\alpha}^2 + \bar{\phi}_1 - \beta\bar{\phi}_1^2}{1-\beta\bar{\phi}_1}\right)\cdot\left(\frac{1}{\bar{s}}\cdot\frac{\beta\bar{\alpha}^2 - \bar{\phi}_1 + \beta\bar{\phi}_1^2}{1-\beta\bar{\phi}_1}\right) \tag{B33}$$

$$= \frac{1}{2}\left(\frac{\beta\bar{\alpha}^2 - \bar{\phi}_1 + \beta\bar{\phi}_1^2}{1-\beta\bar{\phi}_1}\right) \tag{B34}$$

$$= \frac{1}{2}\left(\frac{\beta\bar{\alpha}^2}{1-\beta\bar{\phi}_1} - \bar{\phi}_1\cdot\frac{1-\beta\bar{\phi}_1}{1-\beta\bar{\phi}_1}\right) \tag{B35}$$

$$= \frac{1}{2}\left(3\bar{\phi}_2 - \bar{\phi}_1\right) \tag{B36}$$

$$\bar{\phi}_4 = \frac{3\bar{\phi}_2 - \bar{\phi}_1}{2} \tag{B37}$$

Finally, the fifth shear flexible $\bar{\phi}$ function is given by

$$\bar{\phi}_5 = \frac{\bar{\phi}_1\bar{s}(1+\bar{c})}{6} \tag{B38}$$

By substituting for $\bar{s}$ and $\bar{c}$ it can be shown that this function is

$$= \frac{\bar{\phi}_1}{6}\left(\frac{\beta\bar{\alpha}^2 + \bar{\phi}_1 - \beta\bar{\phi}_1^2}{1-\beta\bar{\phi}_1}\right)\cdot\left(\left(1+\frac{1}{\bar{s}}\right)\cdot\left(\frac{\beta\bar{\alpha}^2 - \bar{\phi}_1 + \beta\bar{\phi}_1^2}{1-\beta\bar{\phi}_1}\right)\right) \tag{B39}$$

$$= \frac{\bar{\phi}_1}{6}\left(\frac{\beta\bar{\alpha}^2 + \bar{\phi}_1 - \beta\bar{\phi}_1^2}{1-\beta\bar{\phi}_1}\right)\cdot\left(\frac{\dfrac{\beta\bar{\alpha}^2 + \bar{\phi}_1 - \beta\bar{\phi}_1^2}{1-\beta\bar{\phi}_1} + \dfrac{\beta\bar{\alpha}^2 - \bar{\phi}_1 + \beta\bar{\phi}_1^2}{1-\beta\bar{\phi}_1}}{\bar{s}}\right) \tag{B40}$$

$$= \frac{\bar{\phi}_1}{6}\left(\frac{\beta\bar{\alpha}^2 + \bar{\phi}_1 - \beta\bar{\phi}_1^2 + \beta\bar{\alpha}^2 - \bar{\phi}_1 + \beta\bar{\phi}_1^2}{1-\beta\bar{\phi}_1}\right) \tag{B41}$$

$$= \frac{\bar{\phi}_1}{6}\left(\frac{2\beta\bar{\alpha}^2}{1-\beta\bar{\phi}_1}\right) \tag{B42}$$

$$\bar{\phi}_5 = \bar{\phi}_1\bar{\phi}_2 \tag{B43}$$

The five $\bar{\phi}$ functions are used in the element stiffness matrix in Equation (10.24) and their values are calculated from $\bar{\phi}_1 = \bar{\alpha}\cot\bar{\alpha}$. According to Livesly (1956) the solution for $\bar{\phi}_1$ function is given by

$$\bar{\phi}_1 = \frac{64 - 60\bar{\rho} + 5\bar{\rho}^2}{64 - 20\bar{\rho} + \bar{\rho}^2} - \sum_{n=1}^{7}\frac{a_n\bar{\rho}^n}{2^{3n}} \tag{B44}$$

in which $\bar{\rho}$ as defined before and a_i's are

$a_1 = 1.57973627$

$a_2 = 0.15858587$

$a_3 = 0.02748899$

$a_4 = 0.00547590$

$a_5 = 0.00115281$

$a_6 = 0.00024908$

$a_7 = 0.00005452$

Appendix C Guide for using sframe program to analysis plane frames of shear flexible members

The modified version of the program sframe described in Chapter 10 uses the matrix stiffness method to analysis and predicts the elastic critical load for a plane frame structure. The steps required for running the program are detailed in this Appendix.

C.1 How to use the sframe program

The first step to use sframe program is to compile the source code file **sframe.c** to have the executable file, which we shall name **sframe**. This is accomplished through the Unix command

cc –o sframe sframe.c **-lm**

After compiling the executable version will be generated and saved in the file named sframe, which appears in the compilation command line before the source code file name (i.e. before sframe.c). The second step is to construct a data file, with suitable file name and having extension **.dat** (e.g. *Example1.dat*) using any text editor program. Then the following Unix command is to be used for performing the analysis task, with multi options:

sframe -s -n -q -l{f} -d{na} *example1.da*]

The options on execution command line are:

-s to include the effect of semi-rigid connections.

-n to include the shear flexible stability functions that allow for P-Δ analysis

-q to include the shear flexibility the members

-l{f} for load factor, it multiplies the applied loads by a number **f** (e.g. 2, 3,...)

-d{na} is for displaying the n iterative results, in which **n** is an integer number and **a** is to display results of all iterations. The default for these options, is for the rigid frame analysis with load factor is unit, and so the command line would be.

By using the execution command given above, the results will be displayed on the terminal screen. For storing the results in an output file e.g. with name **example1.out**, the following Unix command should be used.

sframe *example1.dat* > *example1.out*

Note that any combination of the five run options can be chosen.

C.2 Preparation of the data file

The data file consists of six main parts and these are

- Basic frame specification data.
- Element properties.
- Displacement boundary conditions.
- Applied Loads.
- Tolerances for moment and maximum number of iteration.
- Semi-rigid connection $M - \varphi$.

C.2.1 Basic frame specification data for Al-Sarraf (1979) frame example

For the Al-Sarraf (1979) frame example given in Section 11.3 and shown in Figure C1 the formatted of the data file is presented in Tables C1 to C6. It should be noted that the tables' headers are for facilitating the construction of the data file and not part of its format. In Figure C1 the single bay two storey

frame problem is given with dimensions, joint load, and element and joint numbering. This information will appear in the data file to be described.

The basic frame specification data gives general information on the frame structure. It includes the number of elements, of joints, of restraints, of loads at joints and of load between joints as presented in Table C.1.

Table C.1 Basic Frame Specification for Al-Sarraf (1979) example

No. of Elements	No. of Joints	No. of Restraints	No. of Loads at Joints	No. of Loads Between Joints
6	6	6	3	0

C.2.2 Element properties

Table C.2 gives information for member length, inclination of element, area of cross-section, second moment of area about axis of flexure, elastic modulus, shear modulus and shear coefficient. To identify the element the node numbers at left and right hand ends are given.

Table C.2 Element Properties

Element Joints No.		Joint Type		Length of Element, mm	Inclination of Element, degree	Area of Section, Mm^2	2^{nd} Moment of Area, mm^4	Elastic Modulus	Shear Modulus	Shear Coefficient
End 1	End 2	End 1	End 2							
1	2	0	0	400	90	56.31	4128	2000	0	0
2	3	0	0	400	90	56.31	4128	2000	0	0
3	4	0	0	400	0	56.31	4128	2000	0	0
4	5	0	0	400	270	56.31	4128	2000	0	0
5	6	0	0	400	270	56.31	4128	2000	0	0
2	5	0	0	400	0	56.31	4128	2000	0	0

Each line of the data is for one element. If the element end is a pinned joint, then a number 1 should be assigned at corresponding cell for joint type columns, otherwise 0.

C.2.3 Boundary Conditions

For each joint, there are three displacement components corresponding to the three degree of freedoms. All joints are numbered for displacements in the X, Y and θ directions (see Figure C1) in the frame's global coordinate system. Numbers in Table C3 correspond to the restraints at each joint. For example, if a frame is fully restrained at joints 1 and 6 the 1, 2 and 3 would is entered for joint 1 and 16, 17 and 18 for joint 6. This mathematically given by $3n-2$, $3n-1$ and $3n$, where n is the number assigned to the element.

Table C.3 Boundary Conditions

Joint No.	1			6		
Restraint	X	Y	θ	X	Y	θ
	1	2	3	16	17	18

C.2.4 Applied Load

The loads data specification is of two parts, loads at joints and loads between joints. For load applied at the joints, the code for the type of load is 1 for distributed load, 2 for vertical concentrated load and 3 for horizontal concentrated load. Whereas when the load is applied between joints, then the type of load, 1 is assigned for a distributed load, 2 for a concentrated vertical load and 3 for a concentrated horizontal load. Table C.4 gives the load data acting on members

Table C.4 Applied Load

1				2					
Load at Joints				Load Between Joints					
Load Value	Displacement Code			Load value	Distance from end1	No. of element applied	Type of load		
	X	Y	θ				Dis.	V	H
	1	2	3				1	2	3
0.01	7								
-5.34		8							
-5.34		11							

C.2.5 Tolerances of Moment and Maximum Number of Iteration

The tolerance in moment at each end of the element is the accuracy of the computation when analysis takes account for P-Δ effect and/or the semi-rigid connections. After each iteration process the calculated moments are compared with previous iteration results. If the difference is smaller than the tolerance value, the analysis will terminate, otherwise the iteration process continues. The maximum number of iterations is used to limit the program running time when convergence is not achieved. For Al-Sarraf frame example the tolerance and maximum number of iterations are listed in Table C.5.

Table C.5 Tolerances of Moment and Maximum Number of Iteration

Tolerances of moment, kN/m	Maximum number of iteration
0.001	300

C.2.6 Semi-Rigid Connection

The semi-rigid connection data starts with a caption line, followed by the number of different semi-rigid connection types, and their moment-rotation

curves data. The caption line is a signal to the program that the informations following are for semi-rigid connections. Table C.6 presented the format of information's need to be provided for semi-rigid analysis option.

Table C.6 Semi-Rigid Connection

Caption line	Number of semi-rigid connection type	Moment rotation curve data	Connection type at each member end
Semi-rigid yes			

The caption line goes at beginning of the semi-rigid connection data entry and it simply states that the following data are for the semi-rigid connections. Number of semi-rigid connection type either 1 or 2 as the program allows two types of semi-rigid connection, which are beam-to-column type 1, and column-to-base connections type 2.

Moment-rotation curve provides the actual connection behavior as physically conducted. In the sframe program these information are handled in piecewise linear discretise manner. For each type of the semi-rigid connection, its M-ϕ curve is defined by moment and rotation values at different points along the curve. The units of moment should be in consistent set of the units used for the element properties and the load, and the rotation ϕ should be in radian. Connection type at each member end is to account for the connection type for each element ends. For semi-rigid type either 1 or 2, but for fixed or pinned end, the connection type is 0 in Table C6.

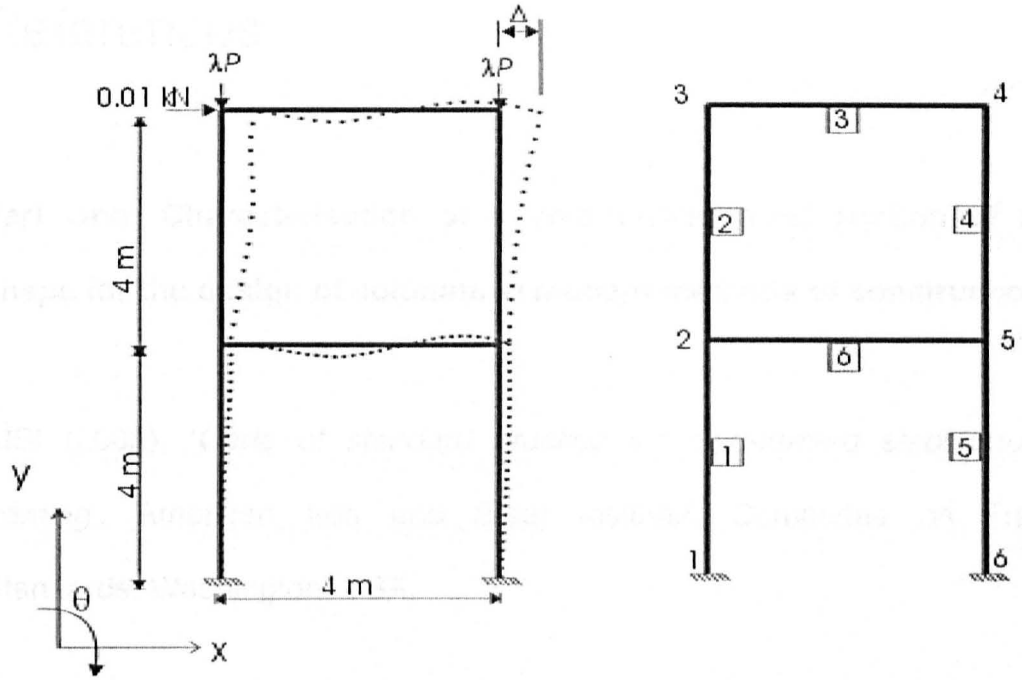

Figure C1: Al-Sarraf (1979) frame example

References

Part One: Characterisation of a cold-formed steel section of novel shape for the design of columns in modern methods of construction

AISI (2005), '*Code of standard practice for cold-formed steel structural framing*', American Iron and Steel Institute, Committee on Framing Standards, Washington, USA.

Azhari, M. and Bradford, M. A. (1993), 'Inelastic initial local buckling of plates with and without residual stresses', *Engineering Structures*, **15**(1), 31-39.

Batdorf, S. B., Stein, M. and Schildcrout, M. (1947), '*Critical shear stress of curved rectangular plates*', Technical Note, NACA, No. 1348.

Bjorhovde, R. and Birkemoe, P. O. (1979). 'Limit state design of H. S. S. columns', *Canadian Journal of Civil Engineering*, **8**(2), 276-291.

Bleich, F. (1952), '*Buckling strength of metal structures*', McGraw-Hill, New York.

Bradford, M. A. and Azhari, M. (1994), 'Local buckling of I-sections bent about the minor axis', *Journal of Constructional Steel Research*, **31**, 73-89.

Bradford, M. A. (1994), 'Inelastic Local buckling behaviour of thin steel plates in profiled composite beams', *The Structural Engineer*, **72**(16), 259-267.

Bradford, M. A. and Pi, Y. L. (2005), 'Flexural-torsional buckling of fixed steel arches under uniform bending', *Journal of Constructional Steel Research,* **62,** 20 – 26.

BS 5950-5 (1998). '*Code of practice for design of cold formed steel sections*,' British Standard Institute.

Bulson, P. L. (1970), '*The stability of flat plates*', Chatto and Windus, London, UK.

Calladine, R. C. (1983). '*Theory of shell structures*', Cambridge University Press, Cambridge, UK.

Chapuis, A. M. J. and Galambos, F. V. T. (1982) 'Restrainted crooked aluminium columns', *Journal of Structural Division*, **108**(ST3), 511-524.

Chen, W. F. and Atsuta, T. (1976). '*Theory of beam-column, Volume 1 In-plane behaviour and design*', Chapman and Hall, London, UK.

Chen, W. F. (1980), 'End restraint and column stability', Journal of Structural Division, ASCE, **106**(ST11), 2279-2295.

Cheng, Y. and Schafer, B. W. (2003). 'Local buckling tests on cold-formed steel beam', *Journal of Structural Engineering* **129** (12) 1596-1606.

Chernenko, D. E. and Kennedy, D. J. (1991). 'An analysis of the performance of welded wide flange columns', *Canadian Journal of Civil Engineering*, **18**, 537-545.

CE139 (2005), '*Building energy efficient buildings using modern methods of construction*', Energy saving trust, London, UK.

Ding, Y., Ghrib, F., Bhattacharjee, S. and Madugula, M. K. S. (2003). 'A novel method for deteriming effective length factors for solid round steel leg members of guyed lattice towers with cross-bracing', *Canadian Journal of Civil Engineers*, **30**, 780-786.

Eatherley, M. and Perera, N. (2003), 'Beaufort Court: new steel homes in London', *The Structural Engineer*, 13-15.

European Committee for Standardisation (CEN). Eurocode 3 (1996). 'design of steel structures', part 1.3: general rules. ENV 1993-1-3

Fertis D. G. (1996), '*Advanced mechanics of structures*', Marcel Dekker, Inc., New York, USA.

Gerard, G. and Becker, H. (1957), '*Handbook of structural stability, Part III buckling of curved plates and shells*', Technical Note, NACA, No. 3783.

Giroud, J. P. (1994), 'Mathematical model of geomembrane stress-strain curves a yield peak', *Geotextiles and Geomembranes*, **13**, 1-22.

Graves Smith, T. R. (1967), '*The ultimate strength of locally buckled columns of arbitrary length*', in Symposium on Thin-Walled Steel Structures Their Design and use in Building, University College of Swansea, Crosby Lockwood & Sons Ltd, London, UK, 35-60.

Hancock G. J., Kwon, Y. B. and Bernard, E. S. (1994). 'Strength design curves for thin-walled sections undergoing distortional buckling', *Journal of Construction Steel Research*, **31**(2-3), 169-186.

Hancock, J. G., Murray, M. T. and Ellifritt, S. D. (2001), '*Cold- formed steel structures to the AISI specification*', Marcel Dekker, Inc., New York, USA.

Hancock G. J. (2003) 'Review article cold-formed steel structures', *Journal of Constructional Steel Research*, **59,** 473-487.

Hopperstad, S. O., Lagseth, M. and Tryland, T. (1999), 'Ultimate strength of aluminium alloy outstands in compression: experiments and simplified analysis', *Thin Walled Structures*, **34**, 279-294.

Horne, M. R. and Merchant, W. (1965) '*The stability of frames*', Pergamon Press Ltd, Oxford, UK.

Ilyushin, A. A. (1947), '*The elasto-plastic stability of plates*', Technical Memorandum, NACA, No. 1188.

Ioannidis, G. I., Ermopoulos, J. H. and Kounadis, A. N. (1999). 'Stability analysis of bars with asymmetric open thin walled cross-sections under eccentric axial thrust', *Mechanics, Automatic Control and Robotics*, **2**(9), 865-876.

Jones, S. W., Kirby, P. A. and Nethercot, D. A. (1983), 'The analysis of frames with semi-rigid connections - A state-of-the-art report', *Journal of Constructional Steel Research*, **3**(2), 2 –13.

von Karman, T., Sechler, E. E., and Donnell, L. H. (1932). 'The strength of thin plates in compression', *Transactions of the American Society of Mechanical Engineers*, **54**(2), 53 - 57.

Kato, B. (1965). 'Buckling strength of plates in the plastic range', *International Association for Bridge and Structural Engineering*, **25**, 127-141.

Khong, P. W. (1994). 'Behaviour of axially loaded lipped channel', *Journal of Constructional Steel Research*, **128**, 243-255.

Kwon, Y. B. and Hancock, G. J. (1992). 'Tests of cold-formed channels with local and distortional buckling', *Journal of Structural Engineering*, **117**(7), 1786-1803.

Lawson, R. M., Chung K. F. and Popo-da, S. O. (2002). 'Building Design using Cold Formed Steel Section: Structural design to BS 5950-5: 1998 – Section Properties and Load Tables', Steel Construction Institute, UK.

Lechner, B. and Pircher, M. (2005). 'Analysis of imperfection measurements of structural members', *Thin-Walled Structures*, **43**, 351-374

Levy, S. (1943), '*Large deflection theory of curved sheet*', Technical Note, NACA, No. 895.

Little, H. G. (1982), 'The collapse of steel model columns', *International Journal of Mechanical Sciences*, **24**(5), 263-278.

Mahendran, M. (1997), 'Local plastic mechanisms in thin steel plates under in-plane compression', *Thin Walled Structures*, **27**(3), 245-261.

Meyzaud, Y. and Parniere, P. (1977). 'High strength cold rolled steel sheets with a high drawability ', *Materials Science and Engineering*, **29**, 41-49.

Moller, M., Johansson, B. and Collin, P. (1997), 'A new analytical model of inelastic local flange buckling', *Journal of Constructional Steel Research*, **43**, 43-63.

Mottram, J. T., Brown, N. D. and Anderson, D. (2003),'Physical testing for concentrically loaded columns of pultruded glass fibre reinforced plastic profile', *Proceedings of the Institution of Civil Engineers, Structures and Buildings Journal*, **156**(2), 205-219.

Murray, N. W. (1984), '*Introduction to the theory of thin-walled structures*', Oxford University Press, Oxford, UK.

Parks, M. B. and Yu W. W. (1989), 'Local buckling behaviour of stiffened curved elements', *Thin Walled Structures*, **7**, 1-22.

Popovic, D., Hancock, G. J. and Rasmussen, K. J. R. (1999). 'Axial compression tests of cold-formed angles', *Journal of Structural Engineering*, **125**(5), 515-523.

Post note (2003), '*Modern methods of house building*', Parliamentary Office of Science and Technology, London, UK.

Pu, Y., Godley, M. H. R., Beale, R. G. and Lau, H. H. (1999). 'Predication of ultimate capacity of perforated lipped channels', *Journal of Structural Engineering*, **125**(5), 510-514.

Rasmussen, K. J. R. and Trahair, N. S. (2004). 'Exact and approximate solutions for the flexural buckling of columns with oblique rotational end restraints', *Thin-Walled Structures*, **43**, 411-426.

Ramberg, W. and Osgood, R. (1943), '*Description of stress-strain curves by three parameters*', Technical Note, NACA, No. 902.

Redshaw, S. C. (1938), 'The elastic stability of a curved panel under axial thrust', *The Aeronautical Journal*, **42**, 536-553.

Rhodes, J. and Harvey, J. (1976). 'Plain channel section struts in compression and bending beyond the local buckling load', *International Journal of Mechanical Science*, **8**, 511-519.

Ros, M. and Eichinger, A. (1932), 'Final report 1st congress', *International Association for Bridge and Structural Engineering*. Paris.

Schafer, B. W. (2002). 'Local Distortional, and Euler Buckling of Thin-Walled Columns', *Journal of Structural Engineering*, **128**, 289 - 299.

SCI P272 (1999), '*Modular Construction using light Steel Framing: An Architect's Guide*', The Steel Construction Institute, UK.

SCI News (2005), '*Design using Modules*', The Steel Construction Institute, UK.

Seah, L. K., Rhodes, J. and Lim, B. S., (1993). 'Influence of lips on thin-walled section', *Thin-Walled Structures*, **16(1-4)**, 145-178.

Sechler, E. E. and Dunn, L. G. (1942), '*Airplane structural analysis and design*', John Wiley and Sons, Inc., New York.

Shanley, F.R. (1947), 'Inelastic column theory', *Journal of the Aeronautical Sciences*, **14**(5), 261-267.

Singer, J., Arbocz, J. and Weller, T. (1998). '*Buckling experiments: Experimental methods in buckling of thin-walled structures*', Volume 1, John Wiley and Sons Ltd, West Sussex, UK.

Stowell, E. Z. (1948), '*A unified theory of plastic buckling of columns and plates*', Technical Note, NACA, No. 1188.

Teter, A. and Kolakowski, Z. (2004), 'Interactive buckling and load carrying capacity of thin-walled beam-columns with intermediate stiffeners', *Thin Walled Structures*, **42**, 211-254.

Timoshenko, S. P. (1961), '*Theory of elastic stability*', McGraw-hill book company, Inc. New York, USA.

Timoshenko, S. P. and Gere, J. M. (1972). '*Mechanics of materials*', Van Vostrand Reinhold Company.

Trahair, N. S. (1993), '*Flexural torsional buckling of structures*', E and FN Spon Chapman and Hall, London, UK.

Ungureanu, V. and Dubina, D. (2004), 'Recent research advances on ECBL approach. Part I: Plastic-elastic interactive buckling of cold-formed steel sections', *Thin Walled Structures*, **42**, 177-194.

Wang, L. R. and Rakotonrainibe, A. (1978), 'Elasto-plastic buckling of curved webs', *Computer and Structures,* **8**, 159 -167.

Wang, C. M., Xiang, Y. and Chakrabarty J. (2001), 'Elastic/plastic buckling of thick plate', *International Journal of Solids and Structures*, **38**, 8617-8640.

Wang, C. W., Wang, C. Y. and Reddy, J. N. (2005). '*Exact solutions for buckling of structural members*', CRC Press LLC, Florida, USA.

Winter, G. and Uribe, J. (1967). '*Effects of cold-work on cold-formed steel members*', in symposium on Thin-Walled Steel Structures Their Design and use in Building, University College of Swansea, Crosby Lockwood & Son Ltd, London, UK, 119-136.

Wood, R. H. (1974), 'effective lengths of columns inmulti-storey building, Part 1', *Structural Engineer*, **52**(7) 235 - 244.

Young, B. and Rasmussen, J. R. (1999). 'Behaviour of cold-formed singly symmetric columns', *Thin-Walled Structures*, **33**, 83 -102.

Young, B. and Rasmussen, J. R. (2000). 'Inelastic bifurcation of cold-formed singly symmetric columns', *Thin-Walled Structures*, **36**, 213 - 230.

Yu, W. W. (1973), '*Cold-formed steel structures*', McGraw-Hill, New York.

Part Two: Determination of the elastic critical buckling load for shear-flexible frames of fibre reinforced polymer sections

Abbaker, A. and Mottram, J. T., (2004), 'The influence of shear-flexibility on the elastic critical elastic load for frames of pultruded fibre reinforced plastic section,' in *Proceedings 2nd International Conference on Advanced Polymer Composites for Structural Applications in Construction* (ACIC04), Woodhead Publishing Ltd., Cambridge, 437-444.

Al-Sarraf, S. Z. (1979). 'Upper and lower bounds of elastic critical loads', *The Structural Engineer*, **57A**(12), 415-421.

Al-Sarraf, S. Z. (1986). 'Shear effect on the elastic stability of frames', *The Structural Engineer*, **64B**(2), 43-47.

Anon, (1989), *'EXTREN Design Manual,'* Strongwell, Bristol VA.

Anderson, D., Colson, A. and Jaspart, J. (1993) 'Connection and Frame Design for Economy', *New Steel Construction*, **1**(6), 30-33.

Anon, (1995), '*Fiberline Design Manual for Structural Profiles in Composite Materials*,' Fiberline Composites A/S, Kolding, Denmark.

Anon, (1999), '*The New and Improved Pultex Pultrusion Design Manual of Pultex Standard and Custom Fiber Reinforced Polymer Structural profiles*,' Creative Pultrusions Inc., Alum, Bank, PA.

Bank, L. C. and Bednarczyk, P. J. (1988). ' A beam theory for thin-walled composite beams', *Composites Sciences and Technology* **32**, Elsevier Applied Science Ltd, London, UK.

Bank, L. C., Mosallam, A. S. and Gonsior, H. E., (1990), 'Beam-to-column connections for pultruded FRP structures' *In Proceedings of the 1st Materials Engineering Congress ASCE,* ASCE NY, 804-813.

Bank, L. C., Mosallam, A. S., (1991), 'Performance of pultruded FRP beam-to-column connections', *In Proceedings of ASCE 9th Structures Congress*, ASCE NY, 389-392.

Bank, L. C. (2006), '*Composites for Construction: Structural Design with FRP Materials*,' Wiley & Sons, New York.

Bass, A. J. and Mottram, J. T., (1994), 'Moment-rotation of polymeric composite connections for pultruded frames', *The Structural Engineer*, **72**(17), 280-285

Brooks, R. J. and Turvey, G. J., (1995), 'Lateral buckling of pultruded GRP I-section cantilevers', *Composite Structures*, **32**(1-4), 203-216.

BS 449-2, (1969), '*Specifications for the use of structural steel in building. Metric units*', British Standard Institute

BS 5950-5, (1998), '*Code of practice for design of cold formed steel sections*,' British Standard Institute.

BS 5950-1, (2000), '*Code of practice for design of cold formed steel sections*,' British Standard Institute.

BS EN 1993-1, (2005), '*Eurocode 3. Design of steel structures. General rules and rules for buildings*', Thomas Telford Ltd.

Chan, S. L. and Chui, P. P. T. (2000). '*Non-linear static and cyclic analysis of steel frames with semi-rigid connections*', Elsevier Science Ltd, London, UK

Chajes, A. (1974), 'Principles of structural stability theory', Prentice- Hall Inc. New Jersey, USA.

Chen, W. F. and Lui, E. M. (1991), '*Stability design of steel frames*', CRC Press, Inc. London, UK.

Coates, R. C., Coutie, M. G. and Kong, F. K., (1994) '*Structural Analysis*', Chapman and Hall, 2-6 Boundary Row London, UK.

Davalos, J. F. and Qiao, P., (1999), 'Computational approach for analysis and optimal design of FRP beams', *Computers and Structures*, **70**(2), 169-183.

Dowling, P.J., Knowles, P.R., Owens, G.W., (1988), '*Structural Steel Design*', Butterworths, London.

ECS (1993), '*Eurocode 3: Design of steel structures*', ENV 1993-1-1:1992E, European Committee for Standardization, Brussels, Belgium.

Galambos, T. V., (1998), '*Guide to stability design criteria for metal structures*', John Wiley and Sons Inc., Canada.

Ghali, A. and Neville A. M., (1997) '*Structural analysis a unified classical and matrix approach*', E & FN SPON, London, UK.

Hollaway, L. C. and Head P. R. (2001). '*Advanced polymer composites and polymers in the civil Infrastructure*', Elsevier Science Ltd, London, UK.

Horne, M. R. and Merchant, W. (1965) '*The stability of frames*', Pergamon Press Ltd, Oxford, UK.

Keller, T. (2003), *'Use of fibre reinforced polymers in bridge construction,'* Structural Engineering Documents 7, Inter. Association for Bridges and Structural Engineering (IABSE-AIPC-IVBH), Zurich.

Lane, A. and Mottram, J. T., (2002), 'The influence of model coupling upon the buckling of concentrically pultruded fibre-reinforced plastic columns', Proceedings of Institution of Mechanical Engineers Part L: *J. Material – Design and Applications*, **216**, 133-144

Livesley, R. K., (1956), 'The application of the electronic digital computer to some problems of structural analysis', *The Structural Engineer*, **34**(1), 1-12

Ludovico, M. D., (2002), '*Experimental behaviour of prestressed concrete beams strengthened with FRP*', Report, Centre for Infrastructures Engineering Studies, Rolla, USA.

Meagher, R. J., (1999), 'The choice of stability functions in second-order analysis', *The Structural Engineer*, **77**(6), 21-23.

Mosallam, A.S., (1990). '*Short and long-term behavior of a pultruded fiber reinforced plastic frame,*' PhD thesis, The Catholic Univ. of America, Washington DC, USA.

Mosallam, A. S., (1994), 'Connections for pultruded composite: A review and evaluation', *In Proceeding of the 3rd Materials Engineering Conference, ASCE,* ASCE NY, 1001-1017.

Mottram, J. T. and Zheng, Y., (1996), 'State-of-the-art review on the design of beam-to-column connections for pultruded frames', *Composite Structures*, **34**(4), 387-401.

Mottram, J.T., (1996), '*Nominally pinned connections for pultruded frames*,' in Clarke, J.L., (Ed.), Structural Design of Polymer Composites - EUROCOMP Design Code and Handbook, S. & F. N. Spon, London, 703-718.

Mottram, J. T. and Zheng, Y., (1999), 'Further tests on beam-to-column connections for pultruded frames: Web-cleated', *J. Composite for Construction*, **3**(1), 3-11.

Mottram, J. T. and Aberle, M., (2002), 'When should shear-flexible stability functions be used in elastic structural analysis?', *Proc. Institution of Civil Engineers: Structures and Buildings*, **152**(1) 31-40.

Mottram, J. T., Brown, N. D. and Anderson, D., (2003), 'Physical testing for concentrically loaded columns of pultruded glass fibre reinforced plastic profile', *Proceedings of the Institution of Civil Engineers, Structures and Building J.*, **156**(2), 205-219.

Mottram, J.T., (2004), 'Shear modulus of standard pultruded FRP material', J. *Composites for Construction*, **8**(2), 141-147.

Owens, G. W., Knowles, P. R. and Dowling, P. J., (1994), '*Steel designers' manual*', Blackwell Scientific publications, Cambridge.

Timoshenko, S. P. and Gere, J. M., (1963), '*Theory of elastic stability*', McGraw-Hill, New York.

Timoshenko, S. P. and Gere, J. M. (1972). '*Mechanics of materials*', Van Vostrand Reinhold Company.

Turvey, G. J. and Cooper, C., (1996), 'Semi-rigid pultruded GRP frame connections: Tests to determine static moment-rotation characteristics', *In Proceedings of the 7th European Conference on Composite Materials*, Woodhead Publishing Ltd., **2**, 295-300

Turvey, G. J., (1997), 'Analysis of pultruded GPR beams with semi-rigid end connections', *Composite Structures*, **38**(4), 3-16

Turvey, G. J., (1999), 'Flexural of pultruded beams with semi-rigid end connections', *Composite Structures*, **47**, 571-580.

Turvey, G. J. and Cooper, C., (2000), 'Semi-rigid column base connections in pultruded GRP frame', *Computers and Structures*, **76**(1-3), 77-88.

Turvey, G. J., (2002), 'Pultruded GRP frames: Simple (conservative) approach to design: a rational alternative and research needs for improved design', Internal Workshop on Composites in Construction, *ASCE Special Publication*, 258-266

Turvey, G.J. and Cooper, C., (2004), 'Review of tests on bolted joints between pultruded GRP profiles, Proceedings of the Institution of Civil Engineers, *Structures and Buildings J.*, **157**(3), 211-233.

Wood, R. H., (1974), 'Effective lengths of columns in multi-storey buildings, Part 1: Effective lengths of single columns and allowances for continuity', *The Structural Engineer*, **52**(7), 235-244.

Zheng, Y. and Mottram, J.T., (1996), 'Analysis of pultruded frames with semi-rigid connections,' *In Proceedings of the 2nd International Conference on Advanced Composite Materials in Bridges and Structures (ACMBS/2)*, The Canadian Society for Civil Engineers (CSCE), 919-927.

Zheng, Y. (1998). 'Connection behaviour and frame analysis for structures of pultruded profiles,' PhD thesis, Dept. of Engrg., University of Warwick, UK.

Zureick, A. and Scott, D., (1997), 'Short-term behaviour and design of fibre reinforced polymeric slender members under axial compression', *ASCE journal of composites for construction*, **1**(4), 140-149.